Responsive, functional materials from self-stabilising and reactive branched addition co-polymers

By Rachel Louisa Harbron

Submitted to Imperial College London
Department of Materials

In fulfilment of the requirements for the award of
Doctor of Philosophy (PhD)

April 2014

The work presented within this thesis is described in my own words, and is my own research. All content relating to others research, or content that has been conducted by others, is appropriately referenced.

Chapter 3; R. L Harbron, Dr. P. H. Findlay, Professor S. P. Rannard, and Dr. J. V. M. Weaver participated in the writing of the presented paper.

Chapter 5; All authors participated in the writing of the presented paper and this is referenced as such within the published document. In chapter 5, specific sections are appropriately acknowledged. Dr. M. Lei and Professor S. Mann conceived the concept; Professor S. Mann directed the research, Dr. M. Li, R. L. Harbron and Dr. J. V. M. Weaver designed and performed the experiments and analysed the data, and Professor B. P. Binks contributed the surface-active nanoparticles and to the discussion on colloid science.

Acknowledgements

Firstly, I would like to thank my industrial sponsors, Parogle Technologies Ltd. and Imperial College London for granting me the opportunity to undertake my Ph.D.

Thank you to my supervisor Dr. Paul Findlay for his constant help and guidance. I did not expect him to support me to the considerable magnitude that he has, and I am forever grateful. He took me on, alongside his own commitments, helping me to finish this thesis.

Thank you to members of Parogle Technologies Ltd., Dr. Roselyn Baudry and Anne-Laure Sanoner.

Thank you to my supervisor Dr. Julian Jones for his continued support and to the Jones research group, especially Dr. Louise Connell and Dr. Oliver Mahony for mercury intrusion measurements included in Chapter 4. Thank you to Professor Molly Stevens, and members of the Stevens research group. Thank you to Dr. Sergio Bertazzo for scanning electron microscopy images included in Chapter 4.

Thank you to Professor Stephan Mann for the great opportunity to collaborate together to complete Chapter 5. Thank you to Dr Mei Li for her contribution to Chapter 5.

Thank you to the University of Liverpool, and a special thank you to Professor Steve Rannard, Dr. Dave Adams and Anita Peacock. Thank you to the Centre for Materials Discovery, Liverpool, for the use of their equipment. Thank you to Dr. Tom McDonald for scanning electron microscopy images used in Chapter 3. Thank you to Dr. Rob Clowes for Brunauer–Emmett–Teller gas adsorption measurements included in Chapter 4.

Thank you to Dr. Robert Woodward, Robert Bell and all the former members of the Weaver group.

Thank you to Dr. Jonathan Weaver; in constant memory.

IMPERIAL COLLEGE LONDON

Rachel Louisa Harbron **Submitted for PhD**

ABSTRACT

A one-component emulsion templating strategy for the preparation of inorganic-organic encapsulated droplets and hollow capsules has been developed. The process exploits, and relies on, both branched addition co-polymer architectures and compositions, which provide simultaneous properties of emulsion droplet steric-stabilisation and cross-linking function. It was demonstrated that high yielding encapsulation of different hydrophobic actives was successful whilst retaining the structural integrity of the capsule compartments.

Responsive capsule surfaces and shell/membrane properties with pre-determined complex functionalities were demonstrated. The incorporation of chemical functionality within the reactive branched addition co-polymer allowed higher order responsive structures to be formed. These materials have been shown to be highly useful in the preparation of large associated aggregates which can be loaded with numerous payloads. The encapsulation of both hydrophobic dyes and an oil-soluble polymer was illustrated.

Protocell constructs with pH-mediated, electrostatically gated permeability were prepared by covalently grafting a multi-responsive functional terpolymer to the outer surface of a cross-linked membrane of silica nanoparticle-based colloidosomes. Terpolymer grafted membrane functionality-mediated uptake and release of small molecules from the colloidosomes was demonstrated.

PRIMARY PUBLICATIONS ARISING FROM THIS THESIS

1. **"One-pot, single-component synthesis of functional emulsions-templated hybrid inorganic-organic polymer capsules"**, R. L. Harbron, T. O. McDonald, S. P. Rannard, P. H. Findlay, J. V. M. Weaver, *Chem. Commun.* **2012**, *48*, 1592-1594.

2. **"Electrostatically gated membrane permeability in inorganic protocells"**, M. Li, R. L. Harbron, J. V. M. Weaver, B. P. Binks, S. Mann, *Nature Chemistry* **2013**, *5*, 529.

3. **"Controlling hybrid capsule surface functionality *via* branched copolymer composition"**, R. L. Harbron, R. T. Woodward, S. Bertazzo, P. H. Findlay, J. V. M. Weaver, *Manuscript in preparation*, **2014**.

Table of Contents

Glossary

ATRP	atom transfer radical polymerisation
BET	Brunauer–Emmett–Teller analysis
CRP	controlled radical polymerisation
CTA	chain transfer agent
CTR	chain transfer reaction
DP	degree of polymerisation
DP_n	number average degree of polymerisation
FRP	free radical polymerisation
FTIR	Fourier Transform infrared spectroscopy
GPC	gel permeation chromatography
MFM	monofunctional monomer
MIP	mercury intrusion porosimetry
M_n	number-average molecular weight
M_w	weight-average molecular weight
NMR	nuclear magnetic resonance
o/w	oil-in-water emulsion
PDI	polydispersity index (M_w/M_n)
RAFT	radical addition-fragmentation chain transfer polymerisation
ref.	reference
rpm	revolutions per minute
SCL	shell cross-linked
SEC	size exclusion chromatography
SEM	scanning electron microscopy
TD-GPC	triple-detection gel permeation chromatography
TEM	transmission electron microscopy
TGA	thermogravimetric analysis
w/o	water-in-oil emulsion
Φoil	volume fraction of oil

Chemical glossary

AIBN	azobis(isobutyronitrile)
$CDCl_3$	deuterated chloroform
D_2O	deuterium oxide
DDT	1-dodecanethiol
DEAEMA	2-(diethylamino)ethyl methacrylate
DiO	Dioctadecyloxacarbocyanine perchlorate
DMAEMA	2-(dimethylamino)ethyl methacrylate
EG	ethylene glycol
EGDMA	ethylene glycol dimethacrylate
EtOAc	ethyl acetate
EtOH	ethanol
GδL	glucono-δ-lactone
HCl	hydrochloric acid
HEMA	2-hydroxyethyl methacrylate
MAA	methacrylic acid
MeOH	methanol
MMA	methyl methacrylate
MPA	mercaptopropionic acid
NaOH	sodium hydroxide
NH_4OH	ammonium hydroxide
PEGDMA	poly(ethylene glycol dimethacrylate)
PEGMA	poly(ethylene glycol) methacrylate
PHEMA	poly(2-hydroxyethyl methacrylate)
PMMA	poly(methyl methacrylate)
*p*NNP	4-nitrophenyl phosphate
PVC	poly(vinyl chloride)
SDS	sodium dodecyl sulfate
TEOS	tetraethoxysilane
TG	1-thioglycerol
THF	tetrahydrofuran
TMOS	tetramethoxysilane
TMSPMA	3-(trimethoxysilyl)propyl methacrylate

Materials Index

Material	Abbreviation	Supplier
Alkaline phosphatase	ALP	Sigma-Aldrich
Aluminium oxide (activated, basic)	-	Sigma-Aldrich
2,2'-Azobis(isobutyronitrile)	AIBN	VWR
2,2'-Bipyridine	bpy	Sigma-Aldrich
4',5'-bis[N,N-	Calcein	Sigma-Aldrich
2-bromoisobutyryl bromide	-	Sigma-Aldrich
Cineole	-	Sigma-Aldrich
3,6-diamino-10-methylacridinium chloride hydrochloride	Acriflavine hydrochloride	Sigma-Aldrich
Deuterated chloroform	$CDCl_3$	Sigma-Aldrich
Deuterium oxide	D_2O	Sigma-Aldrich
2-(Dimethylamino) ethyl methacrylate	DMAEMA	Sigma-Aldrich
3,3'-Dioctadecyloxacarbocyanine perchlorate	DiO	Invitrogen
Dodecane	-	Sigma-Aldrich
1-Dodecanethiol	DDT	Sigma-Aldrich
Ethyl alcohol	EtOH	Sigma-Aldrich
Ethylene glycol dimethacrylate	EGDMA	Sigma-Aldrich
Glucono-δ-lactone	GδL	Sigma-Aldrich
Glycine	-	Sigma-Aldrich
Hydrochloric acid (1 M)	HCl	Sigma-Aldrich
Methacrylic acid	MAA	Sigma-Aldrich
Methyl alcohol (standard laboratory grade)	MeOH	Sigma-Aldrich

4-nitrophenyl phosphate	*p*NPP	Sigma-Aldrich
Oil Blue	-	Sigma-Aldrich
Oil Red	-	Sigma-Aldrich
Poly(ethylene glycol) methacrylate (M_w 1,100 g / mol)	PEGMA	Sigma-Aldrich
Poly(vinyl stearate)	PVS	Sigma-Aldrich
Rhodamine 6G	-	Sigma-Aldrich
Sodium Hydroxide (1 M)	NaOH	Sigma-Aldrich
Tetrahydrofuran (standard laboratory grade)	THF	Sigma-Aldrich
1-Thioglycerol	TG	Sigma-Aldrich
Triethylamine	TEA	Sigma-Aldrich
3-(Trimethoxysilyl) propyl methacrylate	TMSPMA	Sigma-Aldrich
(Trimethysilyl) diazomethane solution	TMS-	Sigma-Aldrich
Toluene (standard laboratory grade)	-	Sigma-Aldrich
1-Undecanol	-	Sigma-Aldrich

Polymer Reference Index

ID	Polymer Composition
P1	$TMSPMA_{100}$-$EGDMA_{10}$-DDT_{10}
P2	$TMSPMA_{100}$-$EGDMA_{10}$-TG_{10}
P3	$TMSPMA_{100}$
P4	$TMSPMA_{100}$-DDT_{2}
P5	$TMSPMA_{100}$-TG_{2}
*P6**	$PEGMA_{5}$/$TMSPMA_{95}$-$EGDMA_{10}$-DDT_{10}
P7	$PEGMA_{5}$/$TMSPMA_{95}$-$EGDMA_{10}$-DDT_{5}
P8	$PEGMA_{5}$/$TMSPMA_{95}$-$EGDMA_{10}$-$DDT_{2.5}$
P9	$PEGMA_{5}$/$TMSPMA_{95}$-$EGDMA_{10}$-TG_{10}
P10	$PEGMA_{15}$/$TMSPMA_{85}$-$EGDMA_{10}$-DDT_{10}
P11	$PEGMA_{95}$/$TMSPMA_{5}$-$EGDMA_{10}$-DDT_{10}
P12	$PEGMA_{85}$/$TMSPMA_{15}$-$EGDMA_{10}$-DDT_{10}
P13	$PEGMA_{80}$/$TMSPMA_{20}$-$EGDMA_{10}$-DDT_{10}
P14	$PEGMA_{5}$/$TMSPMA_{95}$
*P15**	$PEGMA_{5}$/$TMSPMA_{95}$-DDT_{2}
P16	$PEGMA_{5}$/$TMSPMA_{95}$-DDT_{10}
P17	$PEGMA_{5}$/$TMSPMA_{95}$-TG_{2}
P18	$TMSPMA_{15}$/MAA_{85}-$EGDMA_{10}$-DDT_{10}
P19	$TMSPMA_{20}$/MAA_{80}-$EGDMA_{10}$-DDT_{10}
P20	$TMSPMA_{30}$/MAA_{70}-$EGDMA_{10}$-DDT_{10}
*P21**	$TMSPMA_{61}$/MAA_{39}-$EGDMA_{10}$-DDT_{10}
*P22**	$TMSPMA_{61}$/MAA_{39}-DDT_{2}
*P23**	$TMSPMA_{22}$/$DMAEMA_{39}$/MAA_{39}–$EGDMA_{10}$–DDT_{10}
** main co-polymer composition used throughout this thesis*	

CHAPTER 1

Introduction

List of Figures

This section will introduce the main topics of this thesis. Firstly, an introduction to polymer science will be presented with particular emphasis on the preparation of branched polymers that are utilised throughout this work. Then a description of emulsions and emulsification will be introduced. These two areas will be combined, and the formation of polymer-stabilised emulsions and higher structures will be defined.

1.1. Macromolecules

The success of polymer technology has been substantial; there have been many advances in this field of synthetic chemistry since the introduction of Staudinger's foundational concept of polymers chains was published in 1920.[1] His research on high molecular weight molecules, or macromolecules, where a large number of smaller simple building blocks called monomers (Ancient Greek translation: *mono* "single", *mer* "parts") link by means of covalent bond formation *via* a process called polymerisation, to compose a high molecular weight *polymer* (*poly* "many", *mer* "parts") sparking a new era in the molecular design of structural and functional polymeric materials; for which Staudinger received the Nobel Prize in 1953.[2] The advancement of polymer science continues to heavily affect our everyday lives.[3]

1.2. Polymer architectures

In recent decades, progression in synthetic methodologies has led to more control over the size and shape of polymer architecture.[2b, 4] Polymer chains can show many different types of architecture and composition, determined by the polymerisation method and the structure of the constituent parts. Complexity spans from relatively simple structures such as linear polymers, to more complex comb or graft structures and furthermore to branched and hyperbranched materials. Some of the more commonly found architectures are illustrated in Figure 1.

A polymer, or macromolecule, as defined in the previous section, is made up of many monomers commonly linked together through a backbone. The backbone atoms form the 'spine' of the polymer chain with other molecules, or elements, pendent from the chain (often referred to as pendent groups or side groups). Where the monomers are linked through the carbon atoms to produce a single continuous backbone with two chain ends, linear polymers are produced. Examples of industrial everyday linear polymers include poly(methyl methacrylate), poly(vinyl chloride) and polystyrene.

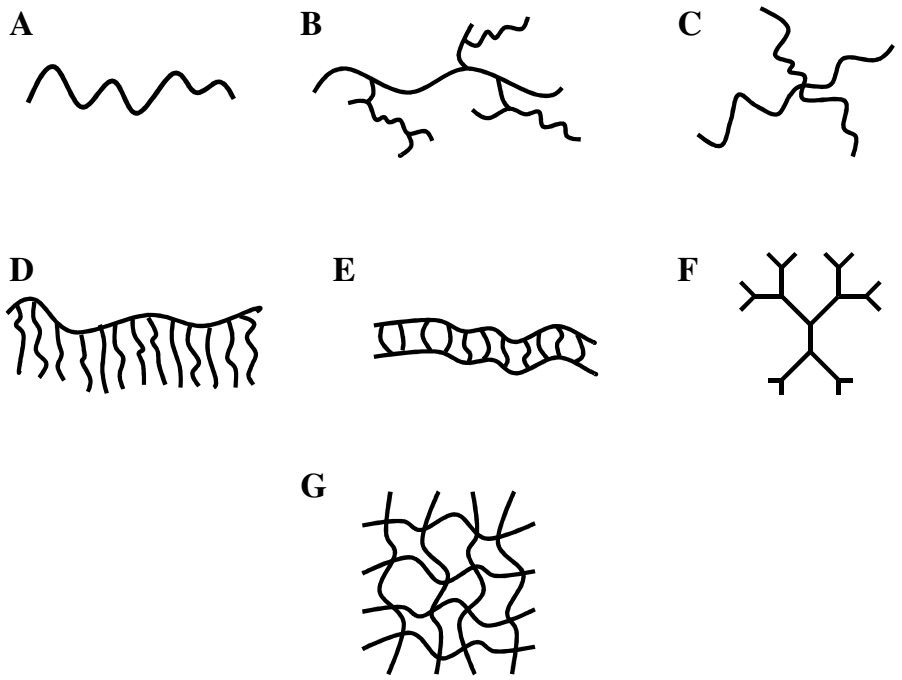

Figure 1. Representation of varied polymer architectures. (A) linear, (B) branched, (C) star, (D) graft or comb, (E) ladder, (F) dendrimer and (G) network polymer architecture.

1.3. Branched polymers

Branched polymers are a class of polymers lying architecturally in-between linear and cross-linked network polymers. Branched polymers differ from less complex polymer structures in that somewhere along the linear or primary chain, branching points have been introduced either during or following their formation. Where a branching point has been introduced into the structure during the polymer's formation, the growing polymer chains typically give rise to side chains or branches due to their increased functionality and by virtue of their ability to react with more than one monomer species, for example the additional double bond in divinyl

monomers e.g. ethylene glycol dimethacrylate.[5] Where the branching is localised at a central point or core star polymers can be formed (Figure 1.c).[6] Where the branching occurs from the polymer backbone, comb polymers (Figure 1.d) and ladder polymers (Figure 1.e) can be formed.[7] These materials are usually prepared through a grafting process following an initial polymerisation step. Highly branched structures include polymer networks, where the polymer chains are interconnected by many cross-links (Figure 1.g), hyperbranched polymers, with many irregular branching points, and dendrimers, which are repetitively and regularly branched structures (Figure 1.f).[8] Dendrimers are extremely interesting materials and can be thought of being "perfectly branched".[9] However, these materials are generally difficult and time-consuming to prepare as they typically require multi-step syntheses, either by convergent or divergent growth, with numerous purification steps and as such are limited in their application. Further complex structures have been produced such as hybrid structures of two or more of the aforementioned types of branched architectures co-existing within the same polymer, for example novel linear chains with pendent dendritic structures.[10]

Branched polymers can be prepared *via* a number of means such as through choice of monomers or polymerisation conditions. A number of industrial polymers are inherently branched by virtue of these properties for example poly(vinyl acetate) (PVAc), a commodity polymer widely utilised in its own right as an adhesive or coating material, or when hydrolysed to poly(vinyl alcohol), as an ubiquitous commodity adhesive. PVAc is branched due to the inherent chain transfer reactions that occur during its formation leading to multiple branching points along the primary chain. This effect is also known for low density

polyethylene, where branching points are formed along the polymer backbone by virtue of the propagating species, therefore short polymer chains "grow" off the primary chain.

Branched polymers are industrially useful as they typically exhibit differing physical properties when compared to equivalent linear species such as solution or melt viscosities (as discussed in section 1.5.2). These materials are useful where the attributes would be beneficial, for example in adhesives or coatings where solutions of high concentration can be prepared with lower amounts of Volatile Organic Compounds (VOC). Additionally, their reduced viscosity and glass transition temperatures (Tg) can be beneficial for adhesive applications. A high concentration of chain ends also affords high functionalities and therefore high degrees of reactivity of a branched compared to a linear system. For example, on comparison of an end-functionalised linear polymer such as poly(ethylene glycol) with a branched poly(ether-alcohol) such as poly(glycidol), the linear polymer would only posses two functional groups whereas the branched chemically similar poly(glycidol) possesses many functional hydroxyl units which could be further reacted as applied in the formation of polyurethane resins or coatings. In this comparison it would be expected that the poly(glycidol) would react faster and more readily than poly(ethylene glycol).

1.4. Molecular weight

Many of the interesting properties of polymers stem from their high molecular weights, or more correctly molecular masses. Molecular mass is the *exact mass* of a molecule calculated

using the most abundant isotope present, whereas molecular weight is the average molecular weight of the different isotopes of a molecule. The determination of this quantity is not as straightforward as in the case for low molar mass molecules. Normally the molar masses are simply expressed as an average value obtained from a specific technique.

The simplest expression for polymer molar masses is an arithmetic mean, usually described as the *number average* molar mass, M_n, as defined by equation 1.

$$(\mathbf{1})\ M_n = \frac{\sum N_i M_i}{\sum N_i}$$

Here M_i represents the molar mass of the molecular species i and N_i is the number of molecules of i in the sample. An alternative expression for molar mass is the *weight average* molar mass, M_w, where we take terms in Mi^2 as shown below in equation 2.

$$(\mathbf{2})\ M_w = \frac{\sum N_i M_i^2}{\sum N_i M_i}$$

For a polymer where all the molecules have the same molar mass, M_n=M_w; in all other cases M_w is greater than M_n because most polymers are composed of varying chain lengths. M_n is calculated using the mole fraction distribution of a number of different sized molecules in a sample. Whereas M_w is calculated considering the weight fraction distribution of different sized polymer chains. A larger molecule will weigh more than a smaller molecule therefore the weight average (M_w) is always greater than the number average (M_n). We can therefore use the ratio of M_w to M_n as an indication of the spread of molar masses within the polymer sample. This ratio is called the *polydispersity* of the polymer and is numerically defined as the polydispersity index (PDI) where PDI=M_w/M_n, and if this value is 1, the polymer is said

to be monodisperse. There are numerous methods, both physical and chemical, to determine the molecular masses of polymers. These include the measurement of colligative properties (lowering of vapour pressure, elevation of boiling point, depression of freezing point and osmotic pressure), end group analysis, light scattering, ultra-centrifugation, viscometry and gel permeation chromatography (GPC) to name but a few.

1.5. Physical properties of branched and linear polymers

The two main characteristics that distinguish branched polymers from their linear analogues are the presence of multiple branching points and the high number of chain ends per molecule. Branched molecules therefore display attractive characteristics such as high solubility, low viscosity and unique thermal properties.

1.5.1. Solubilities of branched and linear polymers

Branched polymers show high solubility in a variety of solvent-media when compared to their linear counterparts. The solubility of homologous linear and highly branched polymers consisting of the same phosphorous-containing repeat unit was investigated by Merino (2001)[11], where highly branched materials were distinguished from their corresponding linear polymers by their solution behaviour. Polymers of branched architectures were found

to be readily soluble in organic solvents, such as tetrahydrofuran, acetone and dichloromethane, whereas homogeneous solutions were difficult to obtain using corresponding linear polymers under similar conditions (temperature and concentration). This difference in solubility behaviour is due to the topography of branched architecture, where multiple branching points create space constraints within the structure resulting in a network of pockets or gaps.[12] These allow a branched structure to become fully solvated for full interaction with the solvent, which is not the case for linear chains.

1.5.2. Viscosities of branched and linear polymers

For a polymer solution, intrinsic viscosity [η] is a measure of the ability of the solute, or polymer molecule, to contribute to the viscosity of a solution. The intrinsic viscosity of a solution is defined in equation 3, where η_o is the viscosity without solvent, and c is the volume fraction of the solute in the solution.

$$(\mathbf{3})\ [\eta] = \lim_{c \to 0} \frac{\eta - \eta_0}{\eta_0 c}$$

Intrinsic viscosity is dependent on the size and shape of the polymer molecule and as such increases with molecular weight (M), as expressed by the Mark-Houwink-Sakurada equation, as shown below in equation 4, where K and α are reaction specific parameter constants.

$$(\mathbf{4})\ [\eta] = KM\alpha$$

When analysing a polymer by size exclusion chromatography, namely gel permeation chromatography (GPC) where polymers are fractionated according to their hydrodynamic volume, the intrinsic viscosity of a polymer is directly related to the elution volume of the polymer. A branched polymer is likely to have a lower solution viscosity than its linear analogue due to the higher degree of branching and a more compact structure as a consequence of its architecture. Additionally, linear polymers are more likely to form chain entanglements than their highly branched polymer counterparts, resulting in higher viscosities.[13] Typically a linear polymer in a good solvent would show a Mark-Houwink value of ~0.7 with a branched material showing a lower value depending on the degree of branching in the structure.[2b]

Nunez, Chiou, Andrady, and Khan (2000)[14], reported a rheological study of highly branched polyester blends with linear poly(2-hydroxyethyl methacrylate) (PHEMA). Using rheological measurements of the polymers, they found the viscosity values obtained for highly branched polymers were independent of the applied shear. This showed almost Newtonian fluid-type behaviour indicating a lack of physical entanglements;[14-15] a Newtonian fluid being a substance where viscosity does not change with changes in the applied shear. The opposite was observed for blends with a high proportion of linear polymer.

The intrinsic viscosities of highly branched poly(methyl methacrylate)s, (PMMAs), were studied by Simon, Muller and Pakula (2001).[16] The viscosity properties were found to be much lower than those of linear PMMA. The intrinsic viscosity of the branched polymer in

solution balances with molecular weight, with a Mark-Houwink exponent of $\alpha = 0.40$ (linear PMMA, $\alpha = 0.688$). This was echoed in a study of polymer topology by Guan (2002),[17] at the same molecular weight, the intrinsic viscosity of highly branched poly(ethylene glycol dimethacrylate)s, (PEGDMA)s, was found to be much lower in comparison with PMMA linear polymers. The intrinsic viscosity of a highly branched PEGDMA, with a M_n of 25.0 k/Da was reported as 0.036 dL/g, whereas for the linear PMMA, with the same M_n, the intrinsic viscosity was 0.11 dL/g.

Typically, the synthesis of branched polymers results in broad molecular weight distributions with high weight-average molecular weights (M_w), which makes it difficult to obtain reliable data.[14, 18] Consequently studies on these systems are relatively rare; however, they are starting to receive more attention. Performing such analytical measurements on polymers with these high levels of architectural and compositional complexity remains challenging.

1.5.3. Thermal properties of branched and linear polymers

The morphology of branched polymers, the physical structure and arrangement in relation to their chemical structure, can be described in 3 different ways. There are either amorphous or crystalline, i.e. lacking molecular order or structurally aligned respectively, or as somewhere in-between the two, known as semicrystalline. Due to the globular shape and architecture of branched polymers they are likely to be amorphous.

Glass transition, T_g, and melting temperatures, T_m, of polymer structures depend on their morphologies, degree of branching, and structural factors such as backbone flexibility and end group interactions. Jayakannan and Ramakrishnan reported (2000)[19] on the investigation of the effect of branching on the thermal properties of novel branched poly(4-ethyleneoxy benzoate), where it was shown that an increase in branching lowered the melting temperature (T_m) and also the enthalpy associated with the melting transition, suggesting a reduction of crystallinity.

1.6. Polymerisation processes

In 1929, Carothers[20] was the first to distinguish between polymers (or macromolecules) by the manner in which they were synthesised. He distinguished *addition* polymers from *condensation* polymers. It was suggested that addition polymers are produced from monomers without the elimination of small molecules during polymerisation, and therefore the monomeric unit within a polymer contains the same number of atoms as the native monomer structure. Condensation polymers contain fewer atoms because small molecules are eliminated during the polymerisation process. Addition and condensation polymers are more correctly referred to as chain-growth and step-growth polymers respectively, as these terms reflect a more accurate understanding of the polymerisation mechanism. Step-growth polymerisations, for example, do not always eliminate a small molecule and are not considered a "polycondensation" reaction such as *via* the ring-opening of a cyclic reactive species such as a lactone to form a polyester.

1.6.1. Step-growth polymerisation (polycondensation)

Step-growth polymerisation occurs when, for instance, two functional groups, A and B are mutually reactive and can form covalent bonds.[2b] A functional monomer can contain both A and B functional groups, for example the formation of polyester from an ω–hydroxycarboxylic acid (Figure 2Figure 1.a), and can also exist on two difunctional monomers, for example the production of polyurethane from diisocyanate and dialcohol (see Figure 2Figure 1.b).

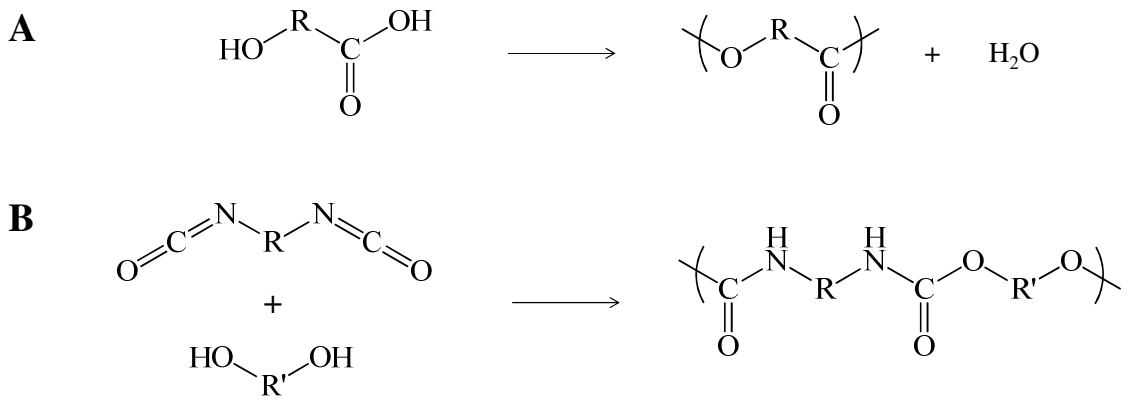

Figure 2. Step-growth polymerisation of (A) an ω-hydroxycarboxylic acid, with both A and B functionality on one monomer, and (B) polyurethane, where one monomer has difunctionality A, and the other, difunctionality B.

A functional monomer containing AB functional groups polymerise to give polymer chains with active sites A and B at either end respectively. However, when a monomer with AA, or

BB, polymerises either functional chain end may be A or B (Figure 3). The two active sites at either end of the growing polymer chain lend to the name of the mechanism, as only one monomer at a time can be added to each end in a stepwise manner. Growth occurs through direct reaction between the two different functionalities A and B, usually without the need for separate activation or deprotection steps.

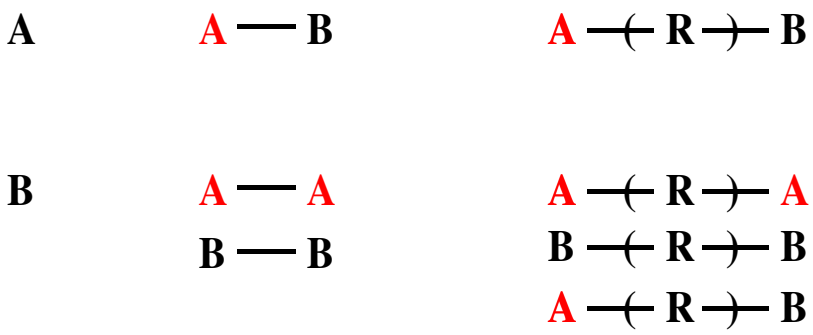

Figure 3. Chain end functionality in the step-growth polymerisation of (A) AB and (B) AA and BB monomers, where 'R' represents a polymer chain.

At the start of a step-growth polymerisation, molecular weight increases slowly because many short chain polymers, or oligomers, are initially formed where monomers are successively linked to reactive chain ends groups. Each small molecule has two active sites enabling further polymerisation between the other oligomers, or polymers. As presented in Figure 4,[21] the reaction rate will slow as the reaction progresses due to the reduction in the number of chain ends and consequently there is a sharp increase in molecular weight as the reaction reaches completion.

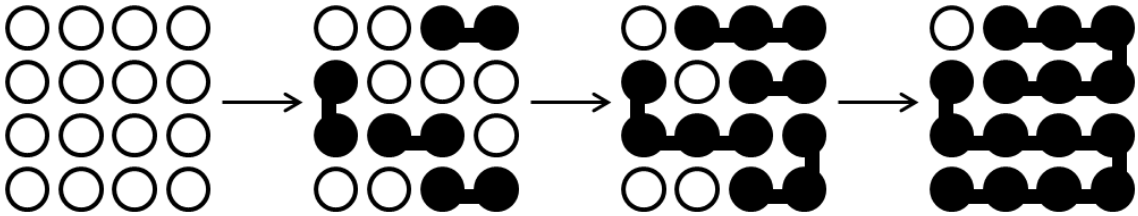

Figure 4. Schematic representation of step-growth polymerisation of an A-B monomer system. White dots represent monomer and black dots represent oligomer/polymer. Adapted from ref. 28.

Branched polymers can be produced *via* step-growth polymerisation from AB_x-type monomers, where there is a functional group A and *x* functional groups B ($x \geq 2$), and was first discussed by Flory in 1952.[22] In Figure 5, this concept is illustrated where x = 2. Disadvantages of this approach are that, as a precondition, the AB_x monomers are usually synthesised beforehand with the possibility of side reactions.

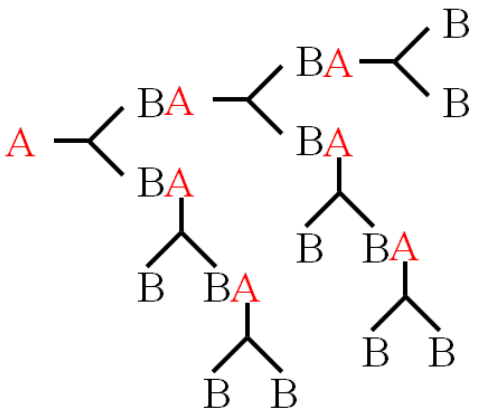

Figure 5. Schematic representation of step-growth polymerisation of a AB_2 monomer.

In 1990, Kim and Webster[23] first reported hyperbranched polymer produced by step-growth polymerisation of AB_2 monomers. Their research was further simplified, and a more generic approach was introduced by Fréchet.[12d, 24] This method uses an AB monomer, which provided a new branching point each time the monomer was linked to the growing polymer chain. Step-growth polymerisation has been used widely in the synthesis of a diverse range of branched systems as it is robust, many different functionalities can be tolerated. e.g. polyester amides,[25] polyimides,[26] polycaprolactones,[27] polyaryl esters,[28] and polyether sulfones[29] etc.

1.6.2. Chain-growth polymerisation (polyaddition)

During a chain-growth polymerisation monomers continually add to a polymer chain terminal reactive site, known as an active centre. The reaction can be divided into four distinct steps: initiation, propagation, chain transfer and termination (these processes are outlined in detail later in this chapter) which are all different reactions occurring at different rates. An example of the initiation and propagation of methacrylic acid is shown in Figure 6.

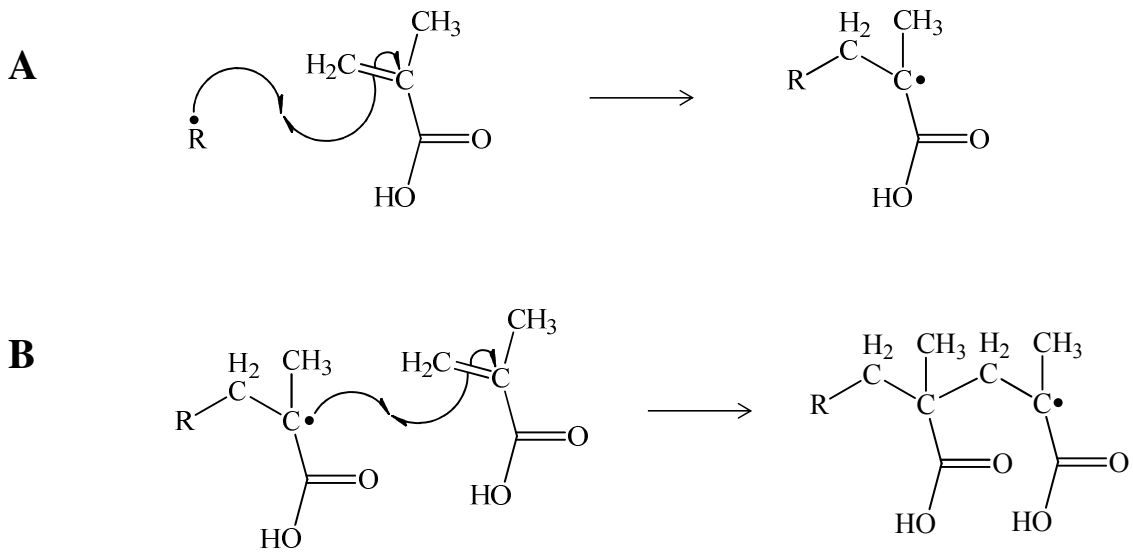

Figure 6. Schematic representation of (A) the initiation and (B) propagation processes of the chain-growth polymerisation of methacrylic acid. 'R' represents a free radical initiator.

Formed as an initiator decomposes, a resultant initiating species, for example a free radical or an anion, is required to start the reaction. However, the presence of an initiator is not always necessary for polymerisation.[2b] Propagation occurs at the active chain end centres successively adding monomer units, undergoing chain transfer reactions, until termination reactions render the chain inactive or all of the available monomer is used up. Chain transfer is the process by where the active centre on a growing polymer chain is transferred to another molecule. In contrast with step-growth polymerisation, where monomer is consumed quickly but molecular weight increases slowly, chain-growth polymerisation rapidly reaches high molecular weight. As chain-growth polymerisation occurs at the chain end, high chain lengths are reached quickly without using up all of the unreacted monomer (see Figure 7).

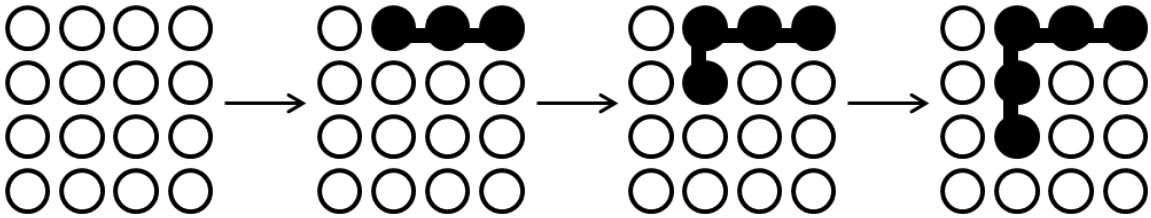

Figure 7. Schematic representation of chain-growth polymerisation. White dots represent monomer and black dots represent polymer. Adapted from ref. 28.

The most common chain-growth polymerisation process is the free radical polymerisation of vinyl monomers, for example ethylene, styrene, vinyl chloride, vinyl acetate, methyl methacrylate, and acrylonitrile to produce a variety of familiar industrial polymers (some of which are shown in Figure 8). Vinyl monomers are popular as they are typically tolerant of impurities, a range of solvents, and different monomer functionalities; they can also be polymerised in bulk, suspension or emulsion.

The work presented in this thesis utilises chain-growth polymerisation. Chain-growth allows for the design of the product, with the option to minimise termination reactions (see section 1.7; Free radical polymerisation).

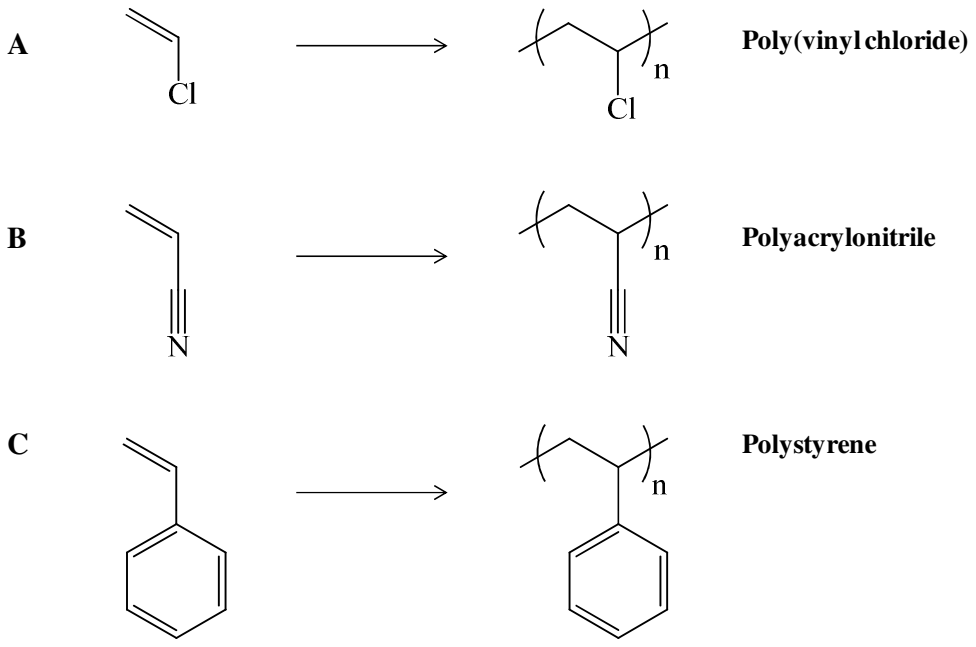

Figure 8. Chain-growth polymerisation of common vinyl monomers, (A) vinyl chloride (B) acrylonitrile and (C) styrene.

1.7. Free radical polymerisation

Free radical addition polymerisation is a chain-growth process, where the polymer is formed by successive addition of monomer units to a terminal free radical active centre on the polymer chain in an uncontrolled manner. As discussed in the previous section, vinyl polymers are the most commercially relevant polymers (see Figure 8), used across a wide range of applications from packaging, cosmetics, and clothing, to insulation, construction and biomaterials. As such, a versatile polymerisation method is required. Free radical polymerisation is one of the most important processes for the production of commodity polymers due to its flexibility, mild reaction conditions, robust tolerance to impurities and a

wide range of monomer functionality. This process is also inexpensive, making it a popular process for the production of vinyl polymers. Furthermore, this innovative technique allows for good architectural control and targeted structures with transfer reactions and chain growth termination, making free radical polymerisation arguably one of the most important relevant advances in polymer science. Free radical polymerisation can be divided into four distinct steps: initiation, propagation, chain transfer and termination.

1.7.1. Initiation

Free radical initiation involves the production of primary radicals by the decomposition of an initiator *via* thermal or photochemical cleavage, followed by addition to a vinyl monomer (scheme represented in Figure 9). Each free radical formed will then attack a monomer molecule to create an active centre, which will then propagate a polymer chain.

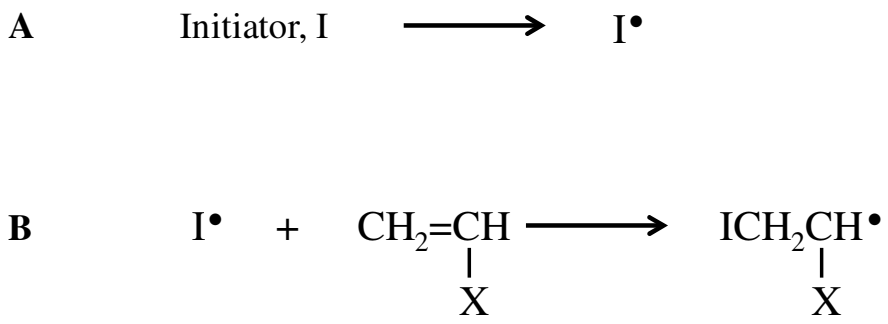

Figure 9. Scheme of the (A) decomposition and (B) initiation. I• is a radical capable of initiating polymerisation of monomer CH_2=CHX.

With the exception of some monomers, for example styrene[30] which can decompose with heat and propagate a reaction without the need for a free radical initiator, an initiator is required to create the radical sites. Common initiators are those which can break down, typically by homolytic fission, to form radical species through a weak bond. Common initiators are azo compounds,[31] peroxides and hydroperoxides,[32] and redox initiators. Initiation can be induced by thermal means or through ultra violet light; gamma radiation has also been known to be used in unusual cases.[33] Thermal decomposition is the most regular method of producing free radicals using peroxides, hydroperoxides and azo compounds.

Benzoyl peroxide is a commonly used initiator in industry; thermal decomposition generates primary benzoyloxyl radicals and secondary phenyl radicals as depicted in Figure 10. Peroxides are popular due to the range of decomposition temperatures afforded by the variety of structures.

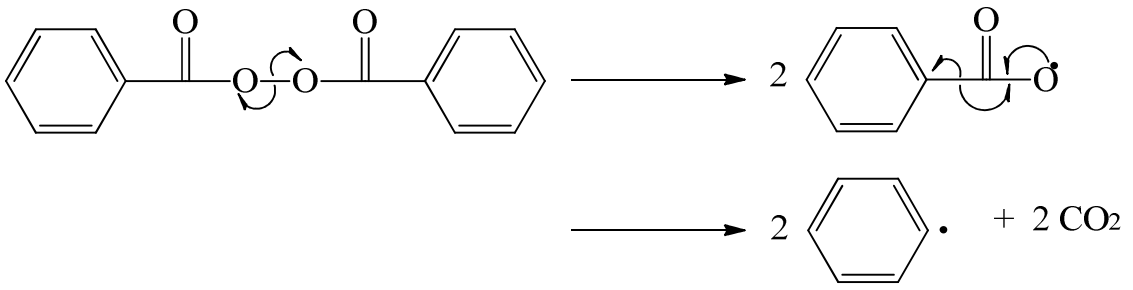

Figure 10. The thermal decomposition of benzoyl peroxide into primary benzoyloxyl radicals and secondary phenyl radicals.

An azo compound, azobisisobutyronitrile (AIBN) decomposes at high temperatures, eliminating a nitrogen molecule to give 2 cyanoprop-2-yl radicals, at all elevated temperatures (see Figure 11).[34] This popular initiator is used throughout this thesis.

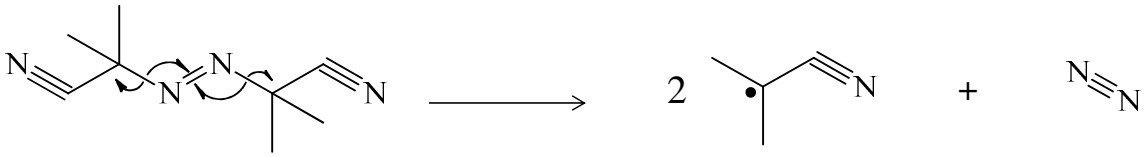

Figure 11. The thermal decomposition of azobisisobutyronitrile (AIBN).

1.7.2. Propagation

Propagation involves growth of the polymer chain by rapid addition of monomer to the radical centre. Monomer units continue to add to the active chain end until all of the monomer is consumed or termination occurs.

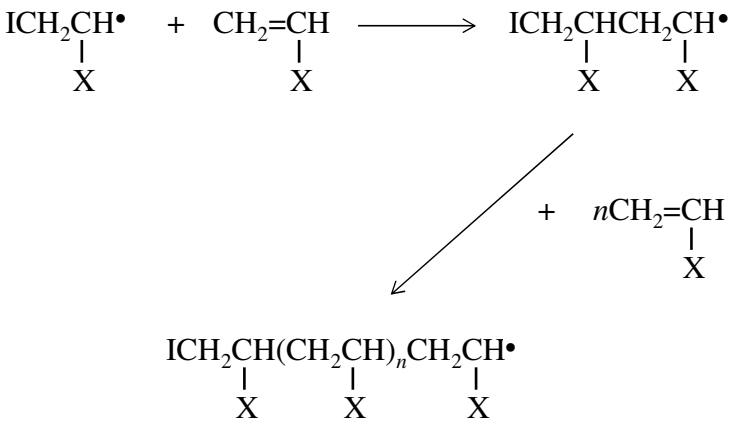

Figure 12. Schematic representation of propagation by head-to-tail addition.

Propagation is generally regiospecific, resulting in head-to-tail addition (see Figure 12) due to both steric and electronic effects, although rare reports indicate that head-to-head addition may occur to some extent.[35] Formation of the most stable radical is favoured, and steric hindrance will result in radical attack at the less hindered chain end. Monomer structure denotes the selectivity of the propagating radical towards the vinyl bond. This is crucial as the free radical end can abstract hydrogen from another or the same polymer chain rather than add to monomer; this would terminate the chain and start the growth of another at the point of hydrogen abstraction, this process is referred to as chain transfer. Chain transfer reactions (CTRs) are the transfer of the active radical from the end of a growing polymer chain to another species. CTRs are exploited during polymerisation methods, by the addition of chain transfer agents (CTAs), to regulate the mean chain length, consequently producing low molecular weight branched polymers with broader polydispersity. Different undesirable CTRs are shown in Figure 13, where the loss of an active radical to an initiator (Figure 13.a), and the abstraction of hydrogen from another polymer chain (Figure 13.b) causes premature termination of the growing polymer chain, furthermore chain "backbiting" where hydrogen is abstracted from the same chain as the active radical (Figure 13.c) creates an unwanted structure with, in this example, a pentyl side chain.

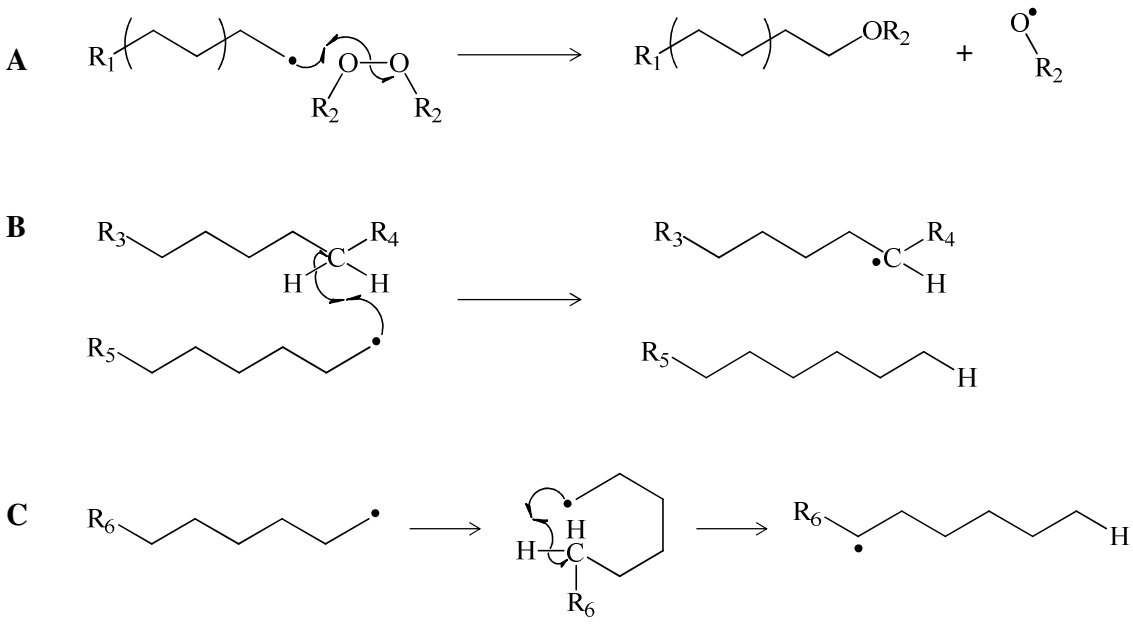

Figure 13. Schematic showing undesirable chain transfer reactions using polyethylene, such as (A) loss of the active radical to the initiator, (B) abstraction of a proton from another polymer chain, and (C) chain backbiting where proton abstraction occurs from the same propagating chain.

1.7.3. Termination

Termination is the discontinuation of polymer chain growth by the annihilation of the growing radical species and is intrinsic to all radical polymerisations. There are two types of termination, combination and disproportionation. It is assumed that both processes occur simultaneously.[2b] However, it has been suggested that the type of termination employed depends on the monomer and the reaction conditions.[36] Combination is the coupling of two chain end radicals forming a new covalent bond either between two polymer chains or between a polymer chain and an initiator fragment as depicted in Figure 14, where 'I' represents initiator.

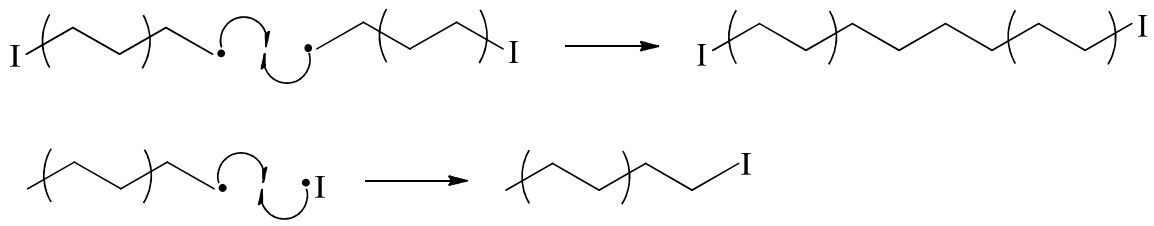

Figure 14. Mechanisms of possible combination reactions using polyethylene resulting in the termination of a propagating polymer chain, where 'I' represents initiator.

Disproportionation is generally the transfer of a radical species between two propagating radicals to form two non-radical moieties, typically an unsaturated group and a saturated group *via* the transfer of a proton. This is demonstrated in Figure 15. A vinyl bond is formed in this process, therefore one of the chains can polymerise further.

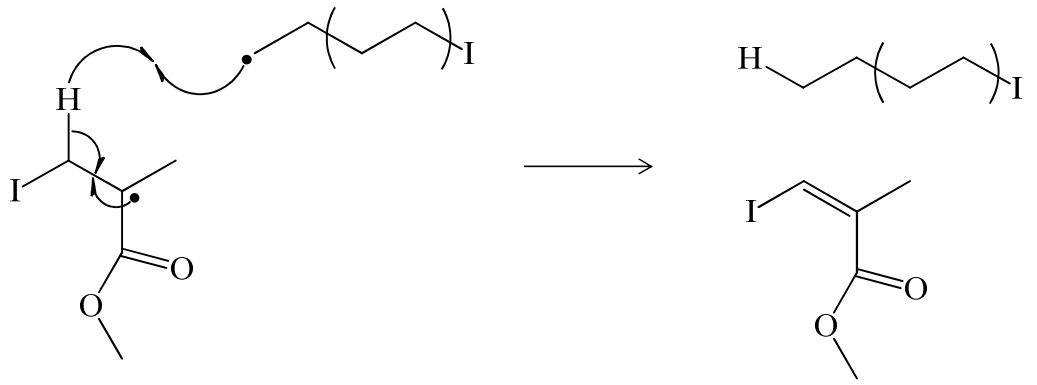

Figure 15. Mechanism of disproportionation reaction using polyethylene and methyl methacrylate resulting in the termination of a propagating polymer chain.

1.8. Kinetics of free radical polymerisation

Mathematical expressions can be derived to describe the kinetics of addition polymerisation since the reaction can be broken down into the well defined steps of initiation, propagation and termination.

1.8.1. Kinetics of initiation

Initiation is a two-stage reaction consisting of the decomposition of an initiator molecule into two free radicals followed by the reaction of these radicals with a monomer molecule are represented by equations 5 and 6, where *I* represents initiator and *M* represents monomer. The latter reaction, equation 6, is usually regarded as being identical to the propagation reaction as far as the reaction kinetics is concerned; k_p represents the rate of propagation.

$$(\mathbf{5}) \quad I \xrightarrow{k_d} 2\,R\cdot$$

$$(\mathbf{6}) \quad 2R\cdot + M \xrightarrow{k_p} 2\,RM\cdot$$

The initial rate of decomposition of the initiator, k_d, is slow compared to the rate of addition to monomer, k_a, and the rate of termination due to the reaction of two radicals. Therefore the

first decomposition step can be thought of as the rate determining step. The rate of initiation can therefore be expressed as equation 7, shown below.

$$(\mathbf{7}) \quad R_i = \frac{d[RM\cdot]}{dt} = 2fk_d[I]$$

The factor 2 is present in the equation due to the generation of two radicals in each decomposition step. The factor *f* is introduced into the equation to account for solvent cage recombination and represents the fraction of radicals, I, which escape from the solvent cage to be available to promote polymerisation. The fraction (1-*f*) of radicals recombine within the solvent cage.

1.8.2. Kinetics of propagation

The propagation step in the reaction is the addition of a monomer radical to another monomer molecule as shown below in equation 7.

$$(\mathbf{7}) \quad RM_n\cdot + M_1 \xrightarrow{k_p} RM_{n+1}\cdot$$

Since propagation is the stage that involves the major consumption of monomers, the rate of monomer loss can be expressed in terms of propagation only. The rate of bimolecular propagation is assumed to be the same for each step (*i.e.* all radicals are assumed to be equally reactive) and the rate of propagation is give by equation 8.

$$(\mathbf{8}) \quad R_p = \frac{-d[M]}{dt} = k_p[M][M\cdot]$$

1.8.3. Kinetics of termination

Termination is the result of reaction of two radicals. This can occur by two mechanisms namely combination and disproportionation as shown below in 9 and 10 respectively.

$$(\mathbf{9}) \quad M_n\cdot + M_m\cdot \xrightarrow{k_{tc}} M_{n+m}$$

$$(\mathbf{10}) \quad M_n\cdot + M_m\cdot \xrightarrow{k_{td}} M_n + M_m$$

However, it is rarely necessary to distinguish between these two mechanisms and so the rate constants are generally combined into a single rate constant: k_t. The rate of termination can therefore be expressed in equation 11, where *Rt* represents the rate of termination and *kt* = *ktc* + *ktd.*

$$(\mathbf{11}) \quad R_t = -\left(\frac{d[M\cdot]}{dt}\right) = 2k_t[M\cdot]^2$$

1.8.4. Steady state kinetics

Early in the polymerisation process the reaction reaches a steady-state concentration of radicals. Here the rate of radical production is equal to the rate of termination. Therefore the rates of initiation and termination are equal; these two equations can then be solved to give an expression for [$M\cdot$] in equation 12.

$$(\mathbf{12}) \quad [M\cdot] = \left(\frac{f k_d [I]}{kt}\right)^2$$

The previous expression can then be substituted into equation 12 to give equation 13.

$$(\mathbf{13}) \quad R_p = k_p \left(\frac{f k_d [I]}{k_t}\right)^{\frac{1}{2}} [M]$$

This mathematical treatment shows that in the early stages of polymerisation the reaction rate should be proportional to the square root of the initiator concentration, assuming f is independent of monomer concentration. This assumption is acceptable for high initiator efficiencies. However with lower efficiencies f may become proportional to [M] making the rate proportional to $[M]^{2/3}$.

1.9. Living polymerisation

Living polymerisation is defined as a chain-growth process without irreversible chain transfer and termination reactions. 'Living' systems were previously observed[37] but 'living' polymers were first defined as *living* by Szwarc in Nature (1956),[38] where after the polymer chains propagate until all the monomer is consumed, the polymer chain ends lie dormant instead of terminated. Szwarc likened this to biological systems where growth continues as food is supplied. In a 'living' polymerisation, the re-introduction of more monomer to the reaction would allow further propagation. A linear plot of molecular weight versus conversion typifies a 'living' polymerisation as the conversion of monomers to polymer, and consequently to molecular weight, is directly proportional. Also, the number of polymer chains remains constant during a 'living' polymerisation, and this together with no termination, produces polymer products with narrow molecular weight distributions.

'Living' polymerisation allows for precise control of polymer structures; a range of different architectures are possible, such as block co-polymers, and as mentioned previously in this chapter, branched architectures such as star, ladder and network polymers. In 1953, Flory[39] presented that since 'living' polymer chains grow at the same rate, the average molecular weight of the polymer product is related to the initial monomer/initiator molar ratio. This is referred to as the degree of polymerisation (DP_n). DP_n is defined in equation 14, assuming

100% monomer conversion, where $[M]_0$ and $[I]_0$ represent the initial concentration of monomer and initiator, respectively.

$$(\mathbf{14}) \quad DP_n = \frac{[M]_0}{[I]_0}$$

The molecular weight of a polymer product synthesised *via* 'living' polymerisation can be pre-determined by variation of the monomer/initiator stoichiometry.

1.10. Controlled/living radical polymerisation

Syntheses of 'true' living polymers, without any termination, are conditionally difficult. One way in which such difficulties were surmounted was to use a transition metal catalyst complex.[40] Transition metal catalysts maintain equilibrium between the active and dormant state of the polymer chain, as first reported by Kato (1995)[41] where an organometallic compound reversibly converted the carbon-chlorine terminal bond into a free radical species.

By establishing equilibrium between the active growing chains and dormancy, an overall reduction in the rate of polymerisation is created. Propagation lifetimes are therefore extended from milliseconds to hours[40] and also giving rise to additional synthetic procedures such as chain-end functionalisation or chain extension.[42] Recently, several controlled/living radical polymerisation processes have been developed, including atom transfer radical

polymerisation (ATRP), nitroxide mediated radical polymerisation (NMRP) and reversible addition-fragmentation transfer process (RAFT).

1.11. Atom transfer radical polymerisation (ATRP)

Atom Transfer Radical Polymerisation was first reported at the same time by the groups of Matyjaszewski[43] and Sawamoto[44] in 1995, and as such both are credited with the discovery. Both suggested using a transition metal/ligand catalyst; Matyjaszewski and co-workers polymerised styrene with a copper catalyst, whereas Sawamoto and co-workers reported the polymerisation of methyl methacrylate with a ruthenium(II) complex. For both reports, polymerisation proceeded with 'living' character; molecular weights of the polymers were found to increase linearly with conversion, giving polydispersity values of less than 1.2, allowing for specific control over composition and architecture. The route reported by Wang and Matyjaszewski is the most commonly used due to the inexpensive copper catalyst, their mechanism of ATRP is shown in Figure 16.

During initiation the alkyl-halogen is cleaved by the transition metal complex (MnY/L) to produce an alkyl radical (R•) which can propagate a polymer chain by addition to monomers units (M) at a constant rate of propagation (k_p). After initiation, control of the polymerisation is afforded by equilibrium between the actively growing polymer chain radicals and a dormant species therefore enabling controlled addition of monomer units that help to grow

polymer chains at the same rate. This equilibrium lies towards the dormant species, slowing propagation and minimising termination reactions giving controlled or living character to the ATRP process.

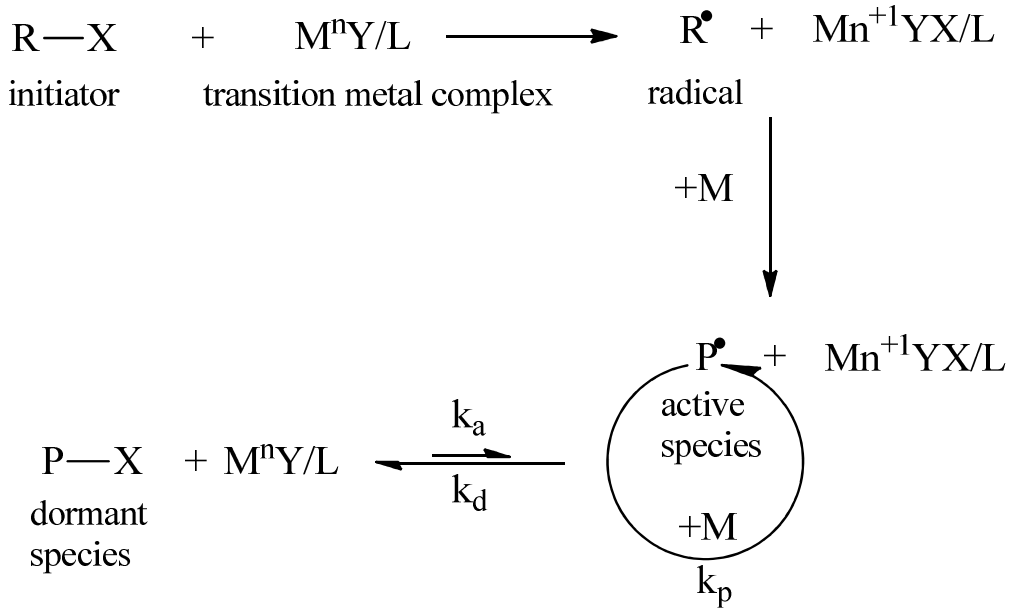

Figure 16. Proposed mechanism of Atom Transfer Radical Polymerisation (ATRP) where k_a, is the rate of activation, k_p is the rate of propagation and k_d is the rate of deactivation. Adapted from ref. 43.

This is an extremely useful technique in a polymer chemist's tool box as it allows for the preparation of extremely controlled structures with a large amount of functional group tolerance. This polymerisation process has been used to prepare monodisperse linear systems, block copolymers, branched and star-like structures to name but a few. The use of a transition metal catalyst, mostly copper, usually at high amounts limits this process industrially as this metal must preferentially be removed after the polymerisation, but

nonetheless it is a simple and convenient process to prepare controlled, highly functional polymers.

1.12. Nitroxide mediated radical polymerisation (NMRP)

Nitroxide mediated radical polymerisation (NMRP) allows for good control of structure, stereochemistry and PDI, and chain length.[45] This is achieved through the thermally stable nitroxide radicals, which behave as a 'trapping agent' in a similar manner to the end capping halogen described in ATRP, reversibly forming the radical and stable alkoxyamine products. The most common nitroxide radical is 2,2,6,6-tetramethyl-1-piperidinyloxy (TEMPO),[46] but others have been reported.

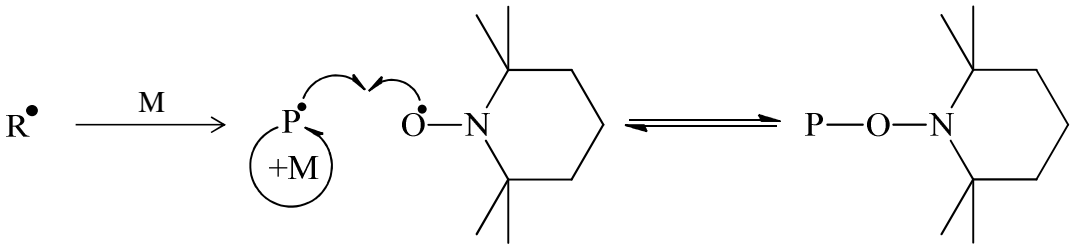

Figure 17. Proposed mechanism of nitroxide mediated radical polymerisation (NMRP) using a TEMPO radical.

1.13. Reversible addition-fragmentation chain transfer polymerisation (RAFT)

RAFT[47] is a radical polymerisation process which relies on the degenerative transfer of radical species to dithioesters compounds (Z-C(=S)-S-R) referred to as RAFT agents.[48] At initiation, a radical is generated by the decomposition of a radical initiator as it reacts with a monomer. The growing polymer chain adds to the C=S bond of the RAFT agent to form an intermediate radical, which then can reversibly fragment between a polymer radical and a temporarily dormant polymer chain, capped with the RAFT agent.[49] This equilibrium between activated and dormant polymer chains allows for uniform chain growth and limits termination reactions. Since the RAFT agent remains on the polymer chain-end, the dormant polymer chains can also act as a chain transfer agents (CTAs). The mechanism is represented in Figure 18. RAFT polymerisation relies on the nature of the Z and R groups. The Z group should activate the C=S bond towards radical addition, and the R group should act as a stable free radical leaving group and be capable of re-initiating the polymerisation. Like ATRP, RAFT produces polymers with predictable molecular weights, narrow molecular weight distributions and a range of architectures. The technique is tolerant of adverse conditions, monomer functionality and a variety of solvents.[49-50] However, the synthesis of co-polymers can be difficult without choice of the correct RAFT agent of monomer addition sequence.

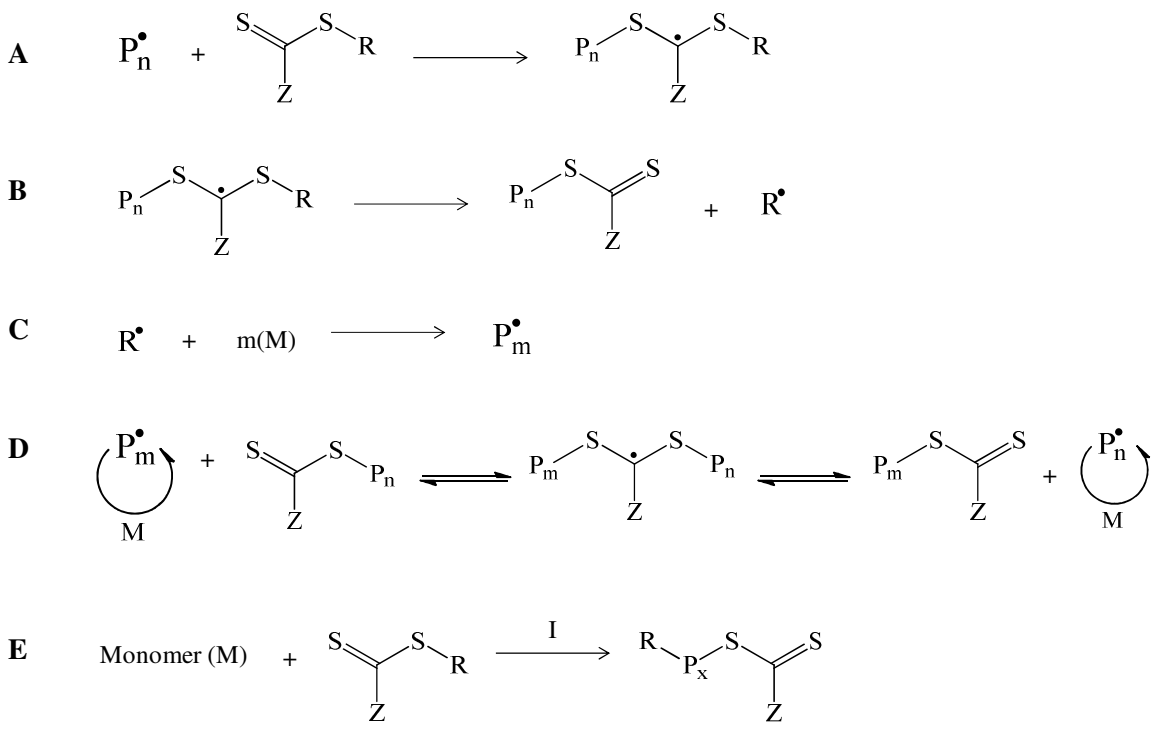

Figure 18. Proposed mechanism of RAFT, which can be divided into (A) addition, (B) fragmentation, (C) re-initiation and (D) equilibration steps. The overall mechanism is represented in (E). P_n, P_m and P_x are polymer chains, M represents monomer, I represents initiator and R is a radical capable of initiating polymerisation. Reproduced with permission from ref. 47.

1.14. Branched addition polymers

In 2000, Sherrington *et al.* [51] described the preparation of branched addition copolymers *via* conventional free radical polymerisation in conjunction with a di- or poly- functional monomer and a chain transfer agent. This empirical study showed that macrogelation can be avoided by using a chain transfer agent which moderates the polymerisation and avoids long

chain branching which would ultimately be the case for using a poly-functional monomer is a conventional polymerisation.

The process is outlined in Figure 19; in the case of the top reaction, polymerisation of a mono-functional monomer in the presence of an initiator yields a soluble, linear polymer. Incorporation of a di- or poly- vinyl monomer in the polymerisation (even at low levels) gives rise to an intractable cross-linked gel. Whilst the incorporation of an amount of chain transfer agent, typically a thiol, moderates the reaction resulting in a soluble branched material.

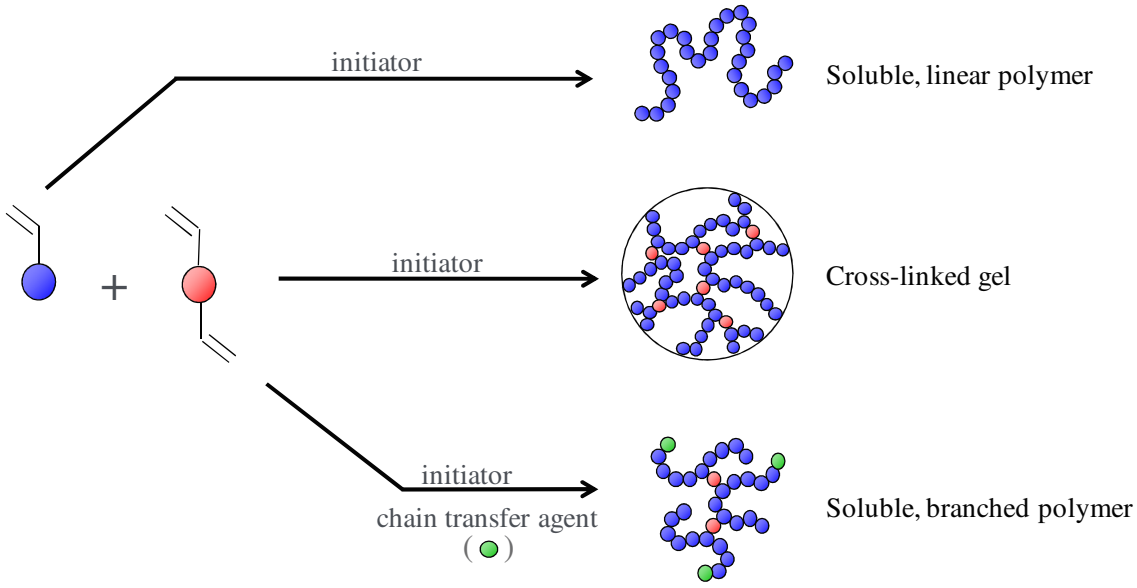

Figure 19. Schematic representation of free radical polymerisation to give a soluble, linear polymer, and the same system with a bifunctional monomer to give a cross-linked gel, and furthermore the inclusion of CTA into this monomer/bifunctional monomer system prevents gelation to produce soluble branched polymers. Adapted from ref. 51.

This so-called *Strathclyde Route* is extremely useful for the preparation of branched architectures in one-step negating the requirement to utilise specific monomers to prepare branched systems.[52] Additionally, since the process is an addition polymerisation there are a numerous number of monomers that can be used to form widely chemically functional branched polymers. This process is typically performed as a solution polymerisation utilising thiols as chain transfer agents, although it has been performed using anionic polymerisation,[53] ATRP,[54] and RAFT[55] processes. Extremely interesting branched architectures can be formed using this straightforward technique although due to the uncontrolled nature of the free-radical process the PDIs of the polymers formed can be considerably higher than those obtained for similar linear systems, this can be thought of as the uncontrolled linking together of propagating linear radicals through the poly-functional monomer which forms the branching node in the system. Through choice of monomers and poly-functional monomers, typically a divinyl species (so-called brancher) and chain transfer agent, it is straightforward to incorporate different functionalities within the polymer structure. For example by choosing a long-chain brancher, such as poly(ethylene glycol) (PEG) dimethacrylate "block" structures can be prepared where the long chain PEG unit can be thought of as linking two primary chains.[56] Because of the functional group tolerance of conventional free radical polymerisation a wide variety of functional groups can also be introduced in one step allowing complex structures to be prepared. Since the chain transfer agent is present at relatively high levels, typically equimolar to the branching agent, and is present in the final polymer, its presence and location at the chain termini can be beneficial.

1.15. Emulsions

Emulsions were defined as metastable colloids in 1999 by Bibette, Calderon and Poulin,[57] which consist of two immiscible fluids, one being dispersed throughout the other. As such, heterogeneous emulsion systems are used extensively in a number of widespread application areas such as food technologies, pharmaceutics, cosmetics, enhanced crude oil recovery, and as templates for the preparation of advanced materials.[58]

Emulsions usually form in spherical droplets. Droplet diameters can range from less than 1 μm[59] (mini- or nano-emulsions) to greater than 100 μm[60] (particulate-stabilised emulsions). Generally, emulsions have a water phase and are described as either oil-in-water or water-in-oil, which denotes the dispersed phase and the continuous phase respectively. Emulsion droplets are stabilised by interfacial surface tension at the liquid-liquid interface. Interfacial tension occurs because the environments of the molecules at the interface and the molecules in the bulk liquid phase are different. At the emulsion droplet interface, interfacial molecules interact less with their surround than the molecules in the bulk phase causing an imbalance of forces between the two liquid surfaces known as interfacial tension. Furthermore, interfacial molecules have a lower binding energy to molecules in the bulk phase. This concept is not to be confused with surface tension (see Figure 20), which occurs at the interface of a gas and a liquid.

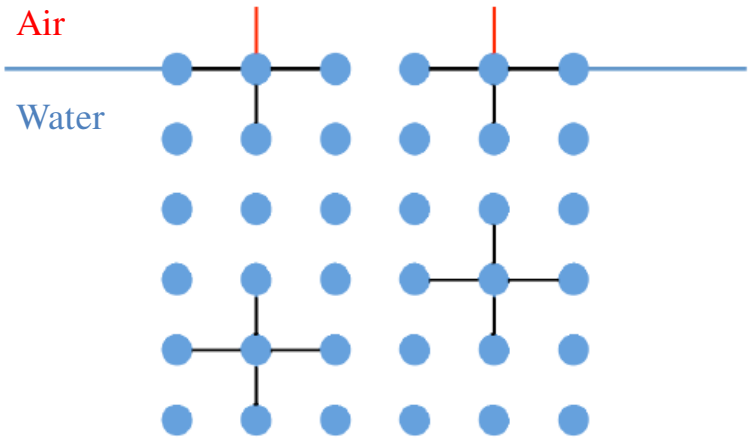

Figure 20. Schematic of the formation of surface tension. Bulk phase molecules have four binding interactions, whereas surface molecules have three. The imbalance at the air/water interface is represented by the red lines.

Emulsions destabilise over time; where two immiscible liquids are in contact, they will act to lower the amount of interfacial energy required in maintaining a high surface area, and high interfacial tension, because they are thermodynamically unstable.[36, 61] Coalescence is the combination of two or more dispersed droplets to form larger droplets. Coalescence of the emulsion droplets increases entropy with the system. Therefore with time, coalescence of the emulsion droplets is favoured over the emulsion droplets remaining dispersed. Entropy increases as the ordering of the water phase molecules, where they act to minimise interactions with hydrophobic molecules (i.e. water-in-oil or oil-in-water), is decreased on coalescence. There are four main mechanisms of emulsion instability, which may transpire simultaneously,[36] sedimentation or creaming (Figure 21.a), coalescence (Figure 21.b), flocculation (Figure 21.c), and Ostwald ripening (Figure 21.d). Sedimentation or creaming is the migration of the dispersed phase of an emulsion; the emulsion droplets separate according to different phase densities. Flocculation is the clustering of dispersed emulsion droplets

without losing their structural integrity; however this is a precursor to coalescence as defined previously. Ostwald ripening is the migration of the dispersed phase from one droplet to a larger droplet, where the dispersed phase is soluble enough to move through the continuous phase.

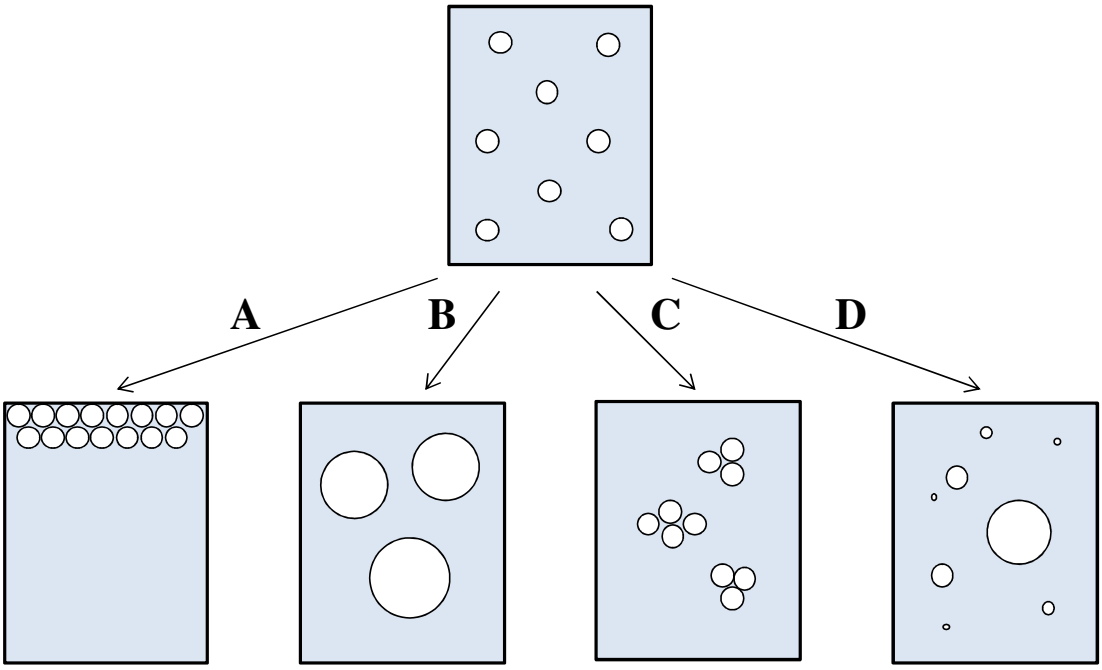

Figure 21. Emulsion instability mechanisms: (A) sedimentation or creaming, (B) coalescence, (C) flocculation, and (D) Ostwald ripening.

If a surface-active agent, or surfactant, is added, its molecules will orientate at the liquid-liquid interface reducing interfacial tension. There is a wide range of capable surface-active agents, or surfactants, such as small molecule surfactants (Figure 22.a),[62] particulate surfactants (Figure 22.b),[63] and polymeric surfactants (Figure 22.c).[64]

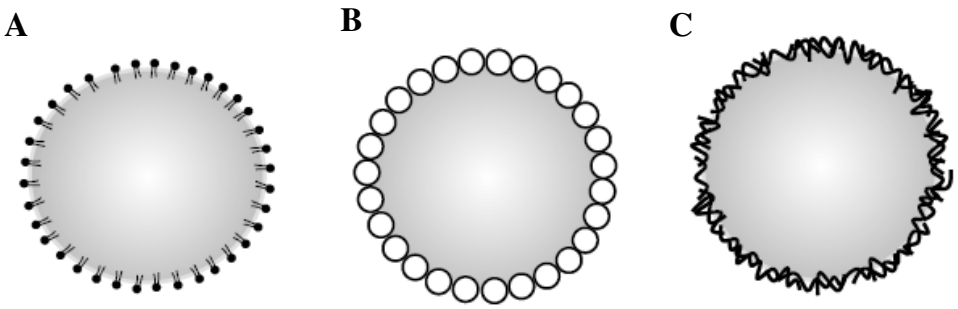

Figure 22. Schematic representation of a water-in-oil emulsion droplet stabilised by a (A) small molecule surfactant, (B) particulate surfactant, and (C) polymeric surfactant.

1.15.1. Small molecule surfactants

Small molecule surfactants, usually amphiphilic organic molecules, consist of a hydrophilic 'head' and a hydrophobic 'tail'. When stabilising an emulsion interface, the hydrophilic part will reside in the water phase and the hydrophobic part in the oil phase, allowing an immiscible liquid to remain dispersed within another. However, the adsorption of small molecule surfactants onto an emulsion droplet surface is reversible, and therefore instability is more common as interfacial tension cannot be lowered to near-zero. Small molecule surfactants are categorised as either ionic (i.e. anionic, cationic, and amphoteric) or non-ionic. Ionic surfactants have a charged group within the composition of the hydrophilic 'head'. A widely used anionic surfactant is sodium dodecyl sulfate (SDS), which is used extensively in the detergent market.[47b] SDS consists of an anionic hydrophilic 'head' and a hydrophobic hydrocarbon 'tail' (see Figure 23.a). Anionic surfactants have no such charged groups, and are commonly alcohols, esters and polyethers. An example of an industrially important non-ionic surfactant is sorbitan oleate (or Span 80) (see Figure 23.b).

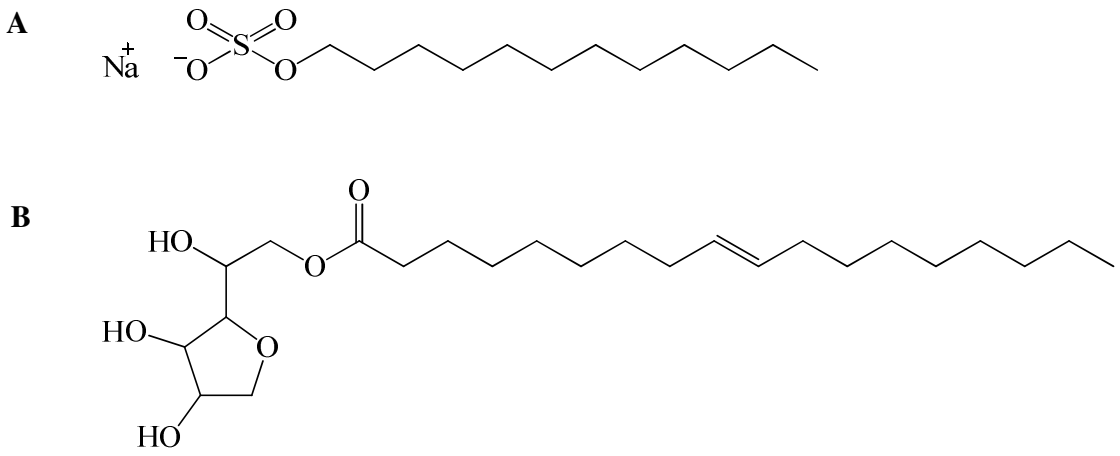

Figure 23. Structure of (A) anionic surfactant, sodium dodecyl sulfate, and (B) non-ionic surfactant, sorbitan oleate (Span 80).

1.15.2. Particulate surfactants

In comparison to small molecule surfactants, particulate surfactants have high interfacial energies and can adsorb strongly onto droplet surfaces to produce stable and reproducible emulsions.[52, 63b] First observed by Ramsden (1903),[55] Pickering (1907)[63a] was the first to describe the stabilisation of emulsion droplets using solid particles and as such they are often referred to as Pickering emulsions (see Figure 22.b). A Pickering emulsion is formed by a reduction in interfacial tension, which drives strong adsorption at the liquid-liquid interface. The large amount of energy required to desorb particulates results in highly stable emulsions. The strength of the adsorption is determined by the contact angle, θ. The stabilising particles are said to be hydrophilic if θ is less than 90° and hydrophobic if θ is greater than 90°, stabilising an oil-in-water and a water-in-oil emulsion respectively.[53] Therefore, the type of emulsion produced (oil-in-water or water-in-oil) can be controlled by changing the ratio of hydrophilicity to hydrophobicity of the particulate surfactant.[53] Particulates can impart

functionality to the emulsion droplet surfaces and as such Pickering emulsions are often used to prepare colloidosomes.[58c]

1.15.3. Polymeric surfactants

Polymeric surfactants offer greater opportunity in terms of flexibility, diversity, and imparting functionality to the resulting polymer-stabilised emulsion. Polymerisation techniques can accommodate for a wide range of functionalities, impurities and reaction conditions (as discussed earlier in this introduction). Due to the amiphilic nature of a polymer, they can be surface-active like small molecule surfactants and are used in coatings, food, and personal care products. Amphiphilic co-polymers containing alternating hydrophilic and hydrophobic segments reside in the water and oil phases respectively stabilising an emulsion droplet interface.[65] A-B and A-B-A block copolymers typically based on ethylene oxide and propylene oxide diblock and triblock systems[65], provide hydrophilic and hydrophobic blocks, which can stabilise an emulsion as represented in Figure 24.

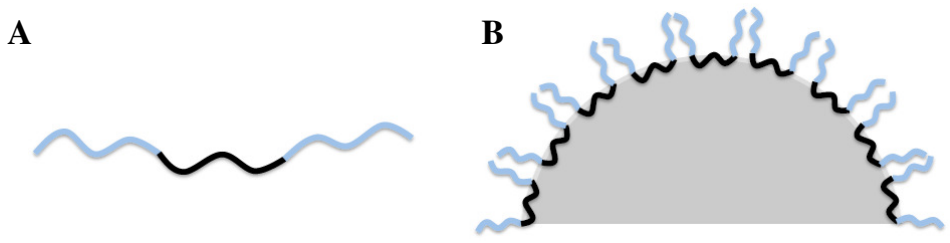

Figure 24. Schematic of how (A) a triblock hydrophilic/hydrophobic/hydrophilic co-polymer stabilises (B) an oil-in-water emulsion droplet interface.

1.15.4. Emulsions as templates

Emulsions, i.e. droplets of oil dispersed through water (or vice versa), have been used as convenient soft templates from which encapsulated materials and hollow capsules can be readily fabricated. Key advantages of these templates include their rapid and simple in-situ formation avoiding the requirement to pre-synthesise the template; the ability to load (*i.e.*, dissolve or disperse) actives within the internal droplet phase which negates the need to post-load the capsules in addition to the simple removal of the liquid phase to produce capsules which avoids core-decomposition steps.

1.16. Capsules

Strategies to encapsulate hydrophobic actives and to fabricate hollow capsules have received significant persistent attention over the last decade.[66] Polymeric capsules have a multitude of proposed applications such as confined reaction vessels, drug carriers, protective shells for cells and enzymes, as a system for heterogeneous catalysis, dye dispersants, or as materials for use in the coatings and fragrance industries, oil field recovery and the removal of contaminated waste.[66-67] Encapsulation is important both academically and commercially since it provides a direct mechanism to site-isolate, or to protect, a material in the presence of

other potentially incompatible substances or environments until they are required. Similarly, pre-formed hollow capsules are highly desirable since they provide a repository, or empty space, into which materials may be sequestered and protected. As such, strategies to prepare these important materials challenges are inherently linked and often exploit either self-assembly of amphiphilic molecules,[68] templated interfacial adsorption,[58c, 69] or direct synthesis.[70] The formation of robust capsules typically requires additional covalent[71] or physical[58c, 69a, 72] stabilisation and the use of cross-linking agents.

1.16.1. Block co-polymer assembly

Appropriate encapsulation strategies should ideally provide control over the size, functionality and membrane properties of the encapsulated material or hollow capsule while also maximising loading efficiency. In addition to the material property requirements, the syntheses should be reproducible, cost-effective and scalable. The most common approaches to produce encapsulated material or hollow capsules have typically involved either template or self-assembly strategies. Amphiphilic block co-polymer self-assembly is a highly elegant process whereby control of polymer-block ratios and molecular weight drives the morphology of the assembled phase-separated structures.[73] Within specific regions of their phase-diagrams amphiphilic block co-polymers can self-assemble into hollow vesicular structures, analogous to liposomes as illustrated by Discher and Eisenberg in 2002.[68b, 73b] They describe prepared block co-polymers of poly(acrylic acid)-*block*-polystyrene (PAA_{52}-*b*-PS_{310}), polystyrene-*block*-poly(isocyano-L-alanine) (PS_{40}-*b*-PIA_{10}), and polyethyleneoxide-

block-polybutadiene ($PEO_{46...250}$-*b*-$PBD_{26...150}$) *via* sequential living anionic polymerisation with an alkyllithium initiator. In aqueous solution or under acidic conditions, these various co-polymers form vesicles as illustrated in Figure 25.i-iii. This one-pot synthetic route is a two-step method, since purification of the alkyllithium initiator is required as it tends to strongly associate with the growing polymer forming ion pairs that can terminate chain propagation, and because of this additional purification step this route is less industrially desirable.

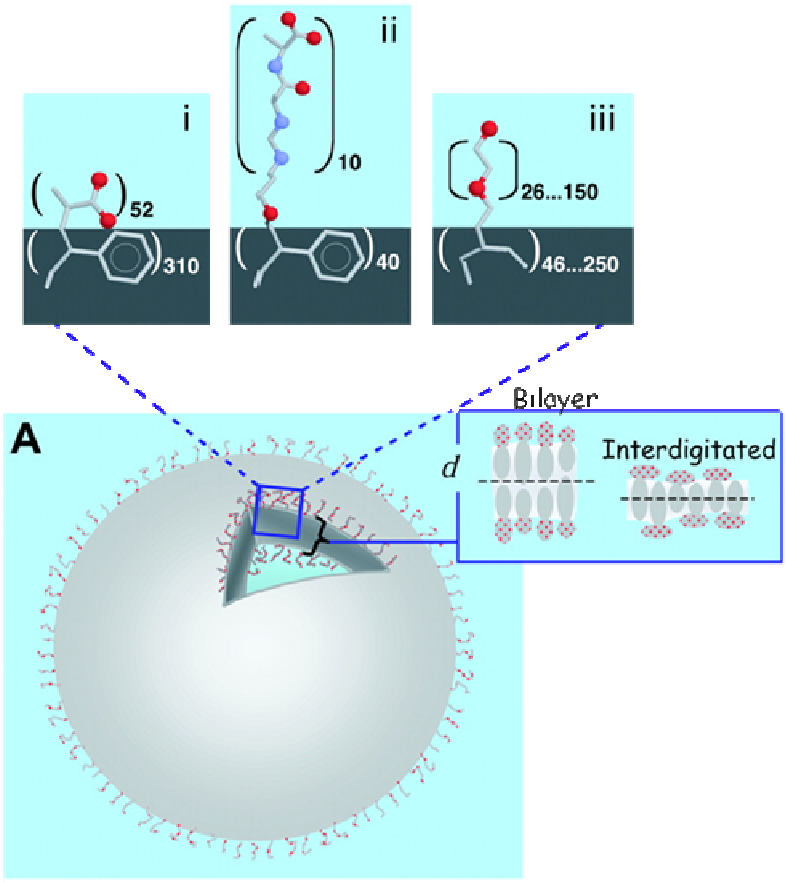

Figure 25. Schematic of vesicle-forming block co-polymers. (A) Vesicle with a section removed to reveal the membrane thickness d, schematically represented by the dark grey regions for (i) PAA_{52}-PS_{310}, (ii) PS_{40}-PIA_{10}, and (iii) $PEO_{46...250}$-$PBD_{26...150}$. Reproduced with permission from ref. 68b.

1.16.2. Templated structures

Complex co-polymer syntheses and purification, sequential assembly steps and loading efficiency concerns render these technologies unsuitable for non-specialised applications.[74] In contrast, templating strategies, as represented in Figure 26 by Réthoré and Pandit in 2010[66c] are comparatively cost effective, generic and can produce highly monodisperse capsules with controlled shell thickness and function.[66b, 69d, 75] However, adsorption of the shell-forming material onto the colloid surface requires a driving force; the process is multi-step and multi-component unless the template is the desired encapsulant. Due to the completely sacrificial nature of the core material, as it must be removed, these approaches are relatively inefficient.

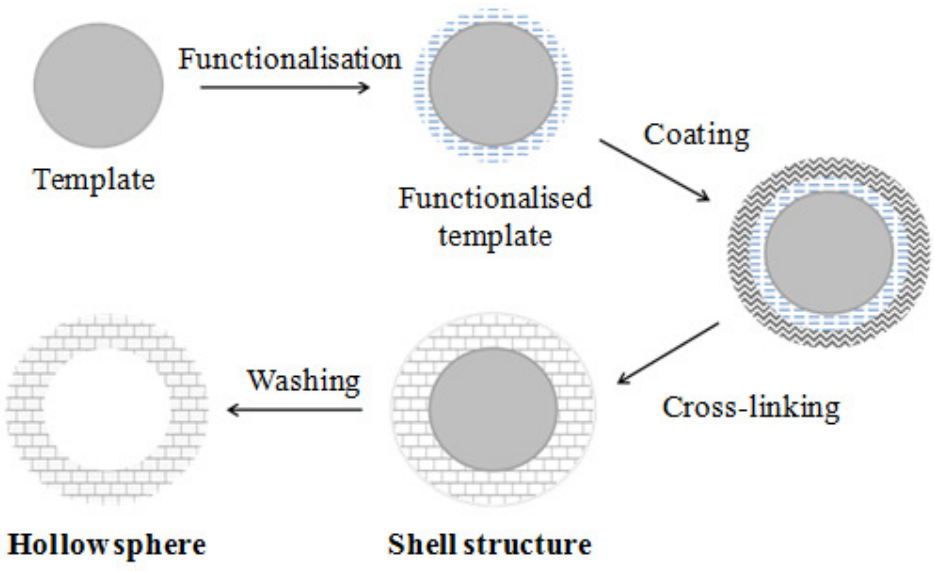

Figure 26. Schematic image of the sacrificial templating process. Adapted from ref. 66c.

Encapsulation and hollow capsule design often requires additional covalent cross-linking steps in order to provide sufficient mechanical integrity to the shell layer.[76] It may be desirable for capsules to retain their integrity during processes required for their formulation and, in terms of biological applications, the higher pressures observed following living cell entrapment, for example the encapsulation of islet cells for sustained hormone delivery in the treatment of diabetes, may induce premature capsule rupturing. [77] Physical or chemical cross-linking provides a convenient route to increased membrane strength. An early example of physically cross-linked SCL micelles was reported by Wooley in 1996, where the pendent styrenyl groups of an amiphilic diblock co-polymer, composed of polystyrene-*block*-poly(4-vinyl pyridine), (PS-*b*-PVP))and formed *via* anionic polymerisation, gave micellar aggregates. Cross-linking through the styrenyl side chains (PS) of the poly(4-vinyl pyridine) (PVP) located in the aqueous peripheral layer produced a shell (see Figure 27).[78] The PVP section of the co-polymer is quarternised to give the hydrophilic block and the cross-linkable group. This change in hydrophilicity allows the co-polymer to organise into micelles in THF with the addition of increasing amounts of MeOH. Cross-linking is initiated between the pendent chains of the peripheral hydrophilic PVP-block, leaving a soft hydrophobic PS core. However, these physical cross-linking methods, while less toxic, require additional components and steps and can be intolerant of ionic environments.[72, 79]

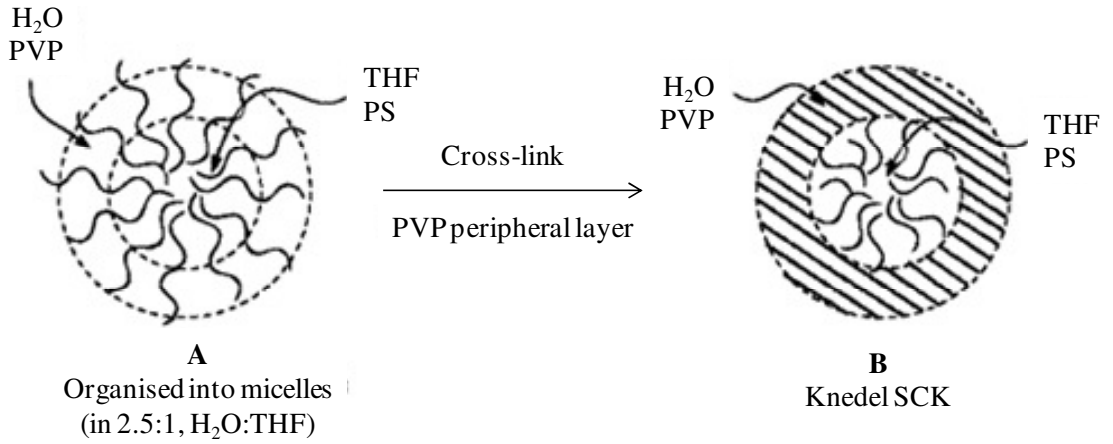

Figure 27. Schematic representation of the basic approach for the formation of shell cross-linked knedel particles (SCKs). Micellisation of amphiphilic block co-polymer in (A) is followed by cross-linking through the styrenyl side chains (PS) of the poly(4-vinyl pyridine) (PVP) located in the aqueous peripheral layer to yield (B). Reproduced with permission from ref. 78.

Typical types of chemical cross-linking strategies, such as the first use of bifunctional small molecules by Armes in 1998 to give diblock co-polymer based shell cross-linked (SCL) micelles, are highly toxic and must be performed at high dilution leading to limited scalability and industrial utility, see Figure 28.[80] Cross-linking the shell of a micellar solution of poly[(2-(dimethylamino)ethyl methacrylate-*block*-2-(*N*-morpholino)ethyl methacrylate] (DMA-*b*-MEMA), synthesised *via* a living polymerisation route, with the bifunctional cross-linker, 1,2-bis(2-iodoethoxy)-ethane (BIEE) must be carried out at low solid content (<0.50% w / v) to avoid inter-micellar cross-linking.

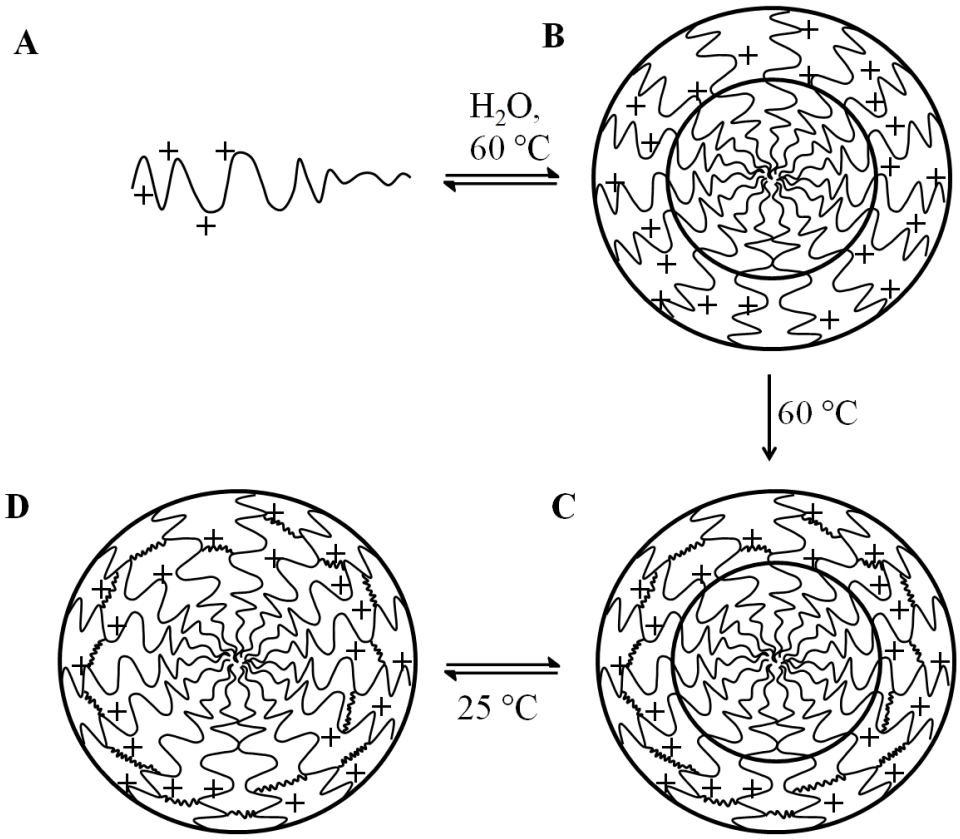

Figure 28. Reaction scheme for the synthesis of shell cross-linked knedel (SCK) micelles using (A) a partially quarternised DMAEMA–MEMA block co-polymer which undergoes (B) reversible micellisation and then (C) shell cross-linking to form a hydrophobic core using $ICH_2CH_2OCH_2CH_2OCH_2CH_2I$ which becomes (D) hydrophilic upon cooling. Adapted with permission from ref. 79.

However in 2002, Armes reported a more efficient synthesis of SCL micelles using triblock co-polymers synthesised *via* ATRP, together with the same bifunctional cross-linker BIEE, which could be carried out at high solid content (>10% w / v) (see Figure 29).[81]

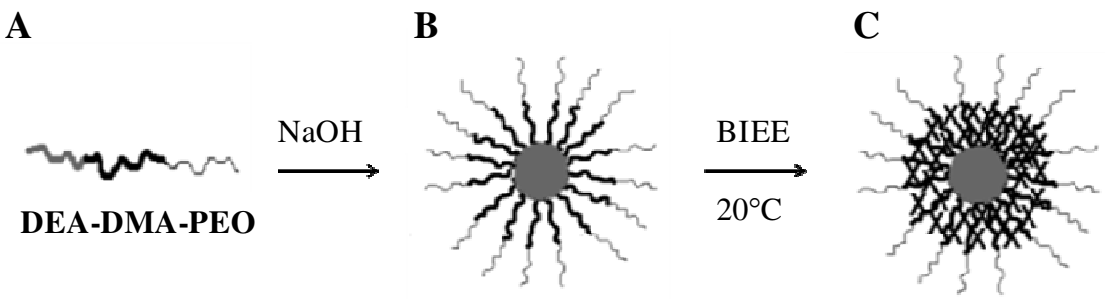

Figure 29. Schematic illustration of the formation of three-layer "onion" micelles and shell cross-linked micelles from PEO-DMA-DEA tri-block co-polymers using 1,2-bis(2-iodoethoxy)ethane as a bifunctional cross-linker. (A) represents the triblock co-polymer at pH 2, (B) depicts a three-layer "onion-like" micelles above pH 7.3, and (C) shows SCL micelles comprising DEA cores, cross-linked DMA inner shells, and PEO coronas. Reproduced and adapted with permission from ref. 81.

Silane chemistry represents an alternative covalent cross-linking approach. This commonly involves the addition of a small alkoxysilane molecule which preferentially adsorbs at the template surface and undergoes hydrolysis and self-condensation to form an inorganic network or sheath.[82] Previous attempts to develop single-component encapsulation strategies have exploited alkoxysilane-containing block co-polymers as amphiphilic materials that will undergo spontaneous self-assembly into vesicular structures after which they are able to self-crosslink.[76b, 83] Armes and Du explored this concept in 2005 (Figure 30), producing an elegant one-pot, single component process.[83] Polymeric vesicles were prepared from the self-assembly of a pH-responsive block co-polymer, poly(ethylene oxide)-*block*-poly[2-(diethylamino)ethyl methacrylate-*stat*-3-(trimethoxysilyl)propyl methacrylate], [PEO-*b*-P(DEA-*stat*-TMSPMA)], prepared *via* ATRP, in an aqueous solution *via* self-catalysis over time. The basic, pH-responsive DEA residues in the co-polymer catalysed the hydrolysis and condensation of TMSPMA groups to form cross-links over time. The paper also shows how this self-condensation was also induced immediately by the addition of a catalyst, TEA.

However, this process requires accurate block co-polymer syntheses and precise self-assembly conditions and as such may limit broader exploitation.

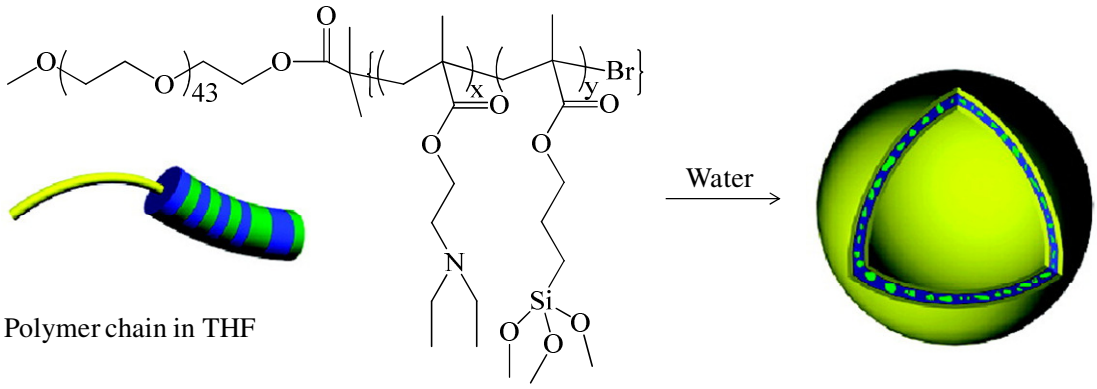

Figure 30. Formation of pH-responsive block co-polymer vesicles using a PEO-*block*-poly(DEA-*stat*-TMSPMA) co-polymer. In yellow, hydrophilic PEO; green, pH-responsive DEA residues; blue, self-cross-linkable TMSPMA residues. Reproduced with permission from ref. 83.

1.17. Present study

In the present work, the versatile role of a branched co-polymer surfactant was demonstrated. Chapter 3 presents a strategy for the formation of organic-inorganic hollow cross-linked capsules. This process was approached *via* an emulsion templating approach using a single component, a multi-functional branched co-polymer. The emulsion droplet stabilisation efficiency of both branched and linear co-polymer analogues was compared. Additionally, the encapsulation of actives within the capsules was demonstrated. Chapter 4 investigates the role of co-polymer composition to impart responsive functionality to the capsule surface. The ability of both branched and linear co-polymer analogues to stabilise an emulsion was

compared. Capsule surface responsiveness was investigated and then utilised to create capsule structures. The responsive and porous nature of the capsule structures was explored. The ability to encapsulate actives was investigated both within the capsules and structures. Chapter 5 describes the judicious design of a branched terpolymer-based membrane which exhibits responsive selectivity. The application of this to protocell constructs was investigated. The uptake and release of small molecules was demonstrated.

1.18. References

[1] H. Staudinger, *Ber. dtsch. Chem. Ges. A/B* **1920**, *53*, 1073–1085.

[2] aR. Mülhaupt, *Angew. Chem. Int. Ed.* **2004**, *43*, 1054-1063; bM. P. Stevens, *Polymer Chemistry: An Introduction*, 3rd ed., Oxford University Press, New York, **1999**.

[3] A. L. Andrady, M. A. Neal, *Philosophical Transactions of the Royal Society B: Biological Sciences* **2009**, *364*, 1977-1984.

[4] P. J. M. Stals, Y. C. Li, J. Burdynska, R. Nicolay, A. Nese, A. R. A. Palmans, E. W. Meijer, K. Matyjaszewski, S. S. Sheiko, *J. Am. Chem. Soc.* **2013**, *135*, 11421-11424.

[5] aF. Isaure, P. A. G. Cormack, D. C. Sherrington, *J. Mater. Chem.* **2003**, *13*, 2701-2710; bI. Bannister, N. C. Billingham, S. P. Armes, S. P. Rannard, P. Findlay, *Macromolecules* **2006**, *39*, 7483-7492.

[6] N. Hadjichristidis, M. Pitsikalis, S. Pispas, H. Iatrou, *Chem. Rev.* **2001**, *101*, 3747-3792.

[7] O. Ikkala, G. ten Brinke, *Science* **2002**, *295*, 2407-2409.

[8] aY. H. Kim, *J. Polym. Sci. Pol. Chem.* **1998**, *36*, 1685-1698; bC. Gao, D. Yan, *Prog. Polym. Sci.* **2004**, *29*, 183-275; cA. W. Bosman, H. M. Janssen, E. W. Meijer, *Chem. Rev.* **1999**, *99*, 1665-1688.

[9] S. M. Grayson, J. M. J. Frechet, *Chem. Rev.* **2001**, *101*, 3819-3867.

[10] K. Aoi, A. Motoda, M. Okada, T. Imae, *Macromol. Rapid Commun.***1997**, *18*, 945-952.

[11] S. Merino, L. Brauge, A. M. Caminade, J. P. Majoral, D. Taton, Y. Gnanou, *Chem.-Eur. J.* **2001**, *7*, 3095-3105.

[12] aC. J. Hawker, J. M. J. Frechet, *J. Am. Chem. Soc.* **1990**, *112*, 7638-7647; bJ. M. J. Frechet, *Science* **1994**, *263*, 1710-1715; cC. J. Hawker, in *Macromolecular Architectures, Vol. 147* (Ed.: J. G. Hilborn), Springer-Verlag Berlin, Berlin, **1999**, pp. 113-160; dC. J. Hawker, J. M. J. Frechet, R. B. Grubbs, J. Dao, *J. Am. Chem. Soc.* **1995**, *117*, 10763-10764.

[13] I. Sendijarevic, M. W. Liberatore, A. J. McHugh, L. J. Markoski, J. S. Moore, *J. Rheol.* **2001**, *45*, 1245-1258.

[14] C. M. Nunez, B. S. Chiou, A. L. Andrady, S. A. Khan, *Macromolecules* **2000**, *33*, 1720-1726.

[15] J. Aerts, *Comput. Theor. Polym. Sci.* **1998**, *8*, 49-54.

[16] P. F. W. Simon, A. H. E. Muller, T. Pakula, *Macromolecules* **2001**, *34*, 1677-1684.

[17] Z. Guan, *J. Am. Chem. Soc.* **2002**, *124*, 5616-5617.

[18] J. V. M. Weaver, D. J. Adams, *Soft Matter* **2010**, *6*, 2575-2582.

[19] M. Jayakannan, S. Ramakrishnan, *J. Polym. Sci. Pol. Chem.* **2000**, *38*, 261-268.

[20] W. H. Carothers, *J. Am. Chem. Soc.* **1929**, *51*, 2548-2559.

[21] V. A. J. M. G. Cowie, *Polymer: Chemistry and Physics of Modern Materials*, 3rd ed., CRC Press, **2007**.

[22] P. J. Flory, *J. Am. Chem. Soc.* **1952**, *74*, 2718-2723.

[23] Y. H. Kim, O. W. Webster, *J. Am. Chem. Soc.* **1990**, *112*, 4592-4593.

[24] J. M. J. Frechet, M. Henmi, I. Gitsov, S. Aoshima, M. R. Leduc, R. B. Grubbs, *Science* **1995**, *269*, 1080-1083.

[25] aE. T. F. Gelade, B. Goderis, C. G. de Koster, N. Meijerink, R. van Benthem, R. Fokkens, N. M. M. Nibbering, K. Mortenssen, *Macromolecules* **2001**, *34*, 3552; bX. R. Li, J. Zhan, Y. S. Li, *Macromolecules* **2004**, *37*, 7584.

[26] J. J. Hao, M. Jikei, M. A. Kakimoto, *Macromolecules* **2003**, *36*, 3519.

[27] J. Choi, S. Y. Kwak, *Macromolecules* **2003**, *36*, 8630.

[28] Q. Lin, T. E. Long, *Macromolecules* **2003**, *36*, 9809.

[29] H. R. Kricheldorf, D. Fritsch, L. Vakhtangishvili, G. Schwarz, *Macromolecules* **2003**, *36*, 4337.

[30] P. J. Flory, *J. Am. Chem. Soc.* **1937**, *59*, 241.

[31] P. S. Engel, *Chem. Rev.* **1980**, *80*, 99.

[32] F. R. Mayo, R. A. Gregg, M. S. Matheson, *J. Am. Chem. Soc.* **1951**, *73*, 1691.

[33] H. Li, D. Y. Gao, *Pigm. Resin. Technol.* **2011**, *40*, 24.

[34] G. Odian, *Principles of Polymerization*, John Wiley & Sons, **2004**.

[35] aB. Liu, W. L. Yu, Y. H. Lai, W. Huang, *Macromolecules* **2000**, *33*, 8945-8952; bK. Van Cauter, V. Van Speybroeck, M. Waroquier, *Chemphyschem* **2007**, *8*, 541-552; cT. Y. Xie, A. E. Hamielec, P. E. Wood, D. R. Woods, *Polymer* **1991**, *32*, 537-557.

[36] M. Buback, F. Gunzler, G. T. Russell, P. Vana, *Macromolecules* **2009**, *42*, 652-662.

[37] K. Ziegler, *Angewandte Chemie* **1936**, *49*, 499-502.

[38] M. Szwarc, *Nature* **1956**, *178*, 1169-1169.

[39] P. J. Flory, *Principles of Polymer Chemistry*, Cornell University Press, Ithaca, NY, **1953**.

[40] W. A. Braunecker, K. Matyjaszewski, *Prog. Polym. Sci.* **2007**, *32*, 93-146.

[41] M. Kato, M. Kamigaito, M. Sawamoto, T. Higashimura, *Macromolecules* **1995**, *28*, 1721-1723.

[42] K. Matyjaszewski, *Macromolecules* **1999**, *32*, 9051-9053.

[43] aJ. S. Wang, K. Matyjaszewski, *J. Am. Chem. Soc.* **1995**, *117*, 5614-5615; bJ. S. Wang, K. Matyjaszewski, *Macromolecules* **1995**, *28*, 7901-7910.

[44] M. Kato, M. Kamigaito, M. Sawamoto, T. Higashimura, *Macromolecules* **1995**, *28*, 1721-1723.

[45] J. Nicolas, Y. Guillaneuf, C. Lefay, D. Bertin, D. Gigmes, B. Charleux, *Prog. Polym. Sci.* **2013**, *38*, 63-235.

[46] M. K. Georges, R. P. N. Veregin, P. M. Kazmaier, G. K. Hamer, *Macromolecules* **1993**, *26*, 2987-2988.

[47] aJ. Chiefari, Y. K. Chong, F. Ercole, J. Krstina, J. Jeffery, T. P. T. Le, R. T. A. Mayadunne, G. F. Meijs, C. L. Moad, G. Moad, E. Rizzardo, S. H. Thang, *Macromolecules* **1998**, *31*, 5559-5562; bG. Moad, E. Rizzardo, S. H. Thang, *Polymer* **2008**, *49*, 1079-1131.

[48] P. Delduc, C. Tailhan, S. Z. Zard, *Journal of the Chemical Society-Chemical Communications* **1988**, 308-310.

[49] R. T. A. Mayadunne, J. Jeffery, G. Moad, E. Rizzardo, *Macromolecules* **2003**, *36*, 1505-1513.

[50] A. B. Lowe, C. L. McCormick, *Prog. Polym. Sci.* **2007**, *32*, 283-351.

[51] N. O'Brien, A. McKee, D. C. Sherrington, A. T. Slark, A. Titterton, *Polymer* **2000**, *41*, 6027-6031.

[52] P. A. Costello, I. K. Martin, A. T. Slark, D. C. Sherrington, A. Titterton, *Polymer* **2002**, *43*, 245-254.

[53] Y. T. Li, S. P. Armes, *Macromolecules* **2005**, *38*, 5002-5009.

[54] F. Isaure, P. A. G. Cormack, S. Graham, D. C. Sherrington, S. P. Armes, V. Butun, *Chem. Commun.* **2004**, 1138-1139.

[55] B. L. Liu, A. Kazlauciunas, J. T. Guthrie, S. Perrier, *Macromolecules* **2005**, *38*, 2131-2136.

[56] A. R. Wang, S. Zhu, *Polym. Eng. Sci.* **2005**, *45*, 720-727.

[57] J. Bibette, F. L. Calderon, P. Poulin, *Rep. Prog. Phys.* **1999**, *62*, 969-1033.

[58] aH. F. Zhang, A. I. Cooper, *Soft Matter* **2005**, *1*, 107-113; bV. N. Manoharan, M. T. Elsesser, D. J. Pine, *Science* **2003**, *301*, 483-487; cA. D. Dinsmore, M. F. Hsu, M. G.

Nikolaides, M. Marquez, A. R. Bausch, D. A. Weitz, *Science* **2002**, *298*, 1006-1009; dB. P. Binks, R. Murakami, *Nat. Mater.* **2006**, *5*, 865-869.

[59] T. Tadros, R. Izquierdo, J. Esquena, C. Solans, *Adv. Colloid Interface Sci.* **2004**, *108*, 303-318.

[60] B. P. Binks, S. O. Lumsdon, *Langmuir* **2001**, *17*, 4540-4547.

[61] T. Tadros, *Emulsion formation and stability*, Wiley VCH, **2013**.

[62] aD. Cochin, A. Laschewsky, F. Nallet, *Macromolecules* **1997**, *30*, 2278-2287; bR. Pichot, F. Spyropoulos, I. T. Norton, *J. Colloid Interface Sci.* ***2010****, 352, 128-135.*

[63] aS. U. Pickering, *J. Chem. Soc., Trans.***1907**, *91*, 2001-2021; bB. P. Binks, *Curr. Opin. Colloid Interface Sci.* **2002**, *7*, 21-41.

[64] aS. Y. Liu, S. P. Armes, *Curr. Opin. Colloid Interface Sci.* **2001**, *6*, 249-256; bS. Y. Liu, S. P. Armes, *Angew. Chem.-Int. Edit.* **2002**, *41*, 1413-1416.

[65] A. M. Mathur, B. Drescher, A. B. Scranton, J. Klier, *Nature* **1998**, *392*, 367-370.

[66] aW. Meier, *Chem. Soc. Rev.* **2000**, *29*, 295-303; bX. W. Lou, L. A. Archer, Z. C. Yang, *Adv. Mater.* **2008**, *20*, 3987-4019; cG. Rethore, A. Pandit, *Small* **2010**, *6*, 488-498.

[67] J. F. Chen, H. M. Ding, J. X. Wang, L. Shao, *Biomaterials* **2004**, *25*, 723-727.

[68] aF. S. Bates, *Science* **1991**, *251*, 898-905; bD. E. Discher, A. Eisenberg, *Science* **2002**, *297*, 967-973; cI. W. Hamley, *Soft Matter* **2005**, *1*, 36-43.

[69] aF. Caruso, R. A. Caruso, H. Mohwald, *Science* **1998**, *282*, 1111-1114; bN. C. Mougin, P. van Rijn, H. Park, A. H. E. Muller, A. Boker, *Adv. Funct. Mater.* **2011**, *21*, 2470-2476; cM. Fujiwara, K. Shiokawa, Y. Tanaka, Y. Nakahara, *Chem. Mater.* **2004**, *16*, 5420-5426; dY. X. Li, Z. Q. Wang, Z. Huang, Y. F. Pan, G. Xue, *J. Mater. Chem.* **2010**, *20*, 5516-5520.

[70] aC. J. McDonald, M. J. Devon, *Adv. Colloid Interface Sci.* **2002**, *99*, 181-213; bG. Delaittre, C. Dire, J. Rieger, J. L. Putaux, B. Charleux, *Chem. Commun.* **2009**, 2887-2889.

[71] aJ. Z. Du, Y. M. Chen, Y. H. Zhang, C. C. Han, K. Fischer, M. Schmidt, *J. Am. Chem. Soc.* **2003**, *125*, 14710-14711; bK. L. Thompson, S. P. Armes, *Chem. Commun.* **2010**, *46*, 5274-5276.

[72] J. V. M. Weaver, Y. Q. Tang, S. Y. Liu, P. D. Iddon, R. Grigg, N. C. Billingham, S. P. Armes, R. Hunter, S. P. Rannard, *Angew. Chem.-Int. Edit.* **2004**, *43*, 1389-1392.

[73] aF. S. Bates, G. H. Fredrickson, *Physics Today* **1999**, *52*, 32-38; bB. M. Discher, Y. Y. Won, D. S. Ege, J. C. M. Lee, F. S. Bates, D. E. Discher, D. A. Hammer, *Science* **1999**, *284*, 1143-1146.

[74] D. J. Adams, S. Adams, D. Atkins, M. F. Butler, S. Furzeland, *J. Controlled Release* **2008**, *128*, 165-170.

[75] aM. Fujiwara, K. Shiokawa, I. Sakakura, Y. Nakahara, *Nano Lett.* **2006**, *6*, 2925-2928; bA. M. Yashchenok, D. N. Bratashov, D. A. Gorin, M. V. Lomova, A. M. Pavlov, A. V. Sapelkin, B. S. Shim, G. B. Khomutov, N. A. Kotov, G. B. Sukhorukov, H. Mohwald, A. G. Skirtach, *Adv. Funct. Mater.* **2010**, *20*, 3136-3142;

cJ. W. Cui, Y. J. Wang, A. Postma, J. C. Hao, L. Hosta-Rigau, F. Caruso, *Adv. Funct. Mater.* **2010**, *20*, 1625-1631.

[76] aA. I. Romoscanu, R. Mezzenga, *Langmuir* **2006**, *22*, 7812-7818; bJ. Z. Du, Y. M. Chen, *Angew. Chem.-Int. Edit.* **2004**, *43*, 5084-5087.

[77] aP. A. L. Fernandes, M. Delcea, A. G. Skirtach, H. Mohwald, A. Fery, *Soft Matter* **2010**, *6*, 1879-1883; bC. Tomaro-Duchesneau, S. Saha, M. Malhotra, I. Kahouli, S. Prakash, *Int. J. Pharm.* **2013**, *2013*, 19.

[78] K. B. Thurmond, T. Kowalewski, K. L. Wooley, *J. Am. Chem. Soc.* **1996**, *118*, 7239-7240.

[79] S. T. Dubas, J. B. Schlenoff, *Macromolecules* **2001**, *34*, 3736-3740.

[80] V. Butun, N. C. Billingham, S. P. Armes, *J. Am. Chem. Soc.* **1998**, *120*, 12135-12136.

[81] S. Y. Liu, J. V. M. Weaver, Y. Q. Tang, N. C. Billingham, S. P. Armes, K. Tribe, *Macromolecules* **2002**, *35*, 6121-6131.

[82] aC. I. Zoldesi, A. Imhof, *Adv. Mater.* **2005**, *17*, 924-+; bH. G. Wang, P. Chen, X. M. Zheng, *J. Mater. Chem.* **2004**, *14*, 1648-1651; cA. Guerrero-Martinez, J. Perez-Juste, L. M. Liz-Marzan, *Adv. Mater.* **2010**, *22*, 1182-1195; dJ. J. Yuan, O. O. Mykhaylyk, A. J. Ryan, S. P. Armes, *J. Am. Chem. Soc.* **2007**, *129*, 1717-1723.

[83] J. Z. Du, S. P. Armes, *J. Am. Chem. Soc.* **2005**, *127*, 12800-12801.

CHAPTER 2

Analytical techniques

2.1 Polymer characterisation techniques

2.1.1. Nuclear magnetic resonance (NMR)

All ^{1}H NMR spectra were recorded using a Bruker DPX-400 spectrometer operating at 400 MHz. ^{1}H NMR was used to determine the chemical composition of the final copolymers.

2.2.1. Size exclusion chromatography (SEC)

SEC measurements were used to determine the molar mass, molar mass distribution, absolute molecular weight and Mark-Houwink values of branched copolymers. A triple-detection Viscotek TDA-302 gel permeation chromatography system (TD-GPC) with refractive index, viscometry and dual-angle light scattering detectors was used. Two Viscotek GMPWXL columns and an additional guard column were used with an oven temperature of 35 °C. The eluent was THF with a flow rate of 1 mL min^{-1}. All samples were prepared at 5 mg/mL.

2.3.1. Dynamic light scattering and zeta potential measurements

Hydrodynamic copolymer size distributions and zeta potential measurements of the responsive branched copolymer were measured by dynamic light scattering (DLS) in a Malvern Zetasizer Nano-ZS ZEN3600 equipped with a 633 nm laser. The scattering angle used was 175°, and all samples were measured in a disposable polystyrene folded capillary cell cuvette. In general, 1 mL of the dilute copolymer solution was added to the dispersion unit at pH values of 10, 9, 7,

5, 4, and 2. The volume-average diameters and zeta potential values were obtained from at least 3 repeated runs.

2.4.1. pKa determination

The pKa of the copolymer was determined by monitoring the rate of change in pH of a copolymer solution initially at pH 10 after addition of 0.025 mL increments of 0.1 M hydrochloric acid to a final pH value of 2. The pKa was determined from an average of 3 repeat runs.

2.2 Emulsion, capsule, and capsule structure characterisation techniques

2.1.2. Measuring capsule formation using light scattering

The formation of cross-linked emulsion droplets was determined and characterised using laser diffraction. All emulsion size distributions were assessed using laser diffraction with a Malvern Mastersizer 2000 equipped with a Hydro 2000 SM dispersion unit. For all emulsion droplet measurements, 100 μL of emulsion was added to the dispersion unit containing 80 mL water (for all MAA-based polymer stabilised emulsions, the pH was adjusted to pH 10 using 1 M NaOH) with a stirring rate of 1,250 rpm. The volume-average droplet diameters were obtained from at least 3 repeat runs. The span is a measure of the width of the droplet size distribution and is expressed mathematically as $(D(0.9) - D(0.1))/D(0.5)$, where $D(0.9)$ is the diameter

under which 90 % of the particles fall, D(0.5) is the diameter under which 50 % of the particles fall and D(0.1) is the diameter under which 10 % of the particles fall.

All emulsions were prepared identically as defined in the chapter descriptions. An uncross-linked emulsion was added to the dispersion unit and monitored for 1 hour. Where MAA-based polymer-stabilised emulsions were analysed the pH of the dispersant was adjusted to pH 10 by the addition of NaOH (1 M) prior to measurement. After monitoring the uncross-linked emulsion, 1 mL of TEA was added to the dispersion unit to induce cross-linking. The solution was monitored for a further hour. Uncross-linked and cross-linked emulsion droplet stability was observed where the change in volume-average droplet diameter was measured as a function of time. This process was repeated to obtain several runs for comparison.

2.2.2. Measuring emulsion droplet aggregation using light scattering

Aggregation and redispersion of dilute dispersions of the emulsions on the addition of acid/base were measured as a function of time using laser diffraction. All emulsions were prepared identically as defined in the chapter descriptions. All measurements were performed under similar conditions, however these runs were monitored for 5 hours where the pH was switched hourly from pH 10 (1M, NaOH) to pH 2 (1M, HCl) repeatedly, and consecutively over this time. The change in volume-average droplet diameter was measured as a function of time. This process was repeated twice.

2.3.2. Optical microscopy

Optical or light microscopy images of emulsion droplets and engineered emulsions were obtained via light microscopy. Two light microscopes were used. Namely a calibrated Meiji Techno MX9300 Series microscope equipped with a Luminera Infinity-1 digital camera, and a calibrated Leica DMIL LED fitted with a Leica DFC295 digital camera.

2.4.2. Confocal microscopy

Confocal images showing emulsions loaded with 0.05 wt. % DiO (Invitrogen) were recorded using a Zeiss LSM710 microscope with a Leica TCS SP5 Spectral Confocal Microscope (40x magnification) with excitation from the 488 nm line of an argon ion laser and emission detected between 497 and 540 nm.

2.5.2. Scanning electron microscopy (SEM)

2.2.5.1. SEM of PEGMA-based capsules

Scanning electron microscope (SEM) images were recorded using a Hitachi S-4800 FE-SEM. A 100 μL aliquot of the particle dispersions was pipetted directly onto aluminium SEM stubs and left to dry for 24 hours. The sample was gold coated for 2 minutes at 25 μA using a sputter-coater (EMITECH K550X) prior to imaging, to avoid charge build-up.

2.2.5.2. SEM of all other capsules and structures

SEM images were recorded on a variable pressure JSM5610LV, using an acceleration voltage of 5kV. 100 μL aliquot of the particle dispersions was pipetted directly onto aluminium SEM stubs and left to dry for 24 hours. The sample was gold coated for 2 minutes at 25 μA using a sputter-coater (EMITECH K550X) prior to imaging, to avoid charge build-up. Capsule structure samples were mounted on carbon tabs and coated with gold for 2 minutes as described previously.

2.6.2. Thermogravimetric analysis (TGA)

Gravimetric weight loss from hollow capsules, encapsulate loaded capsules and aggregated capsule structures was measured using a TA Instruments TGA Q5000 with an automated vertical overhead thermo-balance. Heated analysis was run from 40-1000 °C at a heating ramp of 10 °C per minute in air.

2.7.2. Mercury intrusion porosimetry (MIP)

Intrusion volumes and macropore size distributions were recorded by Dr. Oliver Mahony, Dr. Gowsihan Poologasundarampillai and Dr. Louise Connell at Imperial College London using a Micromeritics Mutopore IV 9500 porosimeter. Capsule aggregates were weighed accurately into a penetrometer. The penetrometer was then sealed and placed into the low-pressure port of the instrument where the sample and penetrometer were evacuated to 50 mmHg and then filled

with mercury. A pressure cycle from 0.5 to 60,000 psi was then performed on the assembly in predefined steps.

2.8.2. Brunauer–Emmett–Teller (BET) gas adsorption[1]

Macropore size distributions were recorded by Dr Rob Clowes at The Centre of Materials Discovery, University of Liverpool using a Micrometrics ASAP 2020 with nitrogen as the analysis adsorptive introduced at a low pressure dose of 0.1388 mmol/g. The analysis bath temperature was -195.8 °C.

2.3 Colloidosome characterisation techniques

2.1.3. FTIR spectroscopy

FTIR spectroscopy was undertaken on air-dried TMOS-cross-linked colloidosomes or TMOS-cross-linked co-polymer-functionalised colloidosomes and air-dried co-polymer from methanol solution, using a Perkin-Elmer Specrum I spectrometer on KBr disks.

2.2.3. Imaging studies of dye-entrapped colloidosomes

Optical and fluorescence microscopy images of the dye-entrapped colloidosomes dispersed in oil or in aqueous solutions at various pH values were recorded using a Leica DMI3000 B manual inverted fluorescence microscope at 10x or 20x magnification. Three band pass filters were used: excitation at 450-490 nm with an emission cut off at 510 nm (I3), excitation at 355-

425 nm with an emission cut off at 455 nm (D), and excitation at 515-560 nm with an emission cut off at 580 nm (N2.1). Line intensity profiles on individual colloidosomes were processed from optical micrographs using Gwyddion software. Fluorescence images were collected at different pH values on over fifty individual colloidosomes and no qualitative difference in permeability behaviour was observed in each case. Calibration curves were determined by fluorescence spectroscopy (Jasco FP-6500) measurements on 0.1 mM bulk aqueous solutions of calcein, acriflavine hydrochloride or rhodamine 6G at pH values between 2 and 10. Excitation at 495 nm (calcein), 416 nm (acriflavine hydrochloride) or 526 nm (rhodamine 6G), and excitation and emission band widths of 3 nm and 1 nm were used, respectively.

2.4 References

[1] S. Brunauer, P. H. Emmett, E. Teller, *J. Am. Chem. Soc.* **1938**, *60*, 309–319.

CHAPTER 3

Synthesis of emulsion-templated hybrid inorganic–organic polymer capsules using a branched co-polymer surfactant for hydrophobic active encapsulation

(Publication arising from this Chapter: **"One-pot, single-component synthesis of functional emulsions-templated hybrid inorganic-organic polymer capsules"**, R. L. Harbron, T. O. McDonald, S. P. Rannard, P. H. Findlay, J. V. M. Weaver, *Chem. Commun.* **2012**, *48*, 1592-1594.)

List of figures

List of tables

3.1. Introduction

Various strategies over the past 15 years have shown increasing progression in the control over particle size, shell thickness and porosity and the incorporation of diverse encapsulated materials using emulsion droplet templates.[1] However, in all these cases pre-formed surfactant-stabilised emulsion droplets are used as templates onto which the shell is precipitated. Therefore these methodologies, even in their simplest states, are fundamentally multi-component and require at least one surfactant and the addition of a metal alkoxide precursor such as tetraethyl orthosilicate (TEOS). Additionally, there are several issues surrounding the use of conventional small-molecule surfactants as emulsifiers, including their toxicity, foaming, and their long-term stability thus giving irreproducible formulations. These drawbacks have stimulated a resurging interest in identifying alternative emulsifiers.[2]

In this chapter, a new hybrid capsule fabrication strategy[3] will be introduced and discussed. This exploits the use of a multi-purpose amphiphilic branched co-polymer which serves as both emulsifier and cross-linker (see Figure 1).

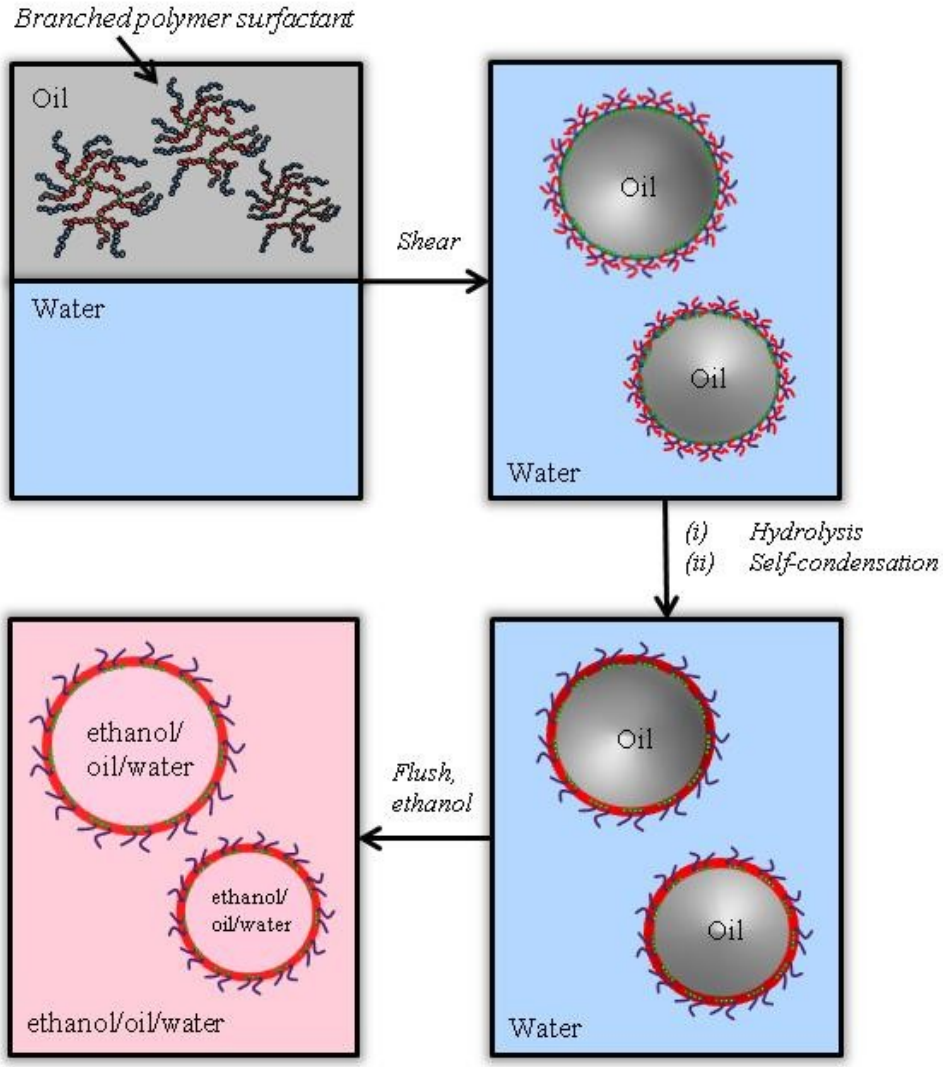

Figure 1. Schematic representation of the one-pot, single-component fabrication of encapsulated emulsion droplets and hollow capsules. Adapted from ref. 3.

In this case, the reactive amphiphilic co-polymers were dissolved in a cineole oil phase which was mixed with an equal quantity of distilled water. This biphasic mixture was agitated at high speed to form oil-in-water emulsion droplets where the amphiphilic co-polymers stabilised the interface. Furthermore, in the presence of water, spontaneous hydrolysis of the methoxy silane residues occurred to form silanol groups on the droplet peripheries (see Figure 2.a). After a cross-linking step, *via* the addition of base to the emulsion dispersion, the silanol residues self-condense to form an inorganic covalently cross-linked inorganic shell around the internal oil

phase (see Figure 2.b). Capsule surface functionality was introduced, and therefore tuned, by the hydrophilic portion of the co-polymer surfactant. The hydrophilic chain ends of the amphiphilic co-polymer were trapped on the surface of the formed cross-linked emulsion droplets. If desired, the internal oil phase could be flushed out with a mutually miscible solvent to give hollow capsules.

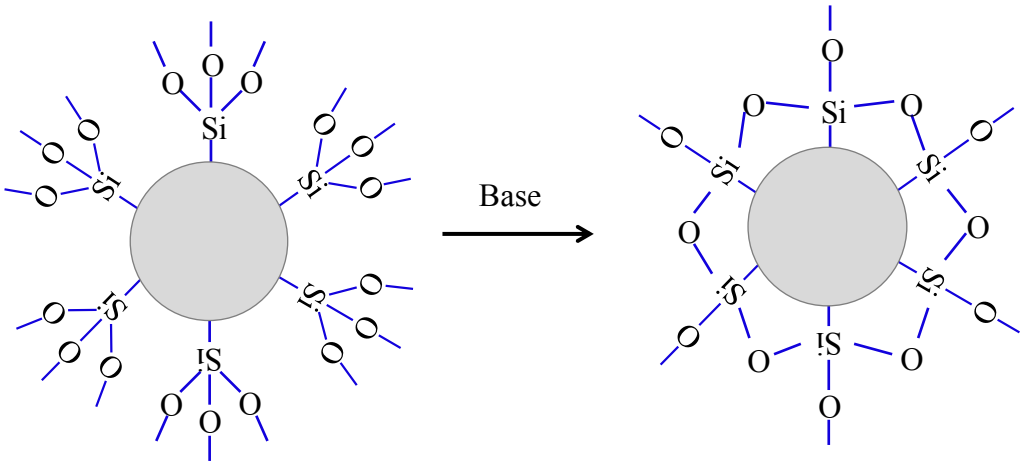

Figure 2. Schematic representation of the surface cross-linking chemistry of capsule formation where silanol groups self-condense on the addition of base to form an inorganic network.

This strategy has the key advantages of: (i) being single-component, (ii) producing stable droplets which can be cross-linked on-demand and (iii) providing additional surface functionalisation—both *in situ* and *via* provision of pre-designed handles by which post-functionalisation can be achieved. This provides a generic and translatable method for encapsulating hydrophobic materials and producing hollow capsules which may have applications in catalysis, delivery and sensing devices.[1d, 4]

3.2. Experimental

The branched co-polymers were synthesised by a free radical polymerisation (FRP) route outlined in Figure 3, namely a thiol-regulated free-radical branching polymerisation process called the 'Strathclyde approach' (see Chapter 1; Introduction for further discussion).[5] Capsule formation occurred by the incorporation of a siloxane-based methacrylate co-monomer into the polymer structure. The resulting polymer was used as an emulsifier to form oil-in-water emulsions. The induction of homocross-linking of the siloxane units, following their hydrolysis during emulsification, produced an inorganic sheath around the droplet.

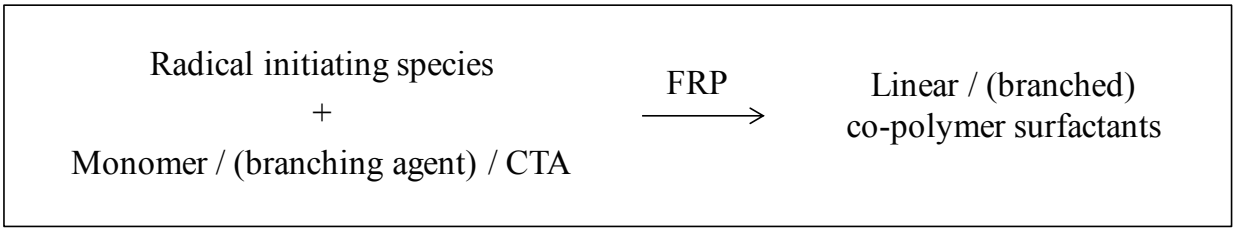

Figure 3. Synthetic strategy towards linear and (branched) co-polymer surfactants via FRP.

Equivalent branched and linear amphiphilic co-polymer analogues based on poly(ethylene glycol)methacrylate (PEGMA) and 3-(trimethoxysilyl)propyl methacrylate (TMSPMA) were prepared. A key component of this thesis concerns the comparison of branched co-polymers with their linear counterparts, and to demonstrate the versatility of branched co-polymers. During synthesis, the use of a chain transfer agent in this system restricted the final molecular weight of the polymer product. This occurred by the transfer of the free-radical of a

propagating polymer chain to another molecule by the CTA. In this section, two CTAs (DDT and TG) were compared and contrasted to find the most effective agent. TG was selected due to its hydrophilic nature whereas in contrast, DDT provides hydrophobic chain ends, allowing multiple points of attachment of the co-polymer to the oil droplet surface. In this chapter, the co-polymer design comprised simultaneous steric stabilisation and self-cross-linking that is pre-designed and multifunctional. The synthetic strategy (Figure 3) for the formation of these complex materials *via* FRP can be simplified into one step.

3.2.1. Preparation of branched and linear co-polymers *via* free radical polymerisation

A library of branched and linear co-polymers were prepared, *via* free radical polymerisation, comprising of PEGMA, TMSPMA, EGDMA (only for the preparation of branched co-polymers), DDT and TG (see Table 3). For the branched analogues, EGDMA was used as the branching agent at 10 mol % relative to the total amount of the monofunctional monomer (MFM). In theory the co-polymers presented in this thesis have compositions of MFM_{100}-$EGDMA_{10}$-CTA_{10} unless stated otherwise. In this case MFM corresponds to PEGMA, TMSPMA or a combination of the two. Molar ratios of PEGMA: TMSPMA were nominally fixed at 5:95 which corresponds to a theoretical overall PEGMA weight/weight (w/w) percentage of 16.6% and 18.3% for the branched and linear analogues, respectively. Furthermore DDT and TG were employed as chain transfer agents (CTAs); polymer analogues were synthesised with either DDT or TG chain ends. The efficiency of the two CTAs in controlling the molecular weight and the architecture of the polymer product and in avoiding gelation was compared.

3.2.2. Representative preparation of $PEGMA_x/TMSPMA_y$ – $EGDMA_{10}/DDT_{10}$ branched co-polymers

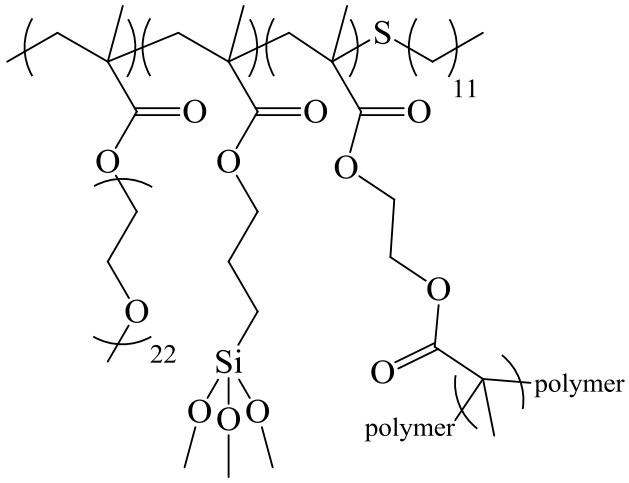

Figure 4. Representative structure of P6, $PEGMA_x/TMSPMA_y$-$EGDMA_{10}$-DDT_{10}.

In order to synthesise the branched co-polymer (P6), $PEGMA_5/TMSPMA_{95}$-$EGDMA_{10}$-DDT_{10}, represented by Figure 4, a mixture of PEGMA (M_w = 1.10 kDa) (2.33 g, 2.12 mmol), TMSPMA (10.00 g, 40.27 mmol), EGDMA (0.84 g, 4.24 mmol), and DDT (0.86 g, 4.21 mmol) was degassed with a nitrogen purge using a Schlenk line. Methanol (140 mL, anhydrous) was degassed separately with a nitrogen purge using a Schlenk line and added to the monomer mixture. After heating to 70^{o}C, the co-polymerisation was initiated by the addition of AIBN (140.3 mg, 0.85 mmol) and was stirred with heating for 48 hours. Methanol was then removed by distillation and the resulting co-polymers were stored under vacuum. No purification steps were required due to almost complete conversion; typically conversions in excess of 97% were achieved as shown by ^{1}H NMR spectroscopy. In order to synthesise co-polymers of varying composition molar ratios of PEGMA to TMSPMA were adjusted, while

the EGDMA and DDT molar ratios were kept unchanged. Linear analogues were also synthesised for comparison. ^{1}H NMR spectroscopy was used to confirm the co-polymer composition; Figure 5 compares P6 with its linear counterpart P15. Molecular weights, molecular weight distributions and Mark-Houwink α-values were determined (see Table 3) using triple detection size exclusion chromatography (TD-SEC) (as discussed in Chapter 1; Introduction).

Example experimental calculation applicable to all polymers synthesised *via* free radical polymerisation within this thesis

P6, $PEGMA_5/TMSPMA_{95}$-$EGDMA_{10}$-DDT_{10}

Mass (g) = Mw x moles (mol)

To start, 10.00 g of TMSPMA (our primary component), is calculated as (10.00 g / 248.35 g/mol) $4.03x10^{-2}$ mol. Since the ratio of monomers equals 5:95:10:10; ($4.03x10^{-2}$ mol / 95) x 5 = moles of PEGMA, ($4.03x10^{-2}$ mol / 95) x 10 = moles of EGDMA and DDT respectively.

Therefore, moles of PEGMA or EGDMA or DDT x Mw = mass of PEGMA or EGDMA or DDT needed to synthesise a polymer with the chosen ratio. All polymers were synthesised at 10 % solids in solvent. The initiator, AIBN, was added at 1 % of the total mass of the constituents (see Table 1).

Table 1. Calculations of the amounts required for the polymerisation of P6.

Chemical	**Empirical formula**	**Mw / g/mol**	**Mass / g**	**Moles / mol**
PEGMA	$C_{49}H_{96}O_{24}$	1100	2.33	2.12×10^{-3}
TMSPMA	$C_{10}H_{20}O_5Si$	248	10.00	4.03×10^{-2}
EGDMA	$C_{10}H_{14}O_4$	198	0.84	4.24×10^{-3}
DDT	$C_{12}H_{26}S$	204	0.86	4.24×10^{-3}
Total Mass = 14.03 g				
Volume of solvent = 140.30 mL				
Mass of initiator = 0.14 g				

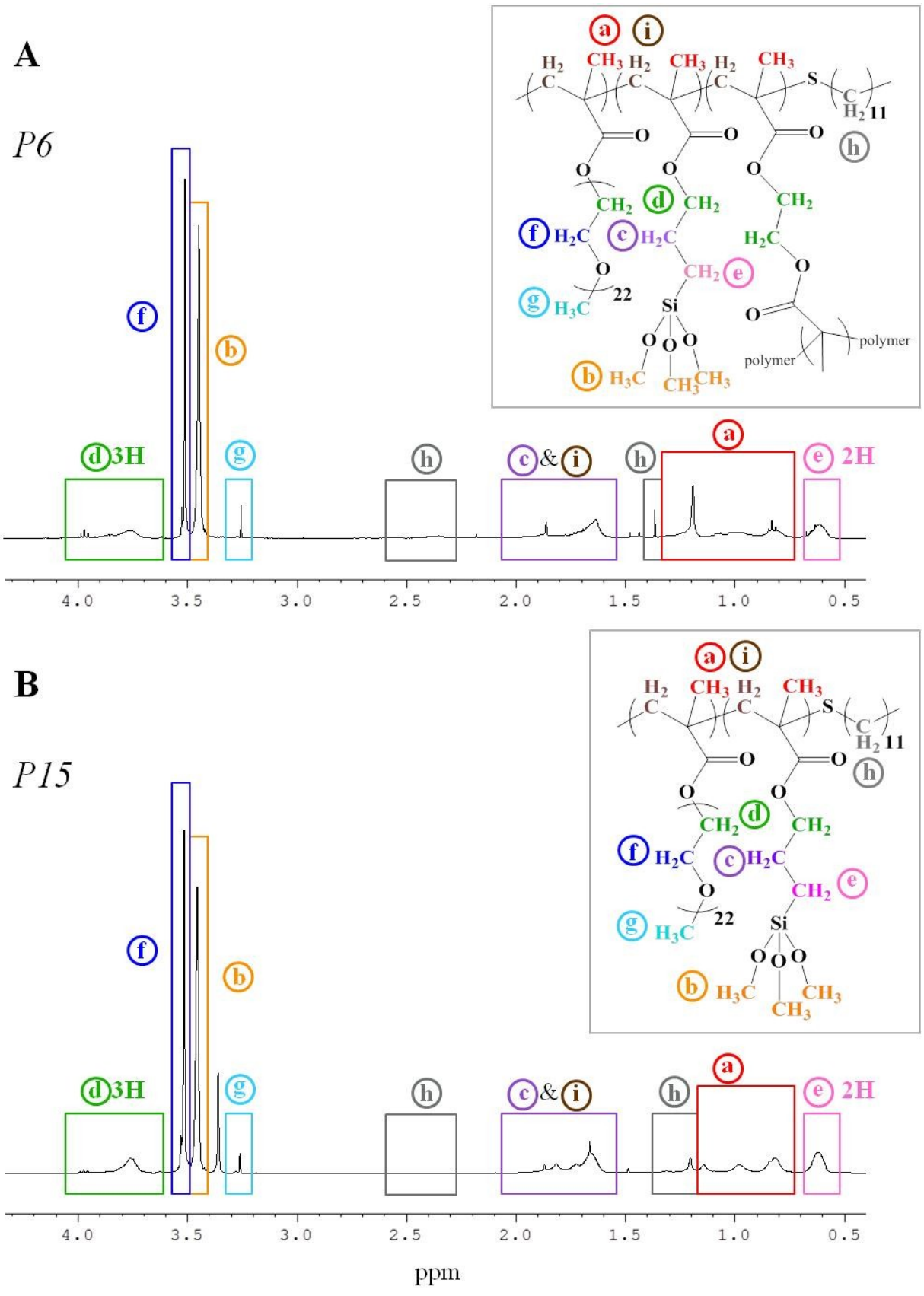

Figure 5. Assigned ^{1}H ($CDCl_3$) NMR spectra of (A) P6, $PEGMA_{5.9}$/$TMSPMA_{94.1}$-$EGDMA_{7.8}$-$DDT_{12.2}$ and (B) P15 linear co-polymer surfactants.

3.2.3. Representative preparation of $PEGMA_x/TMSPMA_y$ – DDT_2 linear co-polymers

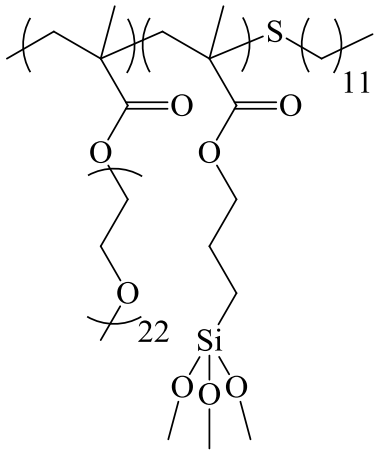

Figure 6. Representative Structure of P15, $PEGMA_x/TMSPMA_y$-DDT_2.

To synthesise the analogous linear co-polymer (P15), $PEGMA_5/TMSPMA_{95}$-DDT_2, (see Table 3) represented by Figure 6, a mixture of PEGMA (M_w = 1100 g / mol) (2.33 g, 2.12 mmol), TMSPMA (10.00 g, 40.27 mmol), and DDT (0.17 g, 0.83 mmol) was degassed with a nitrogen purge using a Schlenk line. Methanol (125 mL, anhydrous) was degassed separately with a nitrogen purge using a Schlenk line and added to the monomer mixture. After heating to 70 ^oC, the co-polymerisation was initiated by the addition of AIBN (125.0 mg, 0.76 mmol) and was stirred with heating for 48 hours. Methanol was then removed by distillation and the resulting co-polymers were stored under vacuum. No purification steps were required due to almost complete conversion, typically in excess of 97% as determined by ^1H NMR spectroscopy. It should be noted that the assumption is made that both end groups of the difunctional brancher have polymerised, this is assumed for all reactions in this thesis. In order to synthesise co-polymers of varying composition, the initial molar ratios of PEGMA to TMSPMA were

adjusted, while the DDT molar ratio was kept unchanged. ^{1}H NMR spectroscopy was used to confirm the co-polymer composition; see Figure 5. Molecular weights, molecular weight distributions and Mark-Houwink α-values were determined (see Table 3) using triple detection size exclusion chromatography (TD-SEC) (as discussed in Chapter 1; Introduction).

Table 2. Calculations of the amounts required for the polymerisation of P15.

Chemical	**Empirical formula**	**Mw**	**Mass / g**	**Moles / mol**
PEGMA	$C_{49}H_{96}O_{24}$	1100	2.33	2.12×10^{-3}
TMSPMA	$C_{10}H_{20}O_5Si$	248.35	10.00	4.03×10^{-2}
DDT	$C_{12}H_{26}S$	204.4	0.17	8.48×10^{-4}
Total Mass = 12.50 g				
Volume of solvent = 125.00 mL				
Mass of initiator = 0.13 g				

3.2.4. Polymer hydrolysis

Hydrolysis of the methoxy silane residues, in the presence of water (see Figure 7), to form silanol groups on the emulsion droplet peripheries was monitored as a function of time *via* ^{1}H NMR kinetic experiments.

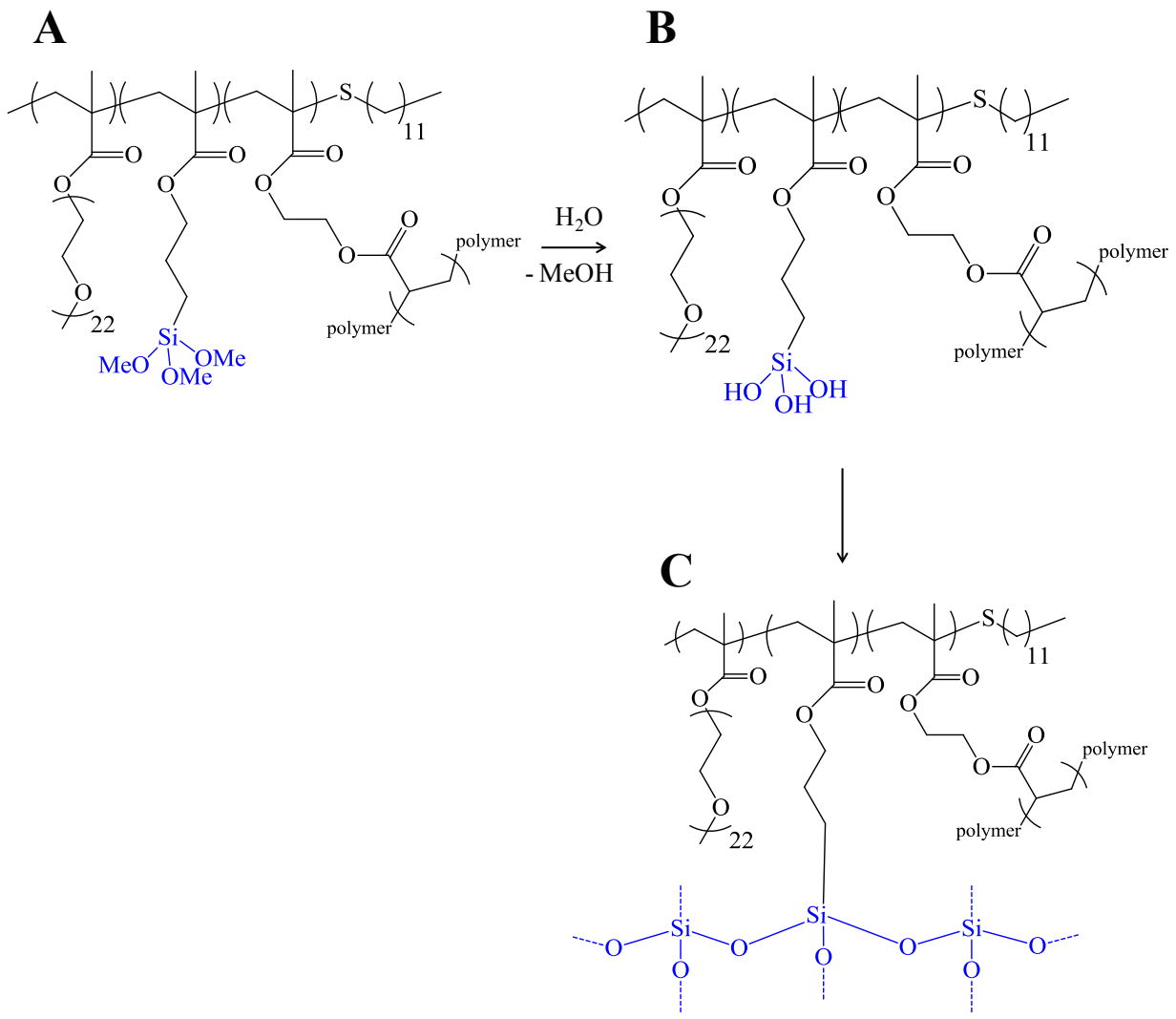

Figure 7. Branched co-polymer P6 (A) in oil. (B) In the presence of water methoxy silane residues spontaneously hydrolyse to form silanol groups. On the addition of base, (C) the silanol residues self-condense to form covalent inorganic cross-links.

Simulated ^{1}H NMR spectroscopy kinetic experiments of the branched co-polymer, P6, initially dissolved in tetrahydrofuran-d_8 (see Figure 8) and then spiked with D_2O confirmed hydrolysis by the evolution of a unique methanol resonance at 3.1 – 3.2 ppm, (as depicted in Figure 9.b) which increased in intensity as a function of time (see Figure 9). This confirms the presence of periphery hydrophilic hydrolysed silanol groups, which are ready available for cross-linking and emulsion droplet stabilisation.

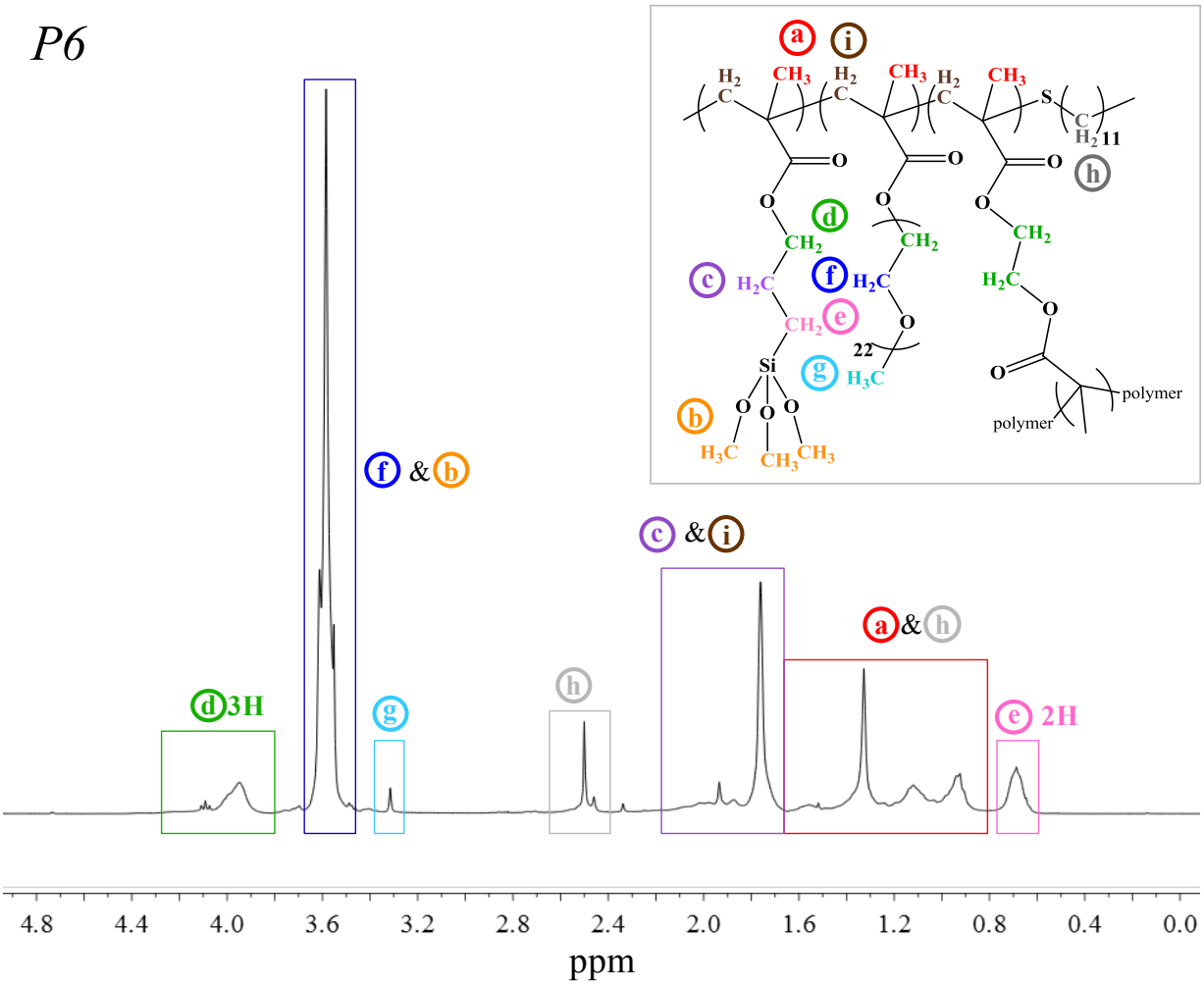

Figure 8. Assigned ^{1}H (d_8-THF) NMR spectra of P6 (before hydrolysis), $PEGMA_{5.9}/TMSPMA_{94.1}$-$EGDMA_{7.8}$-$DDT_{12.2}$.

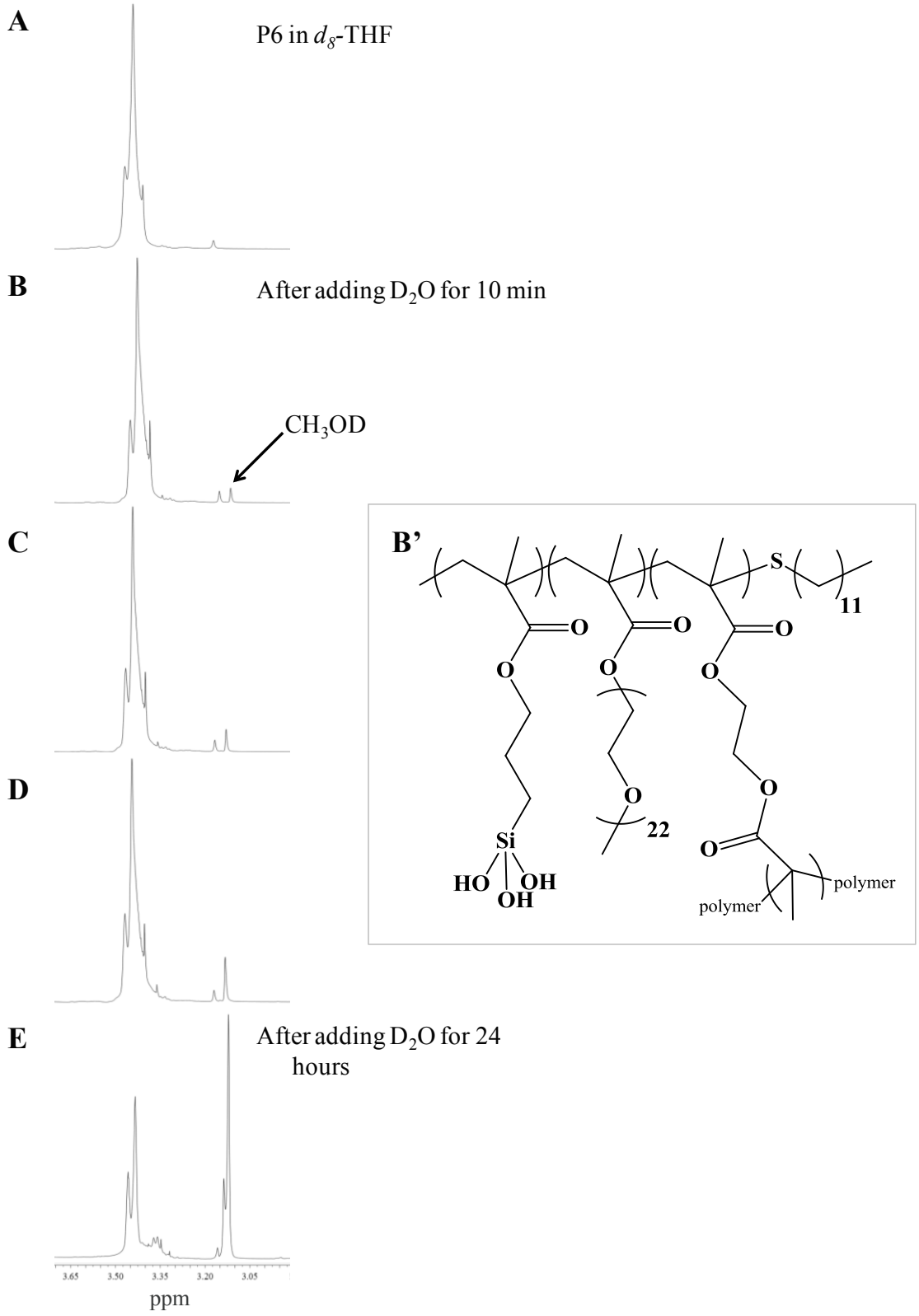

Figure 9. (A) Partial ^{1}H NMR spectra of P6, $PEGMA_{5.9}$/$TMSPMA_{94.1}$-$EGDMA_{7.8}$-$DDT_{12.2}$ in d_8-THF; (B) after adding 0.05mL D_2O into 0.8 mL of d8-THF/P6 for 10 min (note the appearance of a CH_3OD signal due to the hydrolysis of trimethoxysilyl groups as represented in (B')); (C) after a reaction time of 20 min; (D) after a reaction time of 30 min; (E) after a reaction time of 24 hours (note that the peak of CH_3OD becomes sharper).

3.2.5. Emulsion synthetic processes

3.2.5.1. Emulsion preparation

A solution of co-polymer in oil (3.0 w/v %, 3 mL) was prepared and an equal volume of distilled water was added. This biphasic mixture was homogenised at 24,000 rpm for 2 minutes using a T25 digital Ultra-Turrax. Following homogenisation, the emulsions were left to equilibrate for 1 hour before characterisation.

3.2.5.2. Washing of emulsions

The emulsions were washed gently to remove any un-adsorbed polymer by centrifugation using an Eppendorf 5804R (this apparatus was subsequently used for all further centrifugations) (2,800 rpm, 60 minutes). The resulting supernatant was discarded. The polymer-stabilised emulsion droplets were redispersed in distilled water. This process was repeated three times in total.

3.2.5.3. Emulsions with encapsulated guest molecules

A number of emulsions were produced with guest molecules encapsulated within the oil droplets. Guest molecules include Oil Red, Oil Blue, DiO, and PVS (Mw 90 kDa). All emulsions were prepared as per section 3.2.5.1; Emulsion preparation, and all guest molecules

were dissolved into the oil phase before homogenisation. Dyes were always added at 0.1 w/v % unless stated otherwise, DiO at 0.05 w/v % and poly(vinyl stearate) at a maximum of 30 w/v %.

3.2.6. Capsule synthetic processes

3.2.6.1. Cross-linked emulsion and capsule fabrication

Emulsions were prepared and washed identically as per 3.2.5; Emulsion synthetic processes. 1 mL of the creamed emulsion was redispersed in 30 mL distilled water with gentle stirring. 1 mL TEA was added to the dilute emulsion solution whilst stirring and left for 1 hour.

3.2.6.2. Hollow capsule formation

Excavated, hollow cross-linked capsules were formed by flushing the cross-linked emulsions with ethanol to remove the internal and continuous phases.

3.2.6.3. Washing of capsules

In order to wash the capsules to remove any unadsorbed polymer, the cross-linked emulsions were flushed with EtOH, as described in section 3.2.6.2; Hollow capsule formation, the resulting solutions were centrifuged (2,800 rpm, 60 mins) and the resulting supernatant was

discarded. The capsules were redispersed in EtOH after each washing. This process was repeated three times in total.

3.3. Results and discussion

3.3.1. Synthesis of branched and linear co-polymer surfactants

The composition of the prepared statistical branched and linear co-polymers, were pre-designed to include steric stabiliser PEGMA, cross-linker TMSPMA, and CTAs, DDT and TG to provide hydrophobic and hydrophilic polymer chain ends respectively. Table 3 shows the target composition and actual calculated polymer compositional ratios for the branched and linear co-polymers as determined by ^{1}H NMR spectroscopy, using signal ratios, and triple-detection size exclusion chromatography (TD-SEC).

3.3.2. Effect of CTA and polymer architecture

As presented in Table 3, for a given branched co-polymer, mean molecular weight increased with the proportion of branching monomer in the composition. Number average molecular weights were in close agreement for the linear and branched co-polymers, however weight averaged molecular weights differed dramatically due to the inherent statistical conjoining of polymer chains caused by the presence of the branching monomer, EGDMA, which also led to a higher polydispersity. M_w and M_n for each sample are in fair consistency with similar branched co-polymers previously reported.[5b, 6] PDI values ranged up to 12.2 for P6,

suggesting a highly polydisperse system as typically expected of branched co-polymers synthesised *via* free radical polymerisation and the incorporation of bifunctional EGDMA. Polymer architectural information can be inferred by the Mark-Houwink α-values (M-Hα) (as discussed in Chapter 1; Introduction). This value indicates the relationship between intrinsic viscosity and molecular weight, where the exponent α has characteristic values. For a linear homopolymer, such as P3, the M-Hα is typically in the region of 0.7 in a good solvent. M-Hα decreases as the molecular weight increases.[7] All Mark-Houwink α-values are approximately 0.3 or below for the branched co-polymers, indicating relatively compact conformations, as expected with branched polymer architecture.[5a, 6b, 7]

For linear and branched analogues, the level of CTA present affects molecular weight i.e. the lower the amount of CTA, the higher the molecular weight value. On comparison of the co-polymers synthesised with the two aforementioned CTAs, DDT and TG, those synthesised using DDT had a lower molecular weight by GPC (see Table 3). From these results, a conclusion was made that TG has a lower chain transfer efficiency than DDT. DDT was found to be the most effective CTA and was used for the synthesis of polymers throughout the remainder of this thesis. The level of DDT was varied for comparison with P6, where DDT is 10 mol % relative to the total amount of the MFM, to 5 mol % and 2.5 mol %, for PE7 and PE8 respectively. Molecular mass increases with the lower the molecular percentage of DDT. Where an equivalent proportion of DDT, when compared to the MFM with the omission of the EGDMA branching agent, was used to synthesise a linear analogue i.e. P16, short chain oligomers were produced with a low molecular mass and low polydispersity.

Figure 10.a-c, shows that the branched analogue P6 elutes first during analysis suggesting that the co-polymer is much larger in size than the linear counterpart P15, as expected with branched architecture. The plot of P6 in Figure 10.a, shows us that the branched analogue has a wider range of chain lengths and hence a higher polydispersity than the linear (as shown in Table 3) again due to the branching or conjoining of the primary chains during the synthesis of the branched equivalent. In Figure 10.c, at a crossing point of 95.9 kDa, the linear co-polymer is more dense than the branched, although they are chemically similar, it may be the effect of the end chain transfer agent end groups or the fact that there are additional EGDMA units in the branched polymer which gives this effect in this solvent. At higher molecular weights however, it is apparent that the intrinsic viscosity of the linear material increases at a much higher rate than that of the branched material as would be expected. This is due to the increase in entanglement for the linear material even though it has a much reduced Mw than the branched material. The longer the linear chain, the more viscous the polymer product will become.

Table 3. Co-polymer compositions calculated by ^{1}H ($CDCl_3$) NMR and size exclusion chromatography (TD-THF) values.

ID	Target Polymer Composition	Polymer composition [a]	Conv % [a]	Mw/kDa [b]	Mn/kDa [b]	Mw/Mn [b]	M-Hα [b]
P1	$TMSPMA_{100}$-$EGDMA_{10}$-DDT_{10}	$TMSPMA_{98.0}$-$EGDMA_{10.8}$-$DDT_{11.2}$	98.0	55	6	9.5	0.25
P2	$TMSPMA_{100}$-$EGDMA_{10}$-TG_{10}	$TMSPMA_{99.4}$-$EGDMA_{11.8}$-$TG_{8.8}$	97.8	88	22	8.7	0.31
P3	$TMSPMA_{100}$	$TMSPMA_{100}$	95.7	97	39	2.5	0.69
P4	$TMSPMA_{100}$-DDT_2	$TMSPMA_{96.1}$-$DDT_{5.9}$	97.5	21	16	1.3	0.55
P5	$TMSPMA_{100}$-TG_2	$TMSPMA_{97.8}$-$TG_{2.4}$	97.2	54	33	1.6	0.58
*P6**	$PEGMA_5$/$TMSPMA_{95}$-$EGDMA_{10}$-DDT_{10}	$PEGMA_{5.9}$/$TMSPMA_{94.1}$-$EGDMA_{7.8}$-$DDT_{12.2}$	99.2	70	33	12.1	0.35
P7	$PEGMA_5$/$TMSPMA_{95}$-$EGDMA_{10}$-DDT_5	Not performed	-	121	12	5.8	0.40
P8	$PEGMA_5$/$TMSPMA_{95}$-$EGDMA_{10}$-$DDT_{2.5}$	Not performed	-	144	13	3.4	0.51
P9	$PEGMA_5$/$TMSPMA_{95}$-$EGDMA_{10}$-TG_{10}	$PEGMA_{6.2}$/$TMSPMA_{96.5}$-$EGDMA_{8.7}$-$TG_{8.6}$	88.2	220	76	2.8	0.31
P10	$PEGMA_{15}$/$TMSPMA_{85}$-$EGDMA_{10}$-DDT_{10}	$PEGMA_{14.6}$/$TMSPMA_{84.6}$-$EGDMA_{10.1}$-$DDT_{10.7}$	97.3	100	30	11.8	0.34
P11	$PEGMA_{95}$/$TMSPMA_5$-$EGDMA_{10}$-DDT_{10}	$PEGMA_{97.5}$/$TMSPMA_{4.9}$-$EGDMA_{7.5}$-$DDT_{10.1}$	98.0	447	187	14.3	0.27
P12	$PEGMA_{85}$/$TMSPMA_{15}$-$EGDMA_{10}$-DDT_{10}	$PEGMA_{86.7}$/$TMSPMA_{13.2}$-$EGDMA_{8.2}$-$DDT_{11.9}$	97.9	194	90	12.2	0.34
P13	$PEGMA_{80}$/$TMSPMA_{20}$-$EGDMA_{10}$-DDT_{10}	$PEGMA_{83.4}$/$TMSPMA_{19.5}$-$EGDMA_{7.1}$-$DDT_{10.0}$	96.4	128	38	10.5	0.31
P14	$PEGMA_5$/$TMSPMA_{95}$	$PEGMA_5$/$TMSPMA_{95}$	97.8	88	19	1.8	0.63
*P15**	$PEGMA_5$/$TMSPMA_{95}$-DDT_2	$PEGMA_{6.1}$/$TMSPMA_{92.6}$-$DDT_{3.3}$	97.2	26	8	3.2	0.58
P16	$PEGMA_5$/$TMSPMA_{95}$-DDT_{10}	Not performed	-	4	2	1.0	0.36
P17	$PEGMA_5$/$TMSPMA_{95}$-TG_2	$PEGMA_{4.8}$/$TMSPMA_{95.2}$-$TG_{2.0}$	97.0	34	13	1.8	0.54

*[a] as determined by ^{1}H NMR. [b] as determined by THF TD-SEC against polystyrene (99k) standards. * most relevant polymer compositions discussed in this chapter.*

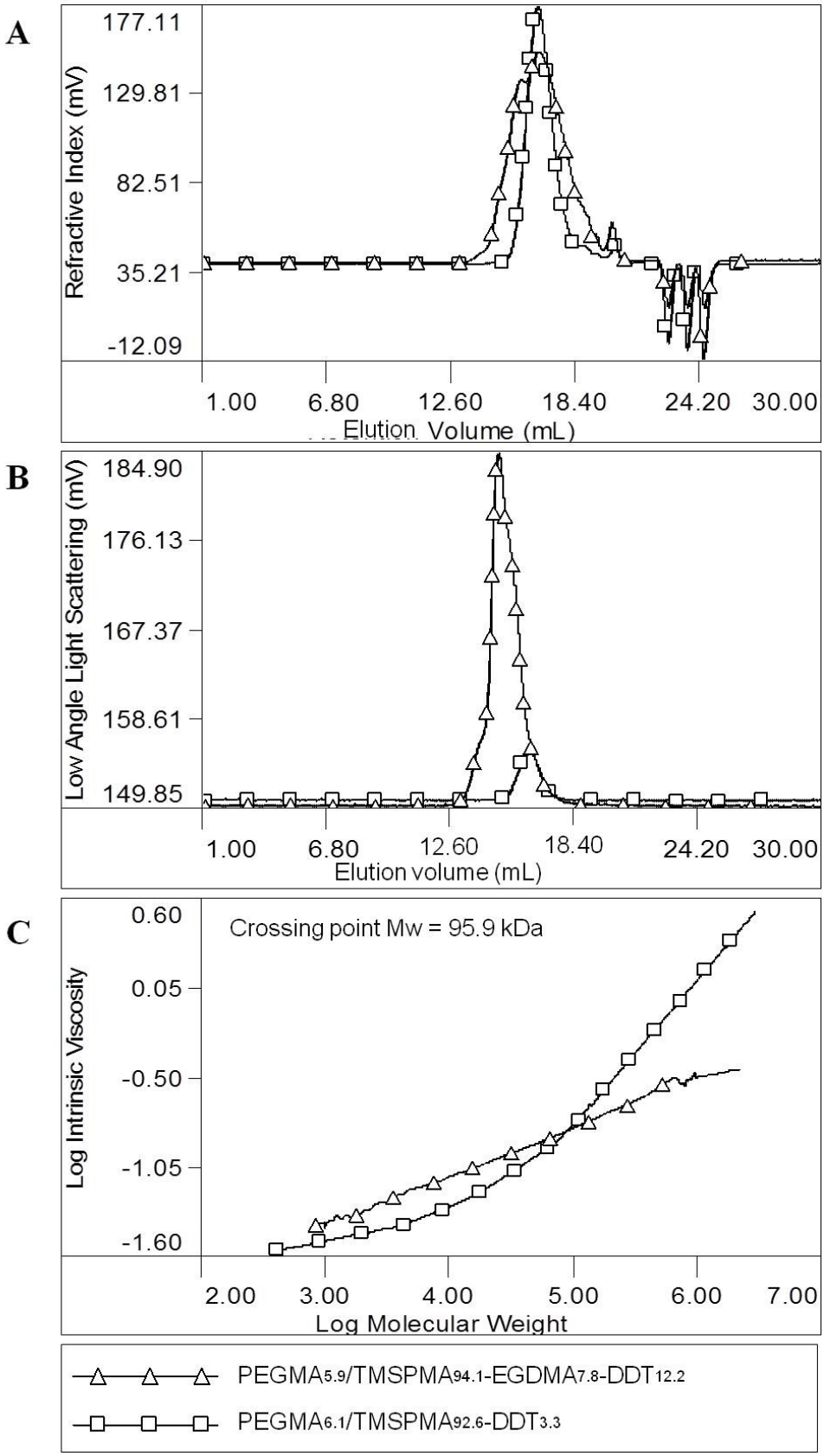

Figure 10. Size exclusion chromatographs depicting differences in (A) refractive index, (B) low angle light scattering, and (C) viscosity between branched P6 and linear P15.

3.3.3. Reproducibility of the branched co-polymer

The applications of P6 as a branched co-polymer surfactant makes up a significant portion of this thesis, therefore a demonstration of reproducibility is presented in Figure 11. Several co-polymers were synthesised separately in order to assess the reproducibility of the free radical co-polymerisation protocol.

^{1}H NMR spectra show good reproducibility between samples, with theoretical co-polymer compositions in good agreement with compositions within error of NMR (see Table 4).

Table 4. Actual polymer compositions as calculated by ^{1}H ($CDCl_3$) NMR.

ID	Conv %[a]	Calculated polymer composition[a]
P6(1)	99.2	$PEGMA_{5.9}/TMSPMA_{94.1}$-$EGDMA_{7.8}$-$DDT_{12.2}$
P6(2)	98.4	$PEGMA_{4.8}/TMSPMA_{95.1}$-$EGDMA_{10.1}$-$DDT_{10.0}$
P6(3)	98.7	$PEGMA_{5.4}/TMSPMA_{96.4}$-$EGDMA_{10.0}$-$DDT_{8.2}$

[a] *as determined by ^{1}H NMR.*

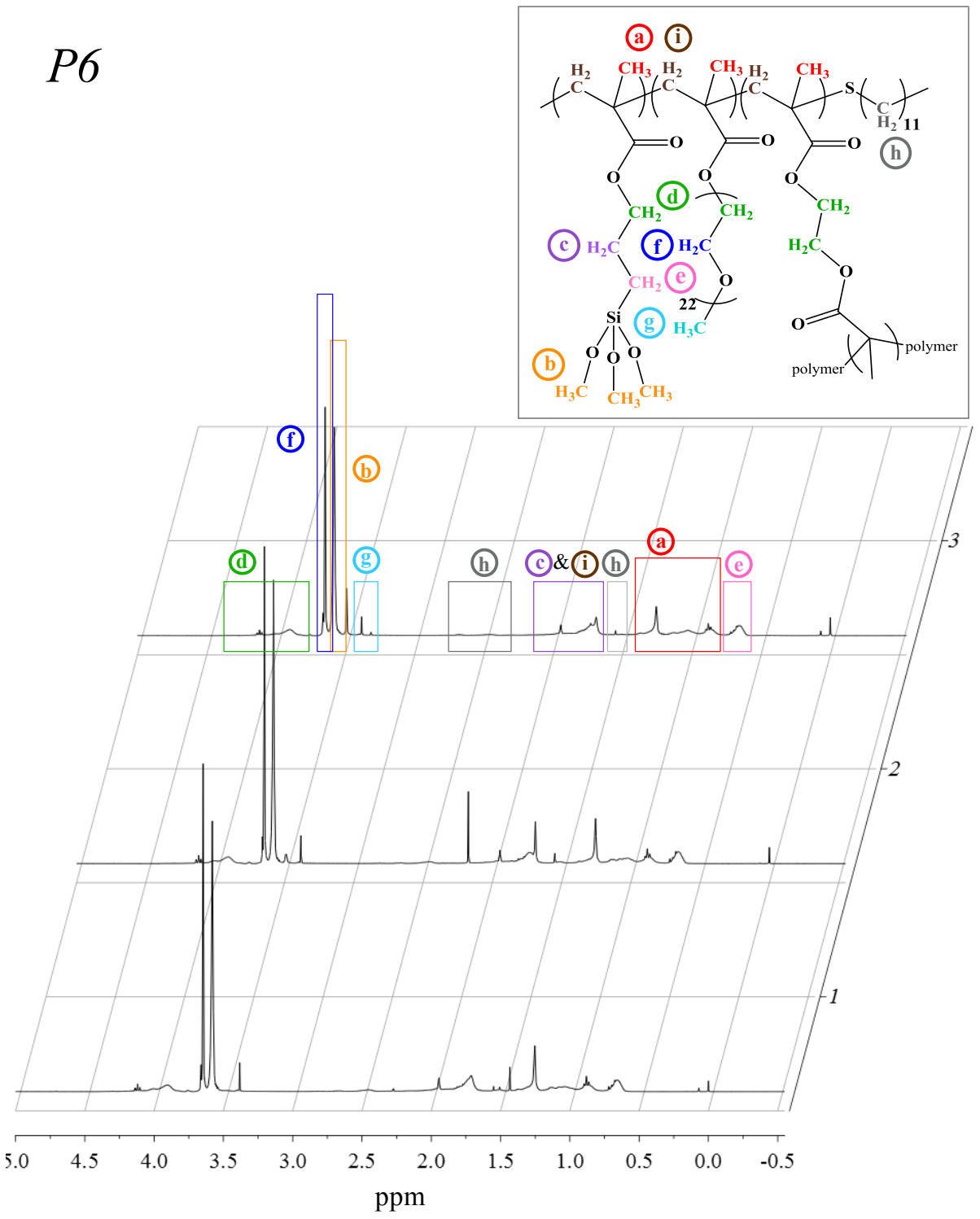

Figure 11. ^{1}H ($CDCl_3$) NMR spectra for three repeat synthesis of P6.

TD-SEC curves overlay well, suggesting similar molecular weight distributions were obtained in all cases (see Figure 12).

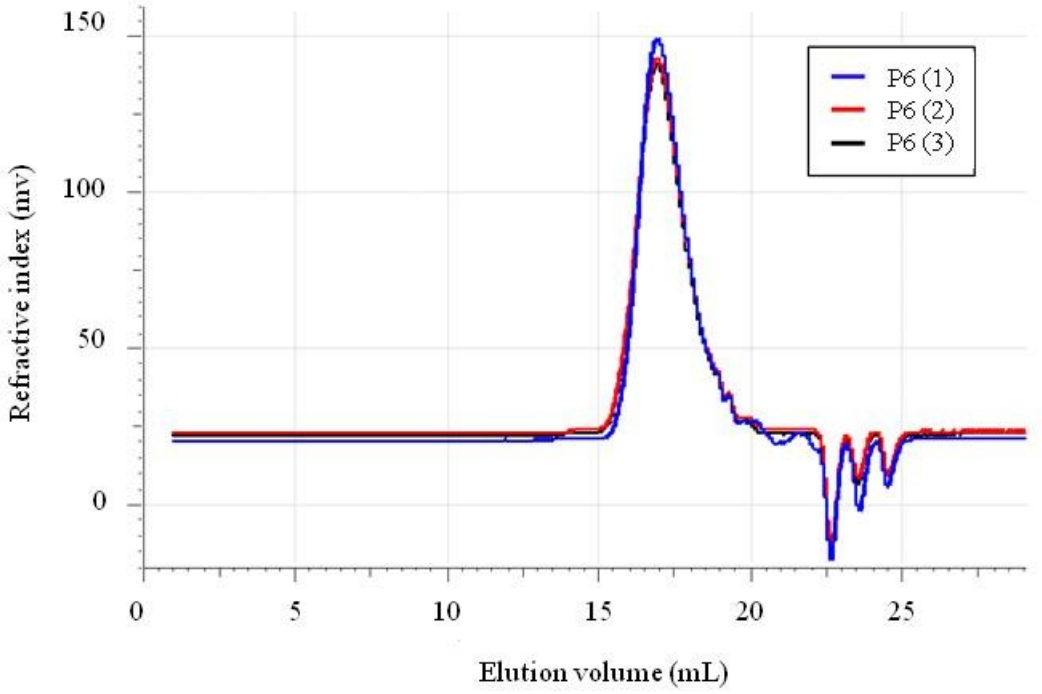

Figure 12. TD-SEC curves obtained for three repeat P6 samples.

M_w, M_n and Mark-Houwink α-values are shown in Table 5; M_n for each sample are in good agreement and all samples showed polydispersity values between 10.4 – 12.1, suggesting a highly polydisperse system as expected of branched co-polymers produced *via* free radical polymerisation that provides minimal control over how the different monomers sequentially arrange to form the polymer. Mark-Houwink α-values are all similar and below 0.34, indicative of relatively compact structures, again suggesting branched architectures as found elsewhere.[5a, 6b, 7] Performing size exclusion chromatography measurements on a branched co-polymer with a high level of architectural and compositional complexity still remains challenging within materials research. Although TD-SEC with the added support of multiple

detectors is a valuable tool for polymer characterisation, its reliable application to complex branched co-polymer systems is still debatable.[8]

Table 5. Table of results comparing M_w, M_n, polydispersity and M-Hα values of the repeat analysis of P6 by GPC.

ID	Mw/kDa[b]	Mn/kDa[b]	Mw/Mn[b]	M-Hα[b]
P6 (1)	70	33	12.1	0.35
P6 (2)	63	34	12.0	0.31
P6 (3)	62	35	10.4	0.32

[b] *as determined by THF TD-SEC against polystyrene (99k) standards.*

3.3.4. Emulsion stability and cross-linking

It has previously been shown by Woodward and Weaver from 2009 to 2011[6a, 9], that similar amphiphilic branched co-polymers, which differ in the nature of the low molecular weight co-monomer component as used in this study, can be used as highly effective, albeit non-reactive, emulsifiers.[6, 9a, 9c] They described a pH-responsive system based on PEGMA, where the PEGMA residues of the polymer provided efficient steric stabilisation of oil droplets dispersed in water whilst the mono-functional co-monomer provided an optionally tunable component (with a pH-response that alters either the polymer hydrophobicity[6a] or inter-polymer hydrogen-bonding potential.[6b] The DDT chain ends, which were present in the co-polymers as dodecane thioether linkages, provided multiple points of attachment of the co-polymer to the oil droplet surface. This multi-functionality is mirrored in the present work producing a co-polymer with simultaneous function which provides the basis of our generic and single-component capsule formation methodology as depicted in Figure 1.

An important consideration when designing a generic capsule formation strategy concerns reproducibility and achieving long-term stabilities of the transient, uncross-linked templates such that the timeframe for cross-linking is as long as possible. Emulsions stabilised by the co-polymers were prepared identically as described in section 3.2.5.1; Emulsion preparation. The choice of oil phase was explored, see Table 6. P6, the main branched co-polymer in this chapter, was utilised to find a suitable oil phase, that is an oil in which this type of polymer composition is fully soluble. Both toluene and cineole were found to be suitable as both were good solvents for the branched and linear co-polymer surfactants and are water-immiscible; however, the general procedure should be applicable to other oils which satisfy these criteria as explored later in this thesis.

Table 6. Dissolution of P6 in various oils.

Oil	Ratio / %	Dissolves Polymer / Y/N
1-Undecanol	-	N
Toluene	-	Y
Toluene/Dodecane	5 : 95	N
Toluene/Dodecane	10 : 90	N
Toluene/Dodecane	50 : 50	N
Cineole	-	Y
Dodecane	-	N

Oil-in-water (o/w) emulsions formed immediately upon homogenisation, with both toluene and cineole, and average diameters of the droplets were measured as a function of time using laser diffraction to assess stabilities (as described in Chapter 2). The stability of the uncross-linked emulsion droplet diameters prepared with toluene and cineole were compared (see Figure 13).

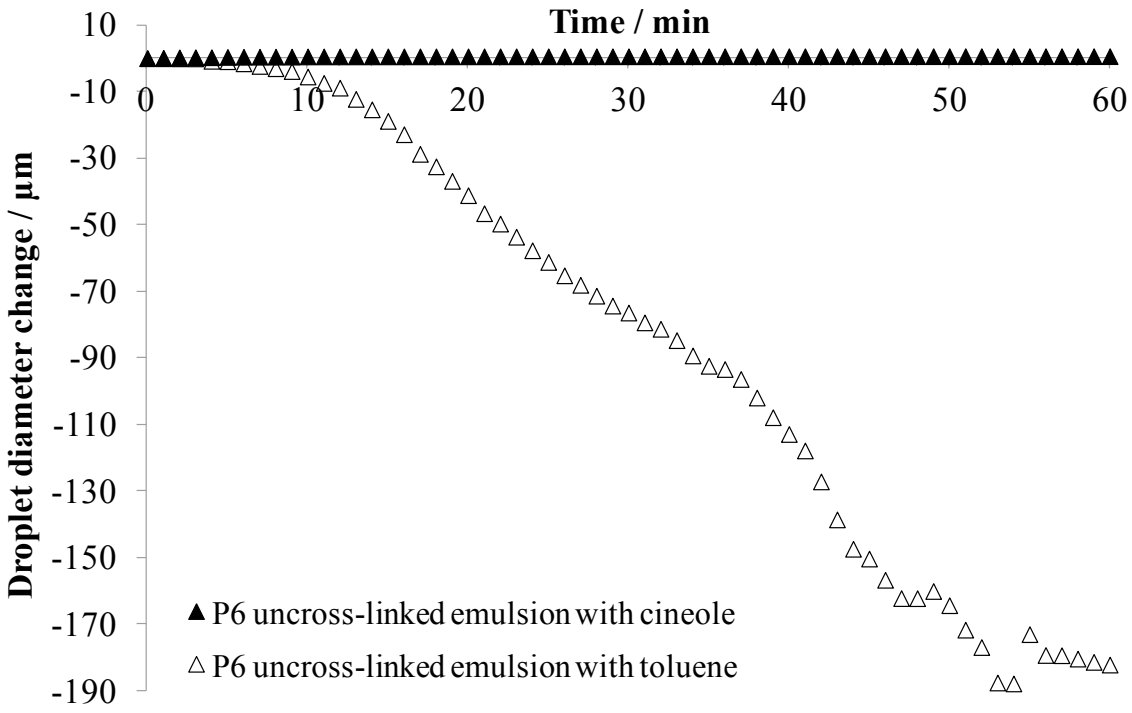

Figure 13. Normalised kinetic experiments monitoring the change in volume-averaged droplet diameters of P6 branched co-polymer stabilised uncross-linked emulsion droplets with either a cineole or toluene oil phase as a function of time.

The initial droplet diameter was compared with the final droplet diameter for each oil phase as shown in Table 7. Cineole was found to give the most stable emulsion with P6 and was therefore used throughout this thesis as the main oil phase.

Table 7. Comparison of initial and final uncross-linked emulsion droplet diameters with changing oil phase.

ID	Oil phase	Initial droplet diameter / µm	Final droplet diameter / µm
P6	Cineole	1.167	1.051
P6	Toluene	6.151	188.354

Branched co-polymer-stabilised droplets (prepared with P6) showed constant droplet diameters over the period of at least 3 hours by light scattering (average droplet diameter = 1.884 μm). In contrast, as depicted in Figure 14, droplets stabilised with P15, the linear co-polymer analogue showed a constant droplet diameter reduction and liberation of phase-separated cineole over longer time frames indicative of emulsion destabilisation. The initial droplet diameter for P6- and P15-stabilised uncross-linked and cross-linked emulsion droplets were compared with the final emulsion droplet diameter for each oil phase as shown in Table 8.

Table 8. Comparison of initial and final uncross-linked and cross-linked emulsion droplet diameters of P6 and P15 co-polymer stabilised emulsion droplets.

ID	Oil phase	Cross-linking	Initial droplet diameter / μm	Final droplet diameter / μm
P6	Cineole	Uncross-linked	1.167	1.051
P6	Cineole	Cross-linked	0.880	0.865
P15	Cineole	Uncross-linked	9.624	4.343
P15	Cineole	Cross-linked	10.609	10.264

Emulsion droplet diameter stability is very important when considering the reproducibility of the system, as an unstable emulsion which demulsifies over time will not provide a suitable template for the preparation of uniform capsules. In the case of the branched co-polymer stabilised emulsions, cross-linking can occur at any point as the uncross-linked droplets do not change size over time. Therefore cross-linking can proceed throughout this 30 min period to give capsules of a similar size. In contrast, in the case of the linear co-polymer stabilised system, the uncross-linked emulsion droplet diameter was changing as it destabilises. This most likely occurs due to the lower number of DDT chain end anchoring points available on

account of its linear architecture. Therefore cross-linking of this system would show a time-dependent size correlation because the emulsion is unstable and therefore demulsifying over time.

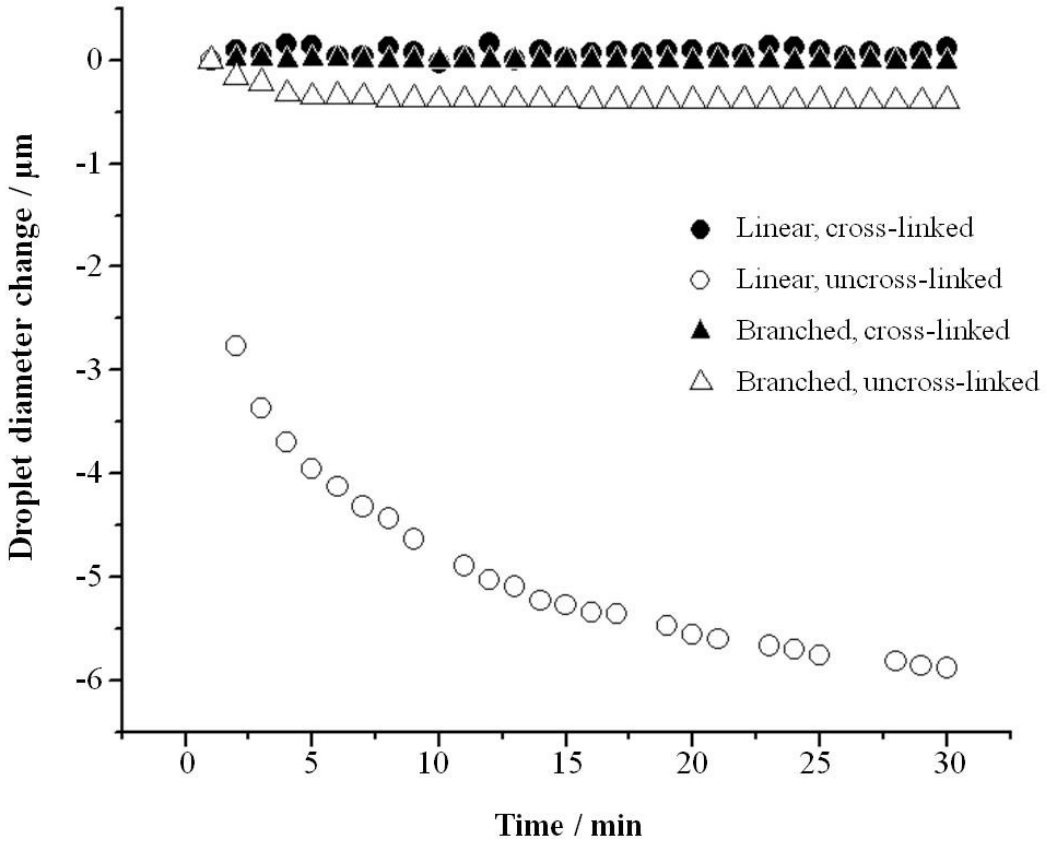

Figure 14. Normalised kinetic experiments monitoring the change in volume-averaged droplet diameters of the branched and linear co-polymer stabilised uncross-linked and cross-linked droplets as a function of time. Reproduced with permission from ref. 3.

This confirms that the branched architectures provide enhanced droplet stabilities compared to linear analogues and is in agreement with observations for related systems using both DDT and TG as CTAs.[6] The rationale for this important observation invokes the higher number of end-groups providing greater surface adhesion and their more globular morphologies and higher molecular weight which provide additional Pickering-type stabilisation.[2a, 10]

3.3.5. Capsule formation and flushing of the contents

The introduction of the aqueous phase during emulsion formation induced spontaneous hydrolysis of the methoxy silane residues to form liberated silanol groups on the droplet peripheries[1e] as represented in Figure 2. The branched co-polymer-stabilised droplets retained their structural integrity during this process despite the inevitable change in the hydrophobe-to-hydrophile balance of these co-polymers. Laser diffraction confirmed that the droplets had volume-averaged droplet diameters of 0.82 µm and light microscopy showed that the droplets were highly spherical, but with obvious indentations, and non-interacting (see Figure 15).

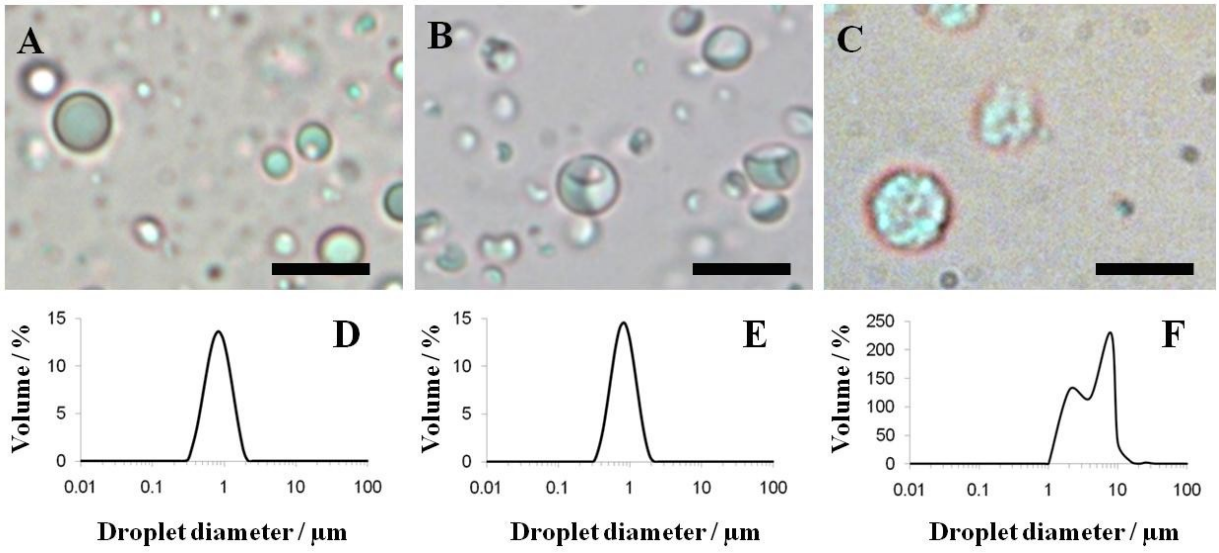

Figure 15. Light micrographs of (a) initial branched co-polymer stabilised emulsion droplets, (b) encapsulated droplets following base-catalysed self-condensation of (a) and (c) hollow capsules following flushing of (b) with ethanol. Scale bars represent 5 µm. (d-f) Droplet size distributions of (a-c), respectively. Note: Distribution in (f) is calculated manually from measuring diameters of 521 dried capsules from light micrographs. Reproduced with permission from ref. 3.

Free silanol residues undergo self-condensation to produce inorganic cross-linked networks in the presence of a base catalyst (see Figure 2). Triethylamine was added to a stirred emulsion dispersion (Φ_{oil} 0.5) to initiate the cross-linking of the branched co-polymer stabilised droplets. Light microscopy revealed low levels of inter-droplet cross-linking events between silanol residues on different droplets despite the presence of the PEGMA steric stabilisation (see Figure 16). Thus the droplets were diluted with water and cross-linked in a more dilute regime (~Φ_{oil} 0.03) and under these conditions no evidence of inter-droplet cross-linking was observed.

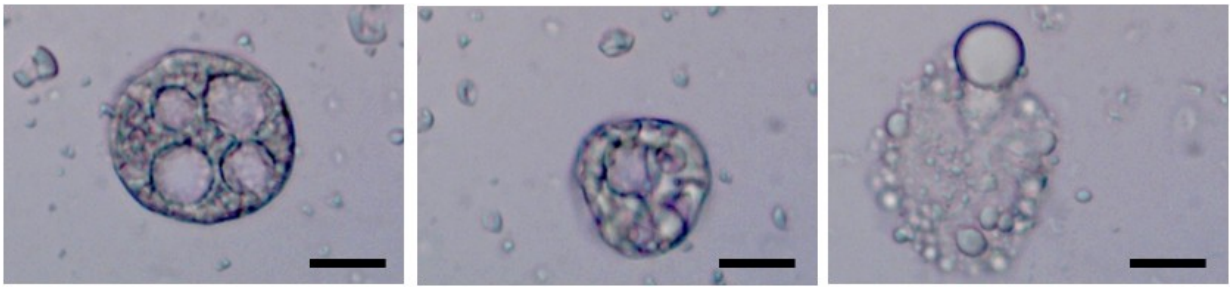

Figure 16. Light micrographs of cross-linked branched co-polymer-stabilised droplets performed at high concentration (Φ_{oil} 0.5). Note presence of droplet aggregation due to inter-droplet covalent cross-links. Scale bars represent 5 μm. Reproduced with permission from ref. 3.

As illustrated in Figure 15.b and Figure 17, light microscopy showed that the droplets became less spherical following cross-linking which implies that the network of covalent bonds that is formed induces a compaction of the sheath around the droplet periphery[11] or a change in osmotic pressure between the disperse and continuous phases.[12] No oil evolution was observed during this process and laser diffraction revealed near-identical droplet size distribution chromatograms before and after cross-linking (0.80 μm, compared to the 0.82 μm for the uncross-linked droplets, Figure 15.d, and Figure 15.e, respectively).

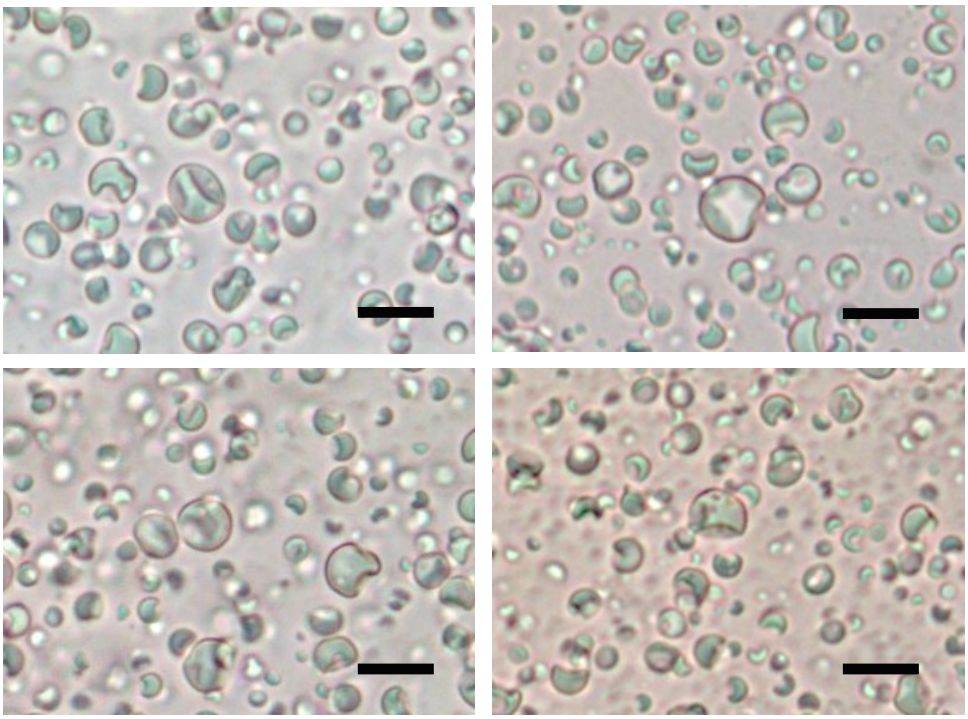

Figure 17. A collective of light micrographs of P6 stabilised cross-linked emulsion droplets. Scale bars represent 3 µm.

Cross-linking experiments were attempted with emulsions stabilised with the less efficient linear co-polymer analogue, P15. Some successful capsule formation was observed and the reactive linear co-polymer was chemically cross-linked around the initial droplet template (Figure 14), however the unavoidable destabilisation of the initial uncross-linked droplets produced inconsistent capsule sizes between batches and liberated oil was also observed over longer timeframes.

3.3.6. Efficiency of polymer-adsorption and cross-linking

Initial light microscopy of the cross-linked droplets showed the presence of background material and it was hypothesised that this material may be unadsorbed PEGMA/TMSPMA branched co-polymer that had cross-linked within the aqueous phase, which is not adsorbed

to the droplet surface. Since the reactive co-polymer surfactant was initially located within the internal oil droplet phase, the contribution of unselectively cross-linked material in the continuous aqueous phase should be negligible. Nevertheless, following initial emulsification the droplets were cleaned by repeat centrifugation and redispersion cycles (as described in 3.2.5.2; Washing of emulsions) using fresh distilled water to ensure that only branched co-polymer present within the system was located at the droplet interface or within the oil droplet. Following cross-linking under identical conditions the presence of background material in light microscopy images was significantly reduced. Centrifugation of emulsion droplets without destabilisation (as evidenced by laser diffraction measurements after each washing, shown in Figure 18, is further supported by the high interfacial stabilisation provided by this class of branched co-polymer emulsifier. However, as seen in Figure 18, the large majority of droplets in all samples fall under a single peak but a small secondary peak is shown for the measurement after homogenisation and after wash 1. This is hypothesised as free unadsorbed polymer that is washed out with further repeated washing cycles. However, the existence of this bimodal droplet distribution could also be due to minor variations in emulsion preparation such as homogenisation times and speeds. It is seen throughout this thesis that both unimodal and bimodal distributions are obtained even when emulsions are produced under the same conditions.

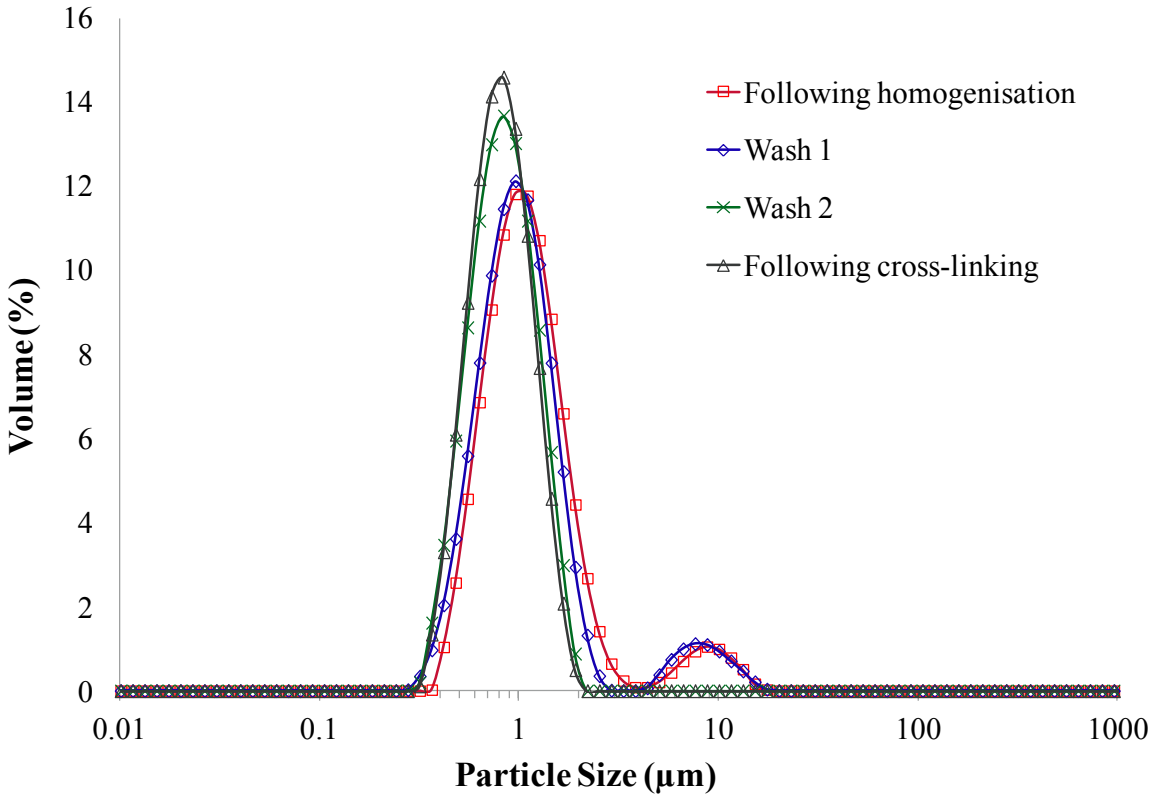

Figure 18. Overlaid laser diffraction chromatograms of the branched co-polymer stabilised emulsion droplets after each centrifugation/redispersion cycle. Note close overlay of the predominant peak which implies no destabilisation occurs under these relatively harsh conditions.

3.3.7. Formation of hollow capsules by solvent flushing

Formation of hollow inorganic-organic hybrid capsules was then attempted by flushing the cross-linked droplets with ethanol, a mutually good solvent for both water and cineole. Drop-wise addition of ethanol with stirring initially showed no visual change to the dispersion which remained turbid and white. However, the dispersion turned transparent as the ethanol entered the capsule cores, solubilised the cineole and reduced the effective refractive index difference within the dispersion (Figure 19).

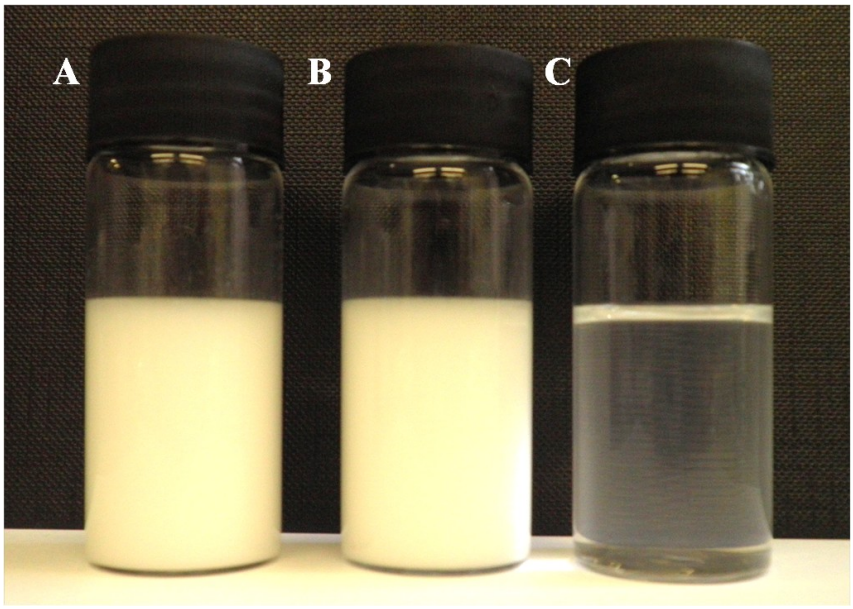

Figure 19. Digital image of branched co-polymer stabilised (a) uncross-linked and (b) cross-linked emulsions. (c) On addition of EtOH, which is mutually miscible with both the internal and external phases, the emulsion dispersion became transparent.

Once the entire solution had turned transparent, a slightly blue tinge to the resulting solution was evident which confirmed the presence of structures capable of scattering light (Figure 19.c). Light microscopy of a dried sample of this transparent solution revealed the presence of collapsed, but structurally intact, capsules or sacks similar to those observed in layer-by-layer approaches (Figure 15.c). Ethanol addition to uncross-linked droplets resulted in the emulsion breaking due to solubilisation which confirmed that the self-condensation step was integral to stable capsule formation. The ethanol-flushed capsules scattered insufficiently to allow the sizes to be determined by laser diffraction, however manual sizing of 521 individual dried capsules by light microscopy revealed diameter distributions which were larger (~1-10 μm) than those recorded in solution. Presumably the discrepancy was due to the inherent resolution limits of light microscopy, preventing the detection of smaller droplets and by the flattening of the capsules on the slide in their dry state (Figure 15.f).

3.3.8. Physical properties of the capsule shells

The hybrid polymer capsules showed closer structural similarities to cross-linked polymer vesicles[13] than reported examples of templated emulsion droplets using small molecule alkoxysilanes.[14] Increasing the concentration of the surfactant employed above the levels reported in this thesis merely changes the average droplet size[13b] whereas, in the case of the small molecule deposition approach, shell thicknesses can be controlled by the concentration of cross-linking agent employed e.g. TEOS.[1e]

Hollow inorganic-organic hybrid capsules were formed by flushing a cross-linked P6 stabilised emulsion, with ethanol as per 3.2.6.2; Hollow capsule formation. The resulting flushed capsule dispersion was dried by supercritical fluid drying (see Chapter 2; Analytical techniques applicable to this thesis), through liquid-gas exchange at critical point by Critical Point Drying (CPD) in order to maintain the structural integrity of the capsules.

Figure 20 shows a P6-hybrid capsule, which has retained its spherical morphology. The rough surface of the capsules is consistent with the presence of a cross-linked matrix of silica on the surface, and may be attributed to the branched architecture of the co-polymer; this could also be an attribute of the gold coating used to image the capsules. The bulky surface can be attributed to the long hydrophilic PEGMA chains.

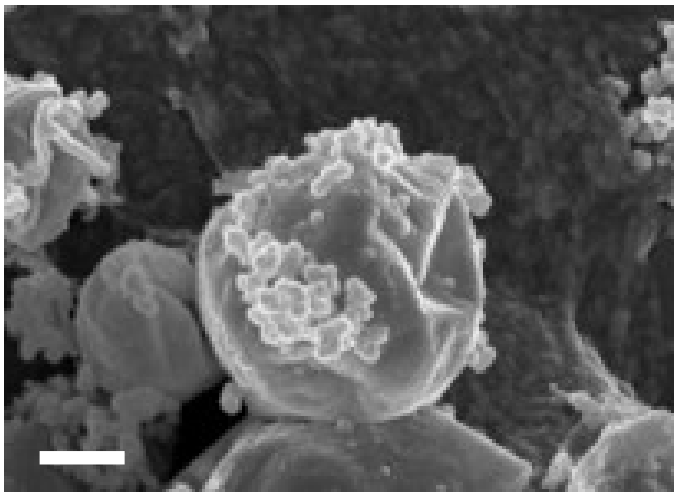

Figure 20. Scanning electron micrograph of a P6-based hybrid capsule dried by supercritical fluid drying. Scale bars represent 2 μm.

Capsules were forcibly broken, however this was difficult due to the tough elastic nature of the co-polymer shell. Also due to this, supercritical drying was not fully successful in all cases with some flattened biconcave structures evident. Scanning electron microscopy of ruptured capsules (see Figure 21) indicated that there is a range of shell thicknesses from 38.5 nm to 53.8 nm. Equivalent branched co-polymer nanoparticles, as described by Weaver (2008),[5b] showed droplet diameters in dilute aqueous solution in the order 16-45 nm which is consistent with the typical membrane thicknesses observed in this thesis.

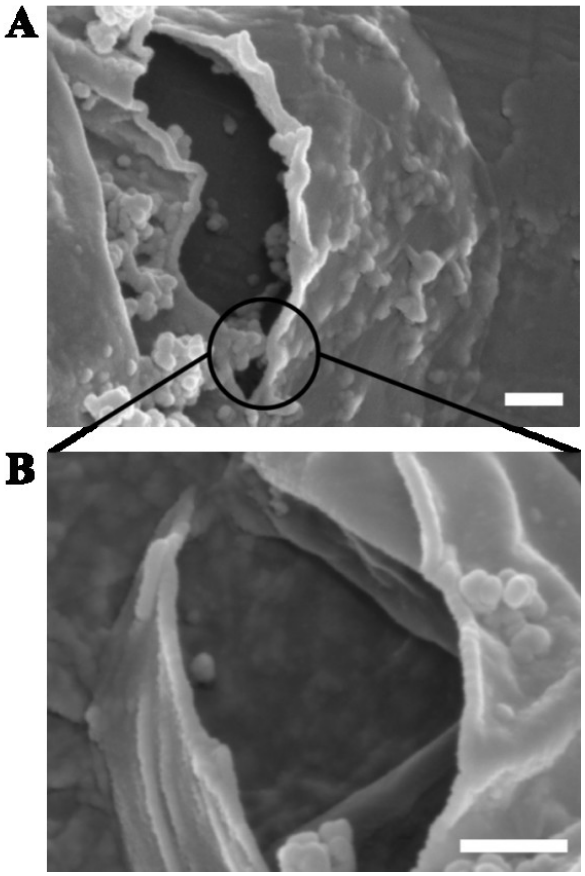

Figure 21. Scanning electron micrographs of (A) a ruptured siloxane capsule and (B), magnification of capsule shell edges on rotation. Scale bars represent 300 nm.

3.3.9. Lowest cross-linking monomer content

A study was made to find the lowest compositional amount of the cross-linking monomer, TMSPMA, required to create a stable emulsion and furthermore stable capsules. Branched co-polymers P11 – P13 (see Table 3) were synthesised *via* free radical polymerisation using the exact same protocol as described in section 3.2.1; Preparation of branched and linear co-polymers *via* free radical polymerisation, but the molar ratio of TMSPMA: PEGMA was varied.

Starting with the lowest amount of cross-linking monomer, P11 was used to create an emulsion in an identical manner as described in 3.2.5.1; Emulsion preparation. Emulsion droplet stability of the corresponding emulsion was monitored as a function of time (see Figure 22). Cross-linked emulsion droplets were formed, by addition of base to the dispersed diluted uncross-linked emulsion, and the stability of the newly cross-linked droplets was observed directly. Average droplet diameters for the uncross-linked and cross-linked emulsion droplets were recorded in Table 9. This process was repeated with further branched co-polymer surfactants, containing increasing amounts of TMSPMA, until the emulsion was efficiently stabilised by the branched co-polymer. This was apparent when there was little or no change in droplet diameter between the uncross-linked and cross-linked emulsion droplets. The lowest MFM molar ratio of cross-inking monomer able to capably stabilise an emulsion for the formation of capsules with consistent sizes was 80:20 (PEGMA: TMSPMA).

Table 9. Average droplet diameter change with varying molar ratio.

ID	Molar ratio (PEGMA : TMSPMA)	Uncross-linked average droplet diameter / µm	Cross-linked average droplet diameter / µm
P11	95 : 5	101.38	74.53
P12	85 : 15	0.86	1.28
P13	80 : 20	0.87	0.87

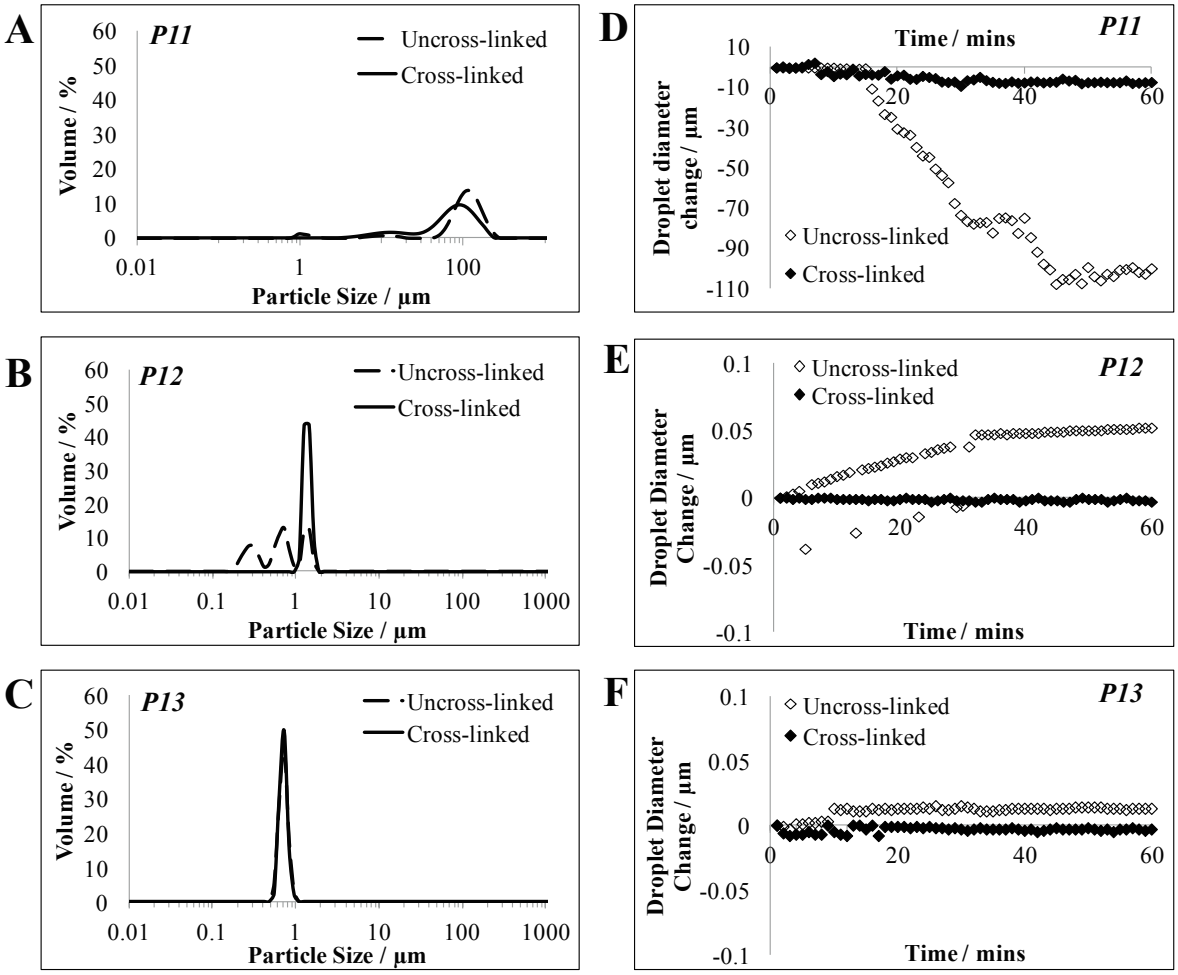

Figure 22. Droplet size distributions of uncross-linked and cross-linked emulsion droplets stabilised with (A) PE11, (B) PE12, and (C) PE13 branched co-polymer surfactants. (D-E) Corresponding normalised kinetic experiments of (A-C) monitoring the change in volume-averaged droplet diameters of the branched co-polymer stabilised uncross-linked and cross-linked droplets as a function of time.

3.3.10. Encapsulation of alternative actives

Having demonstrated the concept of the single-component capsule formation strategy it was decided to extend this to encapsulation of suitable actives. In principle, any material that is soluble in the oil phase and does not influence the emulsification process could be encapsulated using this technique. A hydrophobic fluorescent dialkyl carbocyanine dye, 3,3'-dioctadecyloxacarbocyanine perchlorate (DiO), was dissolved in the oil phase (0.05 w/v %

based on oil) and was encapsulated to provide a marker for confocal microscopy (see Figure 23). Cross-linking of these droplets resulted in a reduction of the fluorescence intensity of the dye. However, this returned on flushing the cross-linked droplets with ethanol to produce hollow capsules indicating a temporary pH quenching effect on addition of triethylamine. Despite its high ethanol solubility, confocal images clearly showed that DiO molecules are retained within the capsule internal void space which implies that either the pores-size of the network formed are smaller than the dye dimension in solution (~ 15 Å)[1] or that the dye is physically or chemically trapped on the capsule surface.

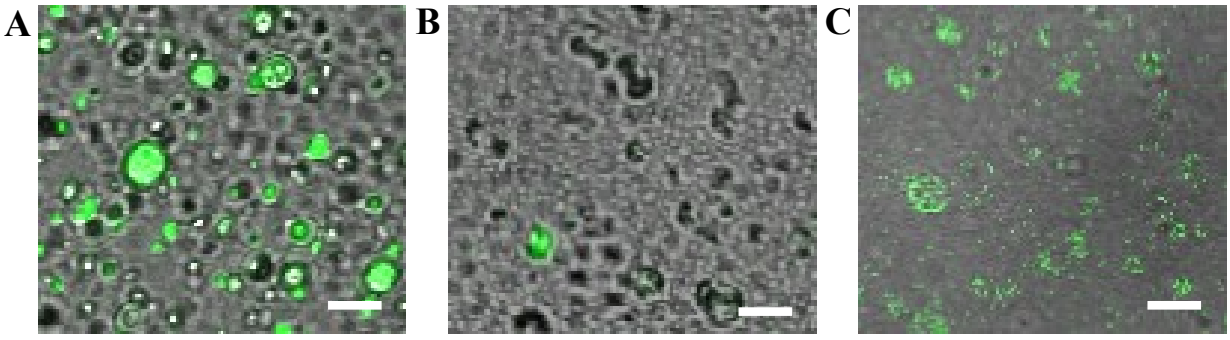

Figure 23. Confocal micrographs of (A) uncross-linked emulsion droplets containing 0.05 w/v % dioctadecyloxacarbocyanine perchlorate (DiO); (B) base catalysed cross-linked emulsion droplets where a temporary pH quenching effect lessens the fluorescence intensity of the dye on addition of TEA; (C) capsules following flushing (B) with EtOH. Scale bars represent 5 µm.

Having demonstrated that a small molecule hydrophobe could be efficiently encapsulated an alternative polymer or small molecule payloads were then investigated, see Table 10. A series of commercially obtained linear polymers were investigated and it was found that both polystyrene and poly(vinyl stearate) were good candidates due to their solubility in cineole,

[1] Estimated using ChemBio 3D software by MM2 energy minimisation.

and their immiscibility with EtOH. Poly(vinyl stearate) was favoured due to its high molecular weight (Mw = 90.0 kDa).

Table 10. Exploration of possible encapsulates.

		Soluble (Y/N)	Miscible (Y/N)		
Encapsulate	**Mw / kDa**	**Cineole**	**EtOH**	**THF**	**Acetone**
Poly(ethylene glycol) dimethyl ether	5.0	N	Y	Y	Y
Poly(ethylene glycol)	3.4	N	Y	Y	Y
Poly(vinyl alcohol)	22.0	N	N	N	N
Polystyrene	30.0	Y	Y	N	Y
Polycaprolactone	10.0	N	Y	Y	Y
Poly(acrylamide)	5.0	N	Y	Y	Y
Poly(vinyl pyrrolidone)	5.0	N	N	Y	Y
Poly(4-vinylpyridine)	0.11	N	Y	Y	Y
Poly(vinyl stearate)	90.0	Y	Y	N	Y
Poly(methyl methacrylate)	15.0	N	Y	Y	Y
Ibuprofen	0.23	N	N	Y	Y
Paracetamol	0.15	N	N	N	N

Poly(vinyl stearate) was dissolved in cineole at different concentrations up to 30 w/v % in the presence of the reactive branched co-polymer emulsifier, P6 (3.0 w/v %). The mixture was then emulsified as before to give stable droplets in all cases (Figure 24). The average droplet diameters were larger than for the unloaded droplets where cineole was the sole internal phase; 9.16 μm for the uncross-linked loaded emulsion droplets and 8.88 μm for the cross-linked loaded emulsion droplets respectively.

.

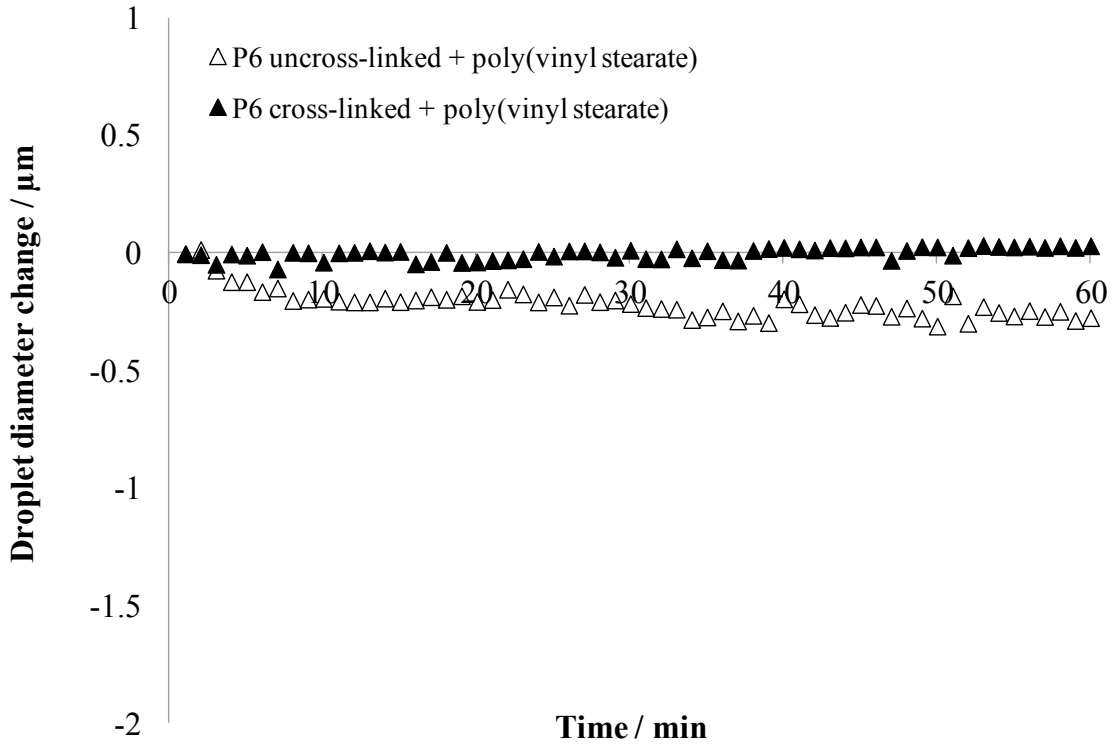

Figure 24. Normalised kinetic experiments monitoring the change in volume-averaged droplet diameters of P6 branched co-polymer stabilised uncross-linked and cross-linked emulsion droplets with a cineole oil phase containing 30 w/v% poly(vinyl stearate) as a function of time.

Table 11 compares the initial and final droplet diameters final uncross-linked and cross-linked emulsion droplet diameters of P6-stabilised emulsion droplets containing 30 w/v% poly(vinyl stearate).

Table 11. Comparison of initial and final uncross-linked and cross-linked emulsion droplet diameters of P6- stabilised emulsion droplets containing 30 w/v% poly(vinyl stearate) (PVS).

ID	Oil phase	Cross-linking	Initial droplet diameter / µm	Final droplet diameter / µm
P6	Cineole + 30 w/v% PVS	Uncross-linked	7.651	10.245
P6	Cineole + 30 w/v% PVS	Cross-linked	8.841	8.899

Cross-linking induced a change in the droplet morphologies similarly to that observed for the unloaded emulsions (Figure 25.b). Upon flushing the unloaded cross-linked droplets, a reduction in turbidity was observed previously. However, the loaded capsules remained more turbid than the corresponding unloaded capsules due to the presence of the hydrophobic polymer, poly(vinyl stearate), that remained insoluble in ethanol (Figure 25.c). Poly(vinyl stearate) was encapsulated at different loadings, and the turbidity of the loaded capsules varied with the concentration of poly(vinyl stearate) see (Figure 26).

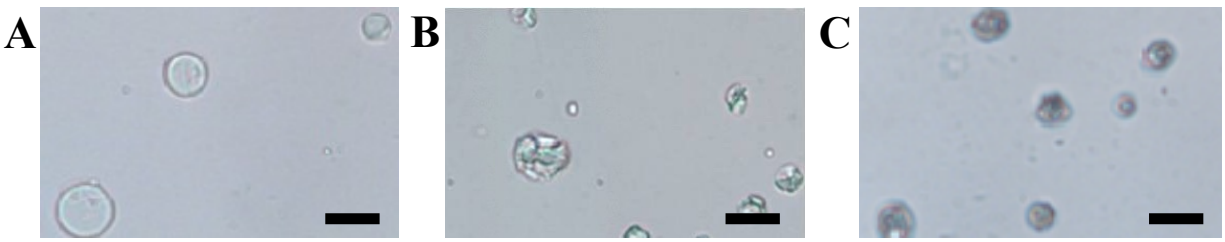

Figure 25. Optical micrographs of (A) polymer-loaded (poly(vinyl stearate), 30.0 w/v %) branched co-polymer-stabilised emulsion droplets; (B) polymer-loaded branched co-polymer stabilised cross-linked droplets following base-catalysed self-condensation of (A); (C) polymer-loaded branched co-polymer-stabilised capsules following flushing of (B) with ethanol. Scale bars represent 10 µm.

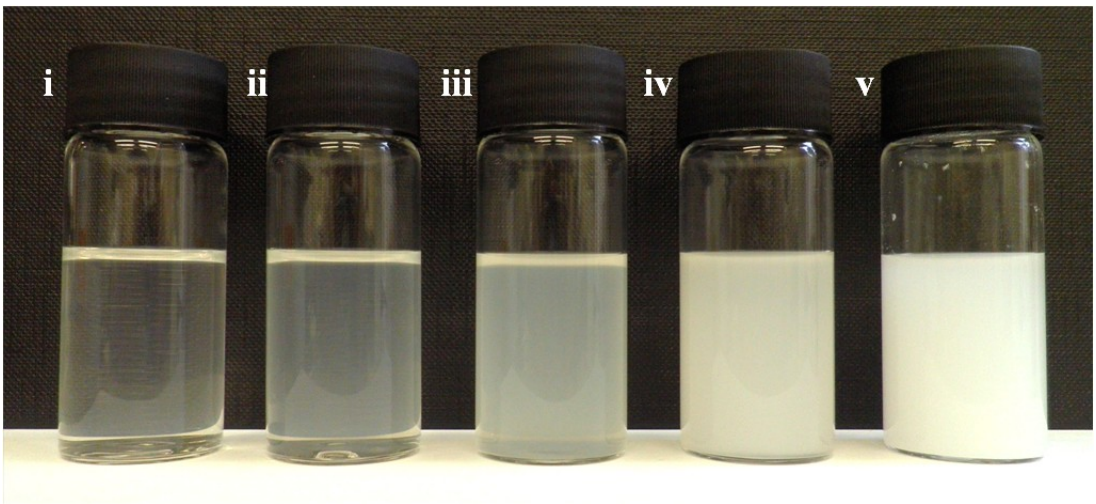

Figure 26. Digital images of the branched co-polymer cross-linked capsules following flushing at different poly(vinyl stearate) loadings. (i) 0 w/v % (unloaded), (ii) 0.5 w/v %, (iii) 2.0 w/v %, (iv) 10.0 w/v % and (v) 30.0 w/v %. Loadings are based on oil volume. Images were recorded at identical concentrations. Reproduced with permission from ref. 3.

Figure 27.a-b, shows comparative digital images of the loaded and unloaded droplets during the capsule formation process. The visible difference between the loaded and unloaded capsules was also visible in the optical micrographs which showed that loaded droplets transmitted less light and thus were observed as dark, as opposed to transparent, micron-sized structures (Figure 27.c-d). Scanning electron microscopy demonstrated that the unloaded capsules collapsed onto surfaces to give flattened biconcave-shaped structures when dried (Figure 27.e) whereas the loaded capsules retained predominantly spherical morphologies (Figure 27.f).

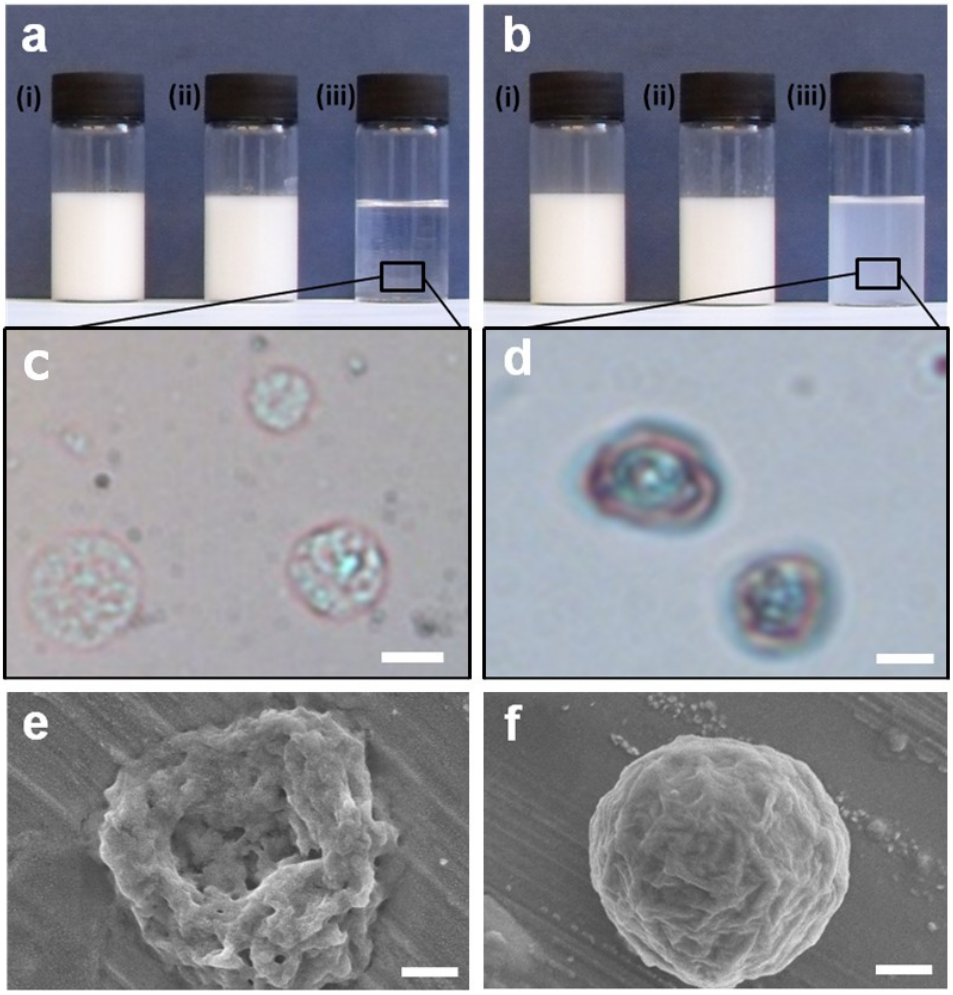

Figure 27. Digital images of the three-step preparation of (a) unloaded and (b) loaded emulsion droplets (i), encapsulated droplets (ii), and capsules (iii). Light micrographs of the flushed (c) unloaded and (d) loaded capsules. Scale bars represent 6 µm. Scanning electron micrographs of the flushed (e) unloaded and (f) loaded capsules. Scale bars represent 500 nm. Reproduced with permission from ref. 3.

3.3.11. Organic/inorganic composition of capsules

Thermal gravimetric analysis (TGA) (see experimental description in Chapter 2; Analysis techniques applicable to this thesis) of the excavated capsules showed that 26 w/w % of the excavated capsule structures comprised inorganic component as compared to the theoretical inorganic component of 24 w/w % based on ^{1}H NMR composition (Figure 28.a). Thermal analysis of identical capsules loaded with poly(vinyl stearate) showed a systematic reduction in the inorganic component of the overall structure as the poly(vinyl stearate) loading increased and this reduction was in close correlation to the predicted mass loss (Figure 28.b). These experiments, in conjunction with the systematic optical difference of the flushed capsules at different poly(vinyl stearate) loadings (see Figure 26), confirmed that predetermined concentrations of hydrophobic material can be readily encapsulated using this technique and that the encapsulation efficiencies appear to be high.

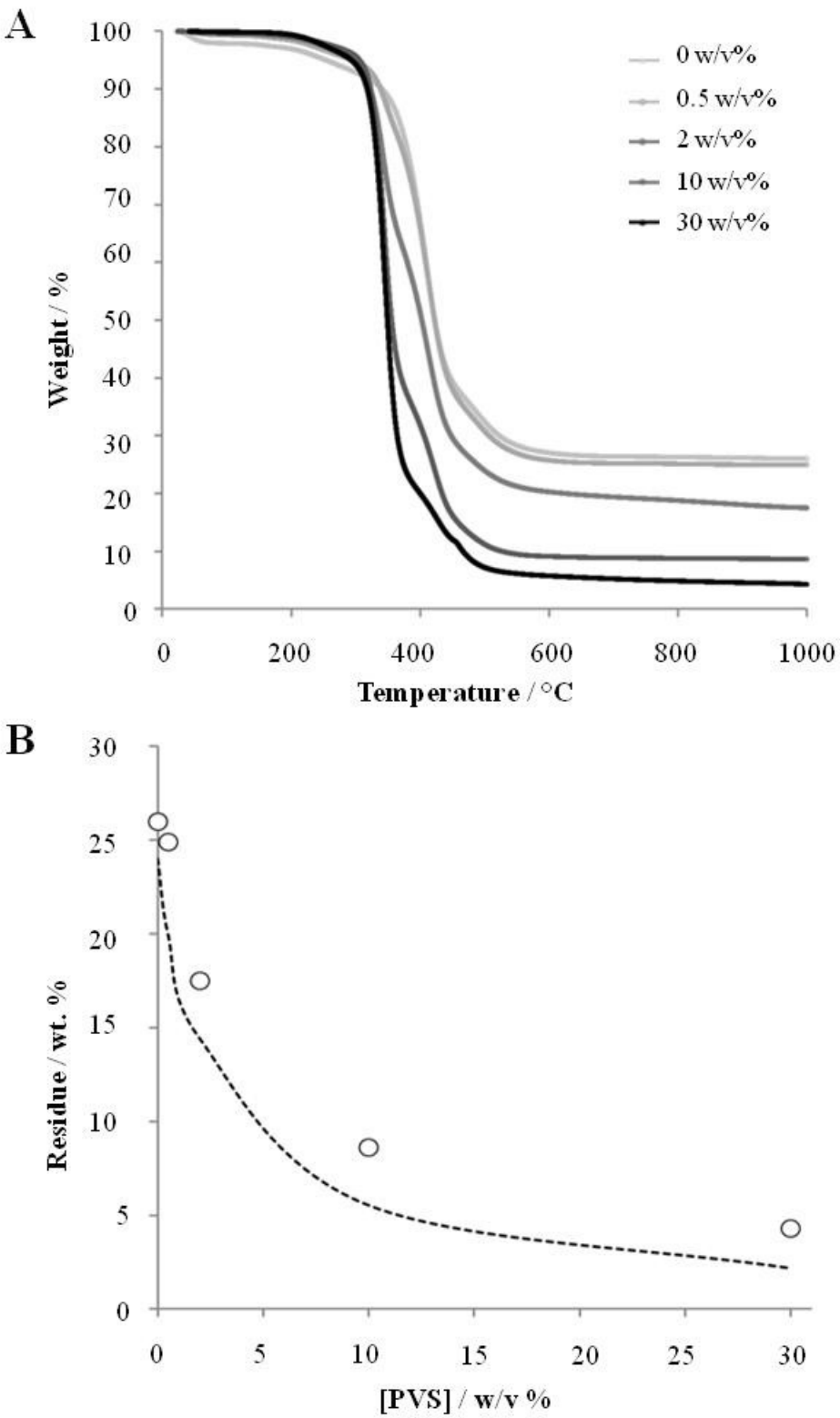

Figure 28. Gravimetric weight loss curves for the capsules and loaded capsules. (b) Graph to show the residual inorganic component of the capsules as a function of the degree of poly(vinyl stearate) loading following thermal treatment. Broken line represents theoretical weight loss. Reproduced with permission from ref. 3.

3.4. Conclusion

In summary, a one-component strategy for the preparation of inorganic-organic encapsulated droplets and hollow capsules has been developed. The process exploits, and relies on, both polymer architecture and composition – the branched architecture providing high droplet stabilities and efficient surfactancy with the compositions providing simultaneous properties of steric-stabilisation and cross-linking function. This approach alleviates the need for addition of multiple small molecule components and ensures that cross-linking is performed selectively at the oil-water interface. It has been demonstrated that high yielding encapsulation of different hydrophobic actives at up to 30 w/w % loading while showing that the initial emulsions, encapsulated droplets and hollow capsules retained their structural integrity. In principle, the diversity of compositions that can be accessed using the branched co-polymer synthetic route can provide a wealth of opportunity in terms of functionalising the capsule surfaces with pre-determined complex moieties and controlling membrane properties and function for tailored applications.

3.5. References

[1] aS. Schacht, Q. Huo, I. G. VoigtMartin, G. D. Stucky, F. Schuth, *Science* **1996**, *273*, 768-771; bG. Fornasieri, W. Badaire, R. Backov, O. Mondain-Monval, U. Zakri, P. Poulin, *Adv. Mater.* **2004**, *16*, 1094-+; cE. Kamio, S. Yonemura, T. Ono, H. Yoshizawa, *Langmuir* **2008**, *24*, 13287-13298; dX. W. Lou, L. A. Archer, Z. C. Yang, *Adv. Mater.* **2008**, *20*, 3987-4019; eC. I. Zoldesi, C. A. van Walree, A. Imhof, *Langmuir* **2006**, *22*, 4343-4352; fA. V. Jovanovic, R. S. Underhill, T. L. Bucholz, R. S. Duran, *Chem. Mater.***2005**, *17*, 3375-3383.

[2] aB. P. Binks, *Curr. Opin. Colloid Interface Sci.* **2003**, *7*, 21-41; bF. Leal-Calderon, V. Schmitt, *Curr. Opin. Colloid Interface Sci.* **2008**, *13*, 217-227.
[3] R. L. Harbron, T. O. McDonald, S. P. Rannard, P. H. Findlay, J. V. M. Weaver, *Chem. Commun.* **2012**, *48*, 1592-1594.
[4] aW. Meier, *Chem. Soc. Rev.* **2000**, *29*, 295-303; bG. Rethore, A. Pandit, *Small* **2010**, *6*, 488-498.
[5] aN. O'Brien, A. McKee, D. C. Sherrington, A. T. Slark, A. Titterton, *Polymer* **2000**, *41*, 6027-6031; bJ. V. M. Weaver, R. T. Williams, B. J. L. Royles, P. H. Findlay, A. I. Cooper, S. P. Rannard, *Soft Matter* **2008**, *4*, 985-992.
[6] aR. T. Woodward, R. A. Slater, S. Higgins, S. P. Rannard, A. I. Cooper, B. J. L. Royles, P. H. Findlay, J. V. M. Weaver, *Chem. Commun.* **2009**, 3554-3556; bJ. V. M. Weaver, S. P. Rannard, A. I. Cooper, *Angew. Chem.-Int. Edit.* **2009**, *48*, 2131-2134.
[7] P. A. Costello, I. K. Martin, A. T. Slark, D. C. Sherrington, A. Titterton, *Polymer* **2002**, *43*, 245-254.
[8] J. V. M. Weaver, D. J. Adams, *Soft Matter* **2012**, *6*, 2575–2582.
[9] aR. T. Woodward, L. Chen, D. J. Adams, J. V. M. Weaver, *J. Mater. Chem.* **2010**, *20*, 5228-5234; bR. T. Woodward, C. Hight, U. Yildiz, N. Schaeffer, E. M. Valliant, J. R. Jones, M. M. Stevens, J. V. M. Weaver, *Soft Matter* **2011**, *7*, 7560-7566; cR. T. Woodward, J. V. M. Weaver, *Polym.Chem.* **2011**, *2*, 403-410.
[10] J. V. M. Weaver, D. J. Adams, *Soft Matter* **2010**, *6*, 2575-2582.
[11] S. Sacanna, W. T. M. Irvine, P. M. Chaikin, D. J. Pine, *Nature* **2010**, *464*, 575-578.
[12] G. Bealle, J. Jestin, D. Carriere, *Soft Matter* **2011**, *7*, 1084-1089.
[13] aJ. Z. Du, Y. M. Chen, *Angew. Chem.-Int. Edit.* **2004**, *43*, 5084-5087; bJ. Z. Du, S. P. Armes, *J. Am. Chem. Soc.* **2005**, *127*, 12800-12801.
[14] aC. E. Fowler, D. Khushalani, S. Mann, *Chem. Commun.* **2001**, 2028-2029; bA. P. R. Johnston, B. J. Battersby, G. A. Lawrie, M. Trau, *Chem. Commun.* **2005**, 848-850.

CHAPTER 4

The role of branched co-polymer composition in controlling hybrid capsule surface functionality

(Publication arising from this Chapter: **"Controlling hybrid capsule surface functionality *via* branched co-polymer composition"**, R. L. Harbron, R. T. Woodward, S. Bertazzo, P. H. Findlay, J. V. M. Weaver, *Manuscript in preparation*, **2015**.)

List of figures

List of tables

4.1. Introduction

Developing design rules for controlled functional stimuli-responsive materials is an increasingly important research area with significant industrial applicability. Natural biological systems, such as protein folding and aggregation[1] that intricately exploit multi-responses with changing conditions,[2] display adaptable properties that are fervently emulated in materials science. Advanced synthetic materials with a number of properties such as self-assembly[3] and self-organisation[4] can also be used to create more complex assemblies such as supramolecular polymers.[5] These intermolecular mechanisms of self-assembly are characteristically non-covalent and generally reversible. Examples include hydrogen bonding,[6] electrostatic interactions,[7] hydrophobic interactions,[8] and π-π stacking.[9] Non-covalent interactions are favoured because of their environmental adaptability, for example the varied strength of hydrogen bonding along a protein backbone.[10]

Polymeric materials are ever-more frequently reported as stimuli-responsive. The responsive polymer may adapt its properties in accordance with the environment; examples of stimuli include pH,[11] temperature,[12] gases,[13] magnetic fields,[14] and light.[15] Reasoned compositional design of polymeric materials allows for the incorporation of functionality into the product on synthesis. Therefore, functional groups become a physical property of the polymer product, which are externally responsive to a stimulus. Linear block co-polymers

based on water soluble tertiary amine methacrylates were reported to undergo self-assembly in response to pH[16] and temperature.[17] Many water soluble polymers show a temperature-based solubility response in water. In 2001, Bütün, Armes, and Billingham,[18] reported a temperature-based solubility response in water of poly (2-(N-morpholino)ethyl methacrylate) (poly(MEMA)). Poly(MEMA) is a weak base and is water soluble at both neutral and acidic pH at ambient temperature, however at elevated temperatures (35 °C – 53 °C, depending on molecular weight) the polymer precipitates from neutral or basic aqueous solutions (see Figure 1). At elevated temperatures, the thermal energy breaks the extensive hydrogen bonding network with the water and the polymer precipitates. This is a fully reversible process. Temperature-responsive behaviour is because of a so called upper critical solution temperature and lower critical solution temperature (UCST and LCST respectively) due to the enthalpy and entropy of mixing within the aqueous solvent.

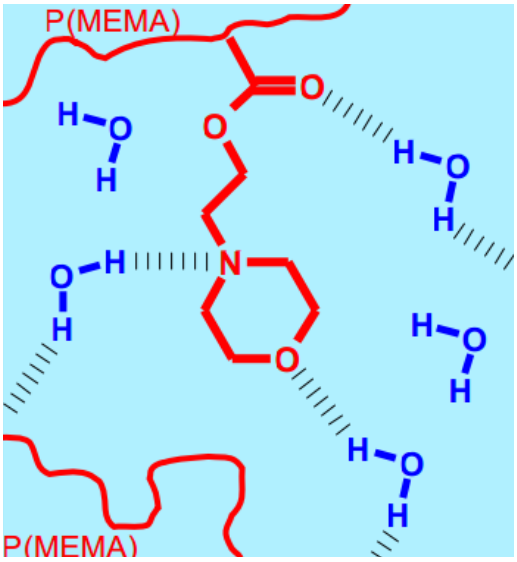

Figure 1. Lower critical temperature solubility (LCST) behaviour of poly(MEMA). Reprinted and adapted with permission from ref. 18.

This effect is utilised for a number of applications including altering the wettability of biological surfaces and drug delivery.[19] A widely studied macromolecule in this field in poly(N-isopropyl acrylamide) (poly(NIPAAm)) which possesses an LCST of 32 ^{o}C and is therefore applicable to many biological systems. It is a common strategy to adjust the LCST of a polymer by incorporating hydrophilic or hydrophobic moieties into the polymer composition such as poly(NIPAAm).[20] Poly(NIPAAm) is frequently used as a thermo-sensitive hydrogel which displays drug-release properties *in vivo* with homeostatic temperature fluctuation.

In 2008, Weaver, Williams, Royles, Findlay, Cooper, and Rannard,[21] reported a new class of responsive branched co-polymers. By selecting a pH-responsive co-monomer and a hydrophilic macromonomer, pH-responsive branched amphiphilic co-polymers were synthesised using poly(ethylene glycol) methacrylate (PEGMA), 2-(diethylamino)ethyl methacrylate (DEAEMA), ethylene glycol dimethacrylate (EGDMA) as the branching agent , 1-dodecanethiol (DDT) or 1-thioglycerol (TG) as the chain transfer agent using 2, 2'-azobis (isobutyronitrile) (AIBN) initiator *via* a thiol-regulated radical polymerisation which is also used to synthesise the majority of co-polymers in this thesis (as discussed in Chapter 1; Introduction).[22] Under acidic-aqueous conditions, at pH 2, these co-polymers were hydrophilic and hydrated due to protonation of the DEAEMA and PEGMA residues. On increasing the pH to 10, the DEAEMA residues deprotonate, becoming more hydrophobic, forming compact structures (see Figure 2). These branched architectures, as opposed to linear structures, could form unimolecular micelle-like structures unlike linear systems that tend to

disassociate. Additionally the ability to control the hydrophilicity or hydrophobicity of the chain-ends through choice of chain transfer agent provides a useful means to adapt their responsive nature.

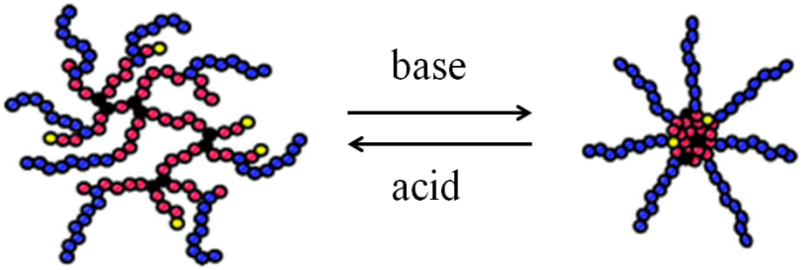

Figure 2. Schematic of the aqueous solution behaviour of pH-responsive branched co-polymer nanoparticles. Reproduced with permission from ref. 21.

Weaver *et al.* (2009)[11b] demonstrated that incredibly stable emulsion droplets could be formed with controlled surface chemistry. Co-polymers of PEGMA, DEAEMA and EGDMA or poly(ethylene glycol) dimethacrylate (PEGDMA) as the branching agents with a choice of CTAs (DDT, TG, and mercaptopropionic acid (MPA)) were prepared and used to prepare responsive emulsions with n-dodecane and water. It was observed that the responsive amphiphilic nature of the co-polymers could be tuned by choice of CTA, and therefore the chain ends of the co-polymers, to give rise to stable, responsive emulsions; this was particularly true for the long-chain brancher PEGDMA. Inherently stable emulsions could be prepared at high pH which could be triggered to fully demulsify upon reducing the pH of the solution below the pKa of the weakly basic unit.

Weaver, Rannard, and Cooper (2009)[23] then extended this work to form higher order structures through the interaction of pH-responsive branched co-polymer emulsifiers. Branched co-polymers were prepared using methacrylic acid (MAA), PEGMA, the branching agent EGDMA, and DDT as the CTA *via* thiol-regulated radical polymerisation.[21-22] The co-polymers were used to prepare oil-in-water emulsions of n-dodecane in water at high pH where the MAA units were fully deprotonated. These emulsions were extremely stable when compared to equivalent linear systems due to the strong hydrophobic interaction of the multiple polymer end groups adsorbed onto the oil phase of the emulsion afforded by the architecture of the branched co-polymer system, and also by the charged periphery of the droplet due to the charged MMA units in the polymer. When the pH of the emulsions was dropped to below the pKa of the carboxylic acid unit, hydrogen-bonding between the protonated carboxylic acid unit and the ether in the PEGMA moiety occurred thus associating the emulsion droplets to form higher structures (see Figure 3).

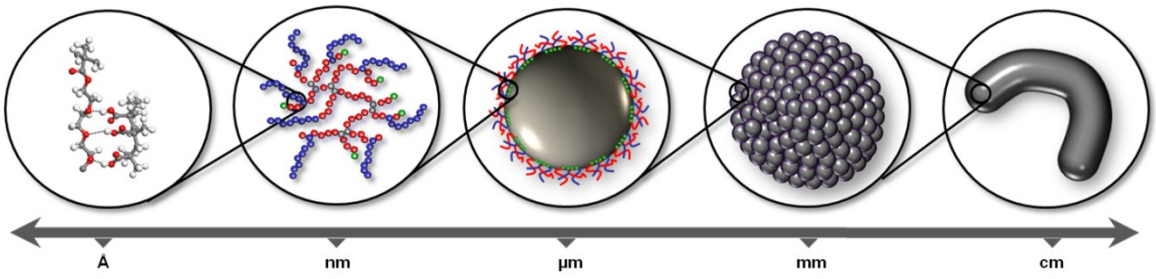

Figure 3. Schematic of reversible hierarchical emulsion droplet assembly. Reproduced and adapted with permission from ref. 23.

The stoichiometry of the carboxylic acid units to the ethylene ether groups was varied from 1:1 to 1:2 to elucidate the role of polymer composition giving fully associating inter-droplet

association, and intra-droplet association respectively (see Figure 4). This so-called emulsion engineering[23-24] showcased how responsive branched polymer emulsifiers could be used to associate upon external stimuli to form stable, robust systems.

In this chapter, the co-polymers have been tailored to create capsules (the formation strategy of such is as described in Chapter 3) with controllable responsive surface behaviour. This was achieved through judicious design of amphiphilic multi-purpose branched co-polymers capable of emulsification, cross-linking, and furthermore responding to pH-stimuli. These reactive amphiphilic co-polymers formed stable oil-in-water emulsion droplets with cineole on homogenisation with basic water at pH 10. Electrostatic repulsion occurred at pH 10 between the hydrophilic anionic MAA residues present on the droplet surfaces allowing the formation of discrete emulsions droplets that could then be used as templates for capsule formation (as described in Chapter 3). A covalently cross-linked inorganic shell was formed on the droplet peripheries around the internal oil phase.

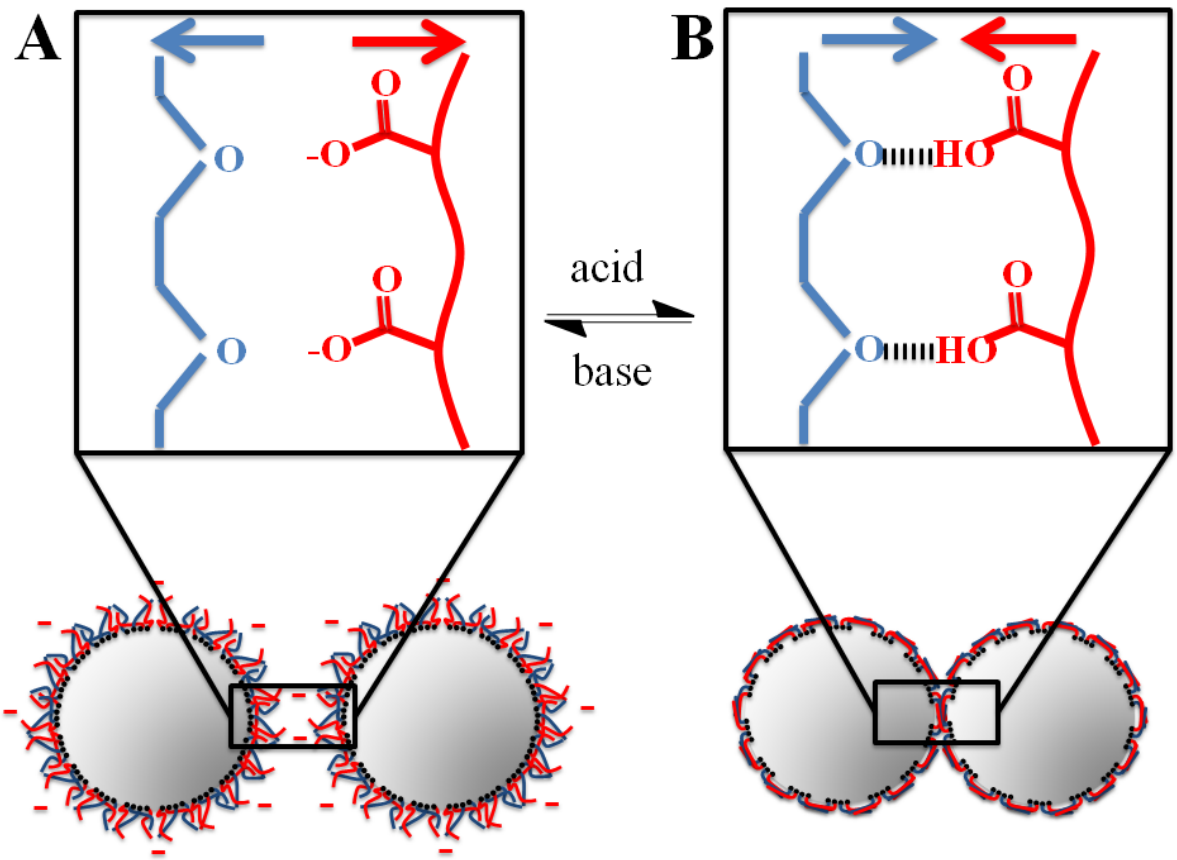

Figure 4. Schematic of the reversible transition from (A) dispersed fluid emulsion droplets to (B) aggregated engineered emulsion droplet association. Adapted with permission from ref. 24a.

Upon shell formation, the hydrophilic MAA chain ends were essentially trapped on the surface giving the resultant capsules an MAA-based pH-responsive surface. Capsule surface functionality was denoted, and therefore tuned, by the hydrophilic portion of the co-polymer surfactant. If desired, the internal oil phase could be flushed out with a mutually miscible solvent to give hollow pH-responsive capsules. The response of the formed capsules was investigated using a reversible pH-switch (see Figure 5). At high solution pH, the discrete capsules were dispersed due to electrostatic repulsion between the anionic MAA residues. On lowering the pH to 2, the MAA residues were protonated becoming more hydrophobic, and the capsules aggregated to reduce their surface interaction with water. The MAA residues

simultaneously formed dimers by hydrogen bonding between the acidic hydrogen and the carbonyl oxygen.

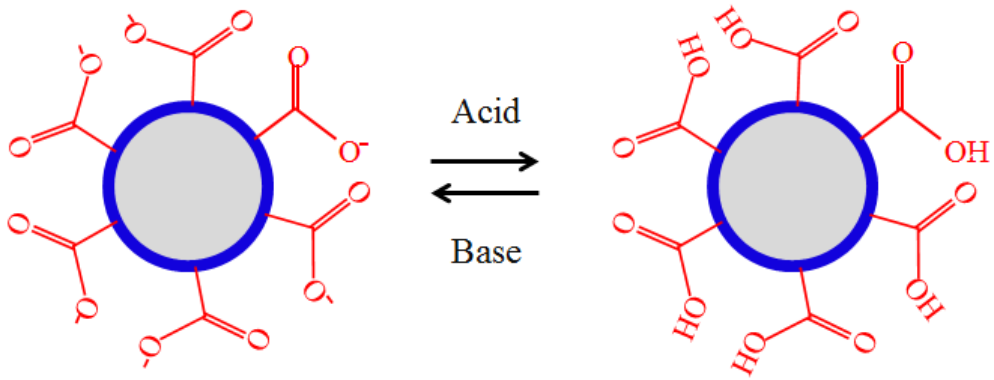

Figure 5. Schematic representation of the reversible responsive behaviour of pH-surface functionalised capsules at (A) high and (B) low solution pH. The blue line represents the cross-linked inorganic capsule shell.

4.2. Experimental

The pH-responsive co-polymers were synthesised by a one-step FRP route using a thiol-regulated polymerisation technique[21-22], as previously used and discussed in Chapter 3 and Chapter 1, where both a siloxane-based methacrylate monomer and a MAA co-monomer were incorporated to give capsule-forming function and pH-responsive functionality respectively. MAA functionality provided the ability to form multiple hydrogen bonds under acidic conditions. The resulting co-polymer was used as an emulsifier to form oil-in-water emulsions. The induction of homocross-linking of the siloxane units, following their hydrolysis during emulsification, produced a cross-linked inorganic sheath around the droplet. Hydrophilic chain ends of the pH-responsive co-monomer were trapped on the capsule surface during shell formation.

Equivalent branched and linear amphiphilic co-polymer analogues based on 3-(trimethoxysilyl)propyl methacrylate (TMSPMA) (capsule forming function) and MAA (pH-responsive functionality) were prepared. As in Chapter 3, both branched and linear analogues were compared to confirm the efficacy of branched co-polymer systems. During synthesis the use of a chain transfer agent (CTA), as selected through investigation in Chapter 3, reduced the final molecular weight of the polymer product. The chosen CTA, 1-dodecanethiol (DDT), provided multiple hydrophobic chain-ends for strong oil-droplet adsorption. Thus, the pre-designed, multifunctional co-polymer simultaneously provided steric stabilisation, self-cross-linking, pH-responsive function and hydrophobic chain ends, as represented in Figure 6.

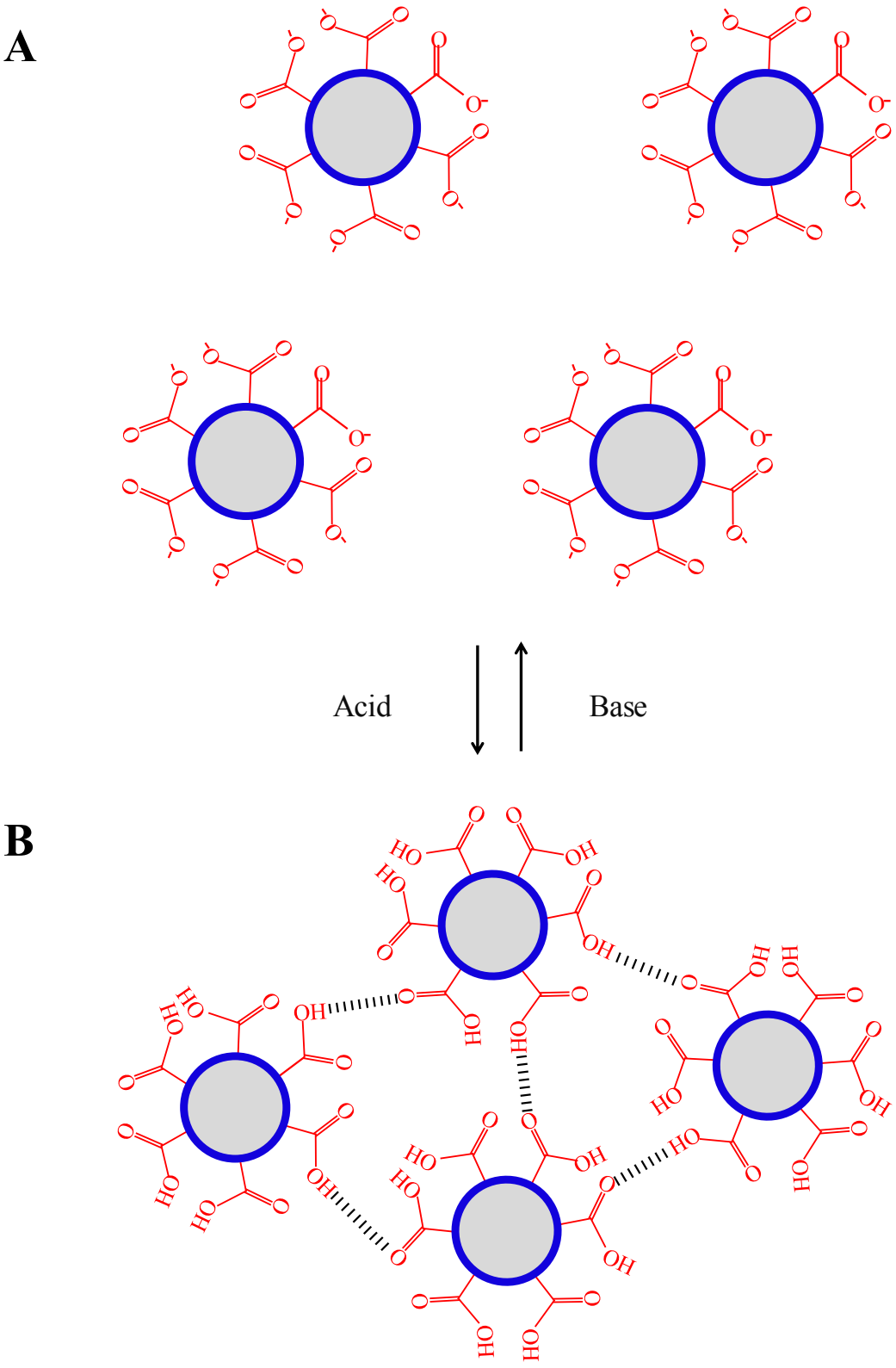

Figure 6. Schematic representation of the responsive behaviour of branched (P21-based) co-polymer capsules in response to pH-stimuli. (A) Cross-linked emulsion droplets are anionic and dispersed at high pH. (B) cross-linked emulsion droplets aggregate at low pH. The blue line represents the cross-linked capsule shell.

4.2.1. Representative preparation of $TMSPMA_x/MAA_y$ – $EGDMA_{10}$ – DDT_{10} branched co-polymers

In order to create these responsive co-polymers (see Table 1) as discussed within the introduction, the PEGMA content of P6 (see Chapter 3; Table 1) was substituted with MAA keeping the estimated stoichiometric ratio of hydrophilic ethylene oxide to carboxylic acid units approximately consistent, and also keeping the ratio of repeat units of hydrophilic to TMSPMA end groups roughly constant, as displayed in Figure 7.a-b.

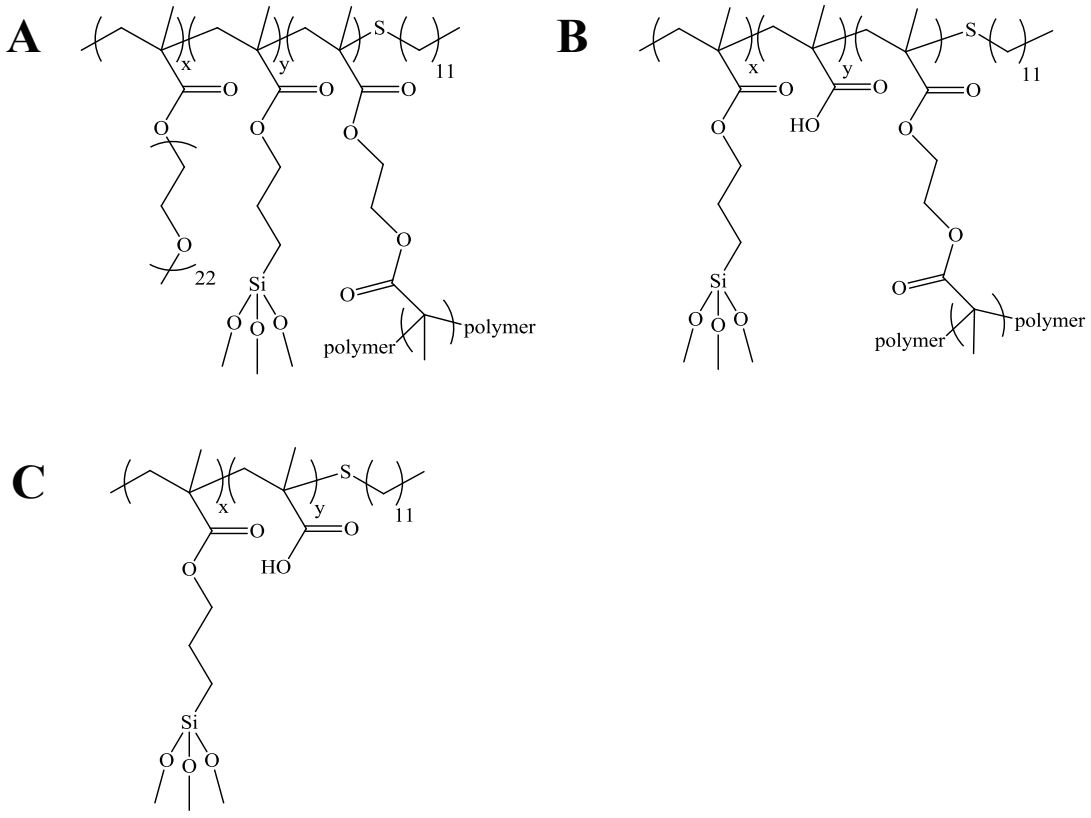

Figure 7. Structural representation of (A) P6, $PEGMA_5/TMSPMA_{95}$-$EGDMA_{10}$-DDT_{10}, (B) P21, $TMSPMA_{61}/MAA_{39}$-$EGDMA_{10}$-DDT_{10} and, (C) the equivalent linear co-polymer analogue P22, $TMSPMA_{61}/MAA_{39}$-DDT_2.

All polymers, branched and linear were prepared using the standard procedure detailed below, as shown by the preparation of branched and linear co-polymers, P6 and P15 respectively (see Chapter 3; Experimental).

4.2.1.1. Preparation of branched co-polymer; P21

In order to synthesise the responsive branched co-polymer P21, $TMSPMA_{61}/MAA_{39}$-$EGDMA_{10}$-$DDT_{10,}$ as represented in Figure 7.b, a mixture of TMSPMA (10.00 g, 40.27 mmol), MAA (2.22 g, 25.79 mmol), EGDMA (1.31 g, 6.61 mmol), and DDT (1.35 g, 6.60 mmol) was degassed with a nitrogen purge using a Schlenk line. Methanol (140 mL, anhydrous) was degassed separately with a nitrogen purge using a Schlenk line and added to the monomer mixture. After heating to 70 ^{o}C, the co-polymerisation was initiated by the addition of AIBN (148.7 mg, 0.91 mmol) and was stirred with heating for 48 hours. The ethanol was then removed by evaporation and the resulting co-polymers were stored under vacuum. No purification steps were required due to almost complete conversion; typically conversions in excess of 98% were achieved as determined by ^{1}H NMR spectroscopy. In order to synthesise co-polymers of varying composition (e.g. those listed in Table 1), the feed molar ratios of MAA to TMSPMA were adjusted, while the EGDMA and DDT molar ratios were kept unchanged. Linear analogues were also synthesised for comparison containing a small amount of DDT to emulate the chain ends present in the branched co-polymers. ^{1}H NMR spectroscopy was used to confirm the co-polymer composition, where the peaks have

been assigned (see Figure 8); however post-esterification of the polymer was required as described in 4.2.2. Esterification of the carboxylic acid units (from the MAA) was performed in order to gain full compositional ratios in ^{1}H NMR analysis. Size exclusion chromatography of the unesterified materials (see Table 2) was performed using a triple detection array (TD-GPC) (as discussed in Chapter 1; Introduction).

Example experimental calculations applicable to all polymers covered within this thesis are represented in Chapter 3; Synthesis of emulsion-templated hybrid inorganic–organic polymer capsules using a branched co-polymer surfactant for hydrophobic active encapsulation.

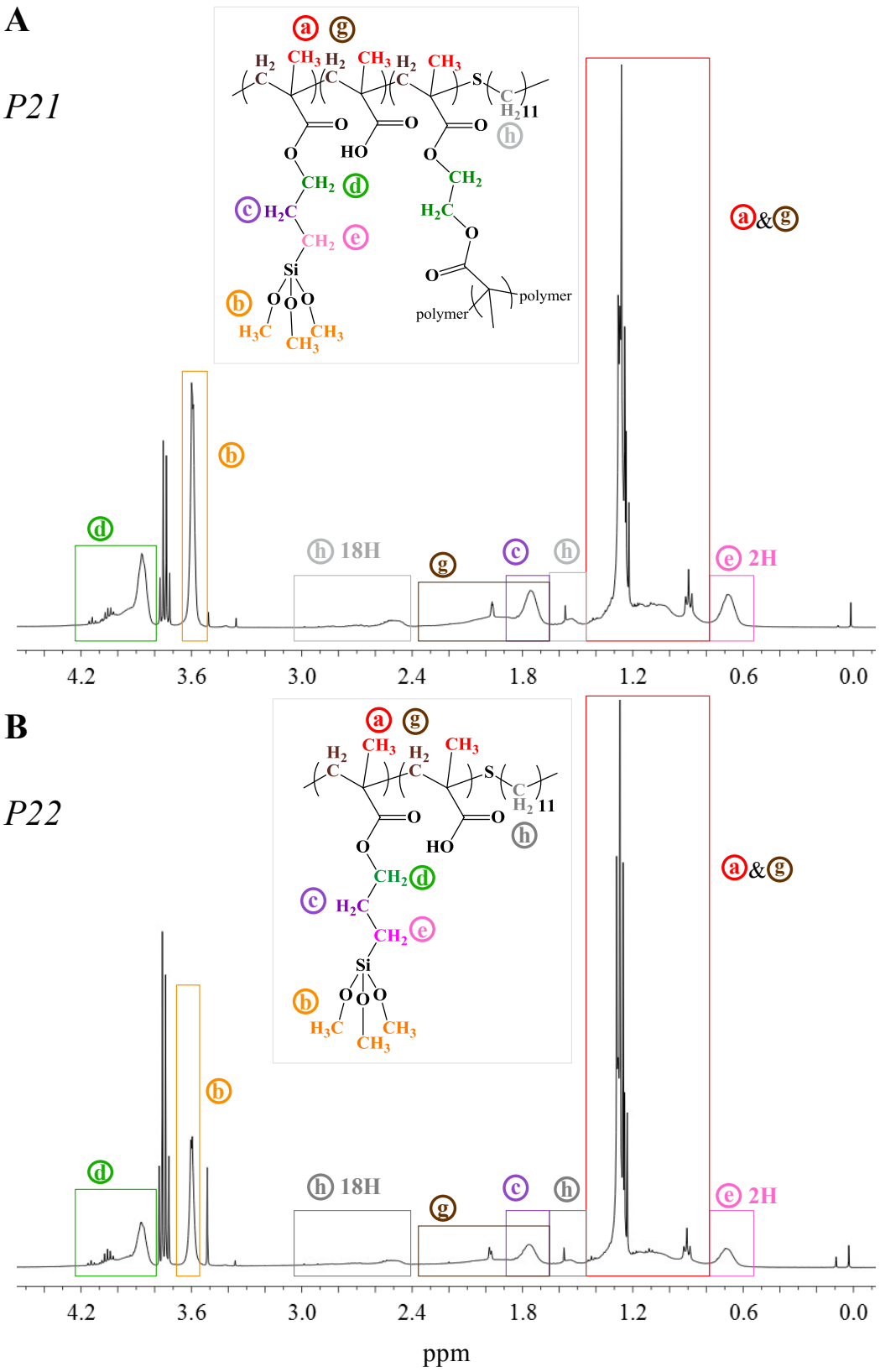

Figure 8. Peak assigned ^{1}H ($CDCl_3$) NMR spectra of (A) P21, $TMSPMA_{63.6}/MAA_{39.8}$-$EGDMA_{9.5}$-$DDT_{7.1}$ and (B) P22, $TMSPMA_{60.3}/MAA_{33.4}$-$DDT_{2.2}$.

4.2.2. Esterification of methacrylic acid containing polymers

The co-polymer surfactants containing MAA were esterified to give the corresponding methyl ester in order to gain full compositional ratios in ^{1}H NMR analysis as the methyl-group of the esterified acid moiety can be easily identified; additionally following this conversion the GPC analysis could be obtained in an organic solvent eluent, thereby alleviating any polymer association typically seen in aqueous chromatography.

4.2.2.1. Typical esterification procedure

The polymer to be esterified (50 mg) was placed in a glass vial, to which MeOH (0.2 mL) was added. The resulting solution was then agitated by hand until a homogeneous solution was formed, after which toluene (0.2 mL) was added, and the vial was again agitated to obtain a homogeneous solution. TMS-diazomethane was then added drop-wise until a yellow colour was just apparent that did not become colourless upon agitation.[25] The resulting solutions were dried *via* evaporation and were placed in a vacuum oven for 30 minutes. ^{1}H NMR spectroscopy was used to confirm the co-polymer composition by comparing the methyl ester peak of MAA to peaks corresponding to TMSPMA residues as shown in Figure 9.

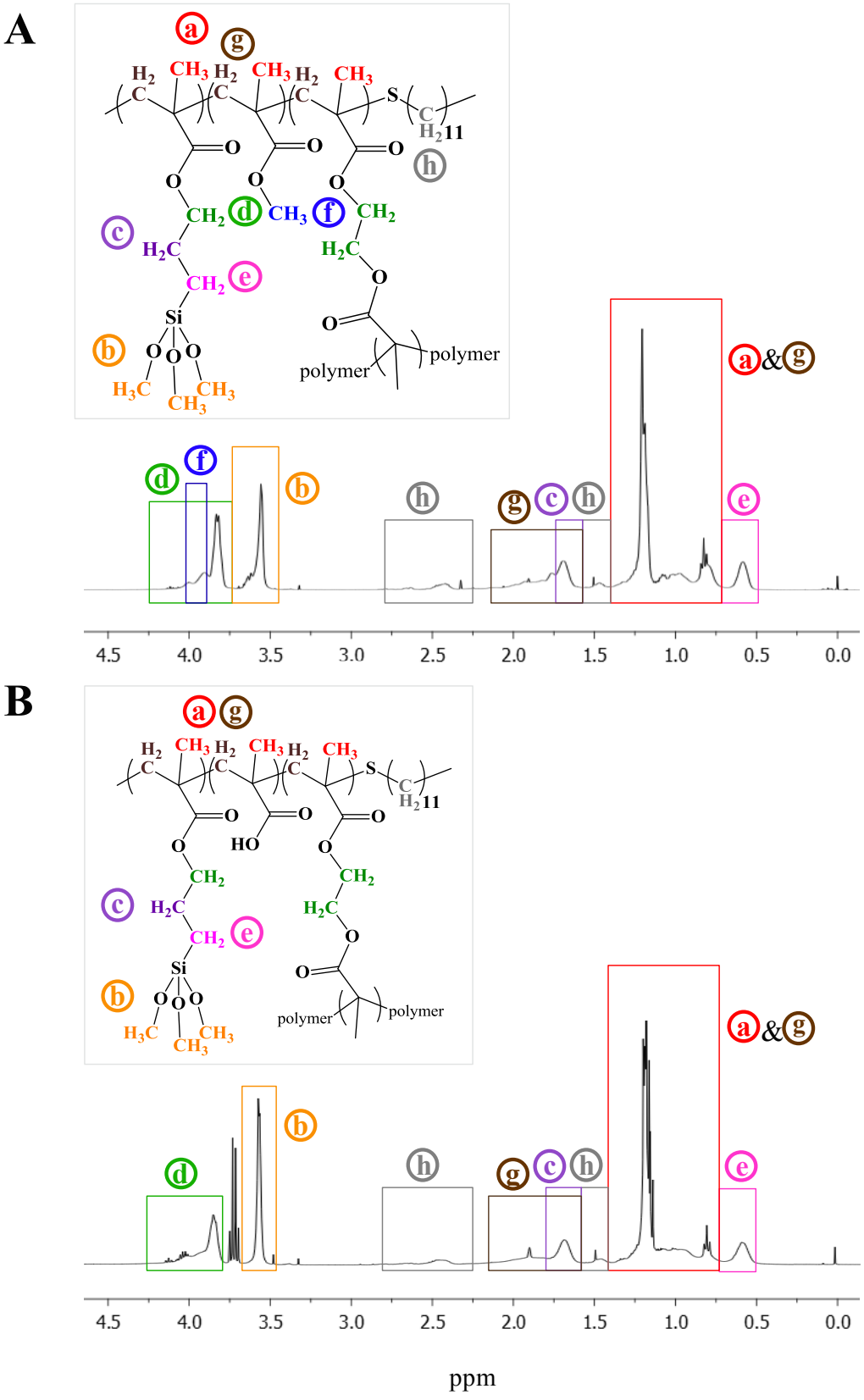

Figure 9. Stacked ^{1}H NMR spectra of (A) unesterified P21 and (B) esterified P21 containing methylated MAA groups.

4.2.3. Emulsion synthetic processes

4.2.3.1. Emulsion preparation

A mixture of co-polymer in oil (3.0 w/v %, 3 mL) was prepared and an equal volume of distilled water at pH 10 (adjusted by the addition of NaOH (1 M)) was added. This biphasic mixture was homogenised at 24,000 rpm for 2 minutes using a T25 digital Ultra-Turrax. Following homogenisation, the emulsions were left to equilibrate for 1 hour before characterisation.

4.2.3.2. Washing of the emulsions

The emulsions were washed gently to remove any un-adsorbed polymer by centrifugation using an Eppendorf 5804R (this apparatus was subsequently used for all further centrifugations) (2,800 rpm, 60 minutes). The resulting supernatant was discarded. The polymer-stabilised emulsion droplets were redispersed in distilled water at pH 10 (adjusted by the addition of NaOH (1 M)). This process was repeated three times in total.

4.2.3.3. Emulsions with encapsulated guest molecules

A number of emulsions were produced with guest molecules encapsulated within the oil droplets. Guest molecules include Oil Red, Oil Blue, DiO, and poly(vinyl stearate) (PVS) (Mw 90.0 kDa). All emulsions were prepared as per 4.2.3.1, where guest molecules were always dissolved in the oil phase before homogenisation. Dyes were always added at 0.1 w/v % unless stated otherwise, DiO at 0.05 w/v % and PVS at a maximum of 30 w/v %.

4.2.4. Capsule synthetic processes

4.2.4.1. Cross-linked emulsion and capsule fabrication

Emulsions were prepared identically as per 4.2.3.1; Emulsion preparation, and gently washed (see 4.2.3.2; Washing of the emulsions). 1 mL creamed emulsion was redispersed in 30 mL distilled water at pH 10 (adjusted by the addition of NaOH (1 M)) with gentle stirring. 1 mL TEA was added to the dilute emulsion solution whilst stirring and left for 1 hour.

4.2.4.2. Hollow capsule formation

Excavated, hollow cross-linked capsules were formed by flushing the cross-linked emulsions with ethanol to remove the internal and continuous phases.

4.2.4.3. Washing of the capsules

In order to wash the capsules to remove any unadsorbed polymer, the cross-linked emulsions were flushed with ethanol as per 4.2.4.2; Hollow capsule formation. The resulting solutions were centrifuged (2,800 rpm, 60 mins) and the resulting supernatant was discarded. The capsules were redispersed in ethanol after each washing. This process was repeated three times in total.

4.2.5. Emulsion droplet- and capsule- structure formation synthetic processes

4.2.5.1. Emulsion droplet structure formation

Emulsions were prepared identically as per 4.2.3.1; Emulsion preparation, and cross-linked as per 4.2.4.1; Cross-linked emulsion and capsule fabrication. The co-polymer stabilised

cineole-in-water cross-linked emulsion was creamed *via* centrifugation at 2,800 rpm, for 60 minutes. A sample of the creamed emulsion layer was pipetted into a template, or mould, and HCl (0.5 M, 75 μL) was added to the top of the sample. This system was then left for 2 hours to aggregate, after which time, any excess HCl solution was removed, and upon removal of the template, or mould, a formed structure was produced. Structures were also produced with this method using uncross-linked emulsion droplets to start.

4.2.5.2. Spheroidal emulsion droplet structure formation

Emulsions were prepared identically as per 4.2.3.1; Emulsion preparation, and the co-polymer stabilised cineole-in-water cross-linked emulsion was creamed *via* centrifugation at 3,000 rpm, for 60 minutes. Spheroidal aggregates were produced by dropping aliquots of the creamed emulsion layer into HCl (0.5M). Spheroidal structures were formed in less than 2 seconds (see Figure 38).

4.2.5.3. GδL emulsion droplet structure formation

Aggregated emulsion droplet structures were created using the concentrated creamed layer of the standard P16-stabilised cineole o/w emulsion, to which glucono-δ-lactone (GδL) (2 wt. % based on the total emulsion volume) was added, stirred slowly and left to stand for at least 1 hour. Formation of specific shapes was achieved by first transferring the creamed emulsion

and GδL mixture into a template. The mixture was left for 2 hours before the template was removed.

4.2.5.4. Hollow capsule structure formation

Excavated, hollow cross-linked capsule structures were formed in an identical manner to 4.2.4.2; Hollow capsule formation.

4.3. Results and discussion

4.3.1. Synthesis of pH-responsive branched and linear co-polymer surfactants

Branched and linear amphiphilic co-polymer analogues based on trimethoxysilypropyl methacrylate (TMSPMA), and methacrylic acid (MAA) were prepared using a thiol-regulated free-radical branching polymerisation process.[22, 26] The composition of the statistical co-polymers was purposely designed so that TMSPMA would provide self-cross-linking residues following hydrolysis and that MAA would provide electrostatic droplet stabilisation. A chain transfer agent, 1-dodecanethiol (DDT), was used to provide hydrophobic polymer chain ends for strong oil-droplet surface adsorption. Molar ratios of TMSPMA: MAA were nominally fixed at 61:39 which exactly reflects the same ratio of hydrophilic to hydrophobic content of the previously described system for non-responsive hollow capsules.[27] Table 1

shows the target composition and actual calculated polymer compositional ratios for the branched and linear co-polymers determined by ^{1}H NMR spectroscopy, using signal ratios, and triple-detection size exclusion chromatographic analysis (TD-SEC), before esterification.

4.3.2. Effect of polymer architecture

As presented in Table 1, values suggest that the copolymers become less polydisperse with increasing TMSPMA content/decreasing MAA content. It is suggested that the architecture of the branched co-polymer produced is similar to that of a brush, or comb, co-polymer because of the difference in chain length between TMSPMA and the MAA co-monomer. Therefore, due to architectural steric hindrance it is possible that with larger compositional amounts of TMSPMA, and hence more longer-length chains, chain growth may be hindered. These SEC results are consistent with previous research on related systems.[11a, 22, 28] SEC chromatograms of the linear and branched analogues (P21 and P22) (Figure 10.a-c) showed that the branched analogue P21 is the first to elute during analysis, suggesting that the co-polymer is larger in size than the linear analogue P22, as expected with branched architecture. Branching or conjoining of the primary chains during the synthesis of the branched analogue gives the wider plot of P21 in Figure 10.a. The branched co-polymer has a broader range of chain lengths and hence a higher polydispersity than the linear (values shown in Table 1). However, as discussed in Chapter 3; Introduction, analytical measurements on polymers with these high levels of architectural and compositional complexity remains challenging.

In Figure 10.c, at a crossing point of approximately 70 kDa, the linear co-polymer is more dense than the branched; although they are chemically similar this may be the effect of the chain transfer agent end groups, or the fact that there are additional EGDMA units in the branched co-polymer, which gives this effect in this solvent. Initially, the linear material shows higher viscosity than the branched material as you would expect since the longer the linear chain, the increased chance of chain entanglement, and consequentially the more viscous the polymer solution will become. However the branched co-polymer is showing an increase in viscosity with increasing Mw, but the difference is reduced at higher molecular weights.

On comparison of responsive P21 with the non-responsive branched P6 co-polymer analogue from the previous chapter, the M_w values are similar; M_w for P6 is 69.7 kDa and P21 is 67.7 kDa. It is suggested that due to the increasing steric hindrance when polymerising long chain PEGMA molecules, chain growth during polymerisation is hindered resulting in smaller chain lengths. Whereas upon polymerisation of the co-polymer that contains a much smaller molecule, i.e. MAA, chain growth is less inhibited. For structural comparison see Figure 7. All Mark-Houwink α-values (M-Hα) were approximately 0.3 or below for the branched co-polymers indicating relatively compact structures as expected with branched co-polymer architectures. The linear analogue, P22, characteristically had an M-Hα value in the region of 0.7, which would be expected for a linear polymer of this composition in this solvent system.[22-23, 29]

Table 1. Co-polymer compositions calculated by ^{1}H ($CDCl_3$) NMR and size exclusion chromatography (TD-THF) values.

ID	Target Polymer Composition	Actual Polymer composition[a]	Conv %[a]	Mw/kDa[b]	Mn/kDa[b]	Mw/Mn[b]	M-Hα[b]
P18	$TMSPMA_{15}/MAA_{85}$-$EGDMA_{10}$-DDT_{10}	Not performed*	-	30	10	4.5	0.28
P19	$TMSPMA_{20}/MAA_{80}$-$EGDMA_{10}$-DDT_{10}	Not performed*	-	31	10	3.9	0.26
P20	$TMSPMA_{30}/MAA_{70}$-$EGDMA_{10}$-DDT_{10}	Not performed*	-	39	9	2.8	0.30
*P21**	$TMSPMA_{60}/MAA_{39}$-$EGDMA_{10}$-DDT_{10}	$TMSPMA_{63.6}/MAA_{39.8}$-$EGDMA_{9.5}$-$DDT_{7.1}$	99.2	68	18	3.0	0.31
*P22**	$TMSPMA_{61}/MAA_{39}$-DDT_{2}	$TMSPMA_{60.3}/MAA_{39.5}$-$DDT_{2.2}$	98.3	44	22	1.6	0.53

*[a] as determined by ^{1}H NMR. [b] As determined by THF TD-SEC against polystyrene (99k) standards. * most relevant co-polymer compositions discussed in this chapter. *NMR not performed for this sample. This sample was synthesised for the comparison of molecular weight and as such is only analysed by GPC.*

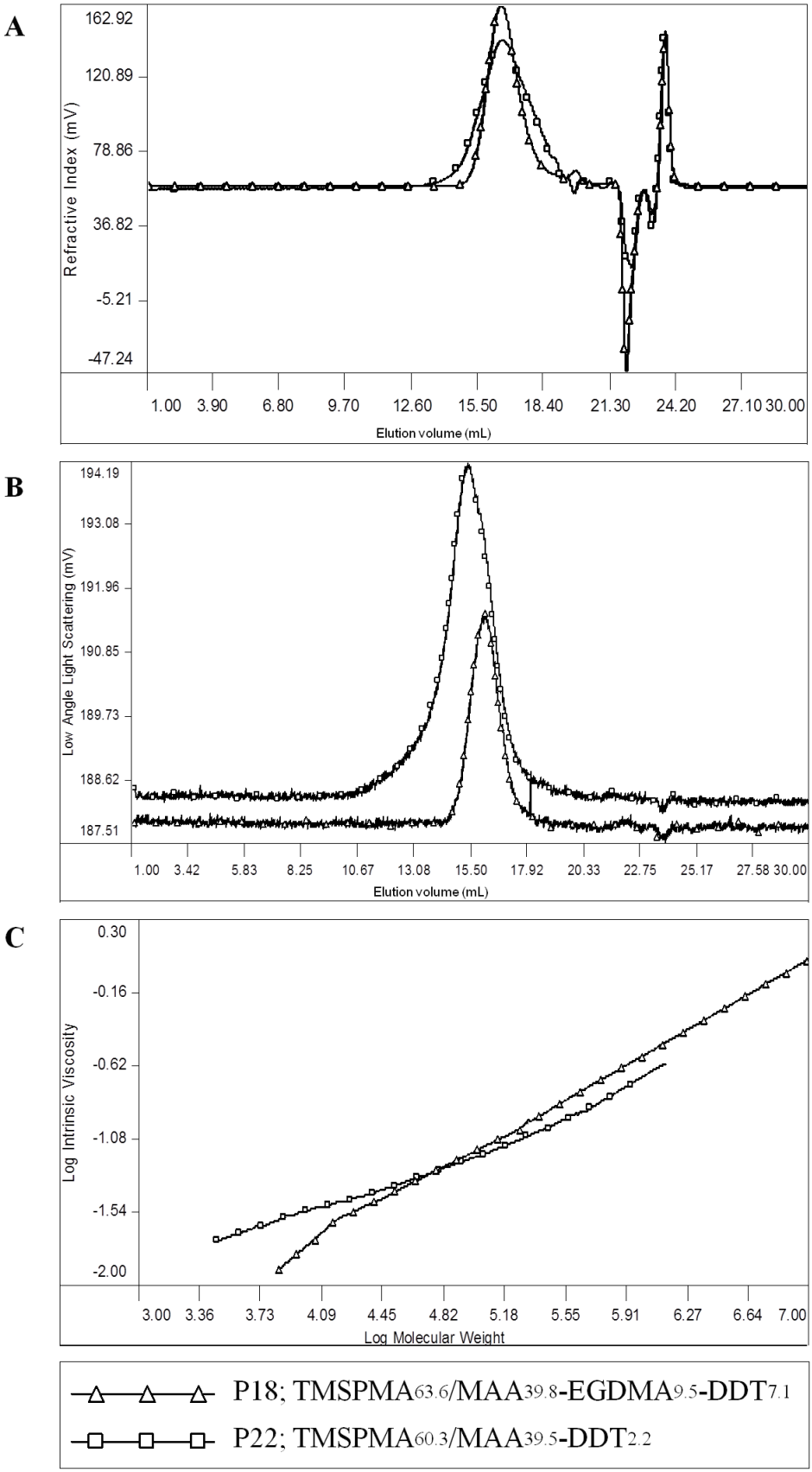

Figure 10. Size exclusion chromatography plots depicting differences in (A) refractive index, (B) low angle light scattering, and (C) viscosity between branched P21 and linear P22.

4.3.3. Synthetic reproducibility of the branched co-polymers

As the applications of P21 as a pH-responsive branched co-polymer surfactant makes up a significant proportion of this thesis, a demonstration of the reproducibility of the polymer synthesis is presented in Figure 11. Three co-polymers were synthesised separately in order to assess the batch-to-batch reproducibility of the free radical co-polymerisation protocol. ^{1}H NMR spectra showed good reproducibility between samples, with theoretical co-polymer compositions in good agreement with compositions calculated by ^{1}H NMR (Table 2).

Table 2. Actual polymer compositions as calculated by ^{1}H ($CDCl_3$) NMR.

ID	Conv/ %[a]	Calculated polymer composition[a]
P21 (1)	99.2	$TMSPMA_{63.6}/MAA_{39.8}$-$EGDMA_{9.5}$-$DDT_{7.1}$
P21 (2)	98.5	$TMSPMA_{64.4}/MAA_{41.9}$-$EGDMA_{9.0}$-$DDT_{4.7}$
P21 (3)	98.6	$TMSPMA_{63.3}/MAA_{41.2}$-$EGDMA_{10.2}$-$DDT_{5.3}$

[a] *as determined by ^{1}H ($CDCl_3$) NMR.*

In Table 2, there is a clear variation in the compositional ratio of DDT between the three separately synthesised P21 branched co-polymers. Quantification of these amounts was obtained *via* ^{1}H NMR integration, and as such within error of the measurement *via* this method. A more accurate method would be to look at the silica content of the obtained polymers. As conversion reached >98 % we can assume that the feed ratio of monomers was

maintained in the resulting polymer and that all of the available vinyl reactive groups have polymerised.

P21

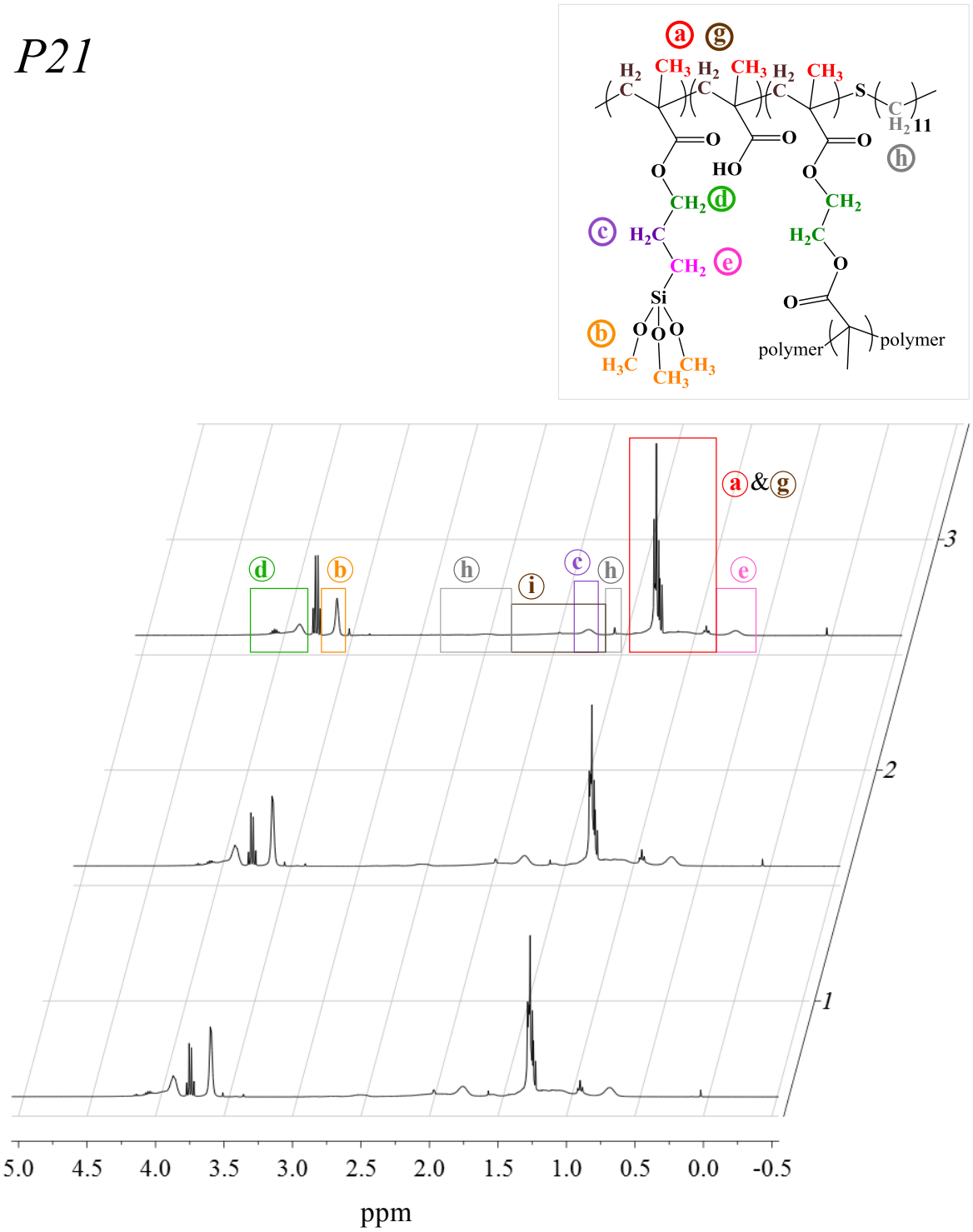

Figure 11. ^{1}H ($CDCl_3$) NMR spectra for three repeat synthesis of P16 (unesterified).

TD-SEC curves overlay well, suggesting similar molecular weight distributions were obtained in all cases (see Figure 12).

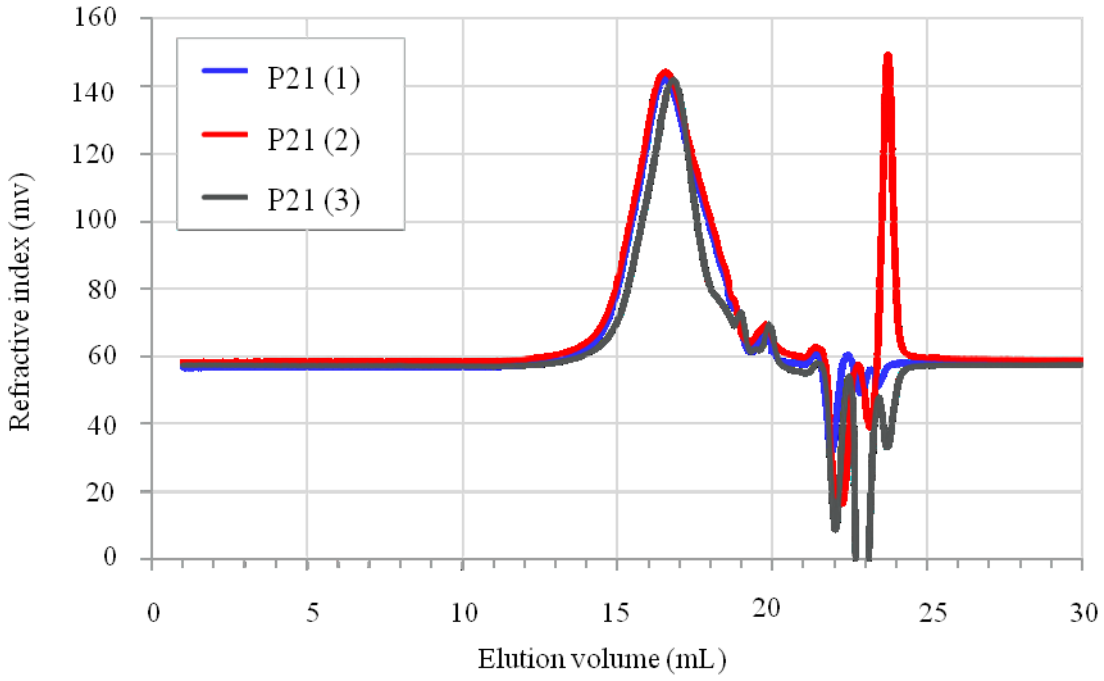

Figure 12. TD-SEC curves obtained for three repeat P21 samples.

M_w, M_n and Mark-Houwink α-values are given in Table 3. M_n for samples P21 (1) and P21 (2) are in good agreement apart from sample P21 (3) that gave a much smaller M_n value. All samples showed polydispersity values between 3.0 – 5.0, suggesting a system with lower polydispersity than seen previously, this is in contrast to the highly polydisperse systems of Chapter 3. Mark-Houwink α-values are all similar and below or equal to 0.34, indicative of relatively compact structures, suggesting branched architectures as found elsewhere.[22-23, 29]

Although TD-SEC with the added support of multiple detectors is a valuable tool for polymer characterisation, its reliable application to complex branched co-polymer systems is still debatable.[30]

Table 3. Comparison of M_w, M_n, polydispersity and M-Hα values for the repeat analysis of P21 by GPC.

ID	Mw/kDa[b]	Mn/kDa[b]	Mw/Mn[b]	M-Hα[b]
P21 (1)	67	18	4.4	0.31
P21 (2)	67	18	5.0	0.34
P21 (2)	66	13	3.0	0.34
[b] *As determined by THF TD-SEC against polystyrene (99k) standards.*				

4.3.4. Size, charge and the effect of architecture on pKa determination of P21; $TMSPMA_{61}/MAA_{39}$-$EGDMA_{10}$-DDT_{10} branched addition co-polymer

Zeta potential measurements for an aqueous solution of P21 gave values of +14 and -25 mV at pH 2 and pH 10, respectively, with an isoelectric point at pH ≈ 4.5 (Figure 13.a). This was consistent with pH titration curves of Figure 13.e, which showed complex behaviour with an averaged pKa value of 4.8. Protonation of the co-polymer P21, on addition of HCl, showed a slight inflection in the pH titration curve and as such the pKa was hard to distinguish due to the distribution of charged polyelectrolyte groups becoming slowly uncharged. It is known that the pKa of branched systems can be different to those for linear systems due to the reduction in chain mobility when fully charged when compared to linear analogues, and this had been shown for the deprotonation of polybases by Weaver and co-workers[21] where pKa determination from the protonation of a branched polybase gave a pKa difference of almost 1

unit when compared to the linear equivalent due to an inability of the branched polyelectrolyte to fully chain extend due to branching points in the structure. Dimerisation occurred between the neutralised acidic hydrogen and the carbonyl oxygen on the MAA residues. This together with dimerisation, occurring also at low pH, caused the mixture to become increasingly viscous. Even with stirring and waiting times, it was difficult to ensure a constant pH throughout the mixture. Dynamic light scattering studies (see Figure 13.c), showed the presence of discrete macromolecules above pH 9, which were 50 - 100 nm in hydrodynamic diameter; in contrast, micrometre-sized aggregates were observed between pH values of 2 and 7, consistent with the low surface charge on the co-polymer under these conditions.

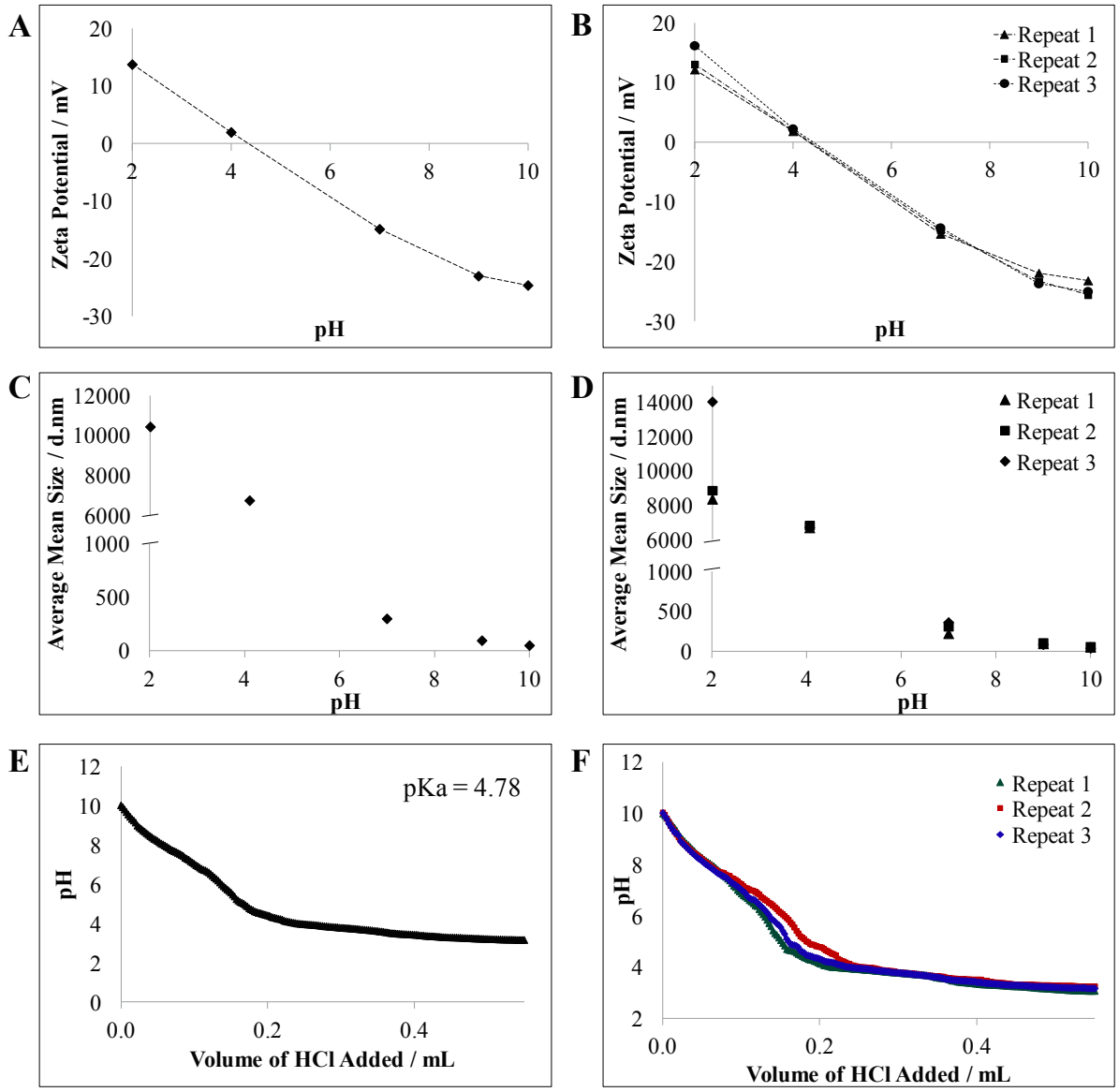

Figure 13. (A) Average zeta potential values and (B) zeta potential repeats, (C) average DLS values and (D) DLS data repeats, (E) average pH titration curve and (F) pH titration curve repeats as a function of pH for the co-polymer, $TMSPMA_{63.6}/MAA_{39.8}$-$EGDMA_{9.5}$-$DDT_{7.1}$ ([co-polymer] = 4.790×10^{-5} mol L-1 in (A) and (C); sample volume = 600 µL in (E).

4.3.5. Emulsion stability and cross-linking

Comparable amphiphilic branched co-polymers used as effective non-reactive emulsifiers, similar to the branched co-polymers produced in this study, were recently reported by Woodward and Weaver.[11b, 24, 31] In those examples, the PEGMA moiety provided efficient steric stabilisation of oil droplets dispersed in water (also seen in Chapter 3), the co-monomer MAA provided an optionally tunable component with a pH-response that altered either the polymer hydrophobicity[11b] or the inter-polymer hydrogen-bonding potential[23] while the DDT moieties, which were present at the chain ends of the co-polymers, as dodecyl thioether groups, provided multiple points of attachment of the co-polymer to the oil droplet surface. This multi-functionality was mirrored in this work where the basic single-component capsule formation methodology, as presented in Chapter 3, was utilised and extended to prepare branched co-polymers with both responsive and cross-linkable functionalities *via* the inclusion of weakly acidic carboxylic acid groups, through incorporation of MAA at polymerisation, and the presence of the cross-linkable moiety arising from the use of TMSPMA as a co-polymer.

Emulsions were prepared using cineole as described in 4.2.3.1; Emulsion preparation. As discussed in the previous chapter, it was important to consider reproducibility and long-term stability of the uncross-linked emulsion droplet templates such that the timeframe for cross-linking was as long as possible. Emulsion droplet diameter stability ensured that capsules of a

similar size could be consistently made upon cross-linking over time. Oil-in-water (o/w) co-polymer stabilised emulsions based on P21 and P22 formed immediately upon homogenisation and average diameters of the droplets were measured as a function of time using laser diffraction to assess stabilities (described in Chapter 2; analytical techniques applicable to this thesis). As shown in Chapter 3, branched co-polymer-stabilised droplets showed constant droplet diameters over the time period. The branched polymer architecture afforded a higher number of hydrophobic end-groups providing adhesion to the oil phase, while a more globular system and the high molecular weights of these materials could provide additional Pickering-type stabilisation, where the large amphiphilic branched co-polymers help to stabilise the oil/water interface more effectively than their linear counterparts.[32] In Figure 14, P21-stabilised emulsion droplets appear to be less stable than those presented in Chapter 3. The composition of co-polymers from the previous chapter contained a long chain permanently hydrophilic monomer, PEGMA, which provides enhanced stability at the emulsion droplet interface due to an increased steric effect. Figure 14 confirms that the branched architecture of P21 provided enhanced droplet stabilities compared to linear analogues as seen with related systems using DDT as a CTA.[11b, 23] Droplets stabilised with the linear co-polymer, P22, showed constant droplet diameter reduction and cineole liberation over time representative of emulsion destabilisation.

Table 4. Comparison of initial and final uncross-linked and cross-linked emulsion droplet diameters of P6 and P15 co-polymer stabilised emulsion droplets.

ID	Oil phase	Cross-linking	Initial droplet diameter / µm	Final droplet diameter / µm
P21	Cineole	Uncross-linked	8.167	7.912
P21	Cineole	Cross-linked	6.741	6.714
P22	Cineole	Uncross-linked	12.547	11.054
P22	Cineole	Cross-linked	8.001	7.798

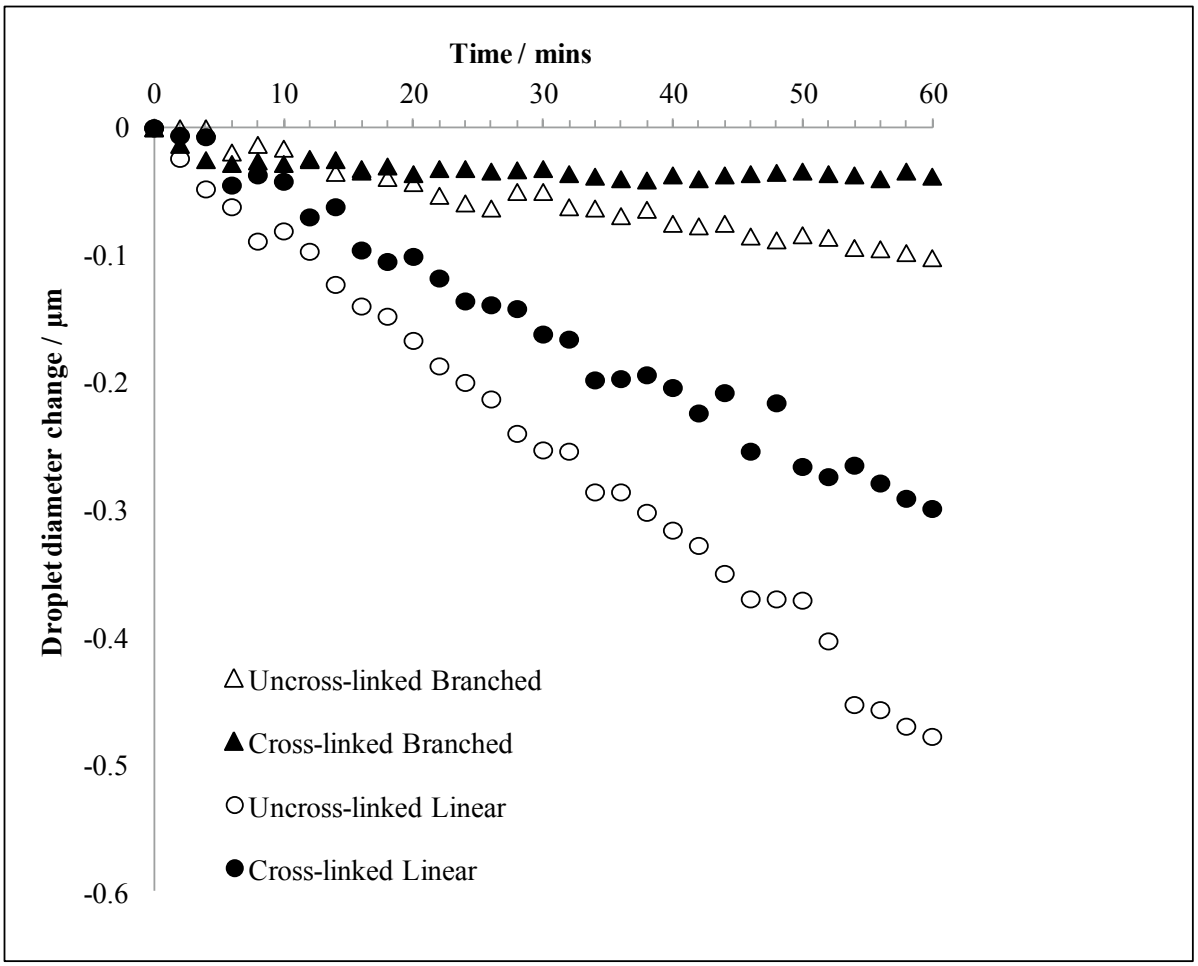

Figure 14. Normalised kinetic experiments monitoring the change in volume-averaged droplet diameters of P21 branched and P22 linear co-polymer stabilised uncross-linked and cross-linked droplets as a function of time.

4.3.6. Responsive capsule formation and flushing of the contents

As previously described in Chapter 3, base-catalysed self-condensation of peripheral silanol groups formed a cross-linked inorganic network on the P21-stabilised emulsion droplet surfaces.[33] Where the hydrophilic pH-responsive MAA groups are also on the periphery, the formation of an inorganic network or capsule shell will trap these on the surface. Therefore

surface pH-responsive capsules are produced. Figure 15 shows that the diluted oil-in-water emulsion droplets (Φ_{oil} 0.5) retain their structural integrity during these processes; laser diffraction confirmed that the droplets had volume-averaged droplet diameters of 6.77 µm and light microscopy showed that the droplets were highly spherical, but with obvious indentations, and non-interacting.

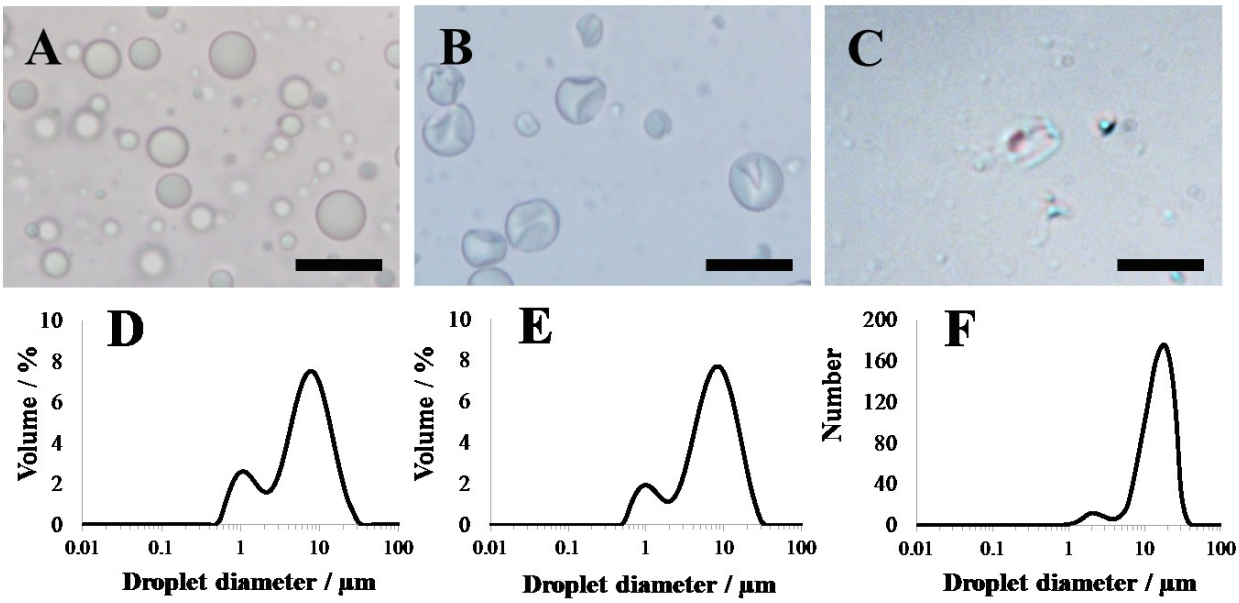

Figure 15. Light micrographs of (a) initial branched co-polymer stabilised emulsion droplets, (b) encapsulated droplets following base-catalysed self-condensation of (a) and (c) hollow capsules following flushing of (b) with ethanol. Scale bars represent 10 µm. (d-f) Droplet size distributions of (a-c), respectively. Note: Distribution in (f) is calculated manually from measuring diameters of 576 dried capsules from light micrographs.

As seen previously in Chapter 3, and illustrated in Figure 15.b and Figure 16, light microscopy showed that the droplets became less spherical following cross-linking where the network of covalent bonds induces a compaction of the sheath around the droplet periphery[34] or a change in osmotic pressure between the disperse and continuous phases.[35] No oil evolution was observed during this process and laser diffraction revealed near-

identical droplet size distribution chromatograms before and after cross-linking (volume-averaged droplet diameters of 6.77 µm, compared to 7.56 µm for the uncross-linked droplets, Figure 15.d-e respectively).

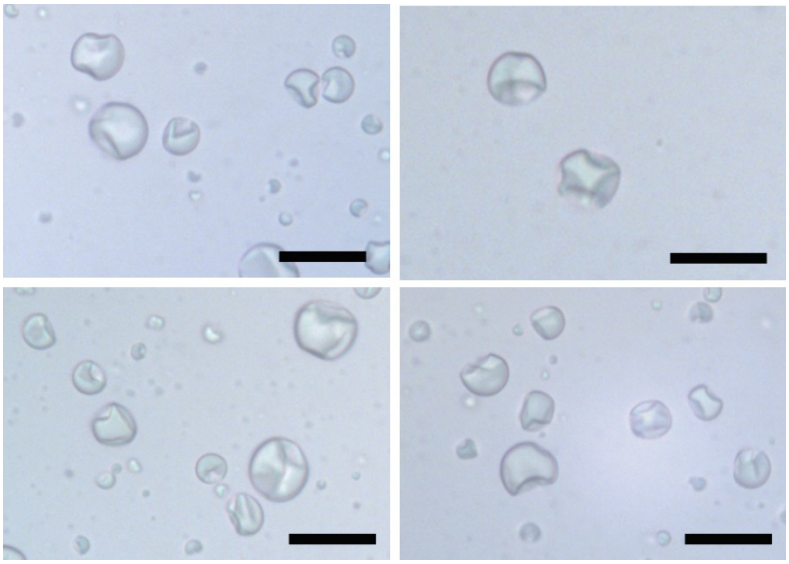

Figure 16. A collective of light micrographs of branched P21-stabilised cross-linked emulsion droplets. Scale bars represent 10 µm.

Cross-linking experiments were attempted with emulsions stabilised with the less efficient linear pH-responsive co-polymer analogue, P22. Some successful capsule formation was observed and the reactive linear co-polymer was chemically cross-linked around the initial droplet template, however the unavoidable destabilisation of the initial uncross-linked droplets produced inconsistent capsule sizes between batches and liberated oil was also observed over longer timeframes (Figure 14).

4.3.7. Efficiency of polymer-adsorption and cross-linking

Background material was observed in initial light micrographs of the P21 polymer-stabilised emulsion. It was hypothesised that this material may be unadsorbed TMSPMA/MAA branched co-polymer. Following initial emulsification, the droplets were cleaned by repeated centrifugation and redispersion cycles (as described in section 4.2.3.1; Emulsion preparation and section 4.2.3.2; Washing of the emulsions). This ensured that only branched co-polymer present within the system was located at the droplet interface or within the oil droplet. Following cross-linking under nominally identical conditions, the presence of background material in light microscopy images was significantly reduced. Centrifugation of emulsion droplets without destabilisation (as evidenced by laser diffraction measurements after each washing (see Figure 17), is further supported by the high interfacial stabilisation provided by this class of branched co-polymer emulsifier.

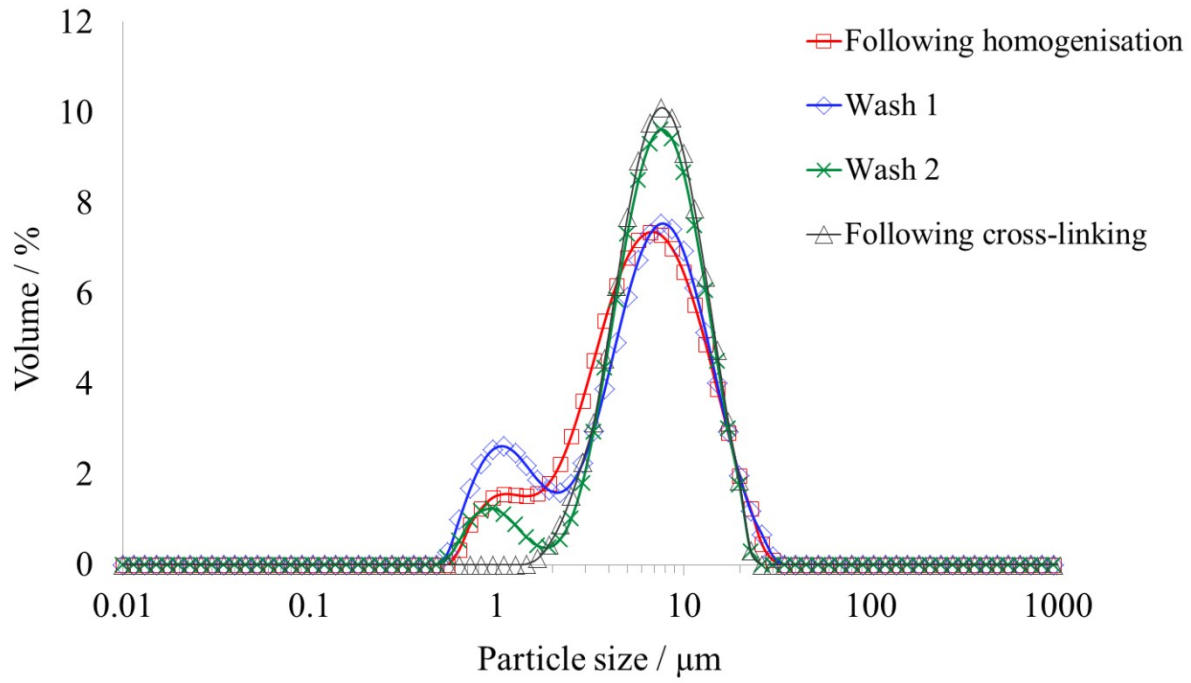

Figure 17. Overlaid laser diffraction chromatograms of branched P21-stabilised emulsion droplets after each centrifugation/redispersion cycle. Note close overlay of the predominant peak which implies no destabilisation occurs under these relatively harsh conditions.

4.3.8. Formation of hollow capsules by solvent flushing

Formation of hollow inorganic-organic hybrid responsive capsules was then attempted by flushing the cross-linked droplets with ethanol, a mutually good solvent for both water and cineole. This process was carried out identically as described in Chapter 3. Light microscopy of a dried sample of this transparent solution showed collapsed, but structurally intact, capsules or sacks as depicted in Figure 15.c and Figure 18.a. Ethanol addition to uncross-linked droplets resulted in the emulsion breaking as described previously.

The ethanol-flushed capsules scattered insufficiently to allow their sizes to be determined by laser diffraction, however manual sizing of 576 individual dried capsules by light microscopy revealed diameter distributions which were larger (~1-10 μm) than those recorded in solution (see Figure 15.f). Presumably the discrepancy was due to the inherent resolution limits of light microscopy, preventing the detection of smaller droplets and by the flattening of the capsules on the slide in their dry state.

4.3.9. Physical properties of the capsule shells

The hybrid pH-responsive polymer capsules again showed closer structural similarities to cross-linked polymer vesicles[36] than reported examples of templated emulsion droplets using small molecule alkoxysilanes,[37] as previously discussed in Chapter 3.

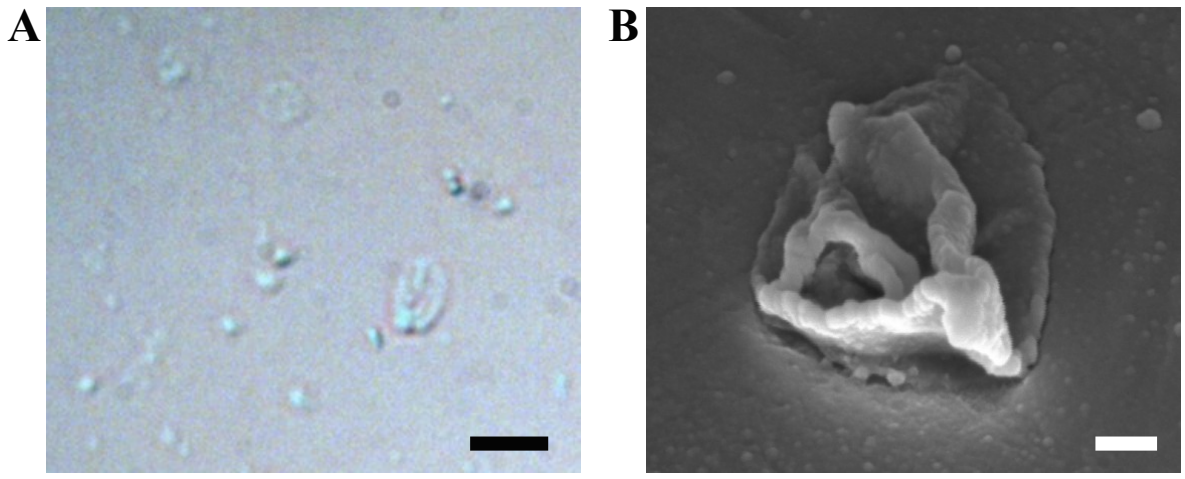

Figure 18. (A) A light micrograph and corresponding (B) scanning electron micrograph of collapsed dried hollow pH-responsive capsules. Scale bars representing 10 μm and 500 nm respectively.

Hollow inorganic-organic pH-responsive capsules were formed by flushing a cross-linked P21 stabilised emulsion, with ethanol as described in 4.2.4.2; Hollow capsule formation. The resulting flushed capsule dispersion was dried by supercritical fluid drying, using Critical Point Drying (CPD), and the dried capsules were forcibly broken in identical conditions as described in Chapter 3. Figure 19.a shows a scanning electron micrograph of a single capsule dried by CPD, which retains its spherical morphology upon critical point drying. A corresponding ruptured capsule is shown in Figure 19.b. The rough external surface of the capsule is consistent with the presence of a cross-linked matrix of silica on the surface, and may be attributed to the branched architecture of the co-polymer; this could also be an attribute of the gold coating used to image the capsules. The smooth interior of the shell indicated that cross-linking occurred predominately in the water phase, close to the surface of the droplet on formation.

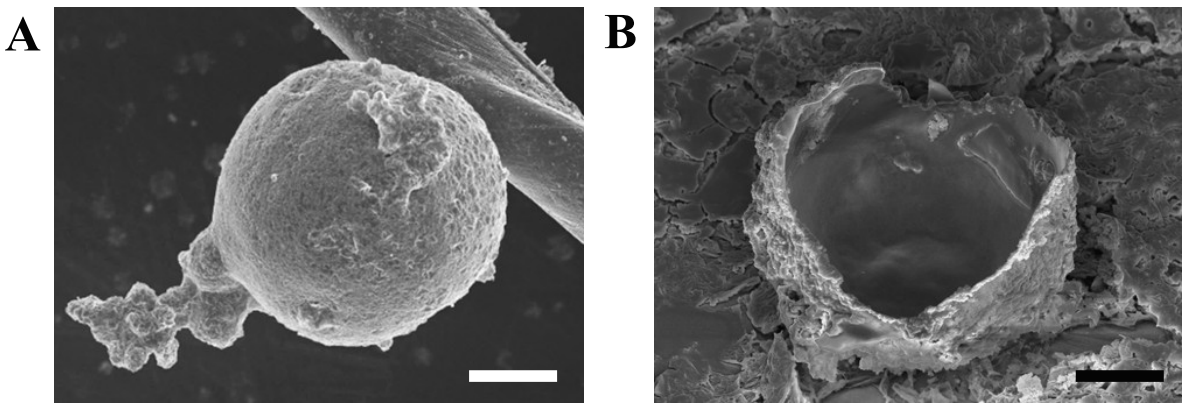

Figure 19. Scanning electron micrographs of (A) a P21-based capsule dried by CPD on a miscellaneous fibre, and (B) a ruptured P21-based capsule dried by CPD. Scale bars represent 2 µm.

Scanning electron micrographs indicated that there is a range of shell thicknesses from 25.7 nm to 45.0 nm (see Figure 20). Equivalent branched co-polymer nanoparticles, as described by Weaver in 2008[21], showed droplet diameters in dilute aqueous solution in the order 16-45 nm which is consistent with the typical membrane thicknesses observed in this thesis.

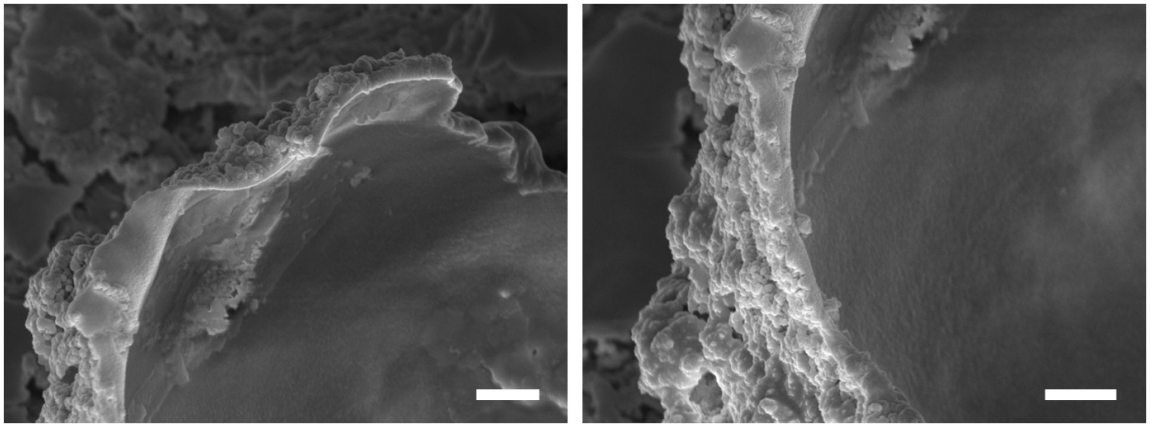

Figure 20. Scanning electron micrographs of the shell of a ruptured P21-based capsule. Scale bars represent 500 nm.

4.3.10. Lowest cross-linking monomer content

As in Chapter 3, a study was made to find the lowest compositional amount of the cross-linking monomer, TMSPMA, required to create a stable emulsion and furthermore stable capsules. Branched co-polymers P19 – P21 (for reference see Table 2) were synthesised *via* free radical polymerisation using the same protocol as described in the experimental section of Chapter 3, however in this case the molar ratio of TMSPMA: MAA was varied. Starting with the lowest amount of cross-linking monomer, P18 was used to create an emulsion as per section 4.2.3.1; Emulsion preparation. Emulsion droplet stability of the corresponding emulsion was monitored as a function of time (as described in Chapter 2; analytical

techniques applicable to this thesis). Cross-linked emulsion droplets were formed by addition of base to the dispersed diluted uncross-linked emulsion, and the stability of the newly cross-linked droplets was observed directly (see Figure 21). Average droplet diameters for the uncross-linked and cross-linked emulsion droplets were recorded (see Table 5).

Table 5. Average droplet diameter change with varying molar ratio.

ID	Molar ratio (TMSPMA:MAA)	Uncross-linked average droplet diameter / µm	Cross-linked average droplet diameter / µm
P18	15 : 85	14.05	8.59
P19	20 : 80	7.72	9.60
P20	30 : 70	7.04	8.10
P21	61 : 39	6.77	7.56
P22	61 : 39	12.97	8.32

This process was repeated with further branched co-polymer surfactants, containing increasing amounts of TMSPMA, until the emulsion was efficiently stabilised by the branched co-polymer. This was apparent when there was little or no change in droplet diameter between the uncross-linked and cross-linked emulsion droplets. The lowest MFM molar ratio of TMSPMA able to capably form capsules with consistent sizes was 30:70 (TMSPMA:MAA).

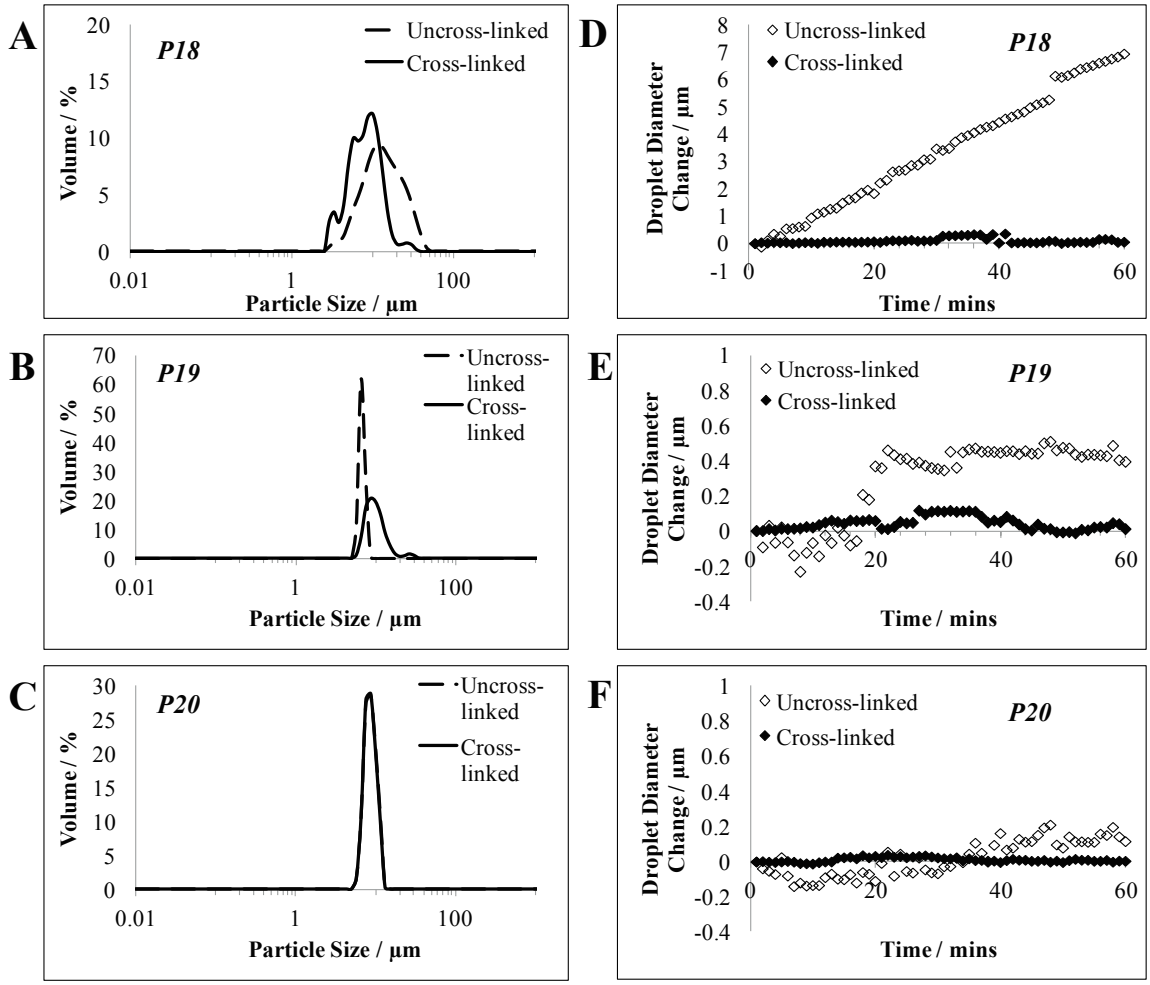

Figure 21. Droplet size distribution chromatograms of uncross-linked and cross-linked emulsion droplets stabilised with (A) P18, (B) P19, and (C) P20 branched co-polymer surfactants. (D-E) Corresponding normalised kinetic experiments of (A-C) monitoring the change in volume-averaged droplet diameters of the branched co-polymer stabilised uncross-linked and cross-linked droplets as a function of time.

4.3.11. Encapsulation of alternative actives

As per Chapter 3, 3.3.10; Encapsulation of alternative actives, it was decided to investigate the encapsulation of suitable actives using the responsive branched co-polymer, P21, using identical conditions. A hydrophobic fluorescent dialkyl carbocyanine dye (DiO) was dissolved in the oil phase (0.05 w/v % based on oil) and was encapsulated to provide a

marker for confocal microscopy (see Figure 22). Again, as described in Chapter 3, cross-linking of these droplets resulted in reduction of the fluorescence intensity of the dye. This returned upon flushing the cross-linked droplets with ethanol to produce hollow capsules indicating a temporary pH quenching effect on addition of triethylamine. Despite their high ethanol solubility, confocal images clearly showed that DiO molecules were retained within the capsule internal void space which implied that either the pore-sizes of the network formed are smaller than the dye dimension in solution (~ 15 Å)[1] or that the dye was physically or chemically trapped on the capsule surface.

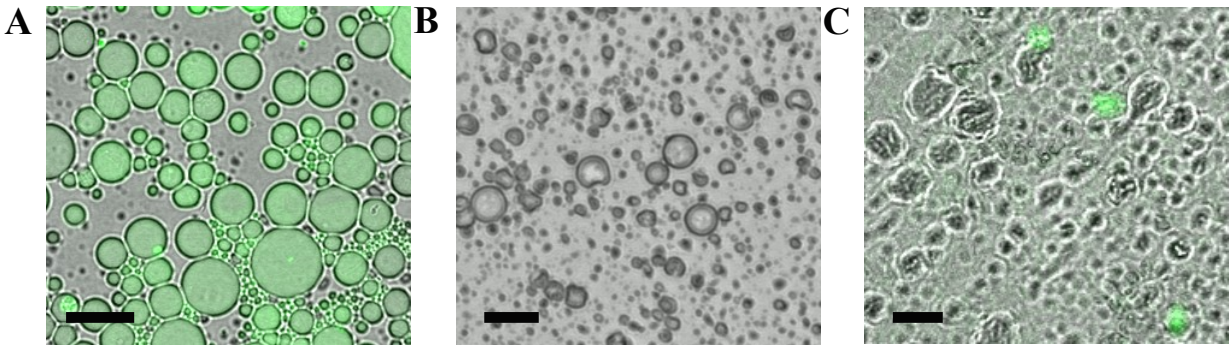

Figure 22. Confocal micrographs of (A) uncross-linked emulsion droplets containing 0.05 w/v % DiO; (B) base-catalysed cross-linked emulsion droplets where a temporary pH quenching effect lessens the fluorescence intensity of the dye on addition of TEA; (C) capsules following flushing (B) with EtOH. Scale bars represent 10µm.

Poly(vinyl stearate) was identified in Chapter 3; section 3.3.10 as a suitable encapsulate for use with a cineole oil phase. Oil-in-water emulsions were prepared using P21 (3.0 w/v %), where poly(vinyl stearate) was dissolved in cineole (30 w/v %), using an identical procedure as outlined in 4.2.3.1; Emulsion preparation. Stable emulsions were formed in all cases with the polymer-loaded droplet diameters being consistent with those of the unloaded droplets.

[1] Estimated using ChemBio 3D software by MM2 energy minimisation.

Cross-linking induced a change in the droplet morphologies similarly to that observed for the unloaded emulsions. Flushing the loaded cross-linked emulsion droplets with ethanol, to give capsules, caused the insoluble encapsulated polymer to precipitate. Comparison of unloaded and loaded capsules by light microscopy showed a visible difference (Figure 23).

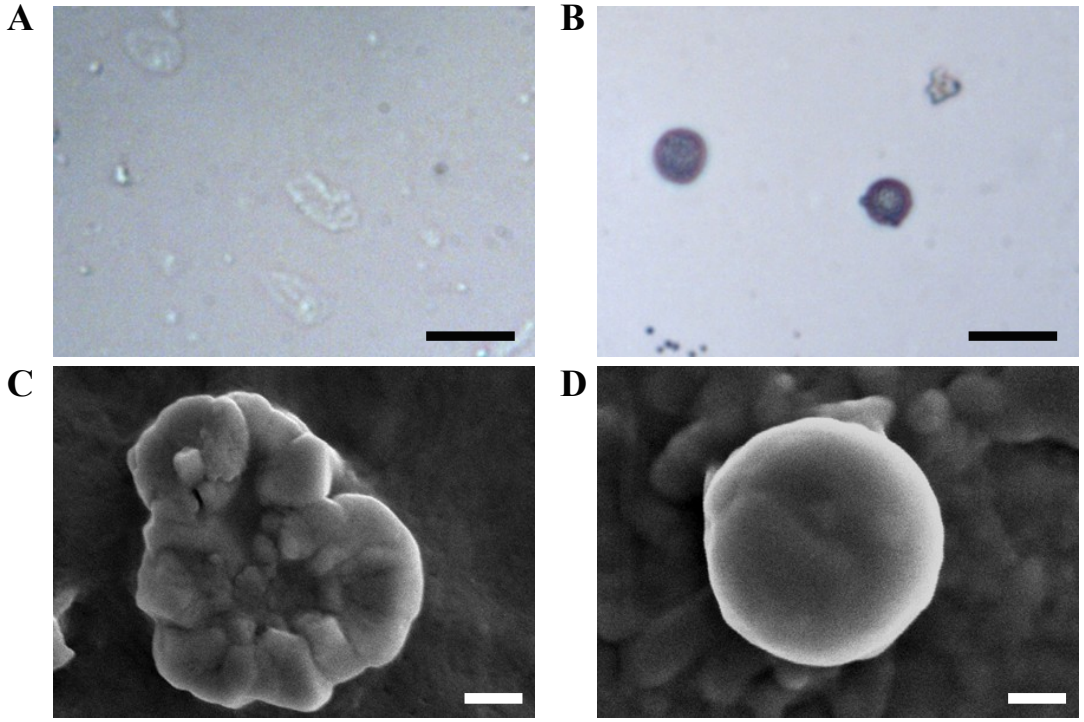

Figure 23. Light micrographs of the flushed (A) unloaded and (B) loaded capsules. Scale bars represent 10 µm. Scanning electron micrographs of the flushed (C) unloaded and (D) loaded capsules. Scale bars represent 500 nm.

Loaded droplets transmitted less light and thus were observed as being opaque (Figure 23.b), as opposed to transparent, micron-sized structures as previously seen in Chapter 3; section 3.3.10 (Figure 23.a). Scanning electron microscopy demonstrated that the unloaded capsules collapsed onto surfaces to give flattened biconcave-shaped structures when dried (Figure

23.c) whereas the loaded capsules retained predominantly spherical morphologies (Figure 23.d).

4.3.12. Capsule surface pH-response

Controllable responsive surface behaviours, as detailed in 4.1; Introduction, was achieved through judicious design of a branched co-polymer capable of emulsification, cross-linking, and responding to pH-stimuli. Essentially through the use of a weakly acidic monomer, MAA, the formed cross-linked capsule could be reversibly associated and disassociated through changes in the external pH. At high solution pH, the discrete capsules were dispersed due to electrostatic repulsion between anionic MAA residues, whereas on lowering the pH to 2 the acid groups protonated becoming more neutral and hydrophobic. This triggered the aggregation of the capsules and simultaneous formation of dimers by hydrogen bonding between the neutralised acidic hydrogens and the carbonyl oxygens (see Figure 24).

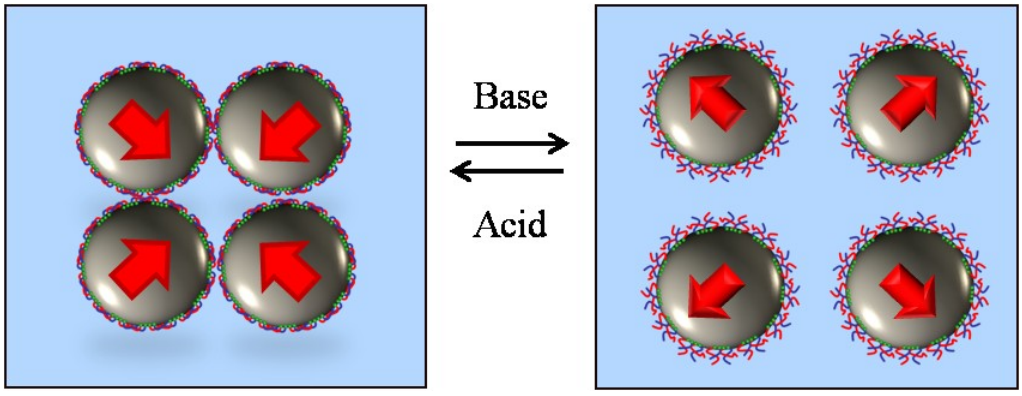

Figure 24. Schematic representation of capsule assembly and redispersion.

This pH-responsive behaviour of capsule aggregation and redispersion was shown by laser diffraction. An emulsion was made under identical conditions as 4.2.3.1; Emulsion preparation, and the average diameters of the uncross-linked and cross-linked droplets were measured as a function of time over 60 minutes each to assess stabilities. The pH-response was also tested by the addition of acid and base consecutively every 60 minutes. The total experiment run was 480 minutes. On lowering the pH to 2, by the addition of HCl, the capsules aggregate and the average droplet diameter increases. On increasing the pH to 10, by addition of NaOH, the capsules redispersed (see Figure 25).

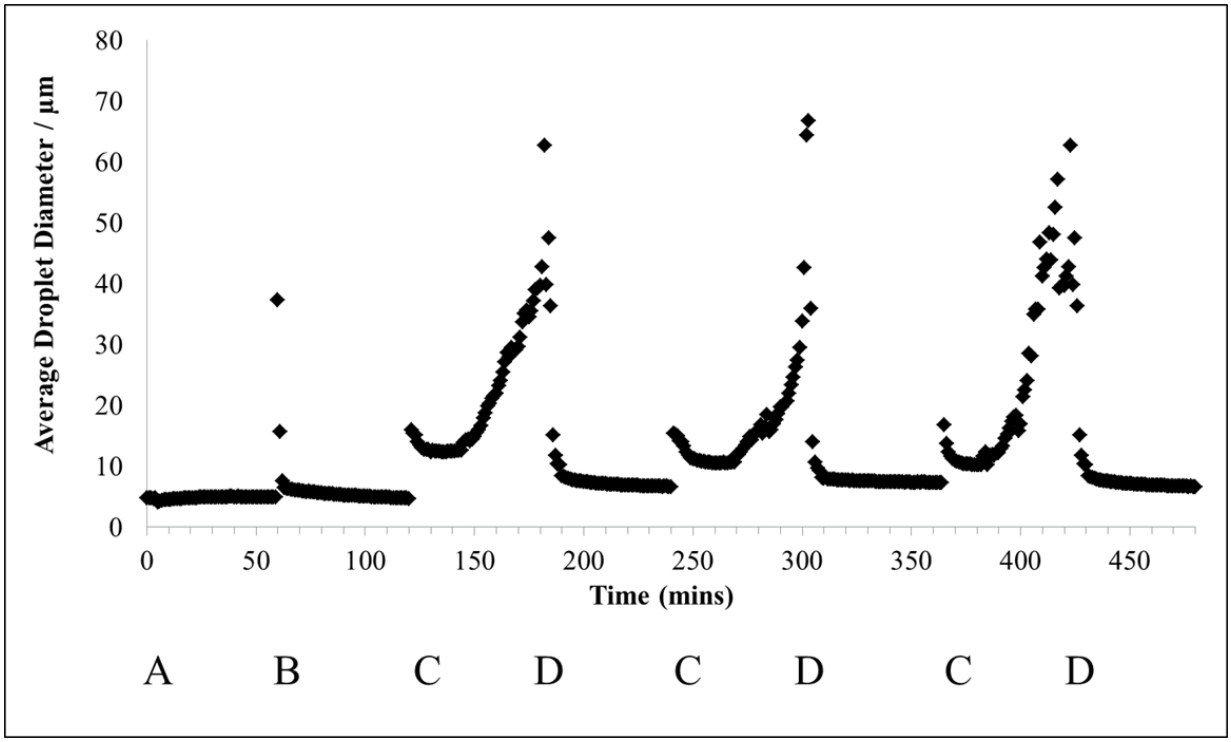

Figure 25. Laser diffraction plot showing the stability of (A) uncross-linked emulsion droplets, and (B) cross-linked emulsion droplets. At (C), the addition of acid causes the emulsion droplets to aggregate, (D) the addition of base causes the emulsion droplets to redisperse, and *vice versa*.

Samples of the analysed solution in Figure 25 were removed and imaged using light microscopy (Figure 26).

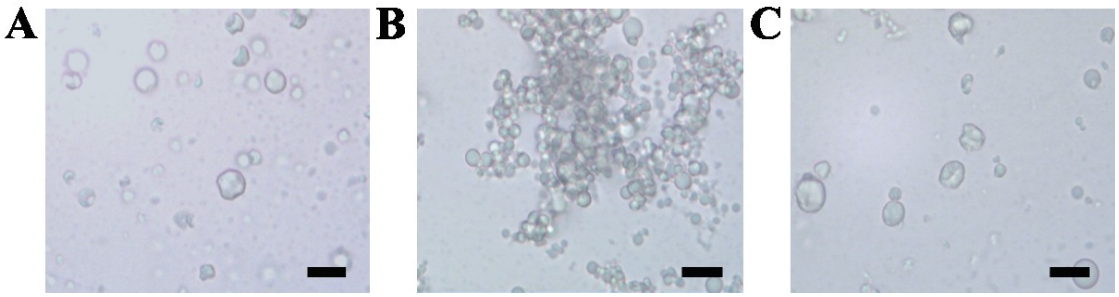

Figure 26. Light microscopy images of samples taken from the laser diffraction solution (of the samples represented in Figure 27) with changing pH. (A) Cross-linked emulsion droplets, (B) the addition of acid causes emulsion droplet aggregation, and (C) the addition of base causes emulsion droplet redispersion.

Figure 25 displays a sharp inflection of the scattering signal of the laser on the addition of base (Figure 25.b), which then settles between approximately two and ten further measurements. This occurred due to non-homogenous mixing of the liquids in the sample, as opposed to localised cross-linking. To evidence that this is the case, the experiment was repeated using a non-responsive co-polymer emulsion (stabilised by P6), a non-responsive wax suspension (Mitrewax NWB73), under the exact same conditions for comparison (see Figure 27). It is indicated that inflection of the laser scattering signal occurs at Figure 25.d also.

A sudden increase in average droplet diameter is also seen at the points of acid addition (Figure 25.c). This is hypothesised to be an area of high acid concentration within the solution at the locus of addition. In this highly concentrated area, the emulsion droplets

aggregated quickly only to be mixed with the remaining solution within a short time period. From these points, aggregation of the emulsion droplets can clearly be seen, the average droplet diameter of the emulsion droplets in solution increases as they interact with each other to form droplet aggregates (Figure 26.b). This initial increase in droplet diameter on the addition of acid was also investigated in Figure 27.c-d, where no increase in diameter is seen on the addition of acid, therefore this observation an artefact of the experiment.

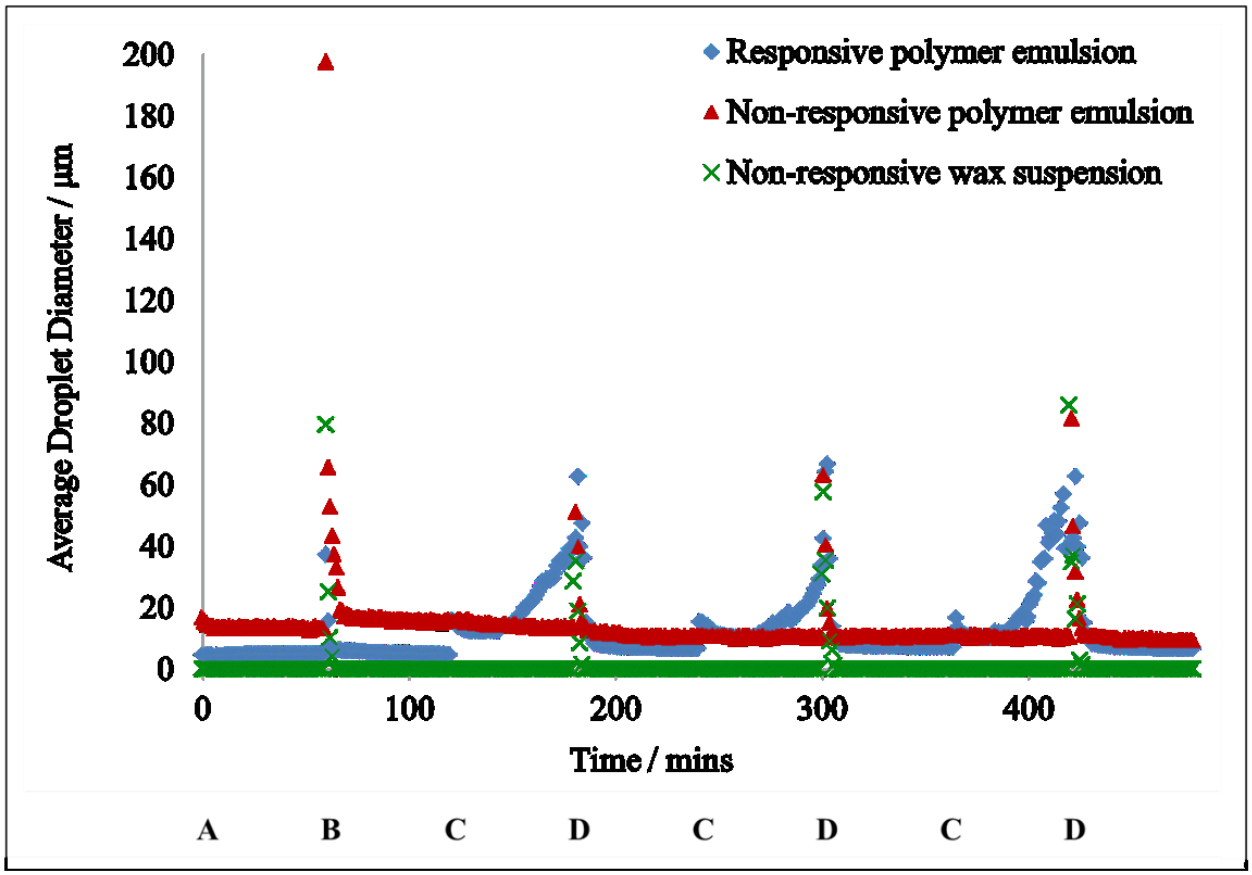

Figure 27. Laser diffraction plot depicting the inflection of the scattering signal with addition of base and acid simultaneously. (A) uncross-linked emulsion droplets, (B) cross-linked emulsion droplets with an initial addition of base. At (C), acid was added, and at (D) base was added, and *vice versa*.

4.3.13. Emulsion droplet structure formation and disassembly

By exploiting the pH-triggered interactions between MAA residues, assembled cross-linked emulsion droplet structures could be formed. Cross-linked emulsion droplets were prepared as per 4.2.4.1; Cross-linked emulsion and capsule fabrication, which were then assembled into structures as detailed in 4.2.5; Emulsion droplet- and capsule- structure formation synthetic processes. Concentrated cross-linked emulsion droplets were poured into a template, or mould, and acid was added on top. As the acid diffused through the concentrated emulsion, the MAA residues neutralised becoming more hydrophobic and the capsules aggregated to reduce their surface interaction with water by interaction with each other through hydrogen bonding. The MAA residues formed dimers by hydrogen bonding between the neutralised acidic hydrogen and the carbonyl oxygen (see Figure 6). The template, or mould, was removed after 1 hour to give an emulsion droplet structure, for example a monolith (see Figure 28).

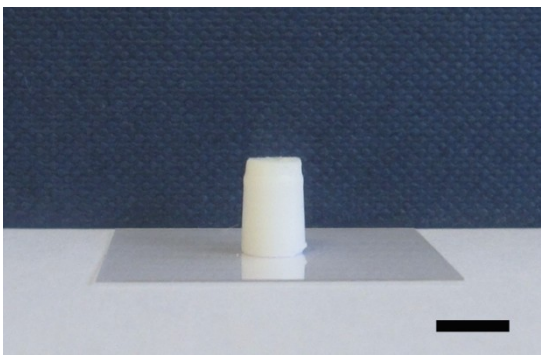

Figure 28. Digital image of an assembled and cross-linked emulsion droplet structure. Scale bar represents 5 mm.

This aggregation, and dimerisation, process was reversible. The addition of base, as per Figure 29, drop-wise onto the monolith caused it to disassemble. On increasing pH, the MAA residues deprotonated and helped to redisperse the capsules due to electrostatic repulsion.

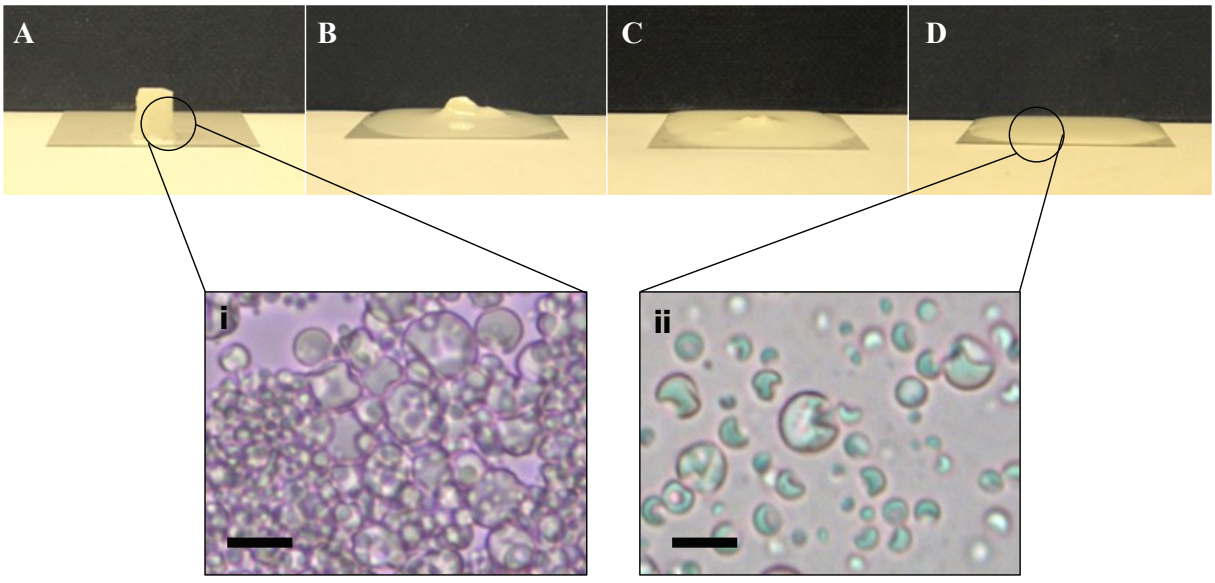

Figure 29. Digital images of the redispersion of an emulsion droplet structure; (A) assembled monolith, (B) t = 1 hr, 1M NaOH was pipetted drop wise onto the monolith – this was repeated occasionally, (C) t = 2 hrs, (D) disassembled monolith, t = 6 hrs. Corresponding light microscopy images of the internal morphology of (A), (i) aggregated capsules at pH 2 and (D), (ii) redispersed capsules at pH 10. Scale bars represent 5 µm.

4.4. Acid-catalysed simultaneous cross-linking and aggregation

So far within this chapter responsive capsule formation was obtained by the addition of base. In 2004, Du and Chen[38] observed cross-linking of silanol groups in the presence of acid on the preparation of novel particles based on an amphiphilic diblock co-polymer, poly(ethylene oxide)-*block*-poly(3-(trimethoxysilyl)propyl methacrylate). Application of this concept to the current system, where acid is used in the place of base as the capsule forming catalyst, the co-

polymer-stabilised uncross-linked emulsion droplets displayed simultaneous cross-linking, dimerisation and aggregation function (as represented by Figure 30). Both inter- and intra-cross-linking occurs due to the close proximity of surface silanol groups afforded by the intermolecular attraction of the MAA residues on the emulsion droplet surfaces at low pH.

This concept was explored by producing a range of assembled and cross-linked emulsion droplet structures, into which encapsulates were sequestered and stored. Where a structure is formed using capsules which can store actives and denote specific surface functionality, there is potential for a wide range of industrial applications such as filtration, catalysis and sustained or triggered release systems.

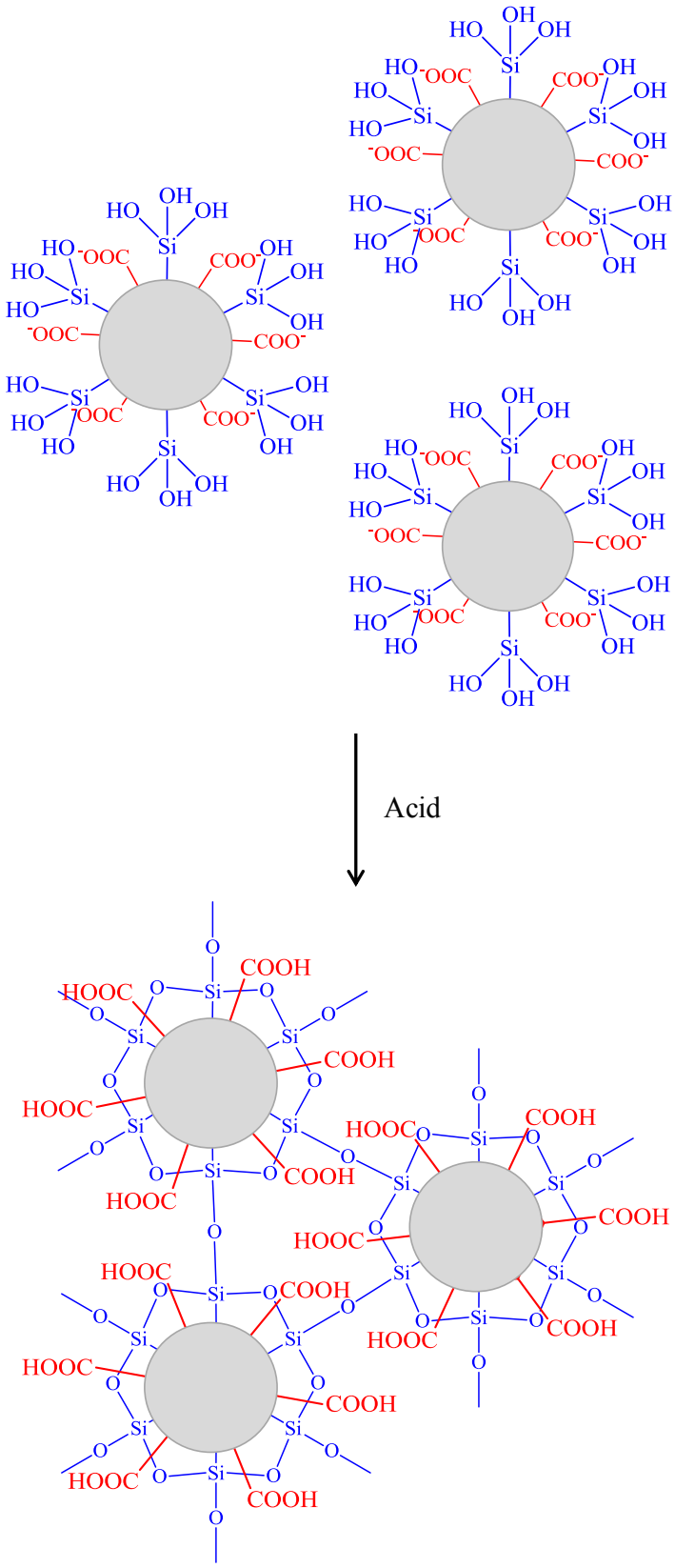

Figure 30. Schematic representation of simultaneous cross-linking, dimerisation and aggregation function of P21-stbailised emulsion droplets on lowering pH.

4.4.1. Emulsion droplet structure formation

A capsule structure was prepared identically to the method used for 4.2.5.1; Emulsion droplet structure formation, except that the emulsion droplets are not previously cross-linked. A concentrated P21-stabilised uncross-linked emulsion was placed into a mould, where acid (HCl, 0.5 M, 75 μL) was placed on top and the mixture was left to acidify. After a set time, the mould was removed leaving a monolith emulsion droplet structure (see Figure 31).

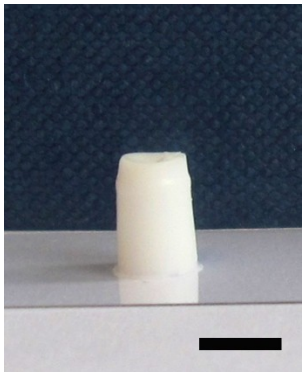

Figure 31. Digital image of a P21-based assembled and cross-linked emulsion droplet structure. Scale bar represents 5 mm

The internal morphology of the monolith structure was investigated using light microscopy (Figure 32.a-d). The arrangement of capsules within the structure can be clearly seen, showing a range of capsule sizes neatly packed together. On dehydration, the monolith became more transparent (Figure 32.b), seeming to decrease in volume with time when left open to air at room temperature. This was previously reported for compositionally similar

structures by Woodward and Weaver (2011)[24] where 'engineered emulsions' formed emulsion droplet structures by exploiting droplet surface interactions. This change in structural appearance was thought to be due to evaporation of the aqueous phase. The internal morphology shows that the cross-linked capsule arrangement compresses with dehydration (Figure 32.b). The monolith was then rehydrated; displaying that the process was reversible, as suggested by the increased opaqueness of the rehydrated sample (Figure 32.c insert) after exposure to HCl (1 M, 1 mL), the emulsion droplet structure was no longer compressed (Figure 32.c). The monolith was then flushed with ethanol, leaving behind the hollow structure (Figure 32.d insert) where the 'skeletal' hollow capsule structure is visible (Figure 32.d).

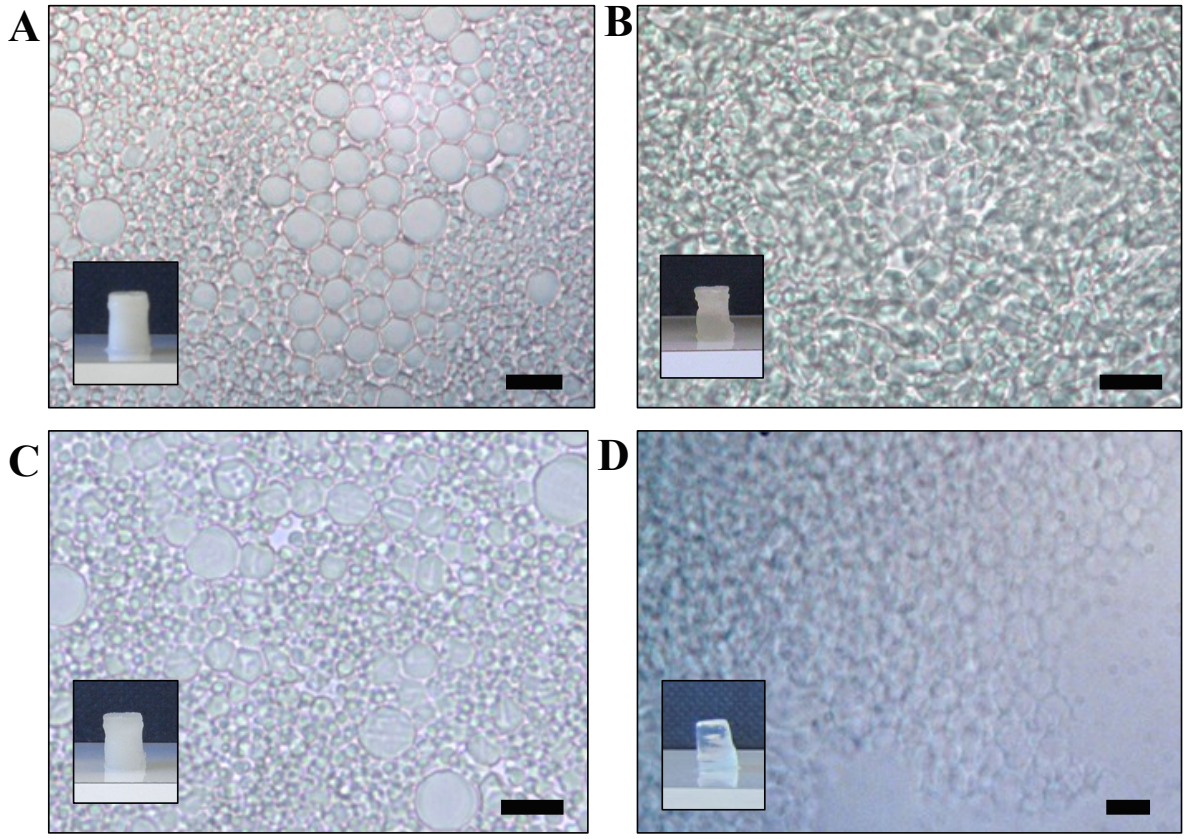

Figure 32. Light microscopy and corresponding insert digital images of (A) monolith assembled and cross-linked emulsion droplet structure, (B) dehydrated monolith structure; insert shows transparency with water loss, (C) rehydrated monolith assembled and cross-linked emulsion droplet structure, insert shows increased opaqueness with hydration, and (D) hollow monolith capsule structure flushed with EtOH. Scale bars represent 10 µm.

4.4.2. Thermogravimetric analysis of an emulsion droplet structure

The dehydration of a monolith (150 µl) emulsion droplet structure, prepared as described in 4.2.5.1; Emulsion droplet structure formation, was monitored as a function of time *via* thermogravimetric analysis (TGA) at room temperature (Figure 33). A 96% loss in mass was indicated, which corresponded to the loss of the water and oil phases. The remaining mass corresponds to the amount of inorganic cross-linked polymer residue, or capsule shell

residue. The TGA plot indicates two distinct losses, first the evaporation of water, followed by a short plateau before loss of the volatile oil phase.

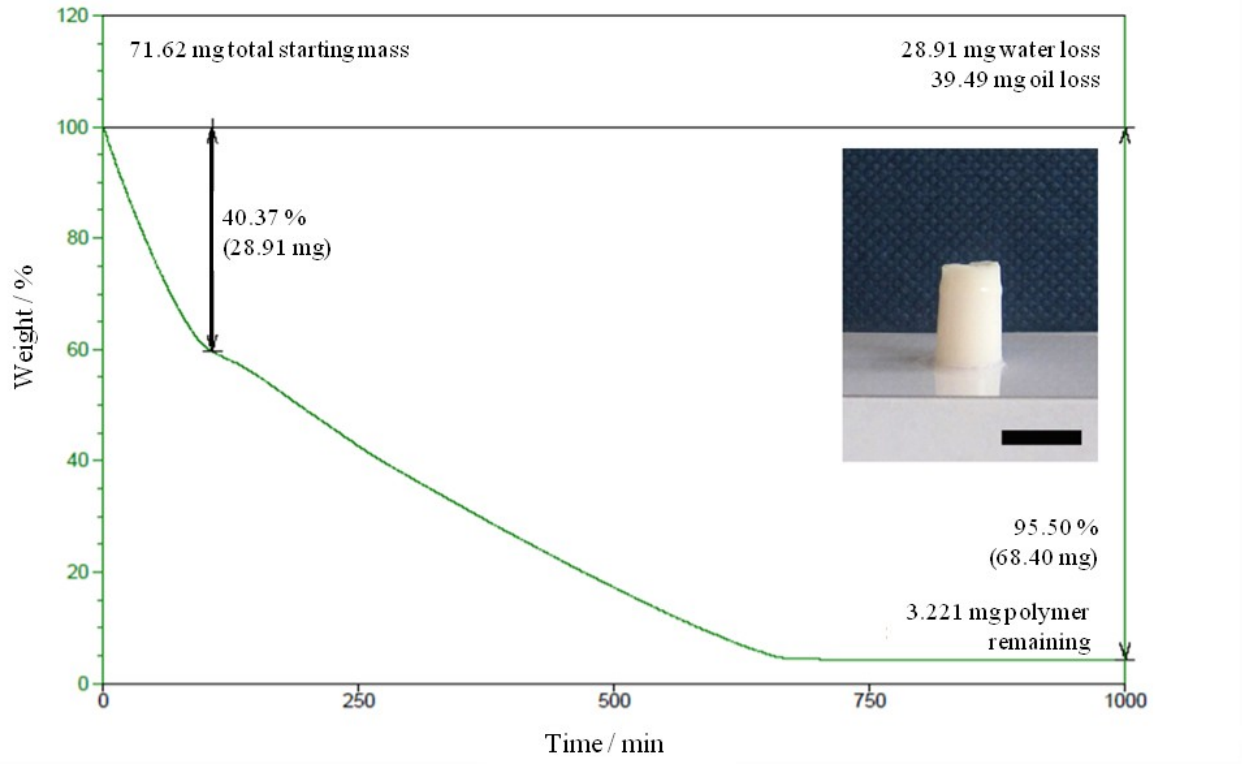

Initial mass / mg	71.62
Amount of water / mg	28.91
Amount of oil / mg	39.49
Amount of cross-linked co-polymer residue / mg	3.22

Figure 33. TGA analysis of the dehydration of a branched co-polymer P21-based capsule monolith structure. Insert shows a digital image of the monolith assembled and cross-linked emulsion droplet structure prior to dehydration. Scale bars indicate 5 mm.

4.4.3. Spheroidal structure formation and flushing of the contents

Spheroid-shaped capsule-structures were produced in preference to monolith structures due to their ease of formation, and as such were made in bulk for analysis (Figure 34). The shape lends itself to macro structures used in industry as catalysts, sustained release systems and filters. Spheroidal structures were prepared as per the method outlined in 4.2.5.2; Spheroidal emulsion droplet structure formation. Aliquots of P21-stabilised creamed emulsion (38.5 µl) were dropped into a 96-well plate filled with HCl (0.5M).

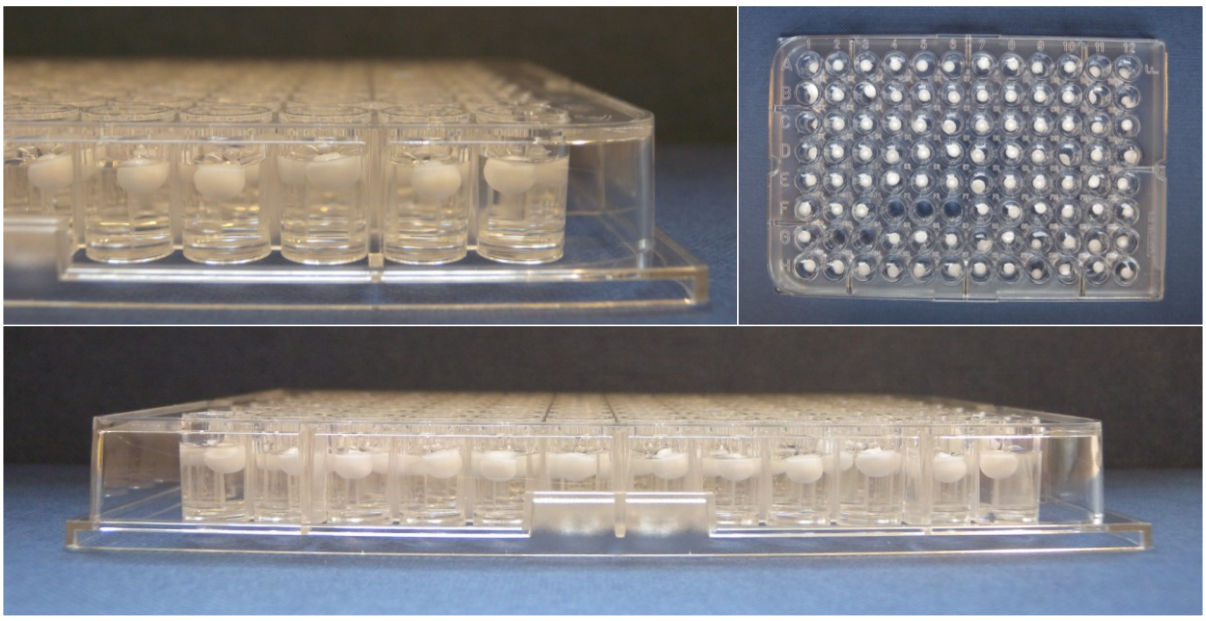

Figure 34. Digital image of P21-based spheroidal structures.

Hollow inorganic-organic spheroidal capsule-structures were formed by flushing with ethanol (see Figure 35).

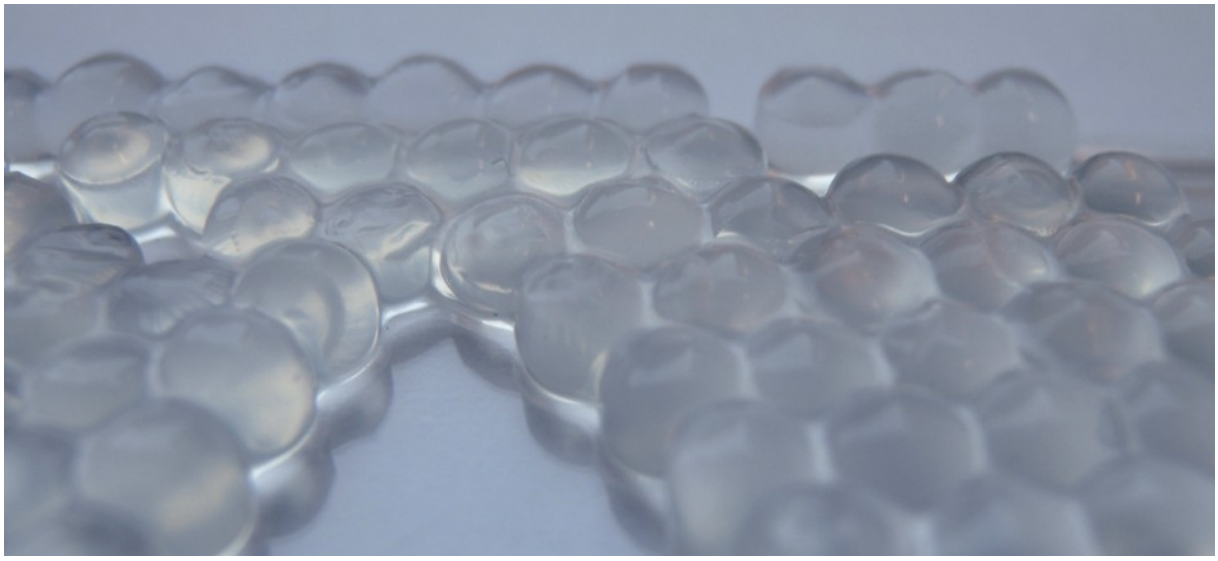

Figure 35. Digital image of hollow inorganic-organic spheroidal structures after flushing the internal phases with ethanol.

The internal morphology of the flushed spheroidal capsule-structure formation process was imaged using light and confocal microscopy (see Figure 36.a-c). Both an emulsion with and without encapsulates was imaged. A hydrophobic fluorescent dye, DiO, was dissolved in the oil phase on emulsification (0.05 w/v % based on oil), to provide a marker for confocal microscopy, as described in section 4.3.11; Encapsulation of alternative actives. Emulsions were prepared as previously described in 4.2.3.3; Emulsions with encapsulated guest molecules.

Figure 36.a. shows a discrete emulsion, where the emulsion droplets are dispersed, highly spherical and non-interacting. The corresponding fluorescence microscopy image clearly shows DiO is successfully encapsulated inside the concentrated emulsion droplets. In Figure 36.b., after the addition of acid (HCl, 0.5 M) to the concentrated emulsion sample, a compact irregular honeycomb-style arrangement is adopted by the emulsion droplets as they undergo simultaneous inter- and intra- cross-linking and assembly by the addition of acid. A higher fluorescence intensity can be seen at the edges of the cross-linked and assembled emulsion droplets due to migration of the encapsulated dye to the now hydrophobic associated periphery of the aggregated particles. This is due to decreased water at the droplet surfaces, which leads the hydrophobic dye to favour the boundary over the internal phase. Hollow capsule structures were achieved by flushing with ethanol, (see 4.2.5.4; Hollow capsule structure formation) where ethanol was simply dropped on top of the acidified sample. Figure 36.c. displays the hollow excavated structure, a 'skeleton' structure of connected capsule compartments or a scaffold. In Figure 36.c, higher fluorescence intensity can be seen at the edges of the capsules, or where the capsules have buckled on cross-linking creating folds or creases, which highlight the scaffold architecture. It is suggested that, as proposed in 4.3.8; Formation of hollow capsules by solvent flushing, the formed inorganic network is thin, scattering light insufficiently for imaging *via* light microscopy; therefore these concentrated areas are simply where there is a higher concentration of DiO due to the amount of the capsule structure within the plain of the image. Another suggestion is that as the internal and continuous phases are removed by solvent flushing, the internal DiO molecules are likely to be dragged to the edge of the capsule. As previously seen in Chapter 3 and earlier in this chapter (see 4.3.11; Encapsulation of alternative actives), DiO molecules are successfully retained within the capsule structure's internal voids even though DiO is highly soluble in

ethanol. The pore sizes of the capsule network formed are smaller than the dye dimension in solution (~ 15 Å)[2] or that the dye is physically or chemically trapped on the capsule surface.

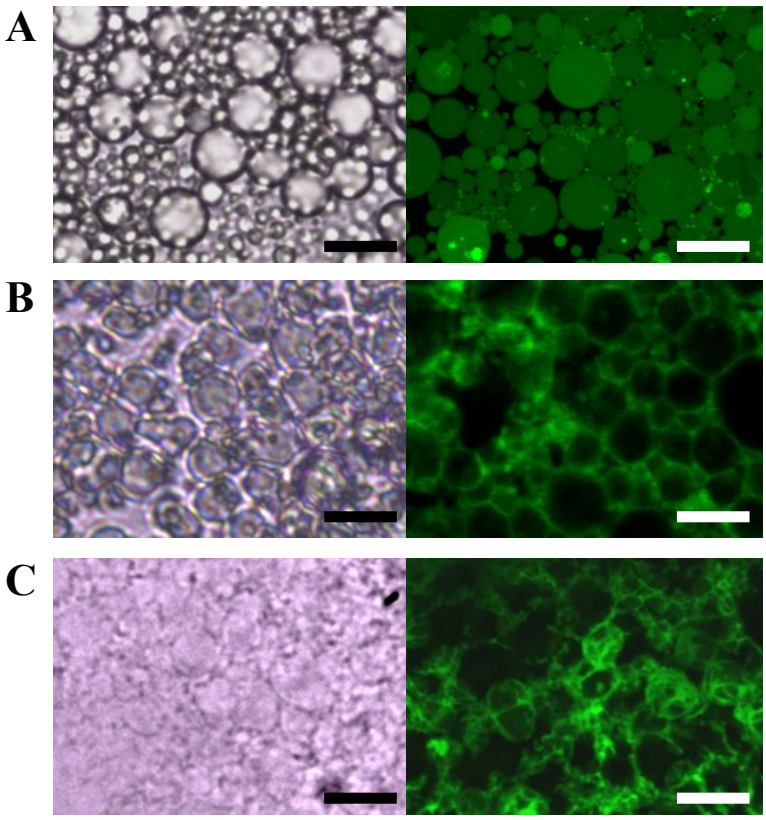

Figure 36. Light microscopy images of (A) uncross-linked concentrated emulsion droplets, (B) assembled and cross-linked emulsion droplets following the addition of acid, and (C) hollow capsule 'scaffold' structure after flushing with EtOH. Scale bars represent 10 µm.

4.4.3.1. Efficiency of acid-catalysed cross-linking

Redispersion of a spheroidal capsule-structure was attempted by introduction of a cross-linked emulsion droplet structure into a high pH environment to assess inter- and intra- cross-

[2] Estimated using ChemBio 3D software by MM2 energy minimisation.

linking obtained *via* acid catalysis (see Figure 37.a-c). A fresh emulsion was prepared, identically as per 4.2.3.1; Emulsion preparation, and concentrated by centrifugation at 2,800 rpm for 60 minutes. An aliquot of creamed P21-stabilised uncross-linked emulsion (41.6 µl) was dropped into acid (HCl, 0.5 M), and then placed into basic water (NaOH) at pH 10 (Figure 37.b.). The spheroidal emulsion droplet structure did not re-disperse suggesting that inter-particle cross-linking was permanent, as proved by flushing a separate spheroidal emulsion droplet structure (41.6 µl) with ethanol (Figure 37.c.). As a control, another aliquot of uncross-linked emulsion (41.6 µl) was dropped into basic water (NaOH, pH 10) which gave the expected redispersion of the emulsion (Figure 37.a.). This ability to form either macro cross-linked structures or associated particles through the choice of either acid or base-catalysed sol-gel formation allows the ability to choose what sort of aggregate or cross-linked structure to prepare.

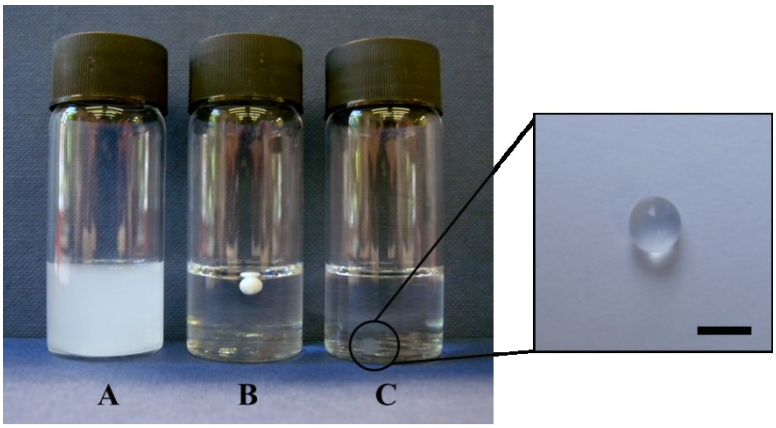

Figure 37. Digital image of (A) an aliquot of uncross-linked concentrated emulsion (41.6 µl) redispersed in pH 10 water, (B) a capsule spheroidal structure in pH 10 water and (C) a capsule spheroidal structure flushed with EtOH. Scale bars represent 3 mm.

The time required for stable spheroidal capsule-structure formation was investigated by dropping aliquots of concentrated emulsion into a reservoir of acidic water (HCl, 0.5 M) for set amounts of time, after which the spheroidal structures were easily removed with a spatula and placed into pH 10 water without redispersion. Figure 38 shows that formation of a stable simultaneously assembled and cross-linked emulsion droplet structure occurs in less than 2 seconds.

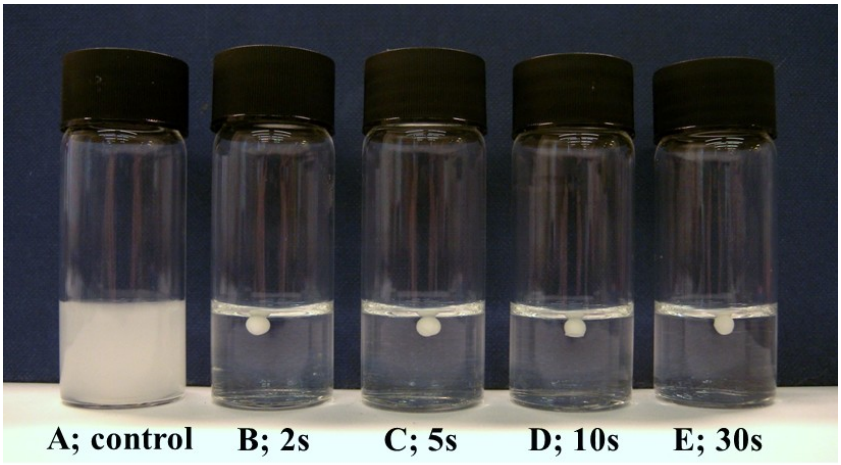

Figure 38. Digital image of the fast and easy formation of emulsion droplet structures. (A) An aliquot of creamed P21-stabilised emulsion was re-dispersed in pH 10 water. (B-E) An aliquot of creamed P21-stabilised emulsion was dropped into HCl (0.5 M) for set time intervals; the formed spheroidal structure was removed with a spatula and placed into pH 10 water.

4.4.4. Encapsulation of small molecules within assembled and cross-linked emulsion droplet structures

Having demonstrated that a small molecule hydrophobe, DiO, could be efficiently encapsulated (see 4.3.11; Encapsulation of alternative actives, where DiO was successfully encapsulated within responsive capsules and also Figure 36, displaying the same

encapsulation within an emulsion droplet), small molecule actives such as dyes were then investigated. All emulsions were made identically as described in 4.2.3.3; Emulsions with encapsulated guest molecules, using commercially available dyes Oil Red and Oil Blue (0.1 w/v %) due to their good solubility in cineole. Spheroidal structures were produced using the method outlined in 4.2.5.2; Spheroidal emulsion droplet structure formation (see Figure 39).

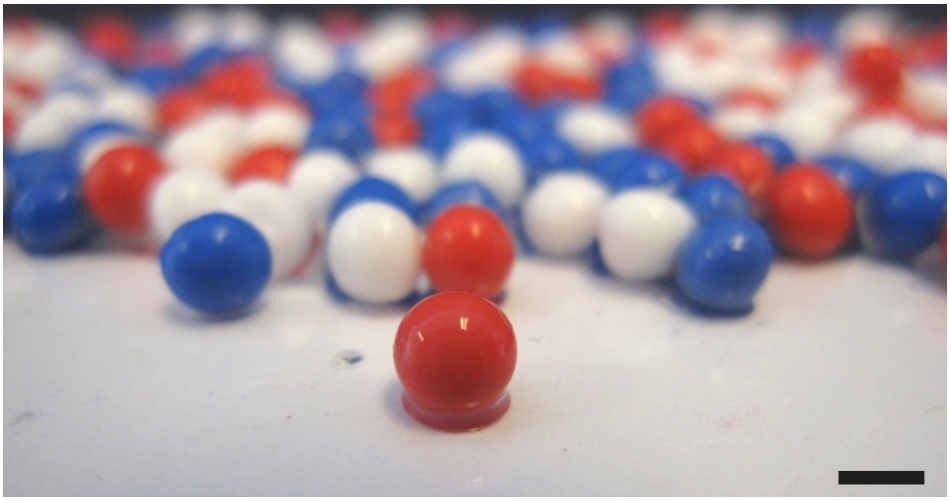

Figure 39. Digital image of spheroidal emulsion droplet structures with encapsulated coloured dyes, Oil Red and Oil Blue at 0.1 w/v %. Scale bar represents 2 mm.

Small molecule dyes were successfully encapsulated within the emulsion droplet structure and furthermore, could be flushed out of the structure using a mutually miscible solvent to give hollow capsules. Figure 40 shows a number of spheroidal structures in basic water (pH 10, 1M NaOH) where the small molecule dyes remained within the hydrophobic environment and did not diffuse into the surrounding bulk aqueous phase until flushed with ethanol, where the dye is released from the structure.

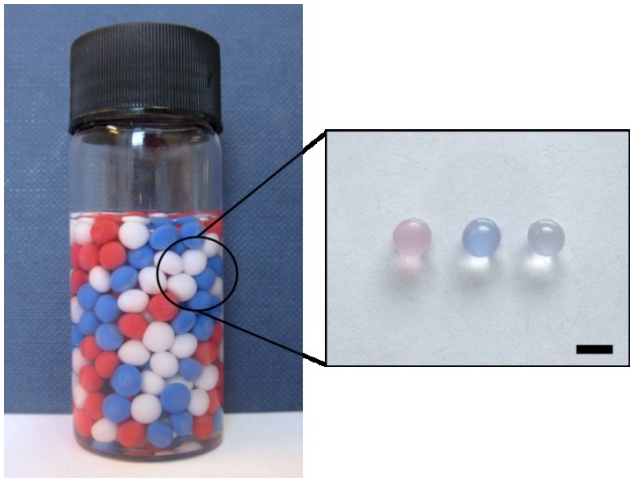

Figure 40. Digital images of a number of spheroidal assembled and cross-linked emulsion droplet structures with encapsulated coloured dyes in bulk pH 10 water, inset shows the removal of dye by flushing with EtOH. Scale bars represent 3 mm.

Furthermore, to demonstrate the versatility and controllability of these structures, spheroidal emulsion droplet structures were made in varying sizes simply by changing the aliquot volume of the concentrated branched co-polymer stabilised emulsion (see Figure 41).

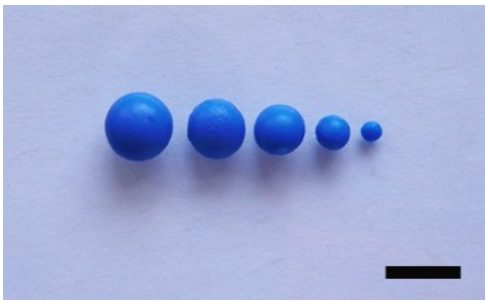

Figure 41. Digital image to demonstrate the versatility and structural control over emulsion droplet structure formation by disparity in spheroidal structure size. Scale bar represents 8 mm.

4.4.5. Structural swelling and shrinking

It was observed that with changing pH, structural swelling and shrinking occurred. The surface MAA residues, of the structurally trapped capsules, are anionic at high pH and electrostatically repel each other causing the structure to swell. At low pH, this charge neutralises and the MAA residues dimerise pulling the capsules together, shrinking the structure (as represented in Figure 42).

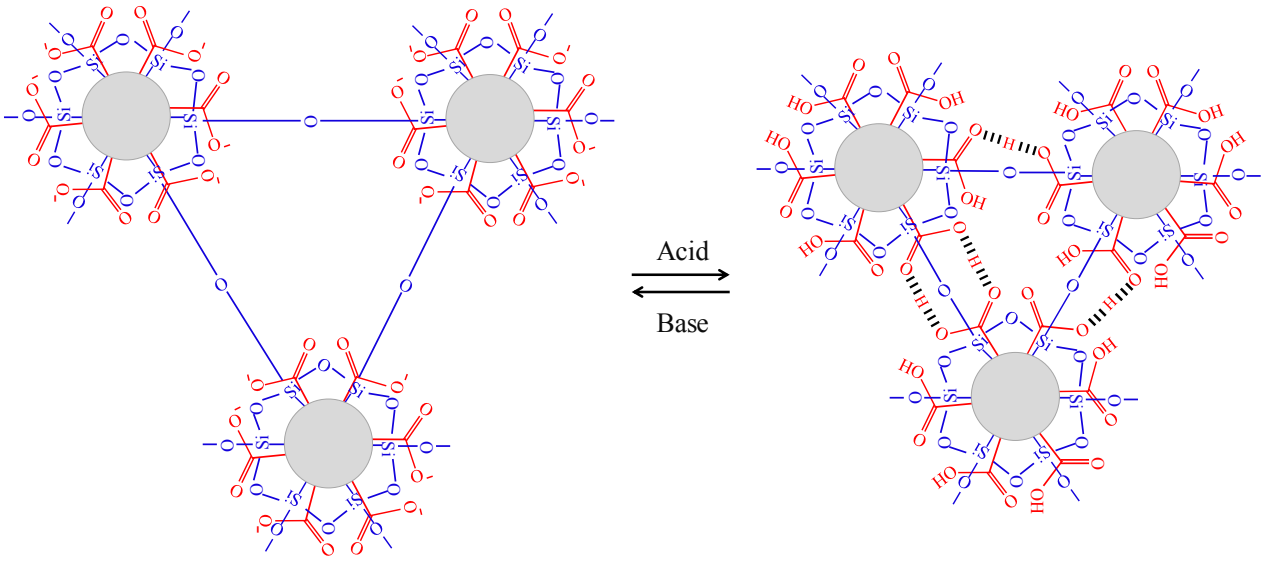

Figure 42. Schematic representation of the structural swelling and shrinking of an emulsion droplet structure with changing pH.

Monolith emulsion droplet structures were used to illustrate the effect of pH on structural size. Seven identical monolith structures were prepared using P21 and cineole as described in

4.2.5.1; Emulsion droplet structure formation, and imaged across a range of pH values (see Figure 43).

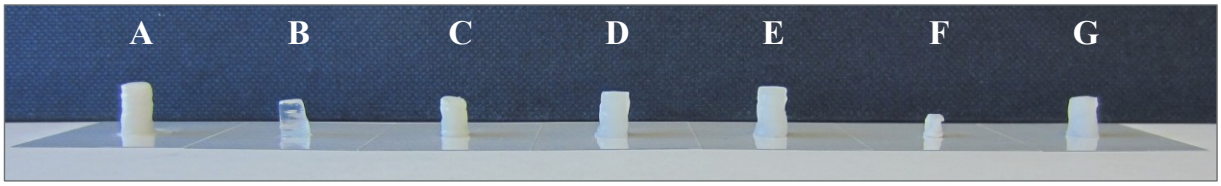

Figure 43. Digital image of (A) emulsion droplet monolith, (B) ethanol flushed monolith, (C) monolith at pH 5, (D) monolith at pH 8, (E) swollen monolith at pH 10, (F) shrunken monolith at pH 2, and (G) pH 2 monolith re-swollen at pH 10.

An ethanol-flushed hollow spheroidal capsule structure was prepared and placed into basic water (pH 10, 1 M NaOH) and then into acidic water (pH 2, 1 M HCl) for a set time of 12 hours repeatedly and the change in size was monitored using optical photography. This process was repeated 3 times, using spheroidal structures made in the same batch, to calculate a margin of error. As shown in Figure 44, the volume of spheroidal structures was plotted as a function of pH, indicating that the change in size fluctuated. Figure 44.a inset shows a digital image of swollen spheroidal structures in basic water at pH 10, whereas Figure 44.b inset shows the same spheroidal structures have shrunk after 12 hours of being placed into acidic water at pH 2.

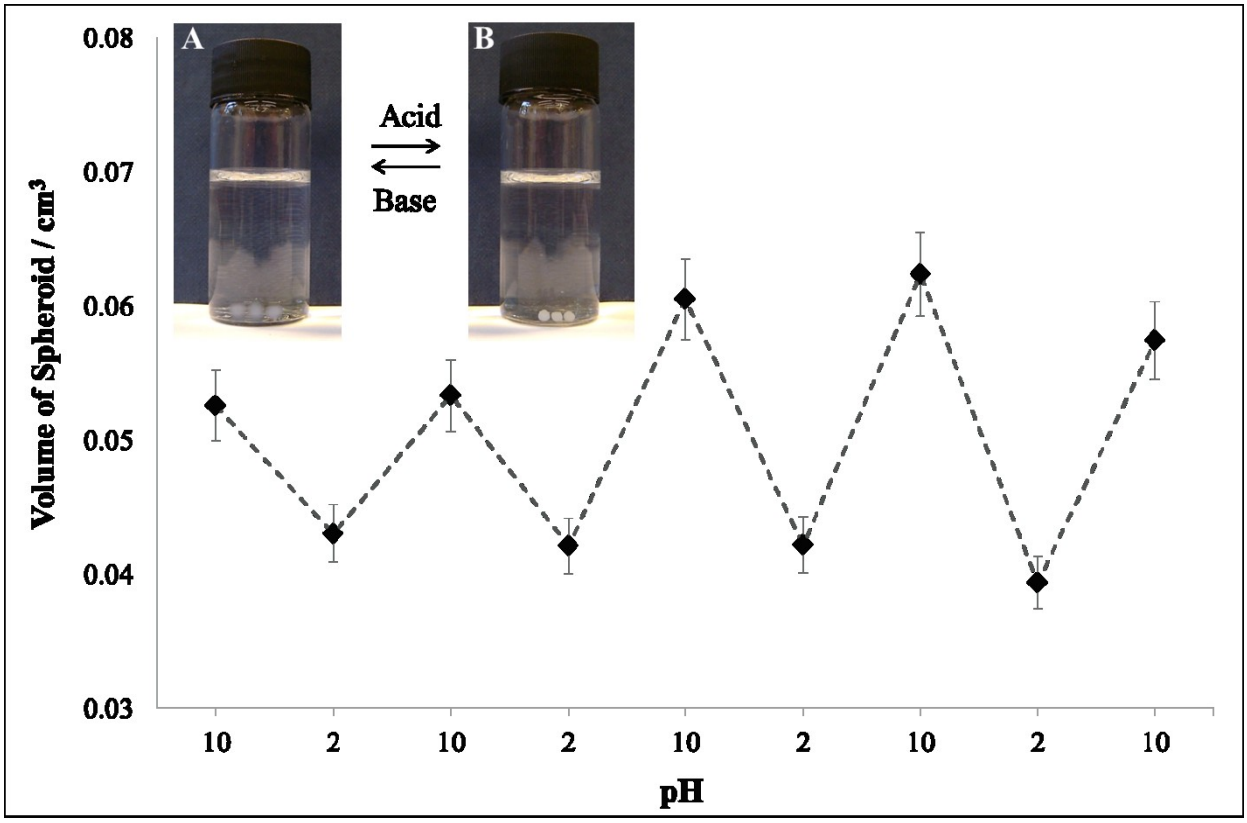

Figure 44. Plot depicting the averaged volume of an ethanol flushed spheroidal capsule structure with changing pH between pH 10 and pH 2. Inset digital image shows (A) swollen spheroidal structures at pH 10 in basic solution (NaOH, 1 M), and (B) shrunken spheroidal structures at pH 2 in acidic solution (0.5 M, HCl).

4.4.6. Physical properties of the capsule structures

The capsule structures showed close structural similarities to polyHIPES; porous emulsion-templated polymers within high internal phase emulsion (HIPEs).[39] HIPEs are highly viscous emulsions where the internal phase, constituting 74% or more of the volume, is dispersed within a minor external phase.[40] If the internal, external, or both, phases contain monomers which can be polymerised typically by FRP, within the HIPE to produce macro-porous materials.[39b, 41] Typically a polyHIPE material's porous structure consists of void

spaces and interconnected holes, which form due to droplet coalescence and/or Ostwald ripening during formation (see Figure 45).[42]

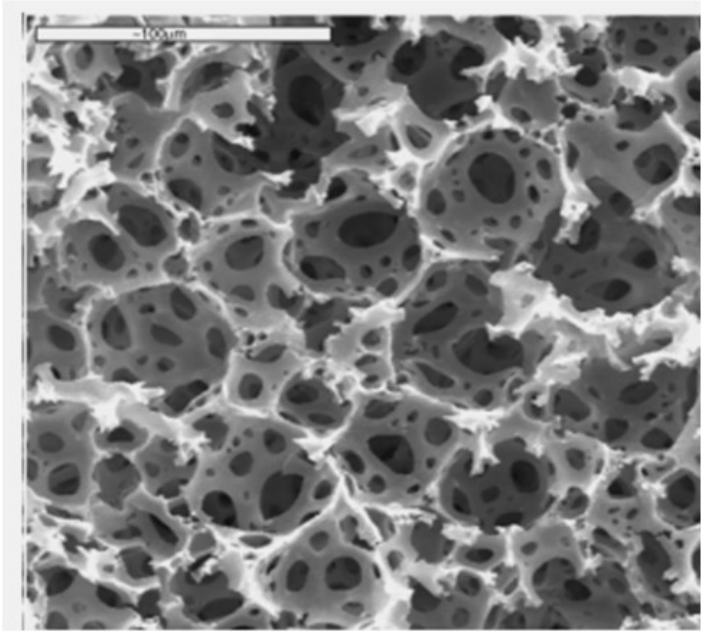

Figure 45. Scanning electron micrograph of a styrene–divinylbenzene polyHIPE structure co-polymerised with an water-in-oil HIPE (90% internal phase volume). Scale bar represents 100 mm. Reproduced with permission from ref. 42.

Barbetta, Cameron and Cooper (2000)[42] produced the polyHIPE (as represented by Figure 45) through the co-polymerisation of styrene and divinylbenzene within a water-in-oil HIPE (90% internal phase volume). This type of porous structure yields materials with low densities and the ability to absorb large quantities of liquids, and are therefore used extensively for a myriad of applications within industries such as food preparation, fuels, oil recovery, cosmetics, agriculture and biomedicines.

Spheroidal structures were made as described in 4.2.5.2; Spheroidal emulsion droplet structure formation, and flushed with ethanol (see 4.2.5.4; Hollow capsule structure formation). Spheroidal capsule structures were placed into either basic water at pH 10 (NaOH, 1M) or acidic water at pH 2 (0.5M. HCl) for 12 hours; the spheroids were then washed repeatedly with absolute ethanol before drying by CPD. Hollow inorganic-organic spheroidal structures were dried by supercritical fluid drying (see Chapter 2; analysis techniques applicable to this thesis), through liquid-gas exchange at their critical point, in order to maintain the structural integrity of the capsule structures. The dried spheroids were then imaged by SEM. SEM images showed an approximate 22.5% reduction in volume of the spheroidal capsule structure from pH 10 to pH 2 as hydrogen bonding between the MAA surface residues pulls the inter-cross-linked capsules together (see Figure 46). The shrunken structure in Figure 46.b shows a distinctive crack in the structure. This suggested to have occured due to the quick rate at which the structures shrink, because the swollen structure is hydrophilic it will allow the acid to enter the structure more freely while it is more difficult for base to permeate a hydrophobic shrunken system.

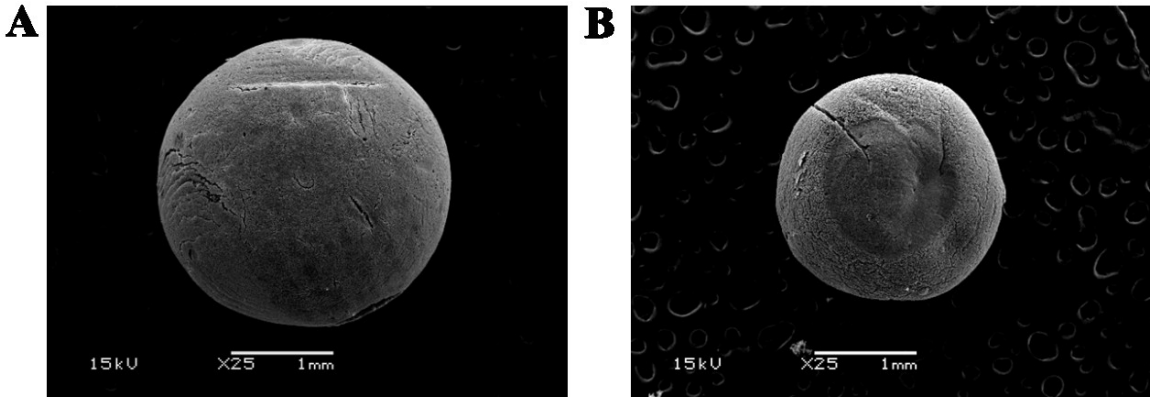

Figure 46. Scanning electron microscopy images of the external morphology of (A) a swollen spheroidal capsule structure at pH 10 dried by CPD, and (B) a shrunken spheroidal capsule structure at pH 2 also dried by CPD. Scale bars represent 1 mm.

The spheroidal structures were sliced in half to view the internal morphology of the structure. However, this was difficult as the capsule structures were soft, but tough and elastic; this was previously found when rupturing capsules to find their shell thickness, see 4.3.9; Physical properties of the capsule shells. SEM images of the internal morphology of a hollow spheroidal capsule structure at high pH (Figure 47.a) showed a swollen network arrangement of capsules. Whereas, the internal morphology of a spheroidal dried at low pH showed a compressed, shrunken capsule network (see Figure 47.b). In comparison with poly-HIPE structural morphology, no interconnected holes are visible suggesting little or no droplet coalescence or Ostwald ripening afforded by the stabilising effect of the co-polymer.

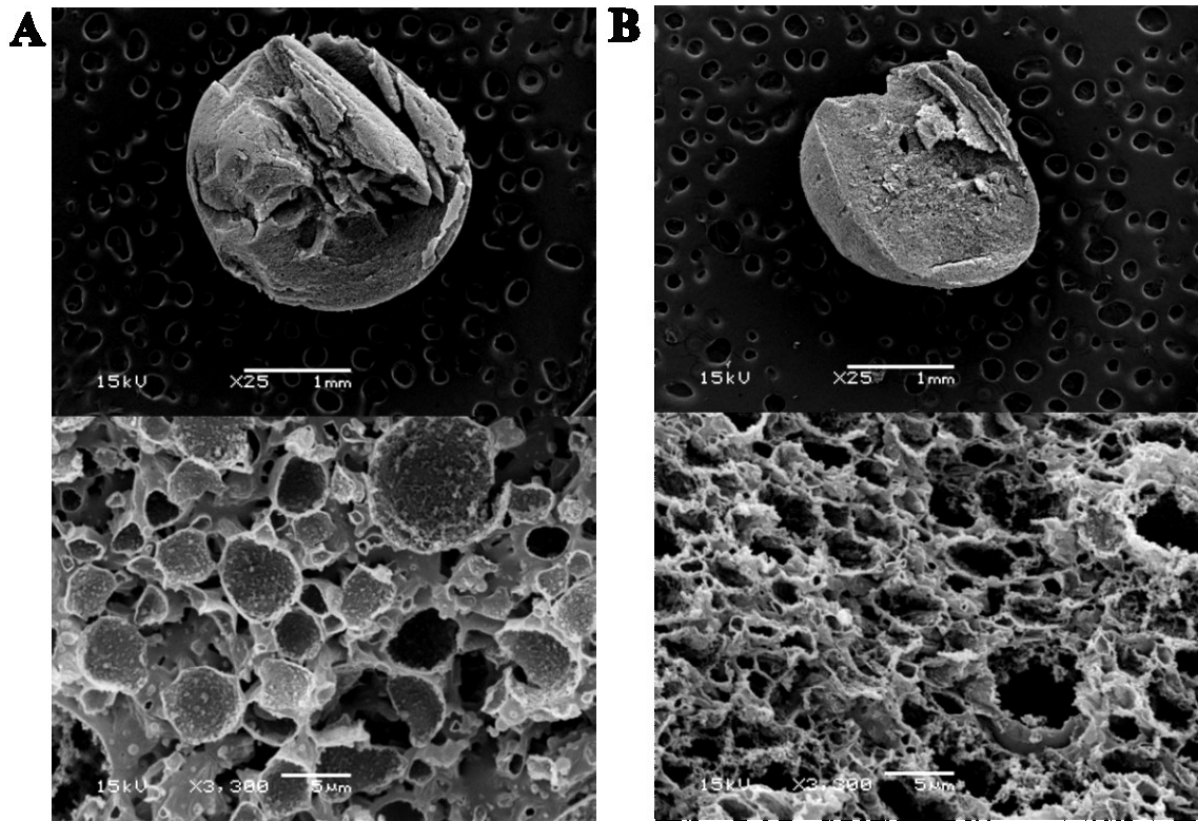

Figure 47. Scanning electron microscopy images of the internal morphology of a (A) swollen spheroidal capsule structure at pH 10 dried by CPD, and (B) a shrunken spheroidal capsule structure at pH 2 also dried by CPD. Scale bars represent 1 mm and 5 µm respectively.

4.4.7. Organic / inorganic composition of hybrid capsule-structures

Hollow spheroidal emulsion droplet structures (prepared identically as outlined in 4.2.5.2; Spheroidal emulsion droplet structure formation) were dried by CPD after the structure was flushed with ethanol to remove both the internal and continuous phases. The structure was then pyrolysed to quantify the amount of organic (MAA, EGDMA, DDT) component relative to inorganic (siloxane from the TMSPMA monomer) component by Thermogravimetric Analysis (TGA) from 40-1000 °C at a heating ramp of 10 °C per minute (see Chapter 2; Analytical techniques applicable to this thesis). It was assumed that the remaining inorganic residue is the cross-linked silica network. The calculated and theoretical amount of inorganic *versus* organic content was compared and was found to be in good agreement (see Figure 48).

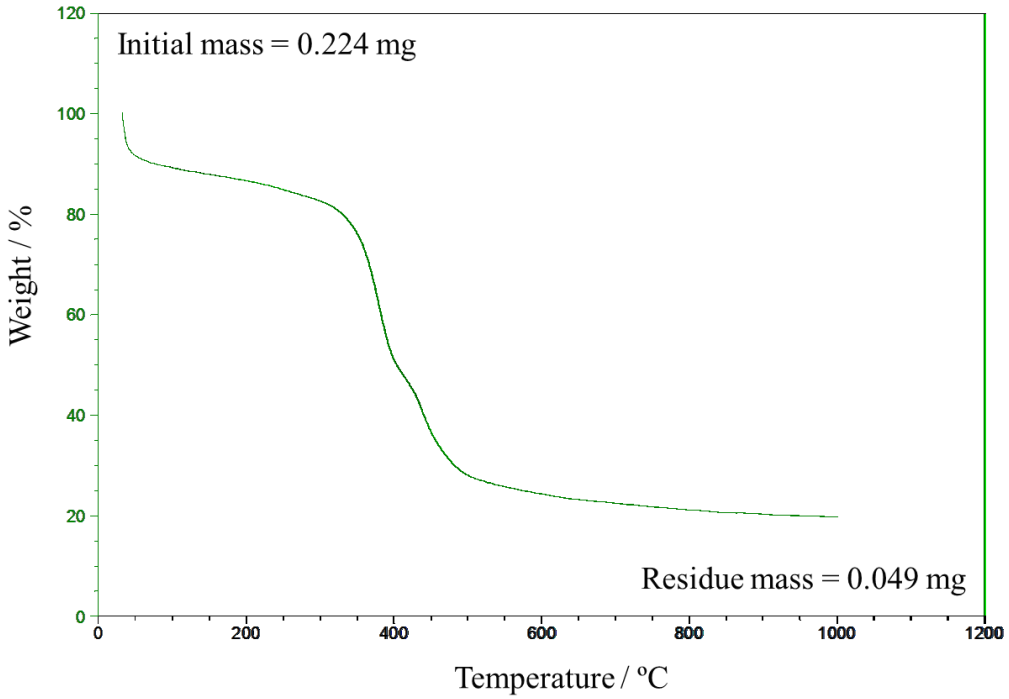

	Calculated	Theoretical [a]
Initial mass of spheroid / mg	0.224	-
Residue / mg	0.049	-
Mass of Organic components* / mg	0.175	0.169
Mass of Inorganic components** / mg	0.049	0.055
Organic component* / %	78.1	75.4
Inorganic component** / %	21.9	24.6

[a] calculated from the initial mass
**Organic component: PMAA, EGDMA, and DDT*
***Inorganic component: TMSPMA*

Figure 48. Quantification of the inorganic vs. organic content of a spheroidal capsule structure analysed *via* thermogravimetric analysis (TGA).

Spheroidal capsule structures were dried by CPD in their swollen (pH 10) and shrunken (pH 2) states, then pyrolysed by TGA from 40-1000 °C at a heating ramp of 10 °C per minute.

Swollen spheroidal structures, allowed to swell in a basic environment, were initially placed into basic water containing sodium hydroxide (NaOH). In Figure 49, the TGA plot of mass loss as a function of temperature for a spheroidal treated with NaOH-based basic water (pH 10) shows a distinct hump from ~400-840 ºC. This was hypothesised to be the salt, NaCl, formed through a neutralisation reaction with trace HCl remaining from the acid-induced assembly and cross-linking. A spheroidal capsule structure was therefore treated with another base, ammonium hydroxide (NH_4OH) for comparison. Spheroidal structures were placed into ammonium hydroxide solution (pH 10), causing them to swell. When using ammonium hydroxide solution (pH 10), no hump was observed during TGA analysis.

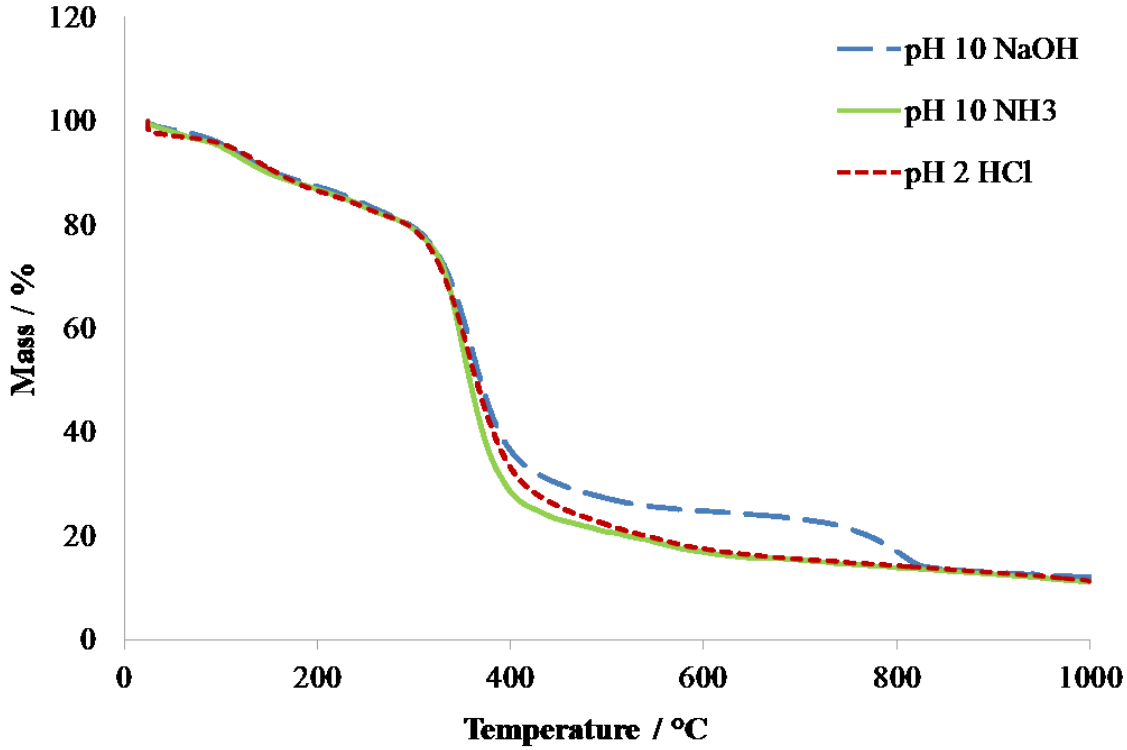

Figure 49. Thermogravimetric analysis of swollen spheroidal capsule structures treated with NaOH-based basic water (pH 10) (blue dashed line) and ammonium hydroxide solution (pH 10) (green line), and shrunken spheroidal capsule structures treated with HCl-based acidic water (pH 2) (red dashed line).

4.4.8. Capsule structure porosity

The network arrangement of capsules, or scaffold architecture, within the structures lends itself to porosity, which was analysed by Mercury Intrusion Porosimetry (MIP) and nitrogen isotherm absorption followed by Brunauer–Emmett–Teller (BET) analysis (procedures outlined in Chapter 2; Analysis techniques applicable to this thesis). Spheroidal emulsion droplet structures were prepared identically as outlined in 4.2.5.2; Spheroidal emulsion droplet structure formation, and flushed with ethanol to remove both the internal and continuous phases. The structures were then dried by CPD in their swollen (pH 10, NaOH) and shrunken (pH 2, HCl) states for analysis (see Figure 50).

A

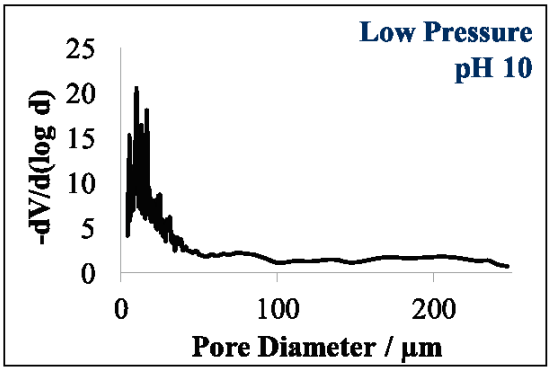

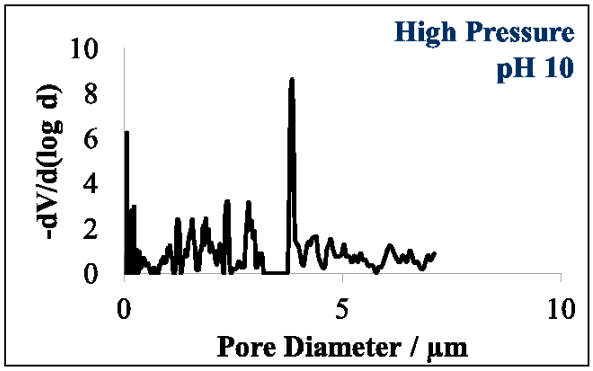

B

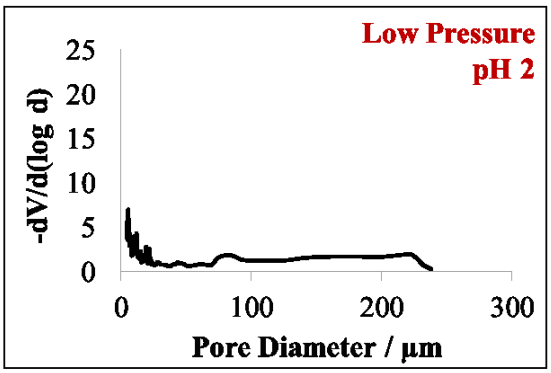

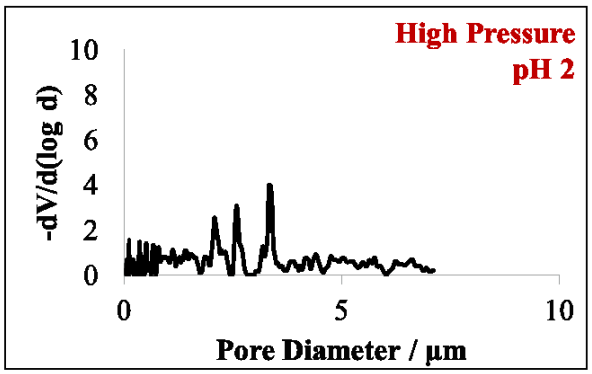

C

Spheroid Structure	Average Pore Diameter at Low Pressure / µm	Average Pore Diameter at High Pressure / µm
pH 10 (NaOH)	25.916	1.407
pH 2 (HCl)	20.600	1.573

Figure 50. Mercury Intrusion Porosimetry (MIP) analysis of (A) swollen spheroidal capsule structure (at pH 10) at low and high pressure, (B) shrunken spheroidal capsule structure (at pH 2) at low and high pressure, and (C) average pore diameters.

Figure 50 shows that swollen structures are more accessible on MIP analysis. However, there is little difference between pore diameters of swollen and shrunken structures (see Figure 50.c). It is suggested that although the shrunken structures are smaller in size, the internal structure is compressed rather than physically smaller. Therefore it is unlikely to see any difference when the structures are filled with a liquid.

Specific surface areas were calculated by BET, using the same spheroidal capsule structures as made previously for MIP, dried by CPD in their swollen (pH 10, NaOH) and shrunken (pH 2, HCl) states for analysis (see Figure 51). Swollen spheroidal structures have a higher specific surface area than their shrunken counterparts, which have a low specific surface area (Figure 51.c).

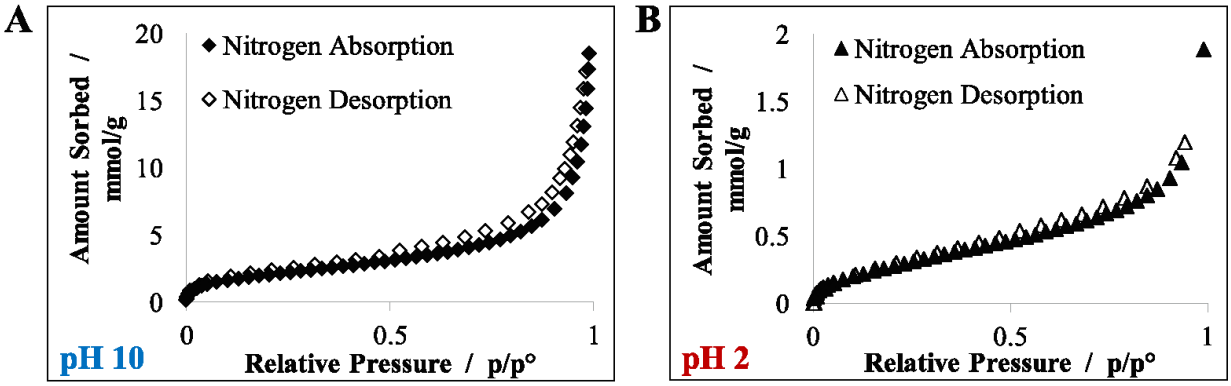

C

Spheroid Structure	Surface Area / m²/g
pH 10 (NaOH)	168.82
pH 2 (HCl)	25.73

Figure 51. Brunauer–Emmett–Teller (BET) analysis of (A) swollen spheroidal capsule structure (at pH 10), (B) shrunken spheroidal capsule structure (at pH 2), and (C) specific surface areas.

4.4.9. Structural control

The ease with which these structures are made, lent to great structural control where the formation of a range of emulsion droplet and capsule structures including fibres, tubing, layers and concentric structures was successful in all manner of shapes and sizes, as well as spheroidal and monolith structures as previously presented. Concentrated emulsions with and

without encapsulated guest dye molecules (Oil Red and Oil Blue at 0.1 w/v %) were prepared identically as defined in section 4.2.5; Emulsion droplet- and capsule- structure formation synthetic processes, and used to make a variety of structures.

Woodward, Chen, Adams, and Weaver (2010)[24b], reported the first use of glucono-δ-lactone (GδL) to induce a homogenous pH change in a pH-responsive co-polymer stabilised emulsion to form large, well-defined 'engineered emulsions.' GδL is a cyclic ester (a lactone), which undergoes hydrolysis in aqueous solution to give gluconic acid in equilibrium (see Figure 52).[43] GδL is highly water-soluble (59 g/100 mL at 20 ºC),[44] and hydrolysis only begins once the solid has been dissolved in water. Hydrolysis of GδL lowers the pH homogeneously throughout an aqueous solution.[43] GδL is a naturally-occurring food additive, acting for example as an acidifier in wines and fruit juices or a curing agent in cured meats.[45] It has also been reported as a homogenous pH trigger in the formation of hydrogels, resulting in reproducible gels with higher strength.[46]

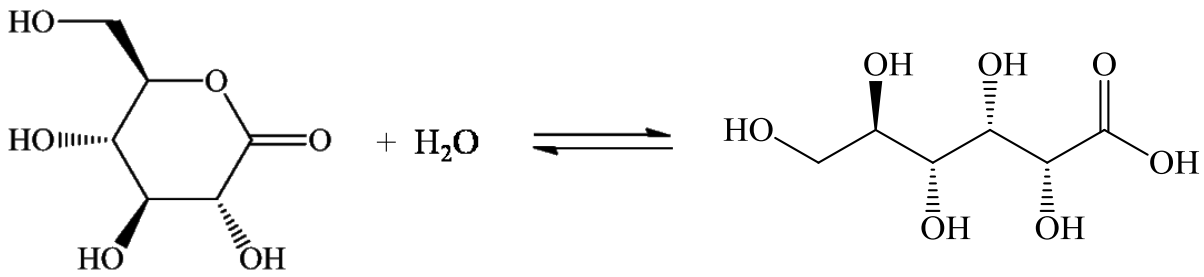

Figure 52. Schematic representation of the hydrolysis of GδL, resulting in chemical equilibrium between the lactone and the acid form.

So far within this chapter, co-polymer stabilised emulsion droplet monoliths and low volume structures were produced as size was limited by the inefficiency of acid diffusion through the structure. By using GδL, larger structures were produced where a more continuous pH change could be generated throughout.

Given the parallel between the internal morphology of capsule or emulsion droplet structures and polyHIPEs, it is anticipated that these structures could be used for similar applications. Successful formation of an enclosed compartment, suggest use for storage of actives or as a chemical reaction environment, where the contents can be removed *via* flushing with a mutually miscible solvent. Furthermore, as good structural control is exhibited allowing for an assortment of shapes and sizes, further industrially relevant applications are possible.

4.4.9.1. Fibres

Concentrated P21-stabilised dye-loaded emulsions were pipetted into acidic water (HCl, 0.5M) forming strands of assembled and cross-linked ‘fibres’ (Figure 53.a), which were then flushed with ethanol (Figure 53.b) removing the encapsulated dye molecules, and the internal and continuous phases.

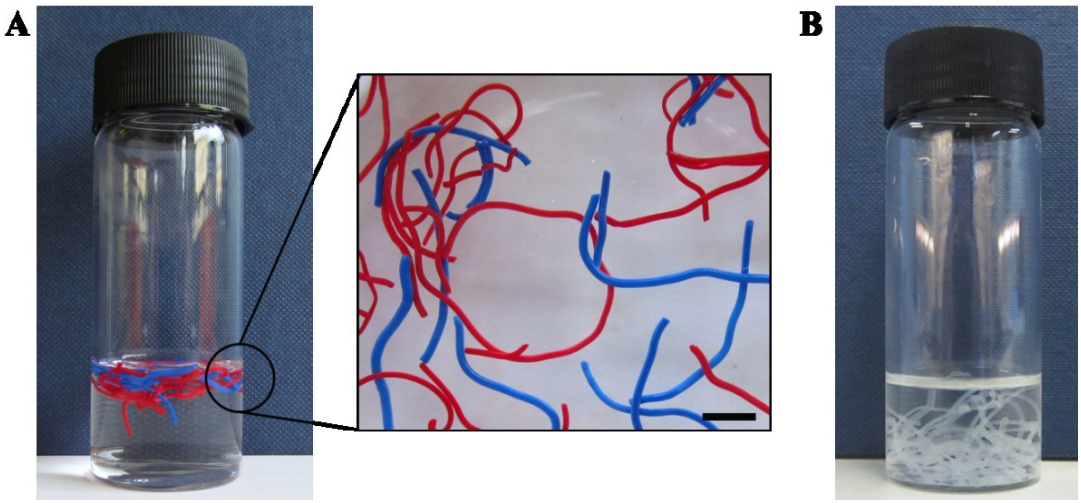

Figure 53. Digital images of (A) 'fibre' emulsion droplet structures with 0.1 w/v % encapsulated Oil Red and Oil Blue dye in acidic water (HCl. 0.5M), insert shows close up image of 'fibres,' and (B) excavated, hollow 'fibre' capsule structures flushed with EtOH. Scale bar represents 5 mm.

4.4.9.2. Tubing

Produced in a similar fashion to 4.4.9.1; Fibres, tubing was produced where a concentric or double needle was designed where there were two different output-channels of the needle-head (Figure 54).

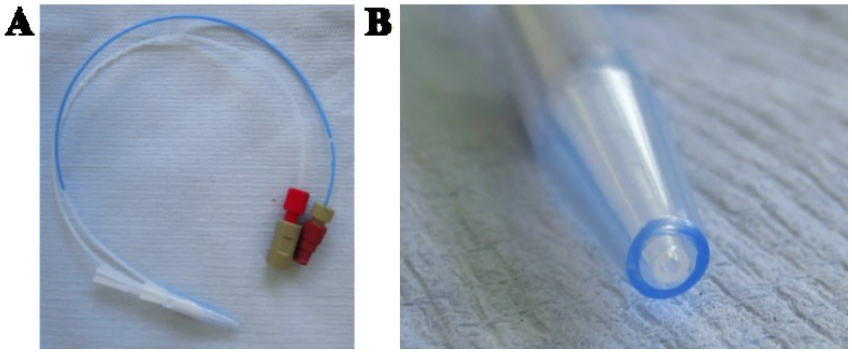

Figure 54. Digital images of the design of (A) the concentric or double needle, (B) shows a close up of the tip of the needle.

The outer needle was filled with concentrated emulsion where Oil Blue was encapsulated at 0.1 w/v % and the internal needle was filled with an oil, cineole. The two needles were attached to a motor and the needle-head dispensed into acidic water (HCl, 0.5M). Capsule 'tubing' structures were produced (Figure 55), and a length of wire was placed through one structure to display that the empty internal tube is continuous.

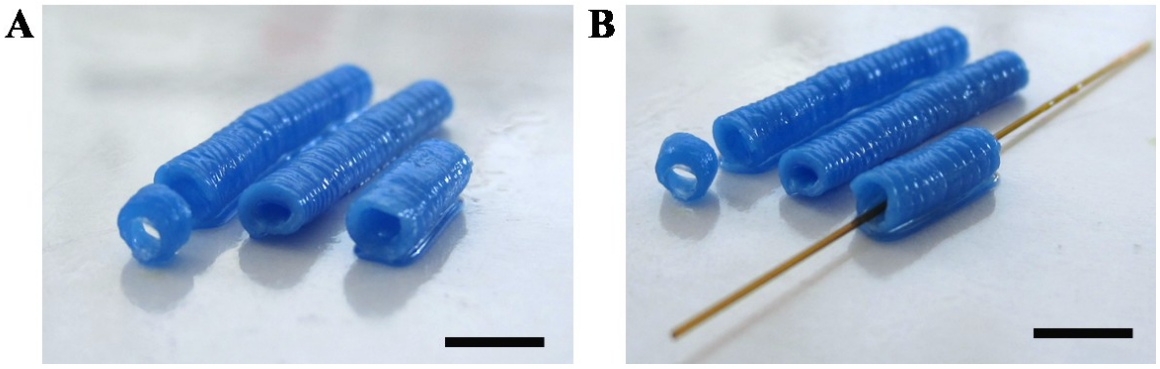

Figure 55. Digital images of (A) capsule 'tubing' structures, and (B) where a length of wire was placed through a capsule 'tubing' structure to show that the empty internal tube is continuous. Scale bars represent 1 cm.

Tubing capsule structures offer a unique reaction environment where an active could be released into a liquid which passes through the permeable tube. These could also be formed into permeable membrane structures, which could be used as separators or as an absorbent for purification (this is discussed further in Chapter 6; Conclusions and further work).

4.4.9.3. Concentric "Scotch egg"

Multi-layered "Scotch egg" emulsion droplet structures were prepared using unloaded and dye-loaded concentrated emulsions (see 4.2.3.3; Emulsions with encapsulated guest molecules). A spheroidal structure was prepared as per 4.2.5.2; Spheroidal emulsion droplet structure formation, and then dipped into either an unloaded emulsion, an Oil Blue encapsulate emulsion or an Oil Red encapsulate emulsion followed by dipping into acidic water at pH 2 (HCl, 0.5M) sequentially to build up layers (Figure 56).

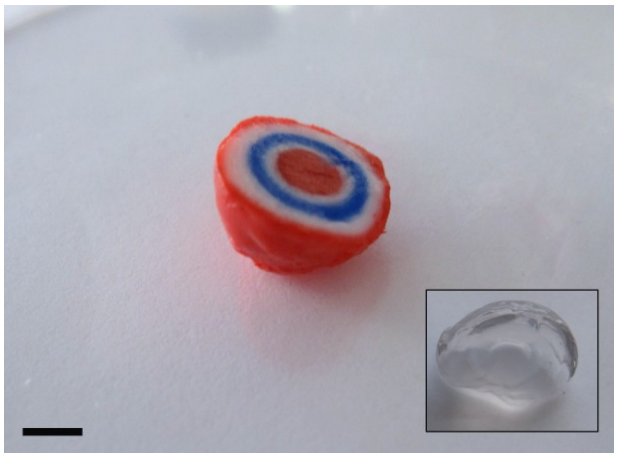

Figure 56. Digital image of a concentric 'Scotch egg' emulsion droplet structure. Inset displays a 'Scotch egg' excavated capsule structure flushed with EtOH where the encapsulate dye, internal and continuous phases have been removed. Scale bar represents 5 mm.

Over time, see Figure 57, the encapsulated blue dye was found to migrate between the layers. The red encapsulated dye did not migrate due to the size of the structure, therefore the spaces, or gaps, within the cross-linked acidified network are smaller than the size of the oil red

molecule. This causes the concentric structure to change colour to purple as the blue and red small molecule dyes mix. If these structures were truly isolated and were responsive they could be used in industry to hold and isolate mutually reactive species where they can be released in close proximity to each other upon changes to the environment.

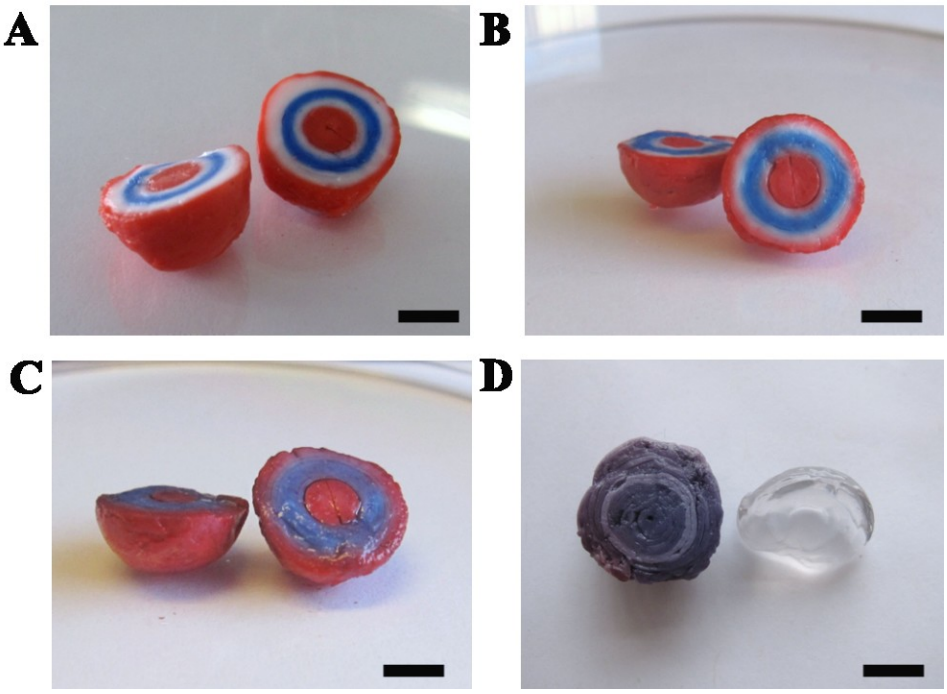

Figure 57. Digital images of (A) concentric 'Scotch egg' emulsion droplet structure where different small molecule dyes are encapsulated at different layers (t = 0 hrs), after time the dye molecules migrate between the layers, (B) t = 1hr, (C) t = 6 hrs, (D) t = 24 hrs, one half of the concentric 'Scotch egg' emulsion droplet structure has turned purple in colour through colour mixing of the blue and red dyes. The other half was flushed with EtOH to remove the encapsulate dye, internal and continuous phases to leave an excavated capsule structure. Scale bars represent 5 mm.

4.4.9.4. Templated bulk shapes

Concentrated dye-loaded emulsion was mixed with GδL and poured into a shaped mould as described in 4.2.5.3; GδL emulsion droplet structure formation. The hydrolysis of GδL to

gluconic acid provided a homogeneous pH trigger for simultaneous assembled and cross-linked emulsion droplet structure formation eliminating the slow diffusion of HCl. This method allowed for a variety of structures where the emulsion fills a mould, permitting a high amount of surface detail (Figure 58.a). The structures were found to be robust, and structurally supportive (Figure 58.b).

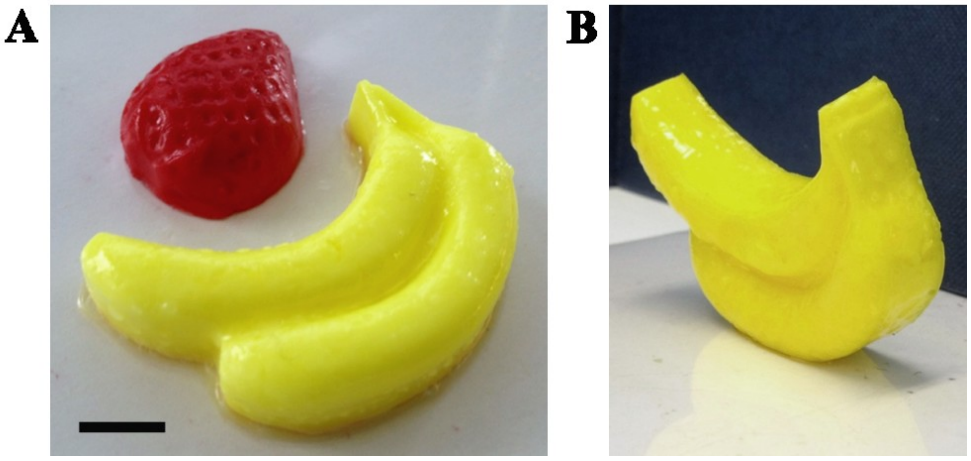

Figure 58. Digital images of (A) emulsion droplet structures formed *via* GδL hydrolysis, where (B) the structures show the ability to maintain the structure when stood upright. Scale bar represents 1 cm.

4.5. Conclusion

In summary, the facile one-component strategy for the preparation of inorganic-organic encapsulated droplets and hollow capsules, as per Chapter 3, can be tailored for specific functionality such as a pH-response. It has been demonstrated that functionalised capsule surfaces and shell/membrane properties with pre-determined complex moieties can be produced. There is a wealth of diversity of composition accessed using the branched co-

polymer synthetic route; creating capsules, able of encapsulating actives, for tailored applications. The incorporation of functionality within the reactive branched addition co-polymer allows higher order responsive structures to be formed. These materials have been shown to be highly useful in the preparation of large associated aggregates which can be loaded with numerous payloads. Both hydrophobic dyes and an oil-soluble polymer were encapsulated, but it is easy to speculate the range of active materials which could be encapsulated and potentially released when desired using this strategy. Examples include biologically active materials and reactive actives where they could be isolated and protected from a harsh environment or formulation. Further encapsulates could include flavours and fragrances or mutually reactive species which could be associated and protected from each other within the same format and released and allowed to react at a further time. This could be useful in reactive adhesives, sealants or coatings. Membranes could be prepared using this methodology where the pore sizes could be controlled and tuned with changes to the pH of the environment.

4.6. References

[1] C. J. Tsai, B. Y. Ma, S. Kumar, H. Wolfson, R. Nussinov, *Crit. Rev. Biochem. Mol. Biol.* **2001**, *36*, 399-433.

[2] A. Klug, *Angew. Chem.-Int. Edit. Engl.* **1983**, *22*, 565-582.

[3] aG. M. Whitesides, B. Grzybowski, *Science* **2002**, *295*, 2418-2421; bJ. Elemans, A. E. Rowan, R. J. M. Nolte, *J. Mater. Chem.* **2003**, *13*, 2661-2670.

[4] J. M. Lehn, *Science* **2002**, *295*, 2400-2403.

[5] aJ. D. Fox, S. J. Rowan, *Macromolecules* **2009**, *42*, 6823-6835; bL. Brunsveld, B. J. B. Folmer, E. W. Meijer, R. P. Sijbesma, *Chem. Rev.* **2001**, *101*, 4071-4097.

[6] D. C. Sherrington, K. A. Taskinen, *Chem. Soc. Rev.* **2001**, *30*, 83-93.

[7] Y. Lvov, K. Ariga, I. Ichinose, T. Kunitake, *J. Am. Chem. Soc.* **1995**, *117*, 6117-6123.

[8] D. E. Discher, A. Eisenberg, *Science* **2002**, *297*, 967-973.

[9] C. G. Claessens, J. F. Stoddart, *J. Phys. Org. Chem.* **1997**, *10*, 254-272.

[10] S. Deechongkit, H. Nguyen, E. T. Powers, P. E. Dawson, M. Gruebele, J. W. Kelly, *Nature* **2004**, *430*, 101-105.

[11] aS. Fujii, Y. L. Cai, J. V. M. Weaver, S. P. Armes, *J. Am. Chem. Soc.* **2005**, *127*, 7304-7305; bR. T. Woodward, R. A. Slater, S. Higgins, S. P. Rannard, A. I. Cooper, B. J. L. Royles, P. H. Findlay, J. V. M. Weaver, *Chem. Commun.* **2009**, 3554-3556.

[12] A. Y. C. Koh, B. R. Saunders, *Chem. Commun.* **2000**, 2461-2462.

[13] Y. X. Liu, P. G. Jessop, M. Cunningham, C. A. Eckert, C. L. Liotta, *Science* **2006**, *313*, 958-960.

[14] P. Brown, A. Bushmelev, C. P. Butts, J. Cheng, J. Eastoe, I. Grillo, R. K. Heenan, A. M. Schmidt, *Angew. Chem.-Int. Edit.* **2012**, *51*, 2414-2416.

[15] aA. Vesperinas, J. Eastoe, P. Wyatt, I. Grillo, R. K. Heenan, J. M. Richards, G. A. Bell, *J. Am. Chem. Soc.* **2006**, *128*, 1468-1469; bS. Khoukh, P. Perrin, F. B. de Berc, C. Tribet, *ChemPhysChem* **2005**, *6*, 2009-2012.

[16] aV. Butun, N. C. Billingham, S. P. Armes, *J. Am. Chem. Soc.* **1998**, *120*, 11818-11819; bS. Y. Liu, S. P. Armes, *Angew. Chem.-Int. Edit.* **2002**, *41*, 1413-1416.

[17] aJ. V. M. Weaver, S. P. Armes, V. Butun, *Chem. Commun.* **2002**, 2122-2123; bS. Y. Liu, N. C. Billingham, S. P. Armes, *Angew. Chem.-Int. Edit.* **2001**, *40*, 2328-+.

[18] V. Butun, S. P. Armes, N. C. Billingham, *Polymer* **2001**, *42*, 5993-6008.

[19] aA. K. Bajpai, S. K. Shukla, S. Bhanu, S. Kankane, *Prog.Polym.Sci* **2008**, *33*, 1088-1118; bM. A. Ward, T. K. Georgiou, *Polymers* **2011**, *3*, 1215-1242.

[20] aC. D. H. Alarcon, S. Pennadam, C. Alexander, *Chem. Soc. Rev.* **2005**, *34*, 276-285; bP. Matricardi, C. Di Meo, T. Coviello, W. E. Hennink, F. Alhaique, *Adv. Drug Deliv. Rev.* **2013**, *65*, 1172-1187.

[21] J. V. M. Weaver, R. T. Williams, B. J. L. Royles, P. H. Findlay, A. I. Cooper, S. P. Rannard, *Soft Matter* **2008**, *4*, 985-992.

[22] N. O'Brien, A. McKee, D. C. Sherrington, A. T. Slark, A. Titterton, *Polymer* **2000**, *41*, 6027-6031.

[23] J. V. M. Weaver, S. P. Rannard, A. I. Cooper, *Angew. Chem.-Int. Edit.* **2009**, *48*, 2131-2134.

[24] aR. T. Woodward, J. V. M. Weaver, *Polym. Chem.***2011**, *2*, 403-410; bR. T. Woodward, L. Chen, D. J. Adams, J. V. M. Weaver, *J. Mater. Chem.* **2010**, *20*, 5228-5234.

[25] S. Graham, P. A. G. Cormack, D. C. Sherrington, *Macromolecules* **2005**, *38*, 86-90.

[26] J. V. M. Weaver, R. T. Williams, B. J. L. Royles, P. H. Findlay, A. I. Cooper, S. P. Rannard, *Soft Matter* **2008**, *4*, 985-992.

[27] R. L. Harbron, T. O. McDonald, S. P. Rannard, P. H. Findlay, J. V. M. Weaver, *Chem. Commun.* **2012**, *48*, 1592-1594.

[28] P. Chambon, L. Chen, S. Furzeland, D. Atkins, J. V. M. Weaver, D. J. Adams, *Polym. Chem.***2011**, *2*, 941-949.

[29] P. A. Costello, I. K. Martin, A. T. Slark, D. C. Sherrington, A. Titterton, *Polymer* **2002**, *43*, 245-254.

[30] J. V. M. Weaver, D. J. Adams, *Soft Matter* **2012**, *6*, 2575–2582.

[31] R. T. Woodward, C. Hight, U. Yildiz, N. Schaeffer, E. M. Valliant, J. R. Jones, M. M. Stevens, J. V. M. Weaver, *Soft Matter* **2011**, *7*, 7560-7566.

[32] B. P. Binks, *Curr. Opin. Colloid Interface Sci.* **2003**, *7*, 21-41.

[33] C. I. Zoldesi, C. A. van Walree, A. Imhof, *Langmuir* **2006**, *22*, 4343-4352.

[34] S. Sacanna, W. T. M. Irvine, P. M. Chaikin, D. J. Pine, *Nature* **2010**, *464*, 575-578.

[35] G. Bealle, J. Jestin, D. Carriere, *Soft Matter* **2011**, *7*, 1084-1089.

[36] aJ. Z. Du, Y. M. Chen, *Angew. Chem.-Int. Edit.* **2004**, *43*, 5084-5087; bJ. Z. Du, S. P. Armes, *J. Am. Chem. Soc.* **2005**, *127*, 12800-12801.

[37] aC. E. Fowler, D. Khushalani, S. Mann, *Chem. Commun.* **2001**, 2028-2029; bA. P. R. Johnston, B. J. Battersby, G. A. Lawrie, M. Trau, *Chem. Commun.* **2005**, 848-850.

[38] J. Z. Du, Y. M. Chen, *Macromolecules* **2004**, *37*, 5710-5716.

[39] aH. Bartl, W. Von Bonin, *Makromol. Chem.* **1962**, *57*, 74-95; bM. S. Silverstein, *Prog. Polym. Sci.***2014**, *39*, 199-234; cH. Bartl, W. Von-Bonin, *Macromol. Chem. Phys.***1963**, *66*, 151-156; dK. Horie, I. Mita, H. Kambe, *J. Appl.Polym.Sci.***1967**, *11*, 57-71.

[40] aK. J. Lissant, *J.Colloid Interface Sci.***1966**, *22*, 462-468; bK. J. Lissant, K. G. Mayhan, *J. Colloid Interface Sci.***1973**, *42*, 201-208; cK. J. Lissant, B. W. Peace, S. H. Wu, K. G. Mayhan, *J.Colloid Interface Sci.***1974**, *47*, 416-423.

[41] M. S. Silverstein, N. R. Cameron, in *Encyclopedia of Polymer Science and Technology*, John Wiley & Sons, Inc., **2002**.

[42] A. Barbetta, N. R. Cameron, S. J. Cooper, *Chem. Commun.* **2000**, 221-222.

[43] Y. Pocker, E. Green, *J. Am. Chem. Soc.* **1973**, *95*, 113-119.

[44] R. Igoe, *Dictionary of Food Ingredients*, Springer, New York, **2011**.

[45] aR. Tarte, *Ingredients in Meat Products: properties, functionality and applications*, Springer, New York, **2008**; bM. Ash, *Handbook of Preservatives*, Synapse Info. Resources, New York, **2004**.

[46] aD. J. Adams, M. F. Butler, W. J. Frith, M. Kirkland, L. Mullen, P. Sanderson, *Soft Matter* **2009**, *5*, 1856-1862; bS. Sutton, N. L. Campbell, A. I. Cooper, M. Kirkland, W. J. Frith, D. J. Adams, *Langmuir* **2009**, *25*, 10285-10291; cJ. Raeburn, G. Pont, L. Chen, Y. Cesbron, R. Levy, D. J. Adams, *Soft Matter* **2012**, *8*, 1168-1174.

CHAPTER 5

Electrostatically gated branched co-polymer-based membrane with selective permeability for inorganic protocell constructs

(Publication arising from this Chapter: **"Electrostatically gated membrane permeability in inorganic protocells"**, M. Li, R. L. Harbron, J. V. M. Weaver, B. P. Binks, S. Mann, *Nature Chemistry* **2013**, *5*, 529.)

List of figures

List of tables

5.1 Introduction

The compartmentalisation, or regional separation, of biochemical reactions within membrane-enclosed water droplets is a promising route towards the organisation and assembly of functional artificial cell systems.[1] In general, research has focused on the design and construction of protocells, aiming to mimic primitive cells, by the spontaneous self-assembly of enclosed organic membranes such as lipid or fatty acid vesicles.[2] Although these systems offer the most plausible route, similar to natural systems, for the primary formation of protocells, other novel approaches have been investigated such as membrane-free peptide polyelectrolyte/nucleotide micro-droplets,[3] or water-filled micro-compartments bound by semi-permeable inorganic membranes.[4]

The preparation of micro-scale compartments in the form of Pickering emulsions, which consisted of a suspension-in-oil of polystyrene and poly(methyl methacrylate) colloidal particles forming semi-permeable capsules or colloidosomes by self-assembly was first presented in Science (2002)[5] by Dinsmore, Hsu, Nikolaides, Marquez, Bausch, and Weitz (see Figure 1). The interstices, or holes, between the particles define the permeability of the colloidosome-membrane and the internal space offers an important step towards the construction of cellular-type reaction environments for processes such as gene expression[4a] and enzyme-mediated catalysis.[4a, 6] However, this, and similar biomimetic systems are limited by the continuous oil medium. When the semi-permeable colloidosome-capsules are transferred into bulk water, the colloidosome-membrane disassembles releasing any entrapped bio-molecular components.

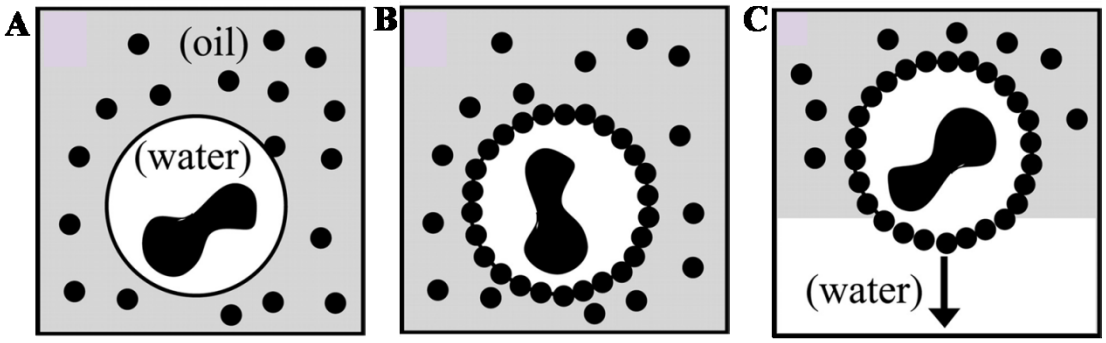

Figure 1. Schematic representation of the ideal self-assembly process of colloidosome structures with the ability to encapsulate materials.[5] (A) Aqueous droplets are dispersed in oil containing colloidal particles, (B) particles adsorb onto the surface of the droplets, and (C) the structure is transferred to water. Reproduced with permission from ref. 5.

The development of a stable membrane, without compromising the level of semi-permeability required for the retention, uptake and release of bio-molecules or small molecule substrates is an important step towards the construction of water-dispersible protocells (as depicted in Figure 1.c). It is also important to consider that once intact colloidosomes are transferred into water, their functionality and usage can be undermined by the diffusion of small low molecular weight substrates through the semi-permeable membrane. Therefore, mechanisms that allow for selective transport are favoured.

Previous studies on colloidosome formation demonstrated that the properties, such as permeability, mechanical strength and responsiveness of the colloidosome-capsules are strongly dependent on the type and size of the component colloidal particles,[5] post-assembly processing and physical state of the interior,[7] and that transfer into water requires prior stabilisation of the membrane by sintering or chemical cross-linking.[5, 8]

Hsu, Nikolaides, Dinsmore, Bausch, Gordon, Chen, Hutchinson, and Weitz (Langmuir, 2005)[8a] reported the construction of particle shells with tunable morphology and mechanical

response using colloidal particles that self-assemble at a water-in-oil emulsion droplet interface (Figure 2). This is achieved by either fusing the particles together through sintering, which not only imparts additional shell stability but also tunes the porosity and subsequent permeability, or by interfacial polymer (poly-L-lysine) absorption that locks the particles together (see Figure 2.b-c), where the amount added allows for variation in mechanical robustness. The viability of these shells as capsules was tested by removal of the internal phase by flushing with a mutually miscible solvent, where some aggregation of the particles was observed. Both sintered and polymer-stabilised shells remained intact.

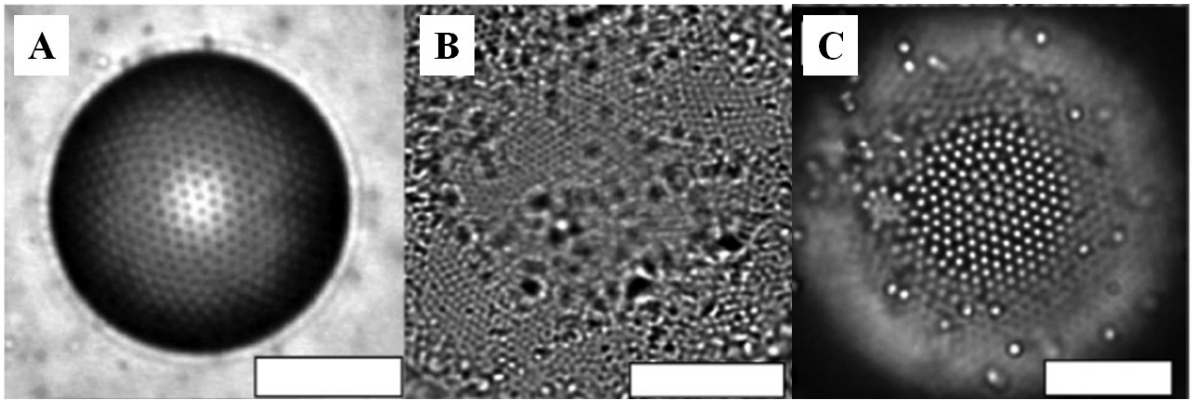

Figure 2. Light micrographs of unfixed and polymer-stabilised particle shells in different oils (b-c). (A) Particles assembled onto water droplets in toluene forming layers of unfixed particles with a high degree of crystalline order. (B) Particles assembled onto droplets of aqueous polymer solution in toluene and (C) vegetable oil exhibit a lower degree of crystalline order. Scale bars represent 10 μm. Reproduced with permission from ref. 8a.

Covalently cross-linked colloidosomes formed by the assembly of Poly(glycerol monomethacrylate) with a degree of polymerisation of 50- (PGMA50) stabilised polystyrene latex particles were reported by Thompson and Armes (2005).[8b] Covalent cross-linking occurred between the end hydroxyl groups of the stabilising PGMA50 chains *via* diisocyanate chemistry forming robust urethane bonds[9] and consequently stable colloidosomes (see Figure 3). The resulting colloidosomes were flushed with a mutually miscible solvent and remained intact, no aggregation of the particles was observed.

Covalently cross-linked colloidosomes were judged as significantly more stable and robust than related systems[5, 8a, 8c] and readily made using a non-volatile, oil-soluble cross-linkable polymeric stabiliser.

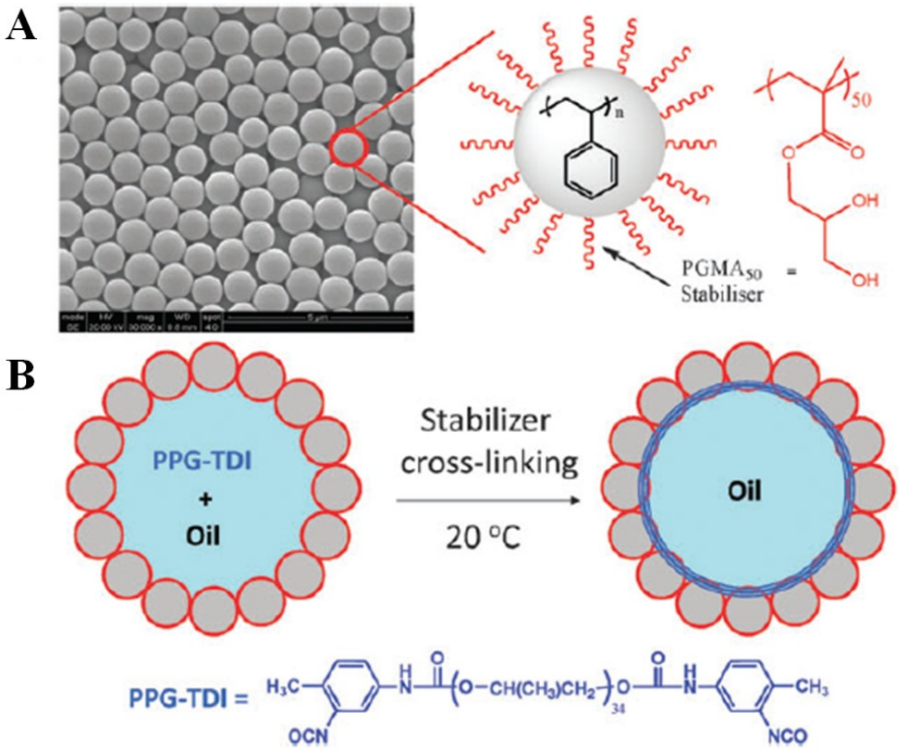

Figure 3. (A) Representative scanning electron micrograph of a poly(glycerol monomethacrylate) (PGMA50)-stabilised polystyrene latex. (B) Covalently cross-linking of the hydroxyl groups of the PGMA50 chains (depicted by the red shell) at the inner surface of the latex particles is adsorbed onto the oil droplets using tolylene 2,4-diisocyanate-terminated poly(propylene glycol) (PPG-TDI) as a cross-linker. Reproduced with permission from ref. 8b.

Permeability of the colloidosome-membrane could be tuned by assembling a colloidosome membrane from polymer gel particles that exhibit temperature-dependent swelling/shrinking behaviour. In 2010, Shah, Kim, and Weitz[7c] prepared water-in-oil emulsions using primary amine-functionalised poly(N-(3-amino propyl)methacrylamide micro-gels. Cross-linking within the aqueous droplets was achieved using a dialdehyde to produce novel thermo-responsive microcapsules. However, aggregation of excess particles occurred during cross-

linking. Kim, Fernandez-Nieves, Dan, Utada, Marquez, and Weitz (2007)[10] had previously shown that a polymer was used as a scaffold for particle assembly such that temperature-dependent buckling of the internal gel causes reversible 'jamming' of the gel particle packed-organic membrane changing the porosity of the structure. In contrast, as reported later by Weitz[11], silica nanoparticle-based colloidosomes were found to be impermeable, and as such examples of inorganic-based reports are rare.

In this chapter[1], the design and construction of inorganic-membrane gated colloidosomes or micro-capsules, which can be transferred intact from oil into water, comprised of a co-polymer-grafted inorganic membrane with self-activated, electrostatically mediated permeability is presented.[12] A functional inorganic-organic branched co-polymer was developed with specific properties *via* tailored design. Polymeric materials are becoming increasingly popular in this application; interest has increased due to ease of preparation and the diversity provided by co-polymer composition. In this case, the charge on the designed branched co-polymer, at the surface of the inorganic membrane, responded to a change in pH providing the responsiveness and ultimately the gated selectivity. This was used to produce intact water-dispersible colloidosomes that exhibit selective permeability for anionic or cationic solutes; this mechanism was exploited for the construction of inorganic protocells with membrane-gated enzymatic activity.

[1] All authors participated in the writing of this paper, specific sections are appropriately acknowledged. Dr. M. Lei and Prof. S. Mann conceived the concept; Prof. S. Mann directed the research, Dr. M. Li, R. L. Harbron and Dr. J. V. M. Weaver designed and performed the experiments and analysed the data, and Prof. B. P. Binks contributed the surface-active nanoparticles and discussions on colloid science.

5.2 Experimental

In brief, initially a Pickering emulsion that consisted of aqueous micro-droplets stabilised with a semi-permeable membrane of closely packed silica nanoparticles (20–30 nm) was prepared in dodecane. Subsequently, the silica nanoparticle-based membrane was stabilised using cross-linking by reaction with tetramethoxysilane (TMOS) followed by covalent grafting of a pH-responsive branched co-polymer in oil (see Figure 4). The surface of the silica nanoparticles was surface-functionalised with *ca.* 50% silanol ($–O_3SiOH$) and 50% dimethylsilane ($–O_2Si(CH_3)_2$) groups (as described in the following sections) to allow for cross-linking between the surface, TMOS and the co-polymer. This stabilised the inorganic network and facilitated the transfer of intact colloidosomes into water.

The covalently grafted responsive branched co-polymer provided an outer layer capable of electrostatically mediating the diffusion of small molecules through the interstices in the shell (see Figure 5). Novel inorganic-organic pH-responsive co-polymers were synthesised by a one-step FRP route using a thiol-regulated branching polymerisation technique[13] as previously used and discussed throughout this thesis, where a siloxane-based methacrylate monomer (TMSPMA), and co-monomers 2-(dimethylamino)ethyl methacrylate (DMAEMA) and MAA were incorporated to give the ability to form cross-links and exhibit pH-responsive functionality.

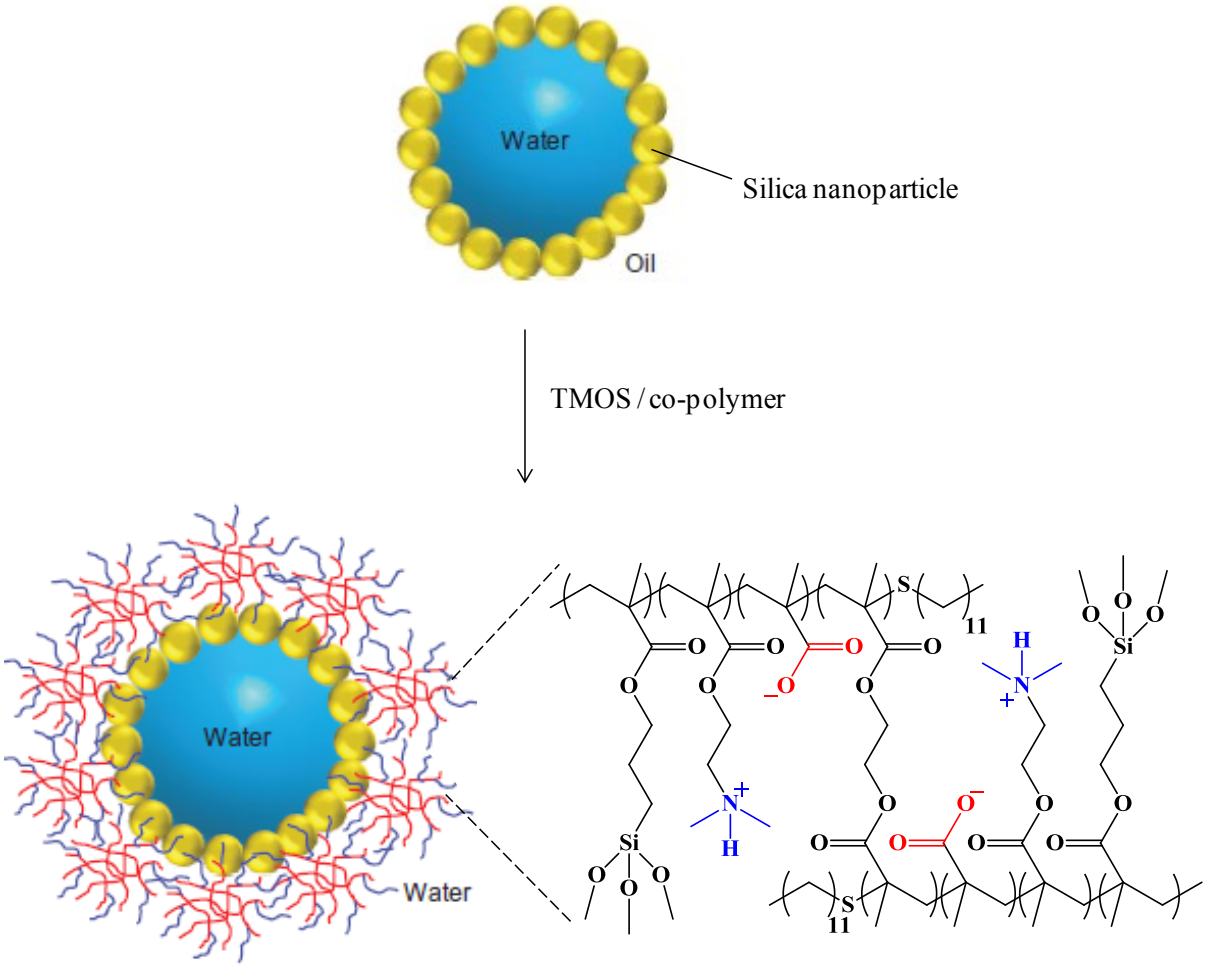

Figure 4. Schematic representation of the design and construction of functionalised colloidosomes prepared by TMOS-induced cross-linking and covalent grafting of a branched co-polymer corona onto the semi-permeable outer surface of a closely packed shell of silica nanoparticles. Reproduced with permission from ref. 12.

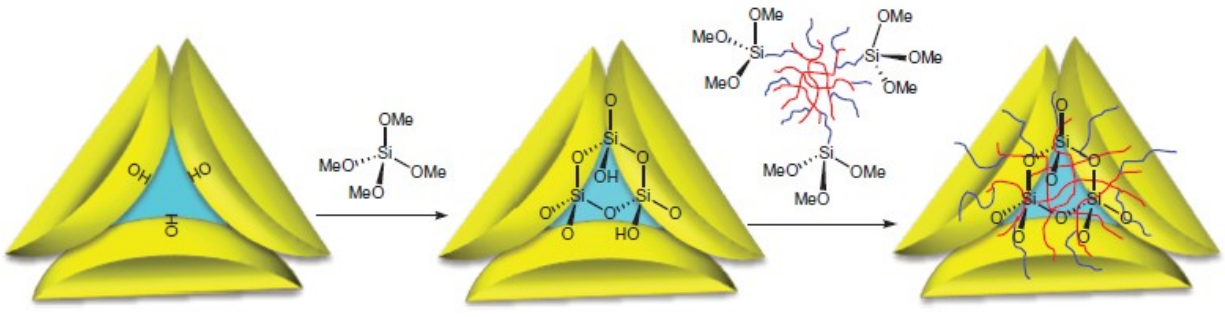

Figure 5. Scheme showing the intersection of three closely packed silica nanoparticles located within the inorganic membrane. Reproduced with permission from ref.12.

5.2.1. Design of pH-responsive branched co-polymer composition

The design of the novel co-polymer was approached in accordance with the desired properties of the end product. This was in continuation from the work discussed in Chapter 4; the role of branched co-polymer composition in controlling hybrid capsule surface functionality, where surface responsive capsules are formed *via* a one-pot single-component process; the single component being a multifunctional branched co-polymer. Initially a further inorganic-organic branched co-polymer, P21 (2) (Figure 6.a) was used (as synthesised in the previous chapter) to try and create a gated-membrane with some success; however, not all of the functional requirements were met. With P21 (2), only an anionic charge (from MAA residues) could be exhibited at high pH on the resulting co-polymer, and therefore it did not provide a full pH range of gated selectivity. The addition of another co-monomer into the composition was required to give a cationic charge when the MAA-residues were neutralised (at low pH). This was facile due to the ease with which chosen functionalities can be incorporated into a polymer product when polymerised by FRP as discussed in Chapter 1; Introduction. The incorporation of 2-(diethylamino)ethyl methacrylate (DEAEMA) was discussed as when applied to the current system it is expected to display a cationic charge at low pH whilst neutral charge at high pH. However, although this was deemed effective in creating a functioning outer coronal layer, it was felt that performance could be improved since DEAEMA is a longer chain molecule than the MAA co-monomer. It was hypothesised that ease of access to the charge by the small molecules for uptake and release from the polymer-stabilised cross-linked silica nanoparticle-based colloidosomes was hindered. In response, DEAEMA was replaced with its shorter chain counterpart, 2-(dimethylamino)ethyl

methacrylate (DMAEMA) and the resulting terpolymer, P23 exhibited successful pH-gated selectivity (Figure 6.b). The molar ratio of DMAEMA was kept exactly the same as MAA to provide equal amounts of charge along the polymer product whether anionic or cationic with changing pH. The novel inorganic-organic pH-responsive co-polymer, P23, targeted composition was $TMSPMA_{22}/DMAEMA_{39}/MAA_{39}–EGDMA_{10}–DDT_{10}$. The co-polymer was designed with branched architecture of TMSPMA, DMAEMA, MAA, ethylene glycol dimethacrylate (EGDMA), and 1-dodecanethiol (DDT) moieties. A branched terpolymer was produced because in the previous chapters of this thesis, branched architectures were found to provide higher interfacial stabilisation. Branched architectures also provide a more accessible network of pH-responsive residues for mediation of small molecules in and out of the protocell constructs.

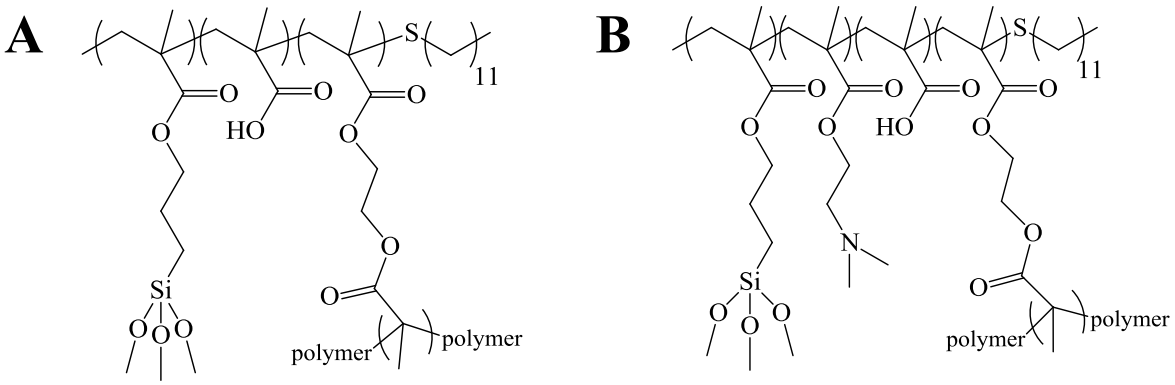

Figure 6. Structural representation of (A) P21 (2), $TMSPMA_{61}/MAA_{39}$-$EGDMA_{10}$-DDT_{10} (B) P23, $TMSPMA_{22}/DEAEMA_{39}/MAA_{39}$-$EGDMA_{10}$-$DDT_{10}$ and, (C) P23, $TMSPMA_{22}/DMAEMA_{39}/MAA_{39}$-$EGDMA_{10}$-$DDT_{10}$.

5.2.2. Preparation of branched co-polymer, P21 (2)

P21 (2) (from Chapter 4) was synthesised as described in Chapter 4; section 4.2.1.1; Preparation of branched co-polymer, P21). ^{1}H NMR spectroscopy was used to confirm the co-polymer composition, where the peaks have been assigned (see Chapter 4; Figure 12);

5.2.3. Representative preparation of $TMSPMA_x/DMAEMA_y/MAA_z$ – $EGDMA_{10}$ – DDT_{10} branched co-polymers

In order to synthesise the responsive branched terpolymer P23 (Figure 6.c), a mixture of TMSPMA (10.00 g, 40.27 mmol), DMAEMA (11.23 g, 71.43 mmol), MAA (6.15 g, 71.44 mmol), EGDMA (3.63 g, 18.31 mmol), and DDT (3.74 g, 18.30 mmol) was degassed separately with a nitrogen purge using a Schlenk line. Methanol (350 mL, anhydrous) was also degassed separately with a nitrogen purge using a Schlenk line and added to the monomer mixture. After heating to 70 ^{o}C, the co-polymerisation was initiated by the addition of AIBN (374 mg, 2.28 mmol) and the reaction mixture was stirred with heating for 48 hours. The methanol was then removed by distillation and the resulting co-polymers were stored under vacuum. No purification steps were required due to almost complete conversion; typically conversions in excess of 97% were achieved as determined by ^{1}H NMR spectroscopy. ^{1}H NMR spectroscopy was used to confirm the mean co-polymer composition where the peaks have been assigned; however post-esterification of the polymer was required, carried out in an identical manner as described in Chapter 4; 4.2.2 Esterification of

methacrylic acid containing polymers, in order to gain full compositional ratios in ^{1}H NMR analysis (see Figure 7). 92.1% of MAA groups were esterified as calculated from ^{1}H NMR spectra. Size exclusion chromatography data of the unesterified materials (see Table 1) was performed by triple detection (TD-SEC) (as discussed in Chapter 1; Introduction).

Example experimental calculations applicable to all polymers covered within this thesis are represented in Chapter 3; Synthesis of emulsion-templated hybrid inorganic–organic polymer capsules using a branched co-polymer surfactant for hydrophobic active encapsulation.

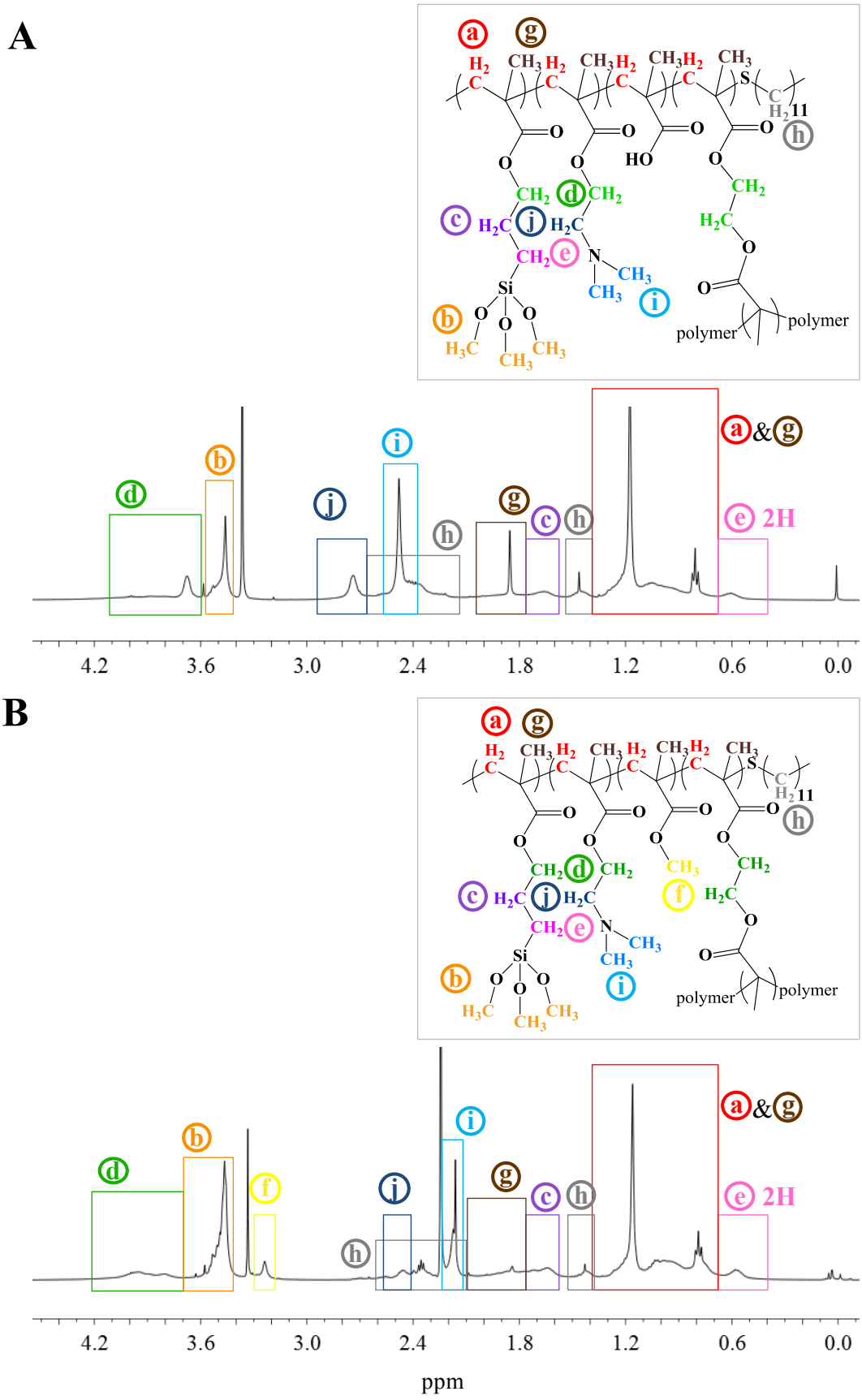

Figure 7. Peak assigned ^{1}H ($CDCl_3$) NMR spectra of (A) unesterified and (b) esterified P23, $TMSPMA_{23.4}$/$DMAEMA_{40.4}$/$MAA_{37.4}$-$EGDMA_{8.4}$-$DDT_{10.4}$. Adapted with permission from ref. 12.

5.2.4. Preparation of silica nanoparticles

Hydrophobic silica nanoparticles with spherical morphology and primary mean diameter of 20–30 nm were prepared as follows. Hydrophilic silica nanoparticles were silylated to various extents by reaction with dichlorodimethylsilane in the presence of water followed by drying at 300 °C for 2 hours. The particular particles used here were surface-functionalised with *ca.* 50% silanol ($–O_3SiOH$) and 50% dimethylsilane ($–O_2Si(CH_3)_2$) groups.

5.2.5. Preparation of nanoparticle-stabilised colloidosomes

Hydrophobic silica nanoparticles (20 mg) were mixed with partially hydrophobic clay particles (1 mg) (the presence of the clay had no effect on the reported results), and then mixed with anhydrous dodecane (3 mL). The resultant mixture was sonicated in an ultrasound bath for 20 seconds to disperse any large aggregates. An aqueous solution (distilled water, enzyme, or fluorescent dye solution) (100 μl) was then added and the mixture was vigorously hand-shaken for 1 minute to produce water droplet formation. The volume fraction of the aqueous phase (φ_w) relative to oil was fixed at 0.033, and the amount of silica nanoparticles used in the aqueous phase was 0.2 mg/μl.

5.2.6. Preparation of co-polymer-grafted nanoparticle-stabilised colloidosomes

Nanoparticle-stabilised colloidosomes were prepared in oil as per section 5.2.5; Preparation of nanoparticle-stabilised colloidosomes.

Whilst in oil, the outer surface of the silica nanoparticle was cross-linked by the addition of oil-soluble TMOS (40 µl, 0.27 mmol) to a preformed Pickering emulsion as prepared in section 5.2.5. The dispersion was gently rotated for 15 minutes in the dark using an Agar Scientific Rotator, or stored in the fridge with occasional rotation for samples containing entrapped fluorescent dyes or enzymes.

The silica cross-linked surface was co-polymer functionalised by addition of the pH-responsive branched co-polymer (8 µl, 0.26 mmol), followed by rotation in either the dark at room temperature (dye-containing colloidosomes), or in the fridge with occasional rotation (enzyme-containing colloidosomes) for 3 days.

5.2.7. Dispersion of co-polymer-grafted nanoparticle-stabilised colloidosomes in water

The successful transfer of co-polymer-grafted nanoparticle-stabilised colloidosomes from the dodecane oil phase, after colloidosome formation (as per section 5.2.5) and co-polymer functionalization (as per section 5.2.6), to a continuous water phase without loss of the compartmentalised microstructure was achieved as follows. Co-polymer-grafted

colloidosomes were transferred from the oil phase into water by the addition of acetone (100 μl) to the colloidosomes in oil (3 mL). The mixture was left at room temperature or in the fridge for 30 minutes and another aliquot of acetone (100 μl) was added, followed by gentle rotation. The mixture was once again left at room temperature or in the fridge for a further 30 minutes. The upper transparent oil phase was discarded. The water phase was redispersed in acetone (1 mL) and centrifuged at 4000 rpm for 30 seconds.

The co-polymer-coated colloidosomes were redispersed in a mixture of acetone and buffer solution (1 mL, 1:1 vol/vol) at various pH values. The dispersion was then centrifuged at 4000 rpm for 1 minute and the clear upper solution was discarded. This was repeated with an aqueous buffer solution (1 mL), and finally the colloidosomes were re-suspended in buffer (3 mL) at various pH values.

5.2.8. Protocall for dye release studies

Ultraviolet-visible (UV-vis) spectroscopy was used to determine release profiles for cross-linked co-polymer-functionalised colloidosomes that contained entrapped calcein or rhodamine 6G when transferred into the continuous water phase.

Cross-linked copolymer-functionalised colloidosomes were prepared in oil using an aqueous (pH 7) solution of calcein (0.2 mM), acriflavine hydrochloride (0.2 mM) or rhodamine 6G (0.2 mM), and then transferred into acetone (0.5 ml). The suspensions were centrifuged and the acetone removed, and the colloidosome dispersion then left for 30–60 minutes in air to remove any residual acetone by evaporation. Buffered water (2 ml) at various pH values was

then added and the concentration of the dye in the continuous aqueous phase measured with time using ultraviolet (UV-vis) spectroscopy (Perkin Lambda II UV-VIS spectrometer). The finite dye concentration point was observed at the first time point (t_0 = 30 minutes) due to the presence of broken colloidosomes in the dispersion originating from the transfer process. This was accounted for in the release profiles.

5.2.9. Protocall for uptake studies

TMOS-cross-linked co-polymer functionalised water-in-oil colloidosomes were transferred into buffer at various pH's and washed twice with buffer. The mixture was centrifuged and afterwards, the buffer was discarded and an aqueous solution of calcein or acriflavine hydrochloride, prepared at varying pH's, was added to the colloidosome dispersion. Fluorescent images were recorded within 2 to 3 hours. Higher apparent fluorescent intensities were observed for dye uptake by the colloidosomes compared with the background values due to the susceptibility of the recorded background intensity to photobleaching during exposure to the light-excitation source. This artefact was minimised by recording images within 30 minutes of exposure to the light source.

5.2.10. Preparation of enzyme–containing co-polymer-grafted nano-particle stabilised colloidosomes

Alkaline phosphatase (ALP) (100 ml of a 0.006 U μl^{-1} solution) in Tris buffer (pH 7.2) was added to anhydrous dodecane (3 ml) that contained 20 mg of partially hydrophobic silica

nanoparticles. The dispersion was hand-shaken to produce a water-in-oil enzyme-containing Pickering emulsion. The Pickering emulsion was cross-linked as described in section 5.2.6; Preparation of co-polymer-grafted nanoparticle-stabilised colloidosomes. These were transferred into a water phase, by the same procedure as that used for the transfer of the colloidosomes as described in 5.2.7; Dispersion of co-polymer-grafted nanoparticle-stabilised colloidosomes in water, as intact enzyme-containing micro compartments.

5.2.11. Influence of membrane permeability on enzymatic activity in inorganic protocells

Glycine buffer (0.5 ml, 100 mM with 1.0 mM magnesium chloride) at various pH values was added to 0.5 ml of the colloidosome dispersion (containing 0.1 U ALP inside the droplets, prepared as described in section 5.2.10; Preparation of enzyme–containing co-polymer-grafted nano-particle stabilised colloidosomes). The dispersions were sedimented and the addition of buffer solutions repeated a few times to ensure that the required final pH was attained, and that no free ALP molecules were present in the continuous phase. The final pH values were 8.4, 9.1 and 9.8. Then, a 0.76 M aqueous solution (10 ml) of the phosphatase substrate, pNPP disodium salt hexahydrate, was added to the continuous aqueous phase and formation of the enzyme-mediated dephosphorylated product 4-nitrophenolate in the continuous aqueous phase at various pH values was monitored over time at 410 nm by UV-vis spectroscopy (Perkin Lambda II UV-VIS spectrometer). The reactions were maintained at 37 °C using a PTP-6 Peltier temperature controller. Control experiments were run at the above pH values in bulk aqueous solutions of ALP in the absence or presence of copolymer-functionalized silica nanoparticles. The former gave calibration curves with a constant molar

extinction constant of (ε = 18,300 M^{-1} cm^{-1}). The latter were prepared by mixing partially hydrophobic silica nanoparticles (20 mg), as previously prepared in section 5.2.4, with dodecane (3 ml), followed by addition of water (3 ml) and sonication for a few minutes to disassemble the silica particle-stabilized droplets. Oil-soluble TMOS (0.27 mmol, 40 ml) was then added to the oil phase followed by addition of the pH-responsive polymer 1 (0.26 mM in methanol, 8 ml) and stirring of the mixture at room temperature for three days. The co-polymer grafted silica nanoparticle aggregates were transferred to water by the same procedure as that used for the transfer of the colloidosomes as described in 5.2.7; Dispersion of co-polymer-grafted nanoparticle-stabilised colloidosomes in water. The copolymer and silica components had no effect on the enzymatic rates over the relevant pH range.

5.3 Results and discussion

5.3.1. Synthesis of pH-responsive branched co-polymer surfactant to create an electrostatically gated membrane

The composition of the statistical terpolymer was purposely designed so that TMSPMA would provide self-cross-linking residues that would cross-link with the same cross-linking residues on TMOS molecules, which are in turn cross-linked to the surface of the silica nanoparticles. MAA and DMAEMA or DEAEMA residues provide anionic and cationic charges respectively with changing pH. As discussed in Chapter 3; Preparation of branched and linear co-polymers *via* free radical polymerisation, the co-polymers presented in this thesis have compositions of MFM_{100}-$EGDMA_{10}$-CTA_{10}. Here, the MFM corresponded to

TMSPMA, DMAEMA or DEAEMA and MAA. Molar ratios of TMSPMA:DMAEMA(or DEAEMA):MAA were nominally fixed at 22:39:39 which was found to be the optimum ratio for purpose as discussed in 5.2.1; Design of pH-responsive branched co-polymer composition. Table 1, shows the target composition and actual calculated polymer compositional ratios for the branched co-polymers determined by ^{1}H NMR spectroscopy, using signal ratios, and triple-detection size exclusion chromatography analysis (TD-SEC), before esterification (see Table 1).

5.3.2. Size exclusion analysis of branched terpolymers by TD-SEC

Table 1. Co-polymer compositions calculated by ^{1}H ($CDCl_3$) NMR and size exclusion chromatography (TD-THF) values.

ID	**Target Polymer Composition**	**Actual Polymer composition[a]**	**Conv %[a]**	**Mw /kDa[b]**	**Mn /kDa[b]**	**Mw/ Mn[b]**	**M-Hα[b]**
P21 (2)	$TMSPMA_{61}/MAA_{39}$-$EGDMA_{10}$-DDT_{10}	$TMSPMA_{63.6}/MAA_{39.8}$-$EGDMA_{9.5}$-$DDT_{7.1}$	98.6	69	25	4.6	0.30
*P23**	$TMSPMA_{22}$/ $DMAEMA_{39}/MAA_{39}$-$EGDMA_{10}$-DDT_{10}	$TMSPMA_{23.4}$/ $DMAEMA_{40.4}/MAA_{37.4}$-$EGDMA_{8.4}$-$DDT_{10.4}$	97.5	270	209	1.3	0.59

*[a] as determined by ^{1}H NMR. [b] As determined by THF TD-SEC against polystyrene (99k) standards. * most relevant co-polymer composition discussed in this chapter.*

The M_w of P23 and P23 was higher than expected. The polydispersity values were also lower than expected. This may be an artefact of the analysis. Performing GPC measurements on a

terpolymer with this level of architectural and compositional complexity remains challenging, and as such examples are rare. Although TD-GPC with the added support of multiple detectors is a valuable tool for polymer characterization, its reliable application to branched co-polymer particles is still debatable.[14]

5.3.3. Size, charge and the effect of architecture on pKa determination of P23; $TMSPMA_{23.4}/DMAEMA_{40.4}$ /$MAA_{37.44}$-$EGDMA_{8.4}$-$DDT_{10.4}$ responsive branched co-polymer

Zeta potential measurements for an aqueous solution of P23 gave values of +20 and -30 mV at pH 2 and pH 10, respectively, with an isoelectric point at pH ≈ 5 (see Figure 8.a). This is consistent with pH titration curves of P23, which shows complex behaviour with an averaged pKa value of = 5.76 in Figure 8.b. Dynamic light scattering studies showed the presence of discrete macromolecules at pH 2 and above pH 7, which were 30–40 nm in hydrodynamic diameter; in contrast, micrometre-sized aggregates were observed between pH values of 4 and 6, consistent with the low surface charge on the co-polymer under these conditions (Figure 8.c). These observations are consistent with those shown in the previous chapter.

The pH-induced protonation / deprotonation of the terpolymer's carboxylic acid (MAA) and amino (DMAEMA) groups was used to induce reversible changes in ionic charge at the surface of the silica nanoparticle-based shell. As confirmed by the zeta potential measurements (Figure 8.a), protonation of both DMAEMA (pKa ≈ 10) and MAA residues (pKa ≈ 4–4.5) produced a substantial positive charge on the co-polymer at pH values between 2 and 4, and a considerable negative charge at pH 9 and above.

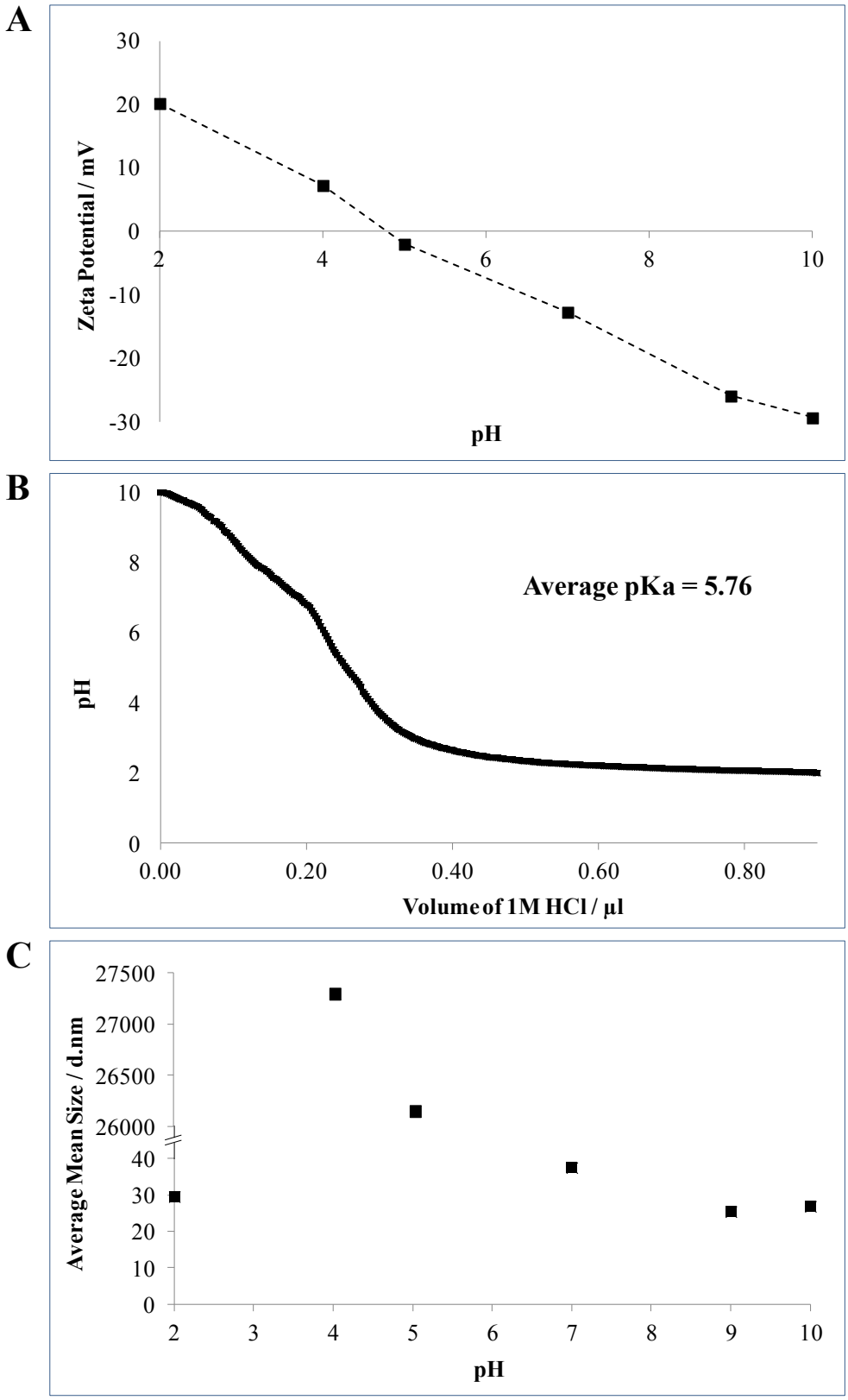

Figure 8. (A) Zeta potential, (B) pH titration curve and (C) DLS values for the co-polymer, P23; $TMSPMA_{23.4}$/DMAEMA40.4/$MAA_{37.4}$-$EGDMA_{8.4}$-$DDT_{10.4}$ ([co-polymer] = $4.790x10^{-4}$ mol L^{-1} in (A) and (C); sample volume = 600 µL in (E). Reproduced with permission from ref. 12.

5.3.4. Formation and physical properties of stable silica nanoparticle-based colloidosomes with a cross-linked and functionalised membrane

A dry powder of surface-active silica nanoparticles was prepared as per section 5.2.4; Preparation of silica nanoparticles. These were added to a water–dodecane mixture at an aqueous volume fraction of 0.033. This produced a suspension of well-defined spherical micro-compartments up to 200 μm in mean diameter (Figure 9.a).

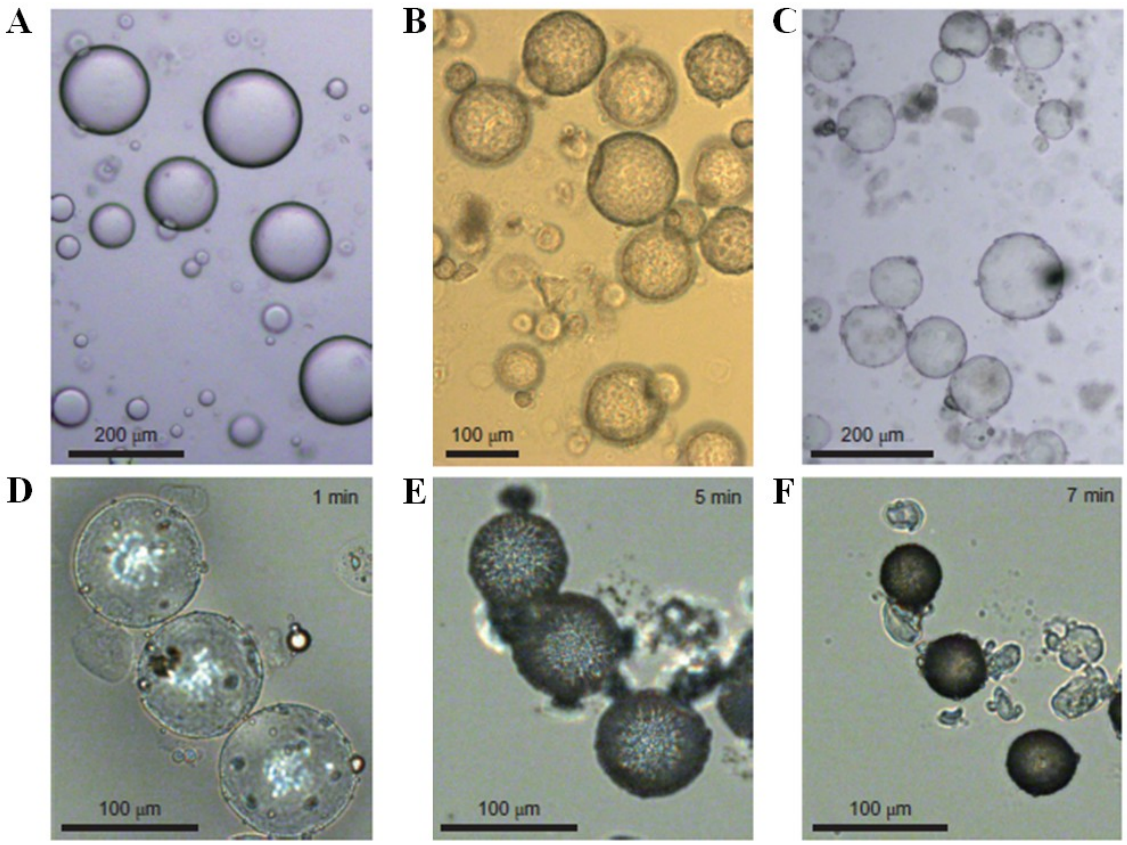

Figure 9. Light micrographs of silica nanoparticle-stabilised colloidosomes. (A) Colloidosomes dispersed in oil before and after (B) TMOS-mediated cross-linking and co-polymer functionalisation of the inorganic membrane. (C) After transfer of (B) into a bulk water phase. (D-F) Structural properties of cross-linked co-polymer-functionalised colloidosomes; the consecutive optical images show deflation and elastic response of the inorganic membrane during air drying. Reproduced with permission from ref. 12.

Although the silica nanoparticle-stabilised colloidosomes were stable in the continuous oil phase, when placed into a bulk water phase the structures disassembled. In contrast, cross-linking of the inorganic shell with TMOS, or using a combination of cross-linking and covalent grafting of P23 pH-responsive co-polymer (prepared as per experimental sections 5.2.5 and 5.2.6), produced spherical colloidosomes that were easily transferred into water without loss of structural integrity in accordance with section 5.2.7; Dispersion of co-polymer-grafted nanoparticle-stabilised colloidosomes in water (see Figure 9.b-c respectively). No successful transfer into water was observed for the polymer-grafted colloidosomes prepared without TMOS cross-linking. Rough external morphology of the surface texture of the inorganic membrane was observed after modification with TMOS (Figure 10) and TMOS/P23 (Figure 9.b). This is consistent with the presence of a cross-linked matrix of silica on the surface of the colloidosomes, the hydrophilic DMAEMA and MAA chains, and to the branched architecture of the co-polymer. The rough surface echoes the work in Chapter 3 and 4, where similar surface morphology was viewed using light and scanning electron microscopy for branched co-polymer cross-linked capsules.

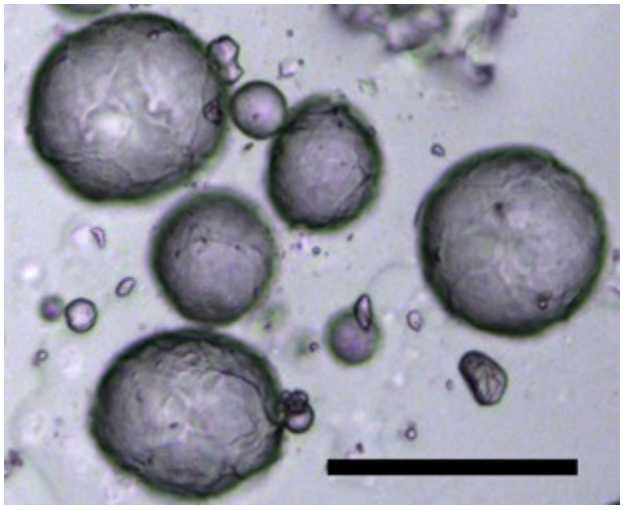

Figure 10. Optical image of an individual water-filled cross-linked colloidosome prepared in the absence of a co-polymer shell and dispersed in dodecane. Note the roughened surface texture. Scale bar represents 200 µm. Reproduced with permission from ref. 12.

It was observed that the cross-linked co-polymer-functionalised colloidosomes did not collapse on air drying, but instead contracted into intact spheres that were approximately half the size of the initial colloidosome and that exhibited an extensively wrinkled outer surface (Figure 9.d-f). Rehydration of the dried colloidosomes restored their initial size, which indicates that the porous silica/co-polymer membrane was structurally intact and elastic even in the dried state. This is similar to assembled and cross-linked capsule structures described in the previous chapter, Chapter 4, which displayed elasticity by shrinking and swelling with dehydration and rehydration respectively whilst maintaining spherical morphology. Moreover, on forcibly breaking capsules prepared in Chapters 3 and 4, difficulty was also encountered also due to the elasticity of the capsule shell.

Spectroscopy was used to successfully confirm the presence of P23 co-polymer within the colloidosomes after transfer into bulk water. Fourier transform infrared spectra (FTIR) of the water dispersed TMOS cross-linked colloidosomes show strong Si-O-Si adsorption bands at around 470 and 1,100 cm^{-1}, and C-H vibrations at 807 cm^{-1} and 2,853–2,927 cm^{-1}, attributed to the inorganic-organic character of the surface membrane. In Figure 11, the spectra of the copolymer-grafted colloidosomes shows C–H deformation vibrations at 1,380 and 1,466 cm^{-1} from n–CH_3 and n–CH_2 or n–CH_3 groups, respectively. A C=O stretching vibration was observed at 1,730 cm^{-1} and C–H bands at 2,853–2,927 cm^{-1} which confirms the presence of the P23 co-polymer in the cross-linked membrane.

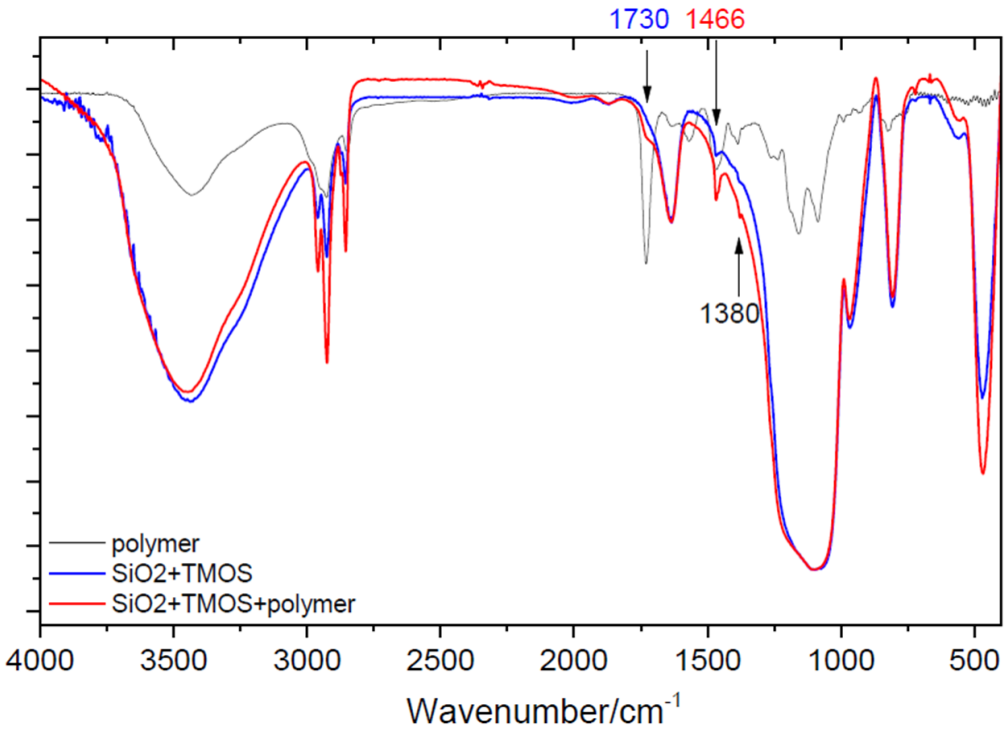

Figure 11. FTIR for P23 branched copolymer (black), TMOS cross-linked colloidosomes (blue) or TMOS cross-linked, P23 co-polymer-functionalised colloidosomes (red). The colloidosome samples were transferred into water and then air-dried before the spectra were recorded. Reproduced with permission from ref.12.

5.3.5. Encapsulation of alternative actives

Anionic (calcein) and cationic (acriflavine hydrochloride, rhodamine 6G) water soluble fluorescent dye molecules (represented in Figure 12) were readily encapsulated at pH 7 within the colloidosomes during self-assembly of the nanoparticle membrane in the oil phase (as described in 5.2.5; Preparation of nanoparticle-stabilised colloidosomes).

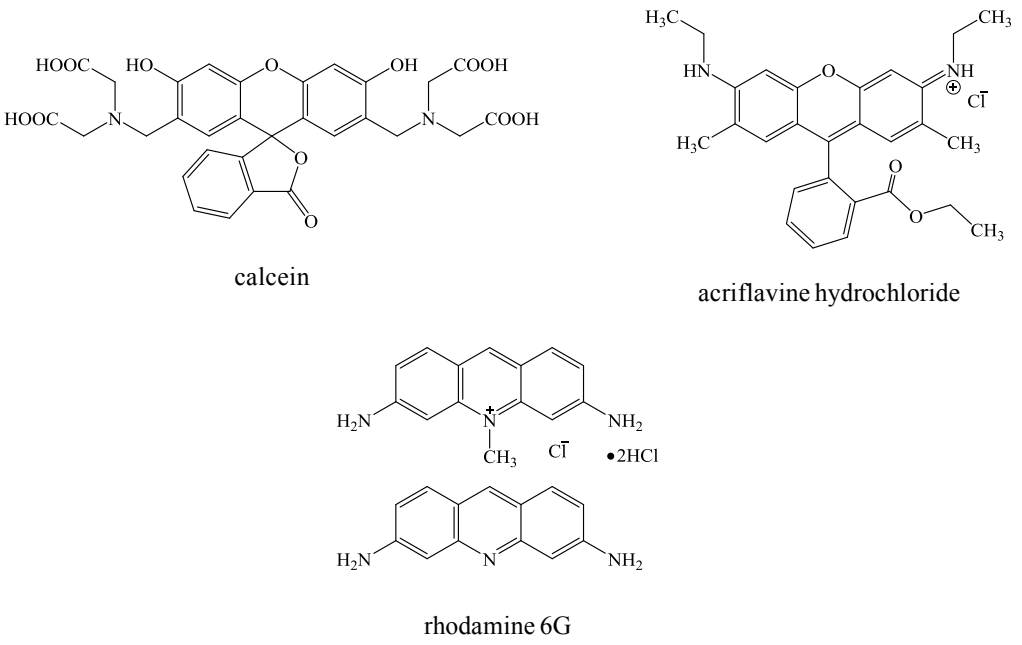

Figure 12. Molecular structures of dyes (pKa values for calcein: carboxylic acids pKa1 = 2.1, pKa2 = 2.9, pKa3 = 4.2, pKa4 = 5.5; amino groups, pKa5 = 10.8, pKa6 = 11.7; rhodamine 6G pKa = 7.5). Reproduced with permission from ref. 12.

Strong fluorescence was observed in each instance, in correspondence with the dye-containing nanoparticle-stabilised micro-compartments (Figure 13 and Figure 16.a.) indicating successful encapsulation of the dyes. Images were taken after 3-5 hours, and further imaging conducted 24 hours later showed no change in fluorescence.[12]

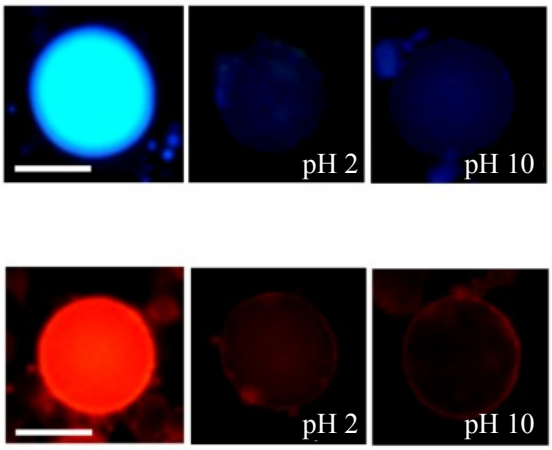

Figure 13.(Top row), fluorescence images fluorescence microscopy images of individual acriflavine hydrochloride-containing TMOS-cross-linked colloidosomes dispersed in oil (left), or water at pH 2 (middle) and 10 (right) showing retention or pH-independent release of the dye in oil and water, respectively. (Bottom row), fluorescence microscopy images of individual rhodamine 6G-containing TMOS-cross-linked colloidosome dispersed in oil (left), or water at pH 2 (middle) and 10 (right) showing retention or pH-independent release of the dye in oil and water, respectively. Scale bars = 50 μm. Reproduced with permission from ref. 12.

Corresponding fluorescence microscopy images of colloidosomes at internal pH values between 2 and 10 also displayed high fluorescence intensities associated with the colloidosomes (Figure 14).

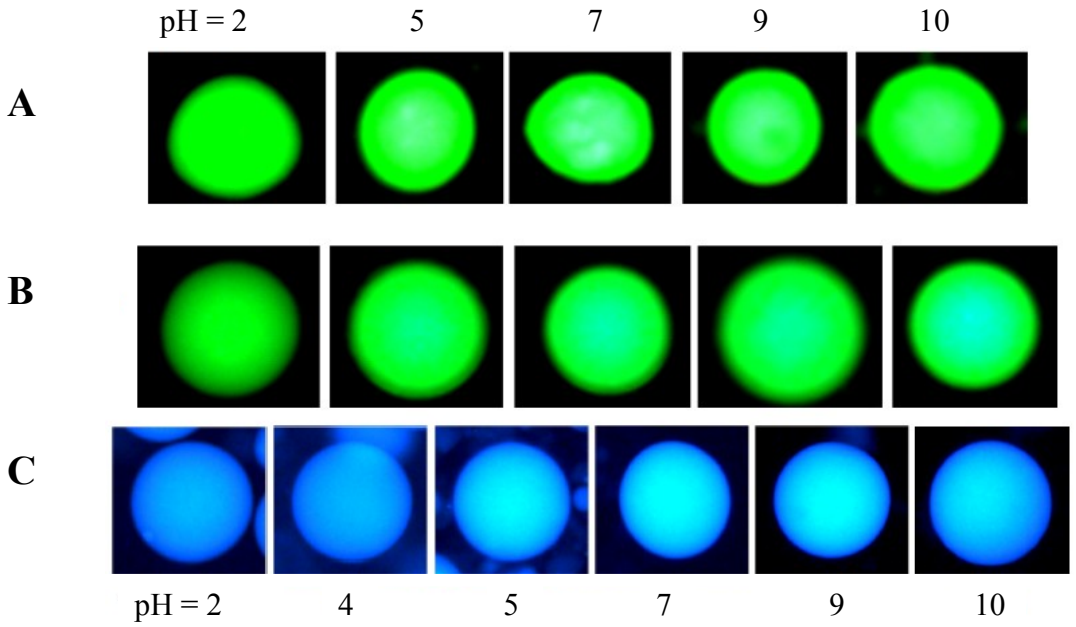

Figure 14. Fluorescence microscopy images of colloidosomes dispersed in oil and comprising (A,B) entrapped aqueous calcein at various pH values after (A) 2 hours, and after (B) 1 day, or (C) entrapped acriflavine hydrochloride. Reproduced with permission from ref. 12.

Even though calcein, and also acriflavine hydrochloride to a lesser extent, showed pH-dependent fluorescence behaviour in control bulk solutions (Figure 15).

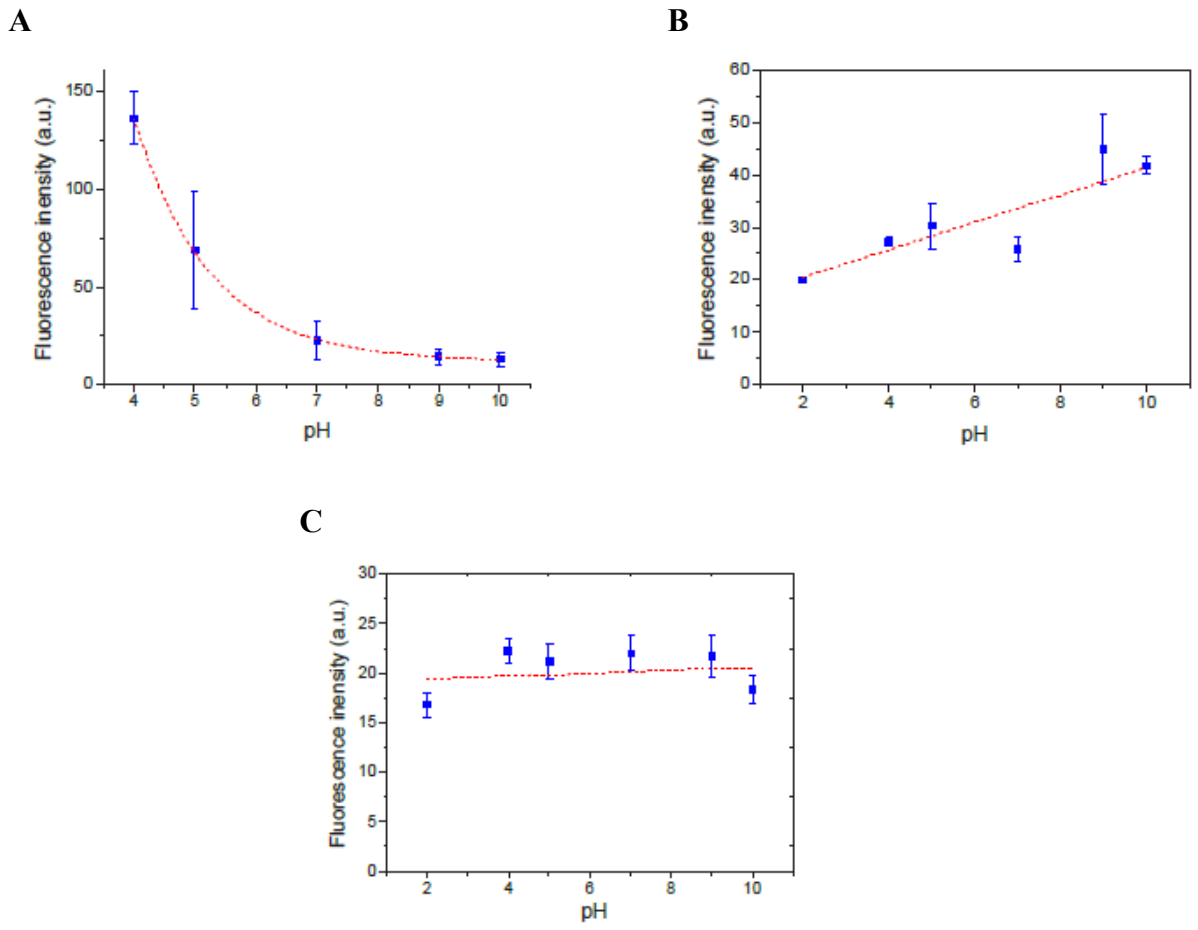

Figure 15. Plots of fluorescence intensity against pH for aqueous solutions of (A) calcein, (B) acriflavine HCl or (C) rhodamine 6G at a concentration of 0.1 mM in each case. The dye concentration was the same as that encapsulated inside the colloidosomes. The error bars were within the standard deviation. Reproduced with permission from ref. 12.

Calcein-containing TMOS cross-linked colloidosomes were dispersed in water at pH 2 (Figure 16.b) and at pH 10 (Figure 16.c) where a loss in fluorescence was attributed to pH-independent release of the dye molecules through the permeable membrane.

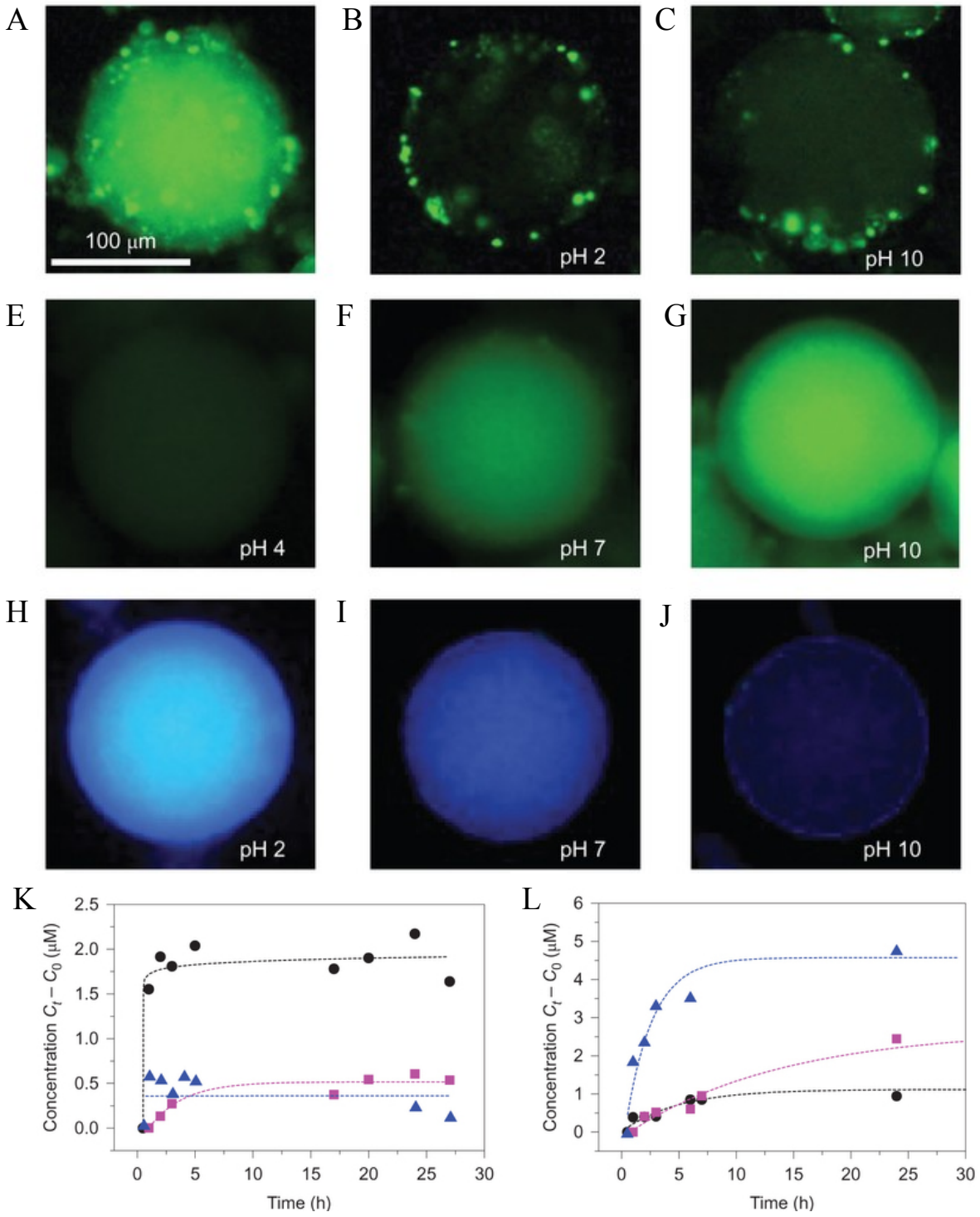

Figure 16. Release properties of inorganic cell-like microstructures. (A–C) Fluorescence microscopy images of an individual calcein-containing TMOS cross-linked colloidosome dispersed in oil showing successful encapsulation of the dye. (A) Fluorescence microscopy images of a single colloidosome dispersed in water at pH 2.5 (B) and pH 10, (C) showing loss of fluorescence intensity attributed to pH-independent release of the dye. (E-G) Fluorescence images of individual calcein-containing cross-linked co-polymer-functionalised colloidosomes prepared at an initial pH of 7 and dispersed in water at (E) pH 4 (F), 7 (G) and 10, showing progressive retention of the entrapped dye with increasing pH. (H-J) Fluorescence images of individual acriflavine hydrochloride-containing cross-linked co-polymer-functionalised colloidosomes dispersed in water at (H) pH 2 (I), 7 (J) and 10, showing progressive leaching of the entrapped dye with increasing pH. (K-L) Concentration of dye molecules released into bulk aqueous solution for cross-linked co-polymer-functionalised colloidosomes that contain (K) entrapped calcein at pH values of 4 (black circles), 7 (pink squares) and 10 (blue triangles), (L), or rhodamine 6G at pH values of 2 (black circles), 7 (pink squares) and 9 (blue triangles). Reproduced with permission from ref. 12.

Despite cross-linking with TMOS alone, the membrane interstices were large enough for free movement of the small molecule dyes. In contrast, fluorescence images of cross-linked co-polymer-functionalised colloidosomes that contained calcein, acriflavine hydrochloride or rhodamine 6G indicated that the dye molecules were retained within the colloidosome interior after transfer into water, depending on the pH of the bulk solution (Figure 16.e-j and Figure 17).

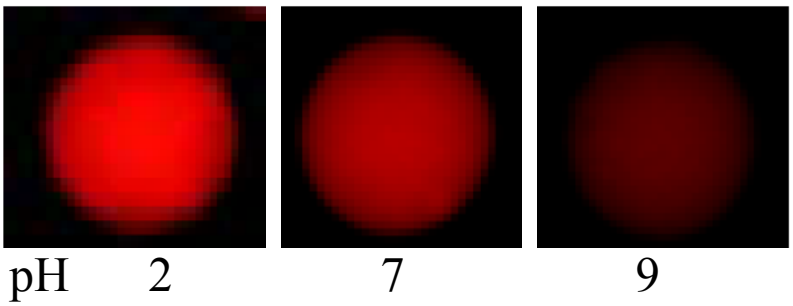

Figure 17. Fluorescence images of individual rhodamine 6G-containing cross-linked co-polymer-functionalised colloidosomes dispersed in water at pH 2, 7 or 9 showing progressive leaching of the entrapped dye with increasing pH. Reproduced with permission from ref. 12.

The anionic and cationic dyes were retained at neutral pH and released under acidic or alkaline conditions. The concentration of the released dyes in the bulk water phase was monitored with changing pH over time (Figure 16.k-l). Comparative experiments with cross-linked co-polymer-functionalised colloidosomes (prepared identically as described in section 5.2.6; Preparation of co-polymer-grafted nanoparticle-stabilised colloidosomes) that encapsulated positively or negatively charged proteins, i.e. cytochrome *c* or ferritin and myoglobin, respectively, showed no leakage from pH 2 – 10. This indicated that the gated mechanism is operated specifically at a molecular level.

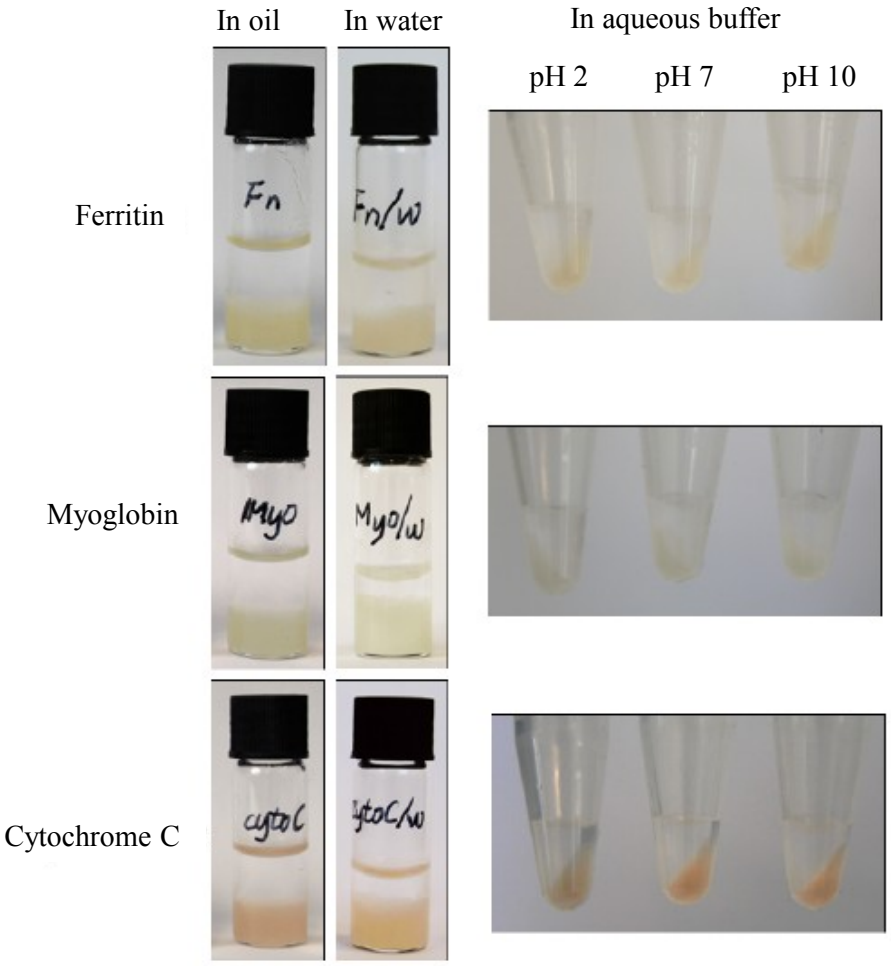

Figure 18. Optical images of sample tubes showing retention of coloration in the colloidosome phase when suspended in oil or water at pHs between 2 and 10, indicating that proteins such as ferritin, myoglobin or cytochrome *c* remain encapsulated within the colloidosome interior. Reproduced with permission from ref. 12.

UV-vis spectroscopy was used to determine the release profiles for calcein or rhodamine 6G encapsulated within the cross-linked copolymer-functionalised colloidosomes dispersed in water at various pH values (see Figure 16.k-l). Figure 16.k indicates that encapsulated calcein was released quickly at pH 4, where 80% was released within an hour and a threshold level for the released dye was reached within two hours of dispersion in water.

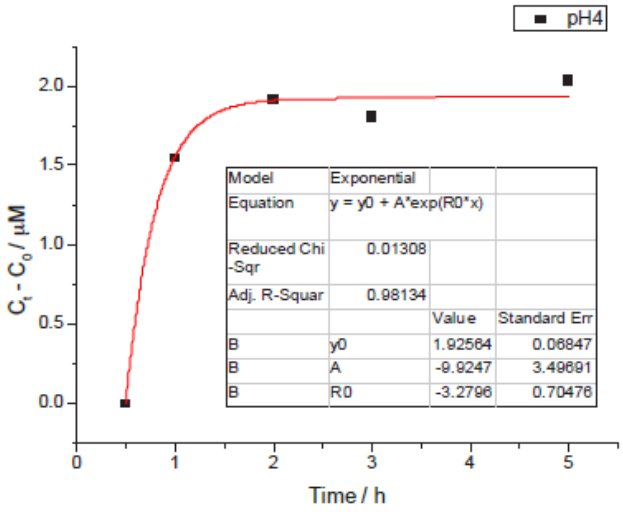

Figure 19. Release profile between 0.5-5 hr for calcein-containing cross-linked co-polymer-functionalised colloidosomes at pH 4. Reproduced with permission from ref. 12.

In comparison, entrapped rhodamine 6G (Figure 16.l) was completely released at pH 9, although at a slower rate (100% after eight hours) than those for calcein transfer through the P23 co-polymer-functionalised inorganic membrane. Little or no release was observed at pH 7 or 10 for calcein-containing colloidosomes, but rhodamine 6G was completely retained at pH 2 and only a slow rate of transfer was exhibited at pH 7.

These results were due to changes in the charge of the P23 co-polymer grafted layer from positive to negative as the pH was increased above the co-polymer isoelectric point (pH ≈ 5) and an average pKa value of 5.76. Consequentially, increased electrostatic repulsion between the co-polymer layer and the negatively charged calcein molecules at high pH, or cationic acriflavine hydrochloride/rhodamine 6G molecules under basic (pH = 10) or acidic (pH ≈ 4) conditions, respectively, created an effective selective gated mechanism for the retention and release of dye molecules within the colloidosome. At intermediary pH values, the multivalent nature of the co-polymer coronal layer appears to be adequately charged at a local level to restrict the diffusion of cationic and anionic small molecules across the nanoparticle membrane. This is particularly evident in the case of calcein, which at neutral pH has a high

spatial charge density associated with four negatively charged carboxylates and two positively charged amino groups.

5.3.6. Uptake of alternative actives

The ability of non-dye-loaded (water-filled) cross-linked P23 co-polymer-functionalised colloidosomes to selectively uptake small molecules from an external solution was investigated. Non-dye-loaded colloidosomes were immersed in aqueous solutions of buffered calcein at different pH values. At pH 10, the membrane was impermeable to anionic calcein molecules, weakly permeable at pH 7, and permeable at pH 4 (Figure 20.a-c), which is consistent with release experiments (Figure 21) as described in 5.2.8; Protocall for dye release studies.

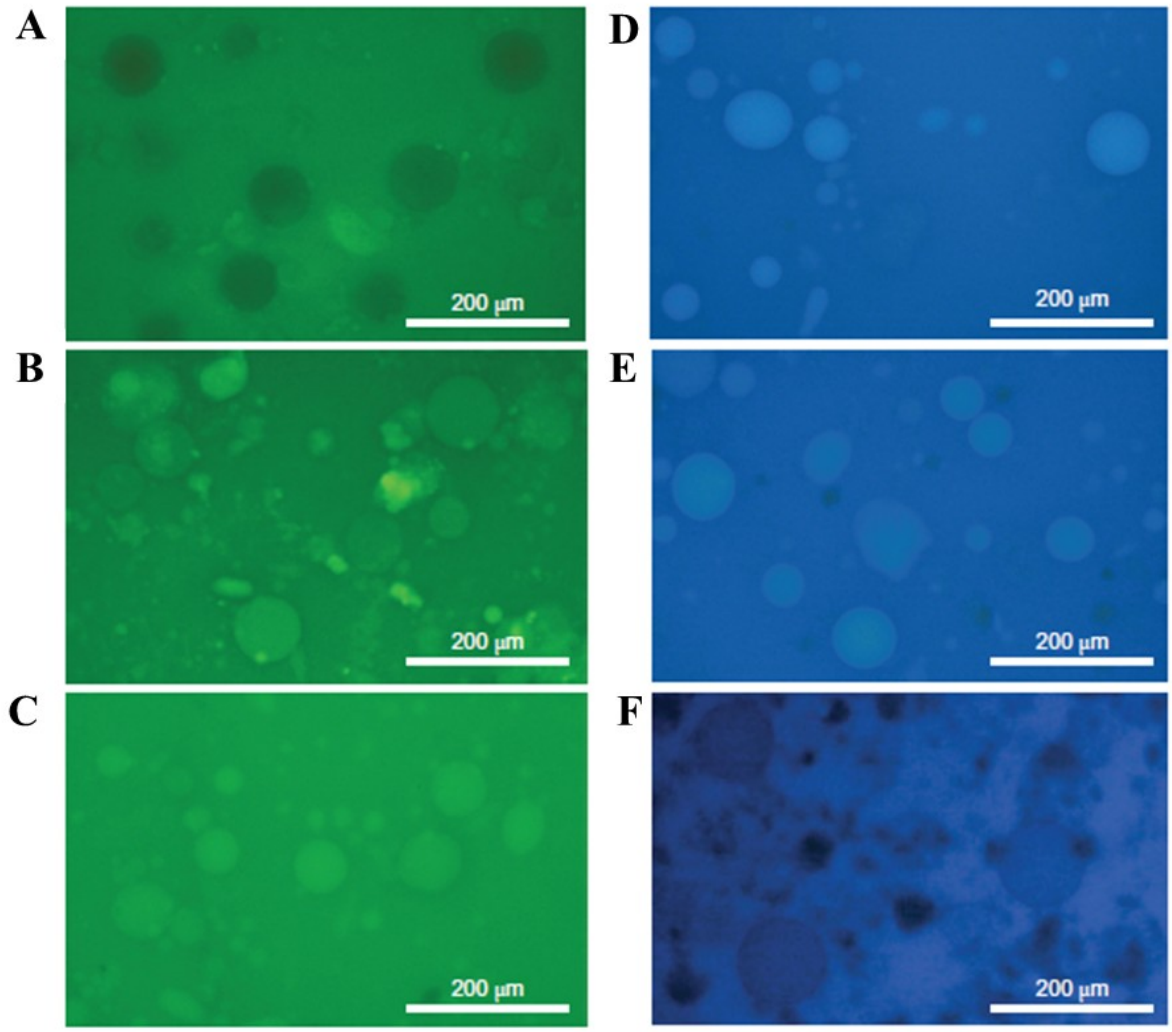

Figure 20. Uptake properties of cross-linked P23-functionalised colloidosomes. (A–F) confocal optical fluorescence micrographs of water-filled colloidosomes immersed in aqueous solutions of anionic calcein at pH values of (A) 10, (B) 7, and (C) 4, or immersed in aqueous solutions of cationic acriflavine hydrochloride at pH values of (D) 10, (E) 7, and (F) 2. Note the absence of dye uptake in (A) and (F). Reproduced with permission from ref. 12.

The experiment was repeated immersing the P23-functionalised colloidosomes in aqueous solutions of buffered acriflavine hydrochloride. Opposite pH-dependent uptake behaviour was observed, where the cationic dye was inhibited at pH 2 (Figure 20.d-f).

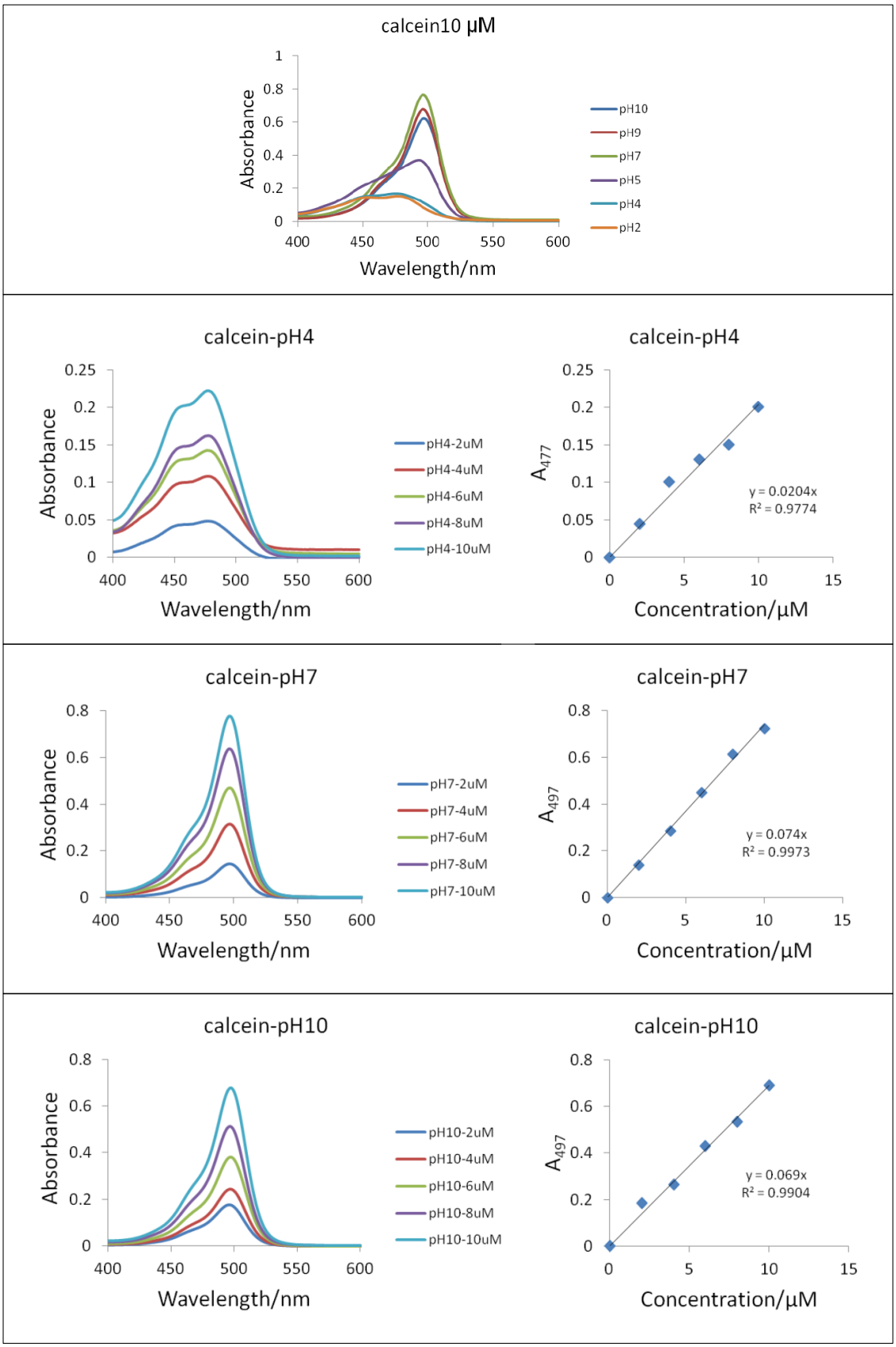

Figure 21. UV-vis spectra and calibration plots for calcein at various pH values in bulk solution. Reproduced with permission from ref. 12.

A control was conducted where pH-independent uptake was observed for cross-linked colloidosomes prepared without the P23 terpolymer. No dye uptake was observed (Figure 22) confirming that the transfer of molecules across the cross-linked co-polymer-functionalised inorganic membrane in either direction is dependent on electrostatically gated transport.

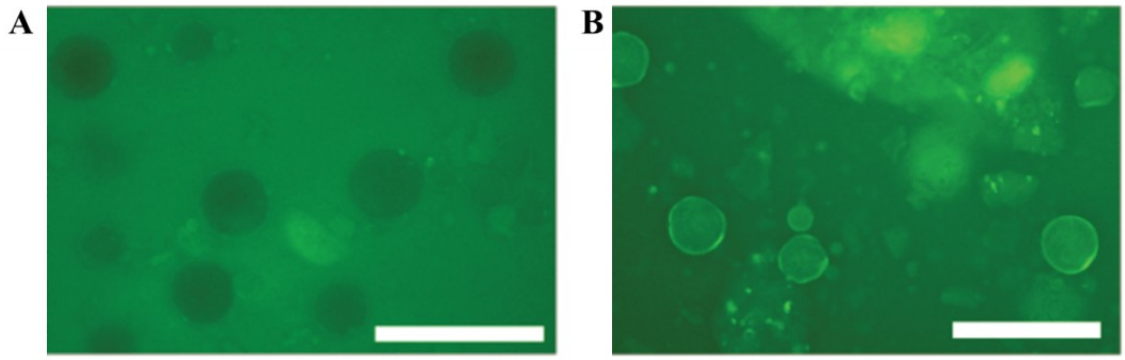

Figure 22. Confocal optical fluorescence micrographs of the uptake properties of (A) water-filled cross-linked copolymer functionalised colloidosomes or (B) water-filled cross-linked colloidosomes immersed in aqueous solutions of calcein at pH values of 10. Note the absence of dye uptake in the presence of the copolymer. Scale bars represent 200 µm. Reproduced with permission from ref. 12.

5.3.7. Enzyme-mediated dephosphorylation in P23-stabilised inorganic protocell constructs

The micro-compartments of the P23-functionalised colloidosomes provide a membrane-enclosed internal space for biochemical reactions (as discussed in 5.1; Introduction). Enzyme-catalysed reactions were carried out inside water-in-water colloidosomes, regulated by pH-gated permeability. ALP was encapsulated within the silica nanoparticle-based Pickering emulsion (prepared as described in section 5.2.5), and after cross-linking and P23-functionalisation of the colloidosome shell in an identical manner as designated in section 5.2.6, the constructs were transferred into water at various pH values (using the method described in section 5.2.7). Anionic 4-nitrophenyl phosphate (*p*NPP) (pKa = 5.2) was added

to the continuous water phase. The concentration of the enzymically produced product, 4-nitrophenolate (pKa = 7.2), was monitored as a function of time (Figure 23). Enzyme-mediated dephosphorylation was monitored against changing pH in cross-linked P23 co-polymer-modified colloidosomes (Figure 23.a.), cross-linked colloidosomes without a co-polymer corona (Figure 23.b.), and bulk aqueous solution (Figure 23.c.). The reaction rate of ALP-mediated dephosphorylation of *p*NPP at a pH of 8.4 was 0.42 µM/min and increased to 0.75 µM/min as pH was increased to 9.1 indicating good enzymic activity. A further increase in pH to 9.8 decreased the reaction rate to 0.14 µM/min suggesting P23-restricted membrane transfer (Figure 23.a).

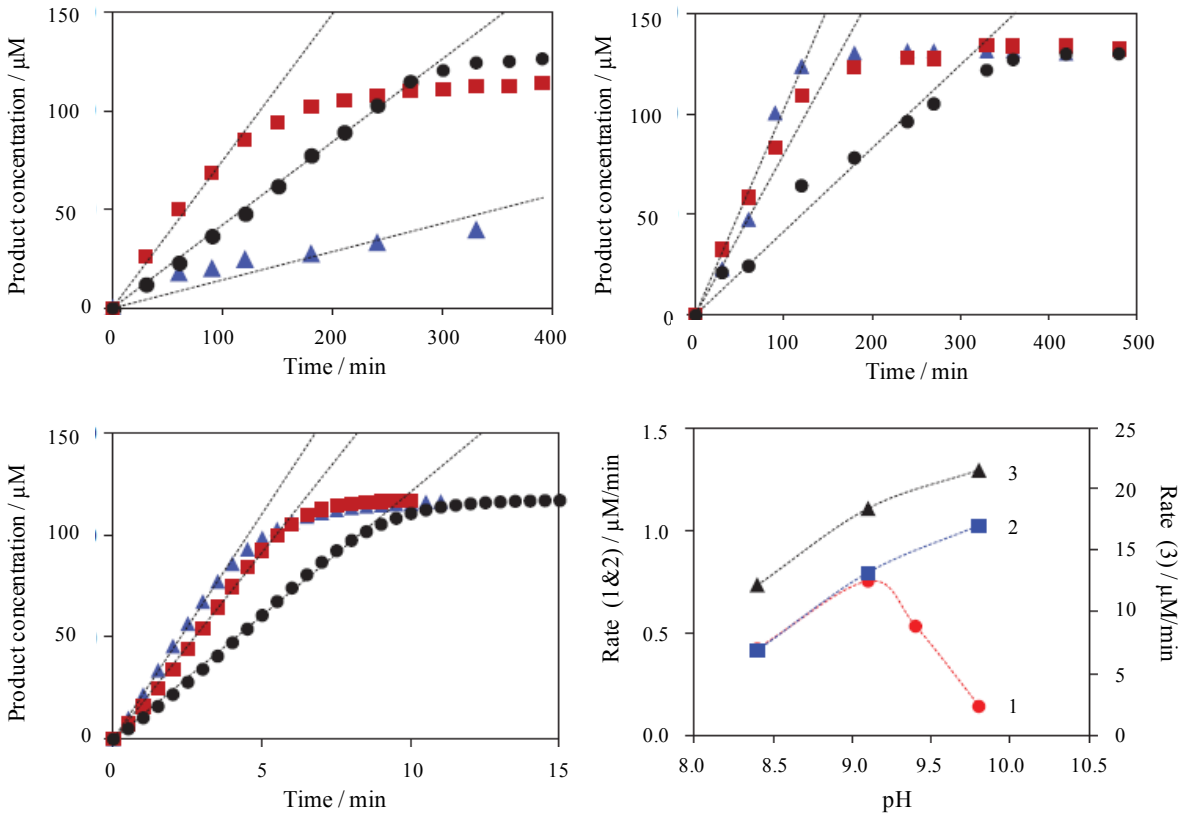

Figure 23. Enzyme-mediated dephosphorylation in inorganic protocells. (A) Time-dependent changes in 4-nitrophenolate concentrations in the continuous aqueous phase of a suspension of ALP contained within P23 co-polymer-grafted cross-linked colloidosomes at pH values of 8.4 (black circles), 9.1 (red squares) and 9.8 (blue triangles); initial rates are shown by dashed lines. Corresponding plots for (B) cross-linked colloidosomes without a co-polymer corona, at pH values of 8.4 (black circles), 9.1 (red squares) and 9.8 (blue triangles), (C) for ALP-mediated *p*NPP dephosphorylation in bulk aqueous solution at pH 8.4 (black circles), 9.1 (red squares) and 9.8 (blue triangles) and (D) for ALP-mediated *p*NPP dephosphorylation in bulk aqueous solution containing P23 co-polymer-grafted cross-linked colloidosomes at pH values of 8.4 (black circles), 9.1 (red squares) and 9.8 (blue triangles). Reproduced with permission from reference 12.

Where the same process was repeated within cross-linked colloidosomes prepared without a P23 co-polymer corona dispersed in water, no pH-mediated inhibition was found at pH 9.8 (Figure 23.b.). However, the reaction rate increased progressively from 0.41 to 0.79 to 1.02 μM/min at pHs of 8.4, 9.1 and 9.8, respectively. This trend was also shown during control reactions at the same pH values, where both ALP and *p*NPP were placed into bulk aqueous solution with and without co-polymer-functionalised silica nanoparticles. When performed in the bulk-phase, reaction rates increased significantly decreasing the reaction time dramatically from hours to minutes (Figure 23.c. and Figure 24). This suggests that the cross-linked P23-functionalised silica nanoparticle membrane acts as an effective barrier.

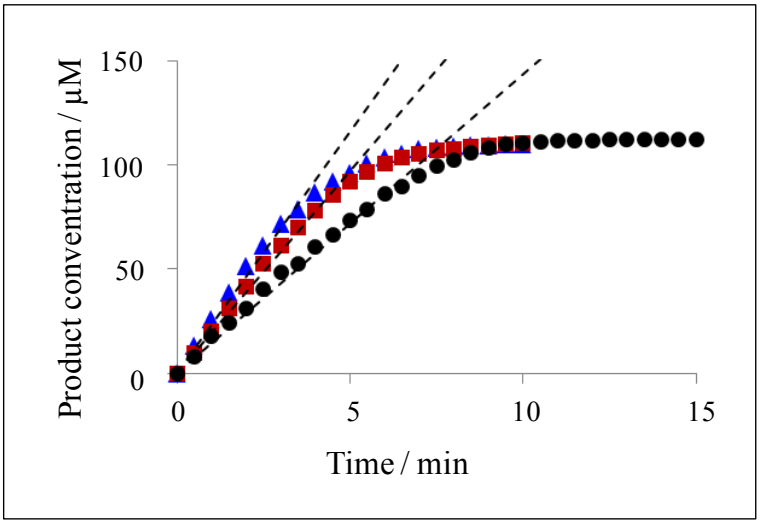

Figure 24.Plots showing time-dependent changes in 4-nitrophenolate concentrations for ALP-mediated pNPP dephosphorylation in bulk aqueous solution containing co-polymer-modified silica nanoparticles at pH 7.5 (black), 8.4 (red) and 9.8 (blue). Reproduced with permission from reference 12.

The absence of yellow colouration within the colloidosome dispersion indicated that the change in enzyme kinetics at pH 9.8 was not associated with the formation or the entrapment of 4-nitrophenolate within the micro-compartments. This observation is attributed to inhibition during the transfer of di-anionic *p*NPP into the cross-linked co-polymer-functionalised colloidosomes because of a high negative charge on the inorganic membrane.

As a result, the enzymatic activity is switched off, but can be switched on by reducing the electrostatic repulsion between the substrate and the co-polymer. This is achieved by lowering the pH (Figure 23.d.).

In contrast, the initial rate of dephosphorylation within the colloidosomes, prepared without the co-polymer corona, remained substantial at pH 9.8 which is consistent with the presence of an inactive semi-permeable membrane. That the rates were so much faster in bulk solution compared with those in the colloidosomes suggests that the nanoscale porosity of the cross-linked silica nanoparticle membrane acts as a considerable diffusion barrier, even in the absence of the pH-gated copolymer coronal layer. However, we cannot rule out the possibility that the presence of sterically hindered or denatured active sites associated with adsorption of the encapsulated proteins onto the silica nanoparticle surfaces was responsible for the differences in enzyme kinetics.

5.4 Conclusion

Chemical construction of water-dispersible protocell constructs with pH-mediated, electrostatically gated permeability was prepared by covalently grafting a responsive co-polymer to the outer surface of a cross-linked membrane of a silica nanoparticle-based colloidosomes. Co-polymer grafted membrane functionality-mediated uptake and release of small molecules from the colloidosomes was successful. Facile grafting of the terpolymer suggests that additional changes to the membrane properties could be accessed *via* judicious design of the multi-functional branched terpolymer, which is straightforward due to the ease of polymer synthesis. The robust, elastic membrane does not lose function on dehydration

and rehydration suggesting that the functionalised colloidosomes could act as compartments into which actives could be sequestered and stored for long periods and released at a later time point. This could be exploited for applications such as the long-term storage of bio-actives, uptake of substrates and enzyme cofactors, or controlled release of drug and bio-active agents. As the micro-compartments retained their structure on heating to 80 °C, these could be used for more complex bio-reactions, for example the replication of DNA by polymerase chain reactions. These alternative structures provide new opportunities for the construction of artificial cells through the advancement of materials design.

5.5 References

[1] aP. Stano, P. Carrara, Y. Kuruma, T. P. de Souza, P. L. Luisi, *J. Mater. Chem.* **2011**, *21*, 18887-18902; bA. Pohorille, D. Deamer, *Trends Biotechnol.* **2002**, *20*, 123-128; cB. Stadler, A. D. Price, R. Chandrawati, L. Hosta-Rigau, A. N. Zelikin, F. Caruso, *Nanoscale* **2009**, *1*, 68-73.

[2] aP. Stano, P. L. Luisi, *Chem. Commun.* **2010**, *46*, 3639-3653; bA. J. Dzieciol, S. Mann, *Chem. Soc. Rev.* **2012**, *41*, 79-85; cP. Walde, *Bioessays* **2010**, *32*, 296-303.

[3] aS. Koga, D. S. Williams, A. W. Perriman, S. Mann, *Nat. Chem.* **2011**, *3*, 720-724; bD. S. Williams, S. Koga, C. R. C. Hak, A. Majrekar, A. J. Patil, A. W. Perriman, S. Mann, *Soft Matter* **2012**, *8*, 6004-6014.

[4] aM. Li, D. C. Green, J. L. R. Anderson, B. P. Binks, S. Mann, *Chem. Sci.* **2011**, *2*, 1739-1745; bG. J. T. Cooper, P. J. Kitson, R. Winter, M. Zagnoni, D. L. Long, L. Cronin, *Angew. Chem.-Int. Edit.* **2011**, *50*, 10373-10376; cA. B. Subramaniam, J. D. Wan, A. Gopinath, H. A. Stone, *Soft Matter* **2011**, *7*, 2600-2612.

[5] A. D. Dinsmore, M. F. Hsu, M. G. Nikolaides, M. Marquez, A. R. Bausch, D. A. Weitz, *Science* **2002**, *298*, 1006-1009.

[6] C. Z. Wu, S. Bai, M. B. Ansorge-Schumacher, D. Y. Wang, *Adv. Mater.* **2011**, *23*, 5694-5699.

[7] aA. Boker, J. He, T. Emrick, T. P. Russell, *Soft Matter* **2007**, *3*, 1231-1248; bD. Y. Wang, H. W. Duan, H. Mohwald, *Soft Matter* **2005**, *1*, 412-416; cR. K. Shah, J. W. Kim, D. A. Weitz, *Langmuir* **2010**, *26*, 1561-1565.

[8] aM. F. Hsu, M. G. Nikolaides, A. D. Dinsmore, A. R. Bausch, V. D. Gordon, X. Chen, J. W. Hutchinson, D. A. Weitz, *Langmuir* **2005**, *21*, 2963-2970; bK. L. Thompson, S. P. Armes, *Chem. Commun.* **2010**, *46*, 5274-5276; cA. B. Subramaniam, M. Abkarian, H. A. Stone, *Nat. Mater.* **2005**, *4*, 553-556.

[9] S. D. Mookhoek, B. J. Blaiszik, H. R. Fischer, N. R. Sottos, S. R. White, S. van der Zwaag, *J. Mater. Chem.* **2008**, *18*, 5390-5394.
[10] J. W. Kim, A. Fernandez-Nieves, N. Dan, A. S. Utada, M. Marquez, D. A. Weitz, *Nano Lett.* **2007**, *7*, 2876-2880.
[11] D. Lee, D. A. Weitz, *Adv. Mater.* **2008**, *20*, 3498-+.
[12] M. Li, R. L. Harbron, J. V. M. Weaver, B. P. Binks, S. Mann, *Nat. Chem.* **2013**, *5*, 529-536.
[13] aN. O'Brien, A. McKee, D. C. Sherrington, A. T. Slark, A. Titterton, *Polymer* **2000**, *41*, 6027-6031; bJ. V. M. Weaver, R. T. Williams, B. J. L. Royles, P. H. Findlay, A. I. Cooper, S. P. Rannard, *Soft Matter* **2008**, *4*, 985-992.
[14] J. V. M. Weaver, D. J. Adams, *Soft Matter* **2010**, *6*, 2575-2582.

CHAPTER 6

Conclusions and future work

This section will briefly summarise and conclude the findings from the main chapters with suggestions for further work.

A single-component strategy for the preparation of inorganic-organic encapsulated droplets and hollow capsules was demonstrated. The process exploits, and relies on, both polymer architecture and composition – the branched architecture providing high droplet stabilities and efficient surfactancy with the compositions providing simultaneous properties of steric-stabilisation and cross-linking function. It has been demonstrated that high yielding encapsulation of different hydrophobic actives at up to 30 w/w % loading, whilst showing that the initial emulsions, encapsulated droplets and hollow capsules retained their structural integrity. The diversity of compositions that could be accessed using the branched co-polymer synthetic route could provide a wealth of opportunity in terms of functionalising the capsule surfaces; further work could include additional functionalisation of the capsule surface. If the produced future polymers were responsive, in principle, the release of encapsulated actives can be controlled by an external trigger. Suitable triggers could of course be pH, UV (*via* the incorporation of cleavable unites in the polymer structure, the easiest being to have cleavable branchers) and ionic strength. To test these hypotheses capsules could be loaded with mutually reactive species, such as Leuco dyes and their respective activator, such as crystal violet lactone and an acid source. The reactivity, or un-reactivity, *via* escape or release from the capsules could then be easily measured.

There is potential for the creation of porous thin films due to the hybrid nature of the co-polymer. When used in spin coating, followed by pyrolysis, the organic section of the co-

polymer will have been burned up, leaving behind interstices in the film. This could be a quick and straightforward route to prepare controlled porosity inorganic membranes.

Functionalised capsule surfaces and shell/membrane properties with pre-determined complex moieties were produced. The facile one-component strategy for the preparation of inorganic-organic encapsulated droplets and hollow capsules, as per Chapter 3, was tailored for specific functionality in this chapter i.e. a pH-response. The incorporation of functionality within the reactive branched addition co-polymer allows higher order responsive structures to be formed. These materials have been shown to be highly useful in the preparation of large associated aggregates which can be loaded with numerous payloads. Both successful encapsulation of hydrophobic dyes and an oil-soluble polymer were illustrated. Future work would include the investigation of the true range of active materials which could be encapsulated and potentially released when desired using this strategy. This could be particularly relevant for biologically active materials and reactive actives where they could be isolated and protected from a harsh environment or formulation such as flavours and fragrances or mutually reactive species.

Industrial applicability: In order to utilise these materials industrially a cheap, non-responsive "bulking monomer" could be introduced into the composition such as butyl methacrylate. This monomer would render the polymer cheaper and more hydrophobic, and through control of the other monomer components a robust and affordable responsive branched addition polymer could be formed. Another drawback from the compositions used throughout this thesis is the use of thiol chain transfer agents, these materials are at best, noxious and can be toxic. The use of a thiol-free route to prepare branched addition polymers could be investigated such as the use of catalytic systems or the use of known chain modifying

compounds such as 2,4 diphenyl-4-methyl-pentene which is readily used as a chain transfer agent for methacrylates and styrenics. The products of these thiol-free routes would need to be compared against materials prepared with DDT, as it is assumed that the long-chain hydrophobic dodecyl units that would be present at the chain termini play an important role in initial emulsion stability.

Membrane structures could be prepared using this methodology where the pore sizes could be controlled and tuned with changes to the pH of the environment. Also, there is potential application in filtration work, where the charge on the capsule or polymer layer could filter for example a solution of charged dye.

Water-dispersible protocell constructs with pH-mediated, electrostatically gated permeability were prepared by covalently grafting a responsive co-polymer to the outer surface of a cross-linked membrane of a silica nanoparticle-based colloidosomes. Co-polymer grafted membrane functionality-mediated uptake and release of small molecules from the colloidosomes was successful. It was demonstrated that the membrane did not lose function on dehydration or rehydration suggesting that it is both robust and elastic. The compartments were also heated to high temperatures without loss of structural integrity. Future work could include further investigation of the storage of actives for long periods of time and followed by controlled released at a later point, this is particularly interesting for bio-actives or controlled release of drug and bio-active agents. Furthermore, the use of the compartments as reaction centres could also be investigated.